

**Leadership-Based Multi-Objective Optimization**  
**with Applications in Energy Systems**

by

**Farid Bourennani**

A Thesis Submitted in Partial Fulfillment  
of the Requirements for the Degree of

**Doctor of Philosophy in Electrical and Computer Engineering**

in

Department of Electrical, Computer, and Software Engineering

Faculty of Engineering and Applied Science

University of Ontario Institute of Technology

Oshawa, Ontario, Canada

© Farid Bourennani, 2013

## **Abstract**

Multi-objective optimization metaheuristics (MOMs) are powerful methods for solving complex optimization problems but can require a large number of function evaluations to find optimal solutions. Thus, an efficient multi-objective optimization method should generate accurate and diverse solutions in a timely manner. Improving MOMs convergence speed is an important and challenging research problem which is the scope of this thesis.

This thesis conducted the most comprehensive comparative study ever in MOMs. Based on the results, multi-objective (MO) versions of particle swarm optimization (PSO) and differential evolution (DE) algorithms achieved the highest performances; therefore, these two MOMs have been selected as bases for further acceleration in this thesis. To accelerate the selected MOMs, this work focuses on the incorporation of leadership concept to MO variants of DE and PSO algorithms. Two complex case studies of MO design of renewable energy systems are proposed to demonstrate the efficiency of the proposed MOMs.

This thesis proposes three new MOMs, namely, leader and speed constraint multi-objective PSO (LSMPSO), opposition-based third evolution step of generalized DE (OGDE3), and multi-objective DE with leadership enhancement (MODEL) which are compared with seven state-of-the-art MOMS using various benchmark problems. LSMPSO was found to be the fastest MOM for the problem undertaken. Further, LSMPSO achieved the highest solutions accuracy for optimal design of a photovoltaic farm in Toronto area.

OGDE3 is the first successful application of OBL to a MOM with single population (no-coevolution) using leadership and self-adaptive concepts; the convergence speed of OGDE3 outperformed the other MOMs for the problems solved. MODEL embodies leadership concept into mutation operator of GDE3 algorithm. MODEL achieved the highest accuracy for the 30 studied benchmark problems. Furthermore, MODEL achieved the highest solution accuracy for a MO optimization problem of hydrogen infrastructures design across the province Ontario between 2008 and 2025 considering electricity infrastructure constraints.

## **Acknowledgements**

I would like to thank my immediately family members as without the continuous encouragement of my parents, constant support of my wife, and the joy of my children it would have been difficult to accomplish this work.

I would like to express my sincere gratitude to my advisors Dr. Shahryar Rahnamayan and Dr. Greg F. Naterer for their expert leadership and continuous support throughout the research work. Especial thanks to Dr. Rahnamayan for his positive attitude; each time I entered his office, I came out with smile and motivation. I greatly appreciate the strategic advices of Dr. Neterer and his great sense of organization.

I would like to thank Dr. Rizvi for offering me to be involved in one of his industrial research projects. Dr. Carlos A. Coello Coello is thanked for his collaboration in one of our research projects. The collaboration of Dr. Hajimiragha in the hydrogen design project is gratefully acknowledged. The collaboration of my friend Amin Ibrahim in variant research works is greatly appreciated. I would also like to thank the entire team at the Software Lab and the Clean Energy Research Lab (CERL) for their assistance especially Haris Mushtaq, Timothy Teatro. I greatly appreciate the discussions and suggestions of various professors, colleagues at UOIT.

I would like to thank the thesis committee members, namely, Dr. Stephen Y. Chen, Dr. Lennaert van Veen, Dr. Mark Rosen, and Dr. Hossam Gaber for their precious comments and review of the thesis. The valuable comments of anonymous referees for my published papers are greatly appreciated as it facilitated the improvement of the thesis.

I would like to thank all the staff at UOIT, especially Joel Stewart, Karla Gomez, Susan Allward for their kindness and support during my graduation years at UOIT.

The financial support of Natural Science and Engineering Council of Canada (NSERC), Ontario Graduate Scholarship (OGS), the Dean Graduate Scholarship, and the Jeffrey Boyce Engineering Award is gratefully acknowledged.

I would like to express my gratitude to all my friends who did whatever they could to help me complete this work.

*To Humanity*

## Table of Contents

Abstract.....	ii
Acknowledgements.....	iv
Table of Contents.....	vii
List of Figures.....	xiv
List of Tables.....	xviii
List of Abbreviations and Acronyms.....	xxii
Nomenclature.....	xxiv
Definitions.....	1
Chapter 1 Introduction.....	3
1.1 Current Trends in Multi-Objective Research.....	5
1.2 Thesis Scope.....	8
1.3 Thesis Objective.....	9
1.4 Thesis Contributions.....	10
1.5 Outline of Thesis.....	11
Chapter 2 Multi-Objective Optimization: A Background Review.....	14
2.1 Global Multi-Objective Optimization.....	15
2.2 Concept of Optimality in Multi-Objective Space.....	15
2.3 Particularities of Multi-Objective Metaheuristics Over Single Objective Optimization Metaheuristics.....	19

2.4	Problems with Transforming Multi-Objective Optimization Problem into Single Objective Problem.....	20
2.4.1	Weighted Sum Method (WSM).....	21
2.4.2	$\epsilon$ -Constraint method.....	22
2.5	Summary .....	23
Chapter 3	Multi-Objective Optimization: A Comparative Study .....	24
3.1	Introduction .....	25
3.2	Previous Comparative Studies: A Literature Review .....	27
3.3	Problems Description .....	29
3.3.1	Variant problem complexities.....	30
3.3.2	The ZDT problems.....	32
3.3.3	The DTLZ problems .....	33
3.3.4	The Van Veldhuizen's test suite .....	33
3.3.5	The WFG problems.....	34
3.3.6	The LZ_09 problems.....	35
3.4	Compared State-Of-The-Art Multi-Objective Metaheuristics .....	36
3.5	Parameter Settings.....	38
3.5.1	Stopping criteria.....	38
3.5.2	Parameters settings.....	40
3.5.3	Performance measures .....	40
3.6	Results .....	42



3.6.1	Bi-objective problems .....	43
3.6.2	Three-objective problems .....	47
3.6.3	LZ_09 problems .....	49
3.6.4	Overall results .....	51
3.7	Conclusions .....	52
Chapter 4 Optimal Design of Hybrid Renewable Energy Systems .....		54
4.1	Introduction .....	55
4.2	Types Renewable Hybrid Energy System.....	56
4.3	Modeling Renewable Energy Systems.....	57
4.3.1	Modeling of photovoltaic systems .....	57
4.3.2	Modeling of wind systems .....	58
4.3.3	Modeling of hydrogen fuel cells .....	59
4.4	Simulation-Based Optimization of Energy System Components .....	60
4.4.1	Simulation-based optimization of photovoltaic systems .....	61
4.4.2	Simulation-based optimization of wind systems .....	62
4.4.3	Simulation-based optimization of fuel-cell systems .....	62
4.4.4	Simulation-based optimization of PV-wind systems .....	63
4.4.5	Simulation-based optimization of solar-wind-fuel-cell systems.....	66
4.5	Optimization of Energy System Components .....	67
4.5.1	Mono objective optimization for hybrid energy systems design .....	68
4.5.2	Multi-Objective optimization for hybrid energy systems design .....	70

4.6	Summary and Future Trends .....	73
4.6.1	Energy system-related observations .....	73
4.6.2	Optimization-related observations .....	74
4.7	Conclusions .....	77
Chapter 5 Leaders and Speed Constraint Multi-Objective Particle Swarm Optimization....		80
5.1	Particle Swarm Optimization .....	82
5.2	Speed Constraints Multi-objective Particle Swarm Optimizer .....	84
5.3	Leadership in PSO Related Work .....	84
5.4	Description of the Proposed Leader Selection Approach .....	86
5.5	Representative Non-Dominance Concept .....	88
5.6	Selection Scheme of Deputy Leaders.....	89
5.7	Experiments Settings.....	92
5.7.1	Benchmark problems .....	92
5.7.2	Comparison of LSMPSO with other MOO algorithms .....	93
5.7.3	Parameters settings.....	93
5.8	Result Analysis.....	95
5.9	Summary .....	102
Chapter 6 Case Study I: Optimal Photovoltaic System Design Using LSMPSO.....		103
6.1	Introduction .....	104
6.2	Related Works .....	106
6.3	Physical System Model .....	108

6.3.1	Solar collector model .....	109
6.3.2	System complexities .....	113
6.3.3	Objectives, variables, and constraints.....	114
6.3.4	Climate information .....	116
6.3.5	PV panel specification .....	116
6.4	Experimental simulations.....	117
6.5	Discussion of the results.....	117
6.6	Summary .....	122
Chapter 7	Opposition-Based Third Generalized Differential Evolution (OGDE3).....	124
7.1	Introduction .....	125
7.2	Opposition-Based Learning (OBL).....	126
7.2.1	Variants of opposition-based Schemes .....	127
7.2.2	Opposition-based learning: Applications in optimization .....	130
7.3	Opposition-based Learning for Multi-Objective Optimization.....	134
7.4	Proposed Algorithm: Opposition-Based Third Generalized Differential Evolution Algorithm (OGDE3) .....	136
7.5	Self-Adaptive Selection of Candidate Solutions for Opposition .....	139
7.6	Experiments.....	142
7.6.1	Benchmarking problems .....	143
7.6.2	Metaheuristics parameter settings.....	143
7.6.3	Evaluation measure .....	143

7.6.4	Experimental simulation results.....	144
7.7	Conclusions .....	150
Chapter 8	Multi-Objective Differential Evolution with Leadership (MODEL).....	152
8.1	Introduction .....	153
8.2	Proposed Mutation Scheme.....	154
8.2.1	Use of leadership in the mutation (GDE3/deputy/1) .....	154
8.2.2	Non-dominance sorting for the difference vector .....	155
8.2.3	Negation of Control Parameter F .....	156
8.3	Multi-Objective Differential Evolution with Leadership.....	158
8.4	Experimental Results.....	160
8.4.1	ZDT, DTLZ, and WFG problems .....	160
8.4.2	LZ_09 problems.....	166
8.5	Conclusions .....	170
Chapter 9	Case Study II: Optimization of Transition to Hydrogen-Fuelled Vehicles in Ontario, Canada Considering Electricity Grid Constraints.....	171
9.1	Introduction .....	172
9.2	Hydrogen-Fueled Vehicles in Canada.....	173
9.3	Electricity Model of Ontario .....	175
9.3.1	Power Transmission.....	175
9.3.2	Power generation .....	177
9.3.3	Import and export of power .....	178

9.3.4	Zonal electricity demand.....	179
9.4	Hydrogen Infrastructure Model.....	180
9.4.1	Hydrogen generation.....	180
9.4.2	Hydrogen demand.....	181
9.4.3	Hydrogen transportation .....	183
9.5	Optimization Model .....	184
9.5.1	Objective Functions .....	186
9.5.2	Variable Bounds.....	187
9.5.3	Constraints .....	189
9.6	Experimental Simulations .....	191
9.6.1	Parameter settings .....	191
9.6.2	Discussion of the results .....	192
9.7	Conclusions .....	197
Chapter 10	Conclusions and Recommendations.....	199
10.1	Conclusions .....	200
10.2	Future Work and Recommendations.....	205
	Appendix A: Multi-Objective Benchmark Problems Description .....	209
	Appendix B: Meteorological Data for Toronto Area Used in the Photovoltaic Energy System Design Case Study.....	242
	Appendix C: Electricity Import/Export Capacities in the Province of Ontario .....	247
	Bibliography.....	249

## List of Figures

Figure 1: Examples of Pareto fronts for minimization bi-objective problems: poor convergence and good-distribution (left), strong convergence and poor distribution (center), strong convergence and uniform-distribution (accuracy) (right).....	6
Figure 2: Classification of optimization methods.....	8
Figure 3: Pareto front schematic .....	17
Figure 4: De Jong is unimodal, scalable, convex, and relatively easy function. ....	18
Figure 5: Griewangk’s function has many, regularly distributed local minima and hard to locate global minimum. ....	18
Figure 6: Illustration of relationships between variables and objectives in single objective space.....	19
Figure 7: Illustration of relationships between variables and objectives in MO space. ....	20
Figure 8: Weighted Sum Method. This example shows the importance of giving the right weights to find Pareto-optimal solutions. ....	21
Figure 9: Difficulties associated with the WSM method such as not finding solutions in non-convex region of the PF .....	22
Figure 10: Pareto front geometries. The Pareto front is composed of mixed components, namely, convex, concave, connected, disconnected, and degenerate components. Degenerate is when the PF is of a dimension $D - 1$ .....	31
Figure 11: Example of a deceptive function for single objective minimization problem .....	32
Figure 12: Projections of Pareto sets of F1–F9 onto the $x_1, x_2, x_3$ space .....	35

Figure 13: Example of a hybrid PV-wind energy system.....	64
Figure 14: Example of modeling of a PV-hydrogen FC energy system.....	67
Figure 15: Example of flock of birds .....	81
Figure 16: Example of fish schools .....	81
Figure 17: Movement of a particle and the velocity update. ....	83
Figure 18: First iteration for the ZDT2 problem.....	87
Figure 19: Iteration 15 <sup>th</sup> (1500 FCs) for the ZDT2 problem.....	88
Figure 20: Example of four selected deputies (full particles) based on the SWR measure....	91
Figure 21: Pareto fronts with different HV values obtained for the ZDT1 problem. ....	94
Figure 22: Boxplots of the number of function evaluations to find the real Pareto front for the ZDT bi-objective problems.....	100
Figure 23: Boxplots of the number of function evaluations to find the real Pareto front for the DTLZ bi-objective problems .....	101
Figure 24: Collectors arrangement in a stationary solar field.....	110
Figure 25. Angle of incidence $\theta$ : angle between a normal to the collector face and the incoming solar beam. ....	112
Figure 26: Collector azimuth with respect to south ( $\gamma_C$ ). ....	113
Figure 27: Median (IGD) solutions found by MOCcell .....	118
Figure 28: Median (IGD) solutions found by AbYSS .....	118
Figure 29: Median (IGD) Solutions found by GDE3 .....	119
Figure 30: Median (IGD) Solutions found by SMPSO .....	119

Figure 31: Median (IGD) solutions found by LSMPSO.....	120
Figure 32: Boxplots of LSMPSO, SMPSO, GDE3, MOCcell, and AbYSS over 100 runs to solve PV design problem .....	121
Figure 33: An opposite point in a one-dimensional search space.....	127
Figure 34: Illustration of an opposite point in 2D search space. ....	128
Figure 35: Simplified representation of quasi-opposites and super-opposites in 2D search space.....	129
Figure 36: Type-I versus type-II opposition.....	130
Figure 37: Taxonomy of parameter control for metaheuristics .....	139
Figure 38: Incorporation of opposition based learning into GDE3. ....	142
Figure 39: Median and IQR of the number of function evaluations for ZDT1. ....	145
Figure 40: Median and IQR of the number of function evaluations for ZDT2. ....	146
Figure 41: Median and IQR of the number of function evaluations for ZDT3. ....	146
Figure 42: Median and IQR for ZDT4.....	147
Figure 43: Median and IQR for ZDT6.....	147
Figure 44: Example of a problem where the distance between the initial population and the PF is reasonable .....	157
Figure 45: Example of a problem where the distance between the initial population and the PF is large .....	157
Figure 46: IGD boxplots for ZDT bi-objective problems.....	164
Figure 47: IGD boxplots for DTLZ bi-objective problems .....	165



Figure 48: IGD boxplots for WFG bi-objective problems.....	166
Figure 49: IGD boxplots for LZ_09 bi-objective problems.....	169
Figure 50: Simplified model of Ontario’s gird zones .....	175
Figure 51: Overview of the expected distribution of power capacity in different zones of Ontario .....	178
Figure 52: Estimated penetration of HFVs in Ontario.....	182
Figure 53: Projected number of light-duty vehicles in 18 years period in the ten zones of Ontario .....	183
Figure 54: Boxplots for the IGD measures for the hydrogen economy problem. ....	192
Figure 55: Pareto optimal sets of median IGDs found for simplified version of the hydrogen economy problem.....	195
Figure 56: Details of an optimal solution found by MODEL with a cost of \$40.5 billion and 5% of hydrogen-fuled vehicles. ....	196
Figure 57: IGD boxplots for DTLZ bi-objective problems .....	230
Figure 58: IGD boxplots for WFG bi-objective problems.....	231
Figure 59: IGD boxplots for ZDT bi-objective problems.....	232
Figure 60: IGD boxplots for Van Veldhuizen’s Bi-Objective problems .....	233
Figure 61: IGD boxplots for the Viennet three-objective problems .....	233
Figure 62: IGD boxplots for DTLZ three-objective problems .....	234
Figure 63: IGD boxplots for WFG three-objective problems.....	235
Figure 64: IGD boxplots of LZ_09 problems .....	236

## List of Tables

Table 1: Control parameter settings .....	39
Table 2: Scores for bi-objective problems .....	44
Table 3: IGD, mean and standard deviation for bi-objective problems taken from ZDT, DTLZ, WFG, and Van Veldhuizen test suites after $10^4$ function evaluations.....	46
Table 4: IGD mmeasure, mean and standard deviation for three-objective problems taken from DTLZ, WFG, and Van Veldhuizen test suites after $10^4$ function evaluations.....	48
Table 5: Scores for three-objective problems .....	49
Table 6: Scores for LZ_09 objective problems.....	50
Table 7: IGD, mean and standard deviation LZ_09 Problems. ....	50
Table 8: Overall score for all the bi-objective problems .....	52
Table 9: Overall score for all the three-objective problems .....	52
Table 10: Overall score for all the bi-objective and three-objective problems.....	52
Table 11: Résumé of reviewed HESs-related works .....	76
Table 12: Example of eight leaders in two-objective space .....	91
Table 13: Utilized bi-objective problems in LSMPSO comparison .....	92
Table 14: Algorithms compared with LSMPSO.....	93
Table 15: Median and interquartile range (IQR) of the number of evaluations for reaching the Pareto front ( $HV \geq 98\%$ ).....	97
Table 16: Average hit rate of the compared MO optimization algorithms.....	98

Table 17: IGD mean and standard deviation .....	120
Table 18: IGD median and IQR.....	120
Table 19: Median and IQR of the number of function evaluations for reaching the PF .....	145
Table 20: Relative difference of the convergence speed between OGDE3 with the other MOMs.....	149
Table 21: Hit Rate of the compared MOMs .....	150
Table 22: IGD, mean and standard deviation for bi-objective problems.....	162
Table 23: Scores for bi-objective problems .....	163
Table 24: IGD, mean and standard deviation for bi-objective problems. Dark grey is the algorithm having the best IGD results followed by light grey in the second position.....	167
Table 25: Scores for LZ_09 problems .....	168
Table 26: Line loading limits of the transmission grid.....	176
Table 27: Transmission corridor enhancements during the study period considered.....	177
Table 28: Estimated zonal peak-load growth rate.....	179
Table 29: Zonal base-load electricity demand [MWh] .....	179
Table 30: Details of the case study model variables.....	188
Table 31: Case study model constraints description.....	189
Table 32: Median and IQR IGD measures for the hydrogen economy problem.....	192
Table 33: Details of two optimal solutions found by the MODEL algorithm.....	193
Table 34: Number of HFVs in every zone based on the solution with a cost of 40.536 \$Million and a ratio of 5% of HFVs. ....	197

Table 35: ZDT test functions (all minimization problems) .....	210
Table 36: DTLZ M-objectives minimization problems.....	212
Table 37: Van Veldhuizen test suite .....	216
Table 38: WFG suite, shape functions of the Pareto front.....	219
Table 39: WFG Suite, Transformation Functions (bias, shift, reduction) .....	220
Table 40: WFG test suite .....	221
Table 41: LZ_09 test suite .....	226
Table 42: HV. Mean and standard deviation for bi-objective problems.....	237
Table 43: HVR. Mean and standard deviation for bi-objective problems.....	238
Table 44: Hypervolume Ratio Mean and Standard Deviation for 3-Objective Problems ....	239
Table 45: HV Mean and Standard Deviation for Three-Objective Problems.....	240
Table 46: Hypervolume Ratio Mean and Standard Deviation for LZ_09 Problems .....	241
Table 47: Hypervolume Mean and Standard Deviation for LZ_09 Problems.....	241
Table 48: Monthly average hourly direct normal beam irradiance: Latitude 43.45° / Longitude -79.25° (kWh/m <sup>2</sup> ).....	243
Table 49: Monthly average hourly horizontal diffuse irradiance: Latitude 43.45° / Longitude -79.25° (kWh/m <sup>2</sup> ).....	243
Table 50: Monthly averaged hourly solar azimuth angles due south (degrees 43.45° / Longitude -79.25°) .....	244
Table 51: Monthly averaged hourly solar Angles relative to the horizon (degrees): 43.45° / Longitude -79.25° .....	244

Table 52: The solutions having achieved the lowest (best) IGD found by LSMPSO. ....	245
Table 53: Zonal electricity maximum import (MWh) .....	248
Table 54: Zonal electricity maximum export (MWh).....	248

## List of Abbreviations and Acronyms

AbYSS	Archive-Based hYbrid Scatter Search
CD	Crowding Distance
DE	Differential Evolution
DTLZ	Deb-Thiele-Laumanns-Zitzler
FC	Function Call
FCV	Fuel Cell Vehicle
GA	Genetic Algorithm
GDE3	Third Generalized Differential Evolution
HES	Hybrid Energy System
HFV	Hydrogen-Fuel Vehicle
HPP	Hydrogen Power Plant
HV	Hypervolume
HVR	Hypervolume Rate
IBEA	Indicator-Based Evolutionary Algorithm
IGD	Inverse Generational Distance
MO	Multi-Objective
MOCcell	Multi-Objective Cellular genetic algorithm
MOEA/D	Multi-Objective Evolutionary Algorithm based on Decomposition
MOM	Multi-Objective Metaheuristic

MOO	Multi-Objective Optimization
MOP	Multi-objective Optimization Problem
NSGA-II	Non-dominated Sorting Genetic Algorithm II
PAES	Pareto Archived Evolution Strategy
PF	Pareto Front
PS	Pareto optimal Set
PSO	Particle Swarm Optimization
PV	Photovoltaic
RESs	Renewable Energy Systems
SMPSO	Speed Constrained Particle Swarm Optimization
SPEA2	Strength Pareto Evolutionary Algorithm 2
SWR	Sum of Weighted Ratios
WFG	Walking-Fish-Group
WSM	Weighted Sum Method
ZDT	Zitzler-Deb-Thiele

## Nomenclature

$A_{max}$	=	maximum collector height above ground, $m$
$a_s$	=	relative shaded area, $m^2$
$D$	=	distance between collector rows, $m$
$D_{min}$	=	minimum distance between collector rows, $m$
$d$	=	normalized distance between collector rows, $m$
$F_d$	=	configuration factor for un-shaded collectors
$F_d^{sh}$	=	configuration factor for shaded collectors
$G_b$	=	direct beam irradiance on the collector perpendicular to solar rays, $kWh/m^2$
$G_{dh}$	=	horizontal diffuse irradiance, $kWh/m^2$
$H$	=	collector height, $m$
$H_s$	=	shadow height, $m$
$h_s$	=	relative shadow height, $m$
$H_{max}$	=	maximum collector height, $m$
$K$	=	number of solar collector rows
$L$	=	solar field length, $m$
$L_s$	=	shadow length, $m$
$l$	=	normalized collector length, $m$
$l_s$	=	relative shadow length, $m$
$Q$	=	yearly energy, $MWh$



$q_b =$	yearly beam irradiation per unit area of an un-shaded collector (first row)
$q_d =$	yearly diffuse irradiation per unit area of an un- shaded collector (first row)
$q_b^{sh} =$	average yearly beam irradiation per unit area of shaded collector ((K-1) rows)
$q_d^{sh} =$	average yearly diffuse irradiation per unit area of shaded collector ((K-1) rows)
$T_R =$	sun rise on the collector for the beam irradiance, $kWh/m^2$
$T_S =$	sun set on the collector for the beam irradiance, $kWh/m^2$
$T_{SR} =$	sun rise for the diffuse irradiance, $kWh/m^2$
$T_{SS} =$	sun set for the diffuse irradiance, $kWh/m^2$
$W =$	solar field width, $m$
$W_{max} =$	maximum solar field width, $m$
$Z^+ =$	natural number set
$\alpha =$	sun elevation angle, <i>degree</i>
$\beta =$	collector inclination angle, <i>degree</i>
$\gamma =$	difference between the sun and collector azimuth, <i>degree</i>
$\gamma_C =$	collector azimuth with respect to south, <i>degree</i>
$\gamma_S =$	sun azimuth with respect to south, <i>degree</i>
$\theta =$	angle between the solar beam and the normal to the collector, <i>degree</i>
$\Delta T =$	time interval

## Definitions

Definitions are provided to clarify the meaning of some terminologies used in this thesis that could be interpreted differently in other fields than multi-objective optimization.

**Accuracy:** Accuracy of solutions refers to a combination of strength of convergence and uniformity of distribution for solutions along the Pareto front.

**Convergence:** Closeness of Pareto optimal solutions the real Pareto front.

**Convergence speed:** measure of number of function evaluations, not computation time, refers to the computational effort required to find accurate approximations of the Pareto front.

**Deceptive function:** a function that deceives an optimizer by leading it away from the global optimum when located in the neighborhood of the global optimum

**Degenerate solutions:** Unusual case where the dimensionality of Pareto optimal solutions is of a lower number than the number of objectives; for example, optima is only a single solution for a bi-objective problem.

**Experiments:** In optimization field, it refers to a set of simulations in metaheuristics to solve either synthetic or real optimization problems. In other fields such as mechanical engineering it

refers to physical experiments but in computational context, the contributions are also computation therefore the word experiment is used

**Heuristic:** an algorithm that is problem dependent.

**Metaheuristic:** a computational method that optimizes a problem by iteratively improving a candidate solution. Contrary to heuristic, it can be applied to wide range of problems; it can also be tailored for specific types of problems.

**Robustness:** is accuracy quality of an algorithm when solving optimization problems of variant complexities (features).

# **Chapter 1**

## **Introduction**

Real-world problems require optimization in multiplicity of conflicting objectives. For example, while designing a power system, electrical engineers are targeting competing objectives such as cost minimization, performance maximization, supply-demand balancing, pollution minimization, to name a few. Such problems are called multi-objective optimization problems (MOPs). Furthermore, real-world problems often encompass multiple complexities which make them non-solvable using classical optimization methods. Examples of such complexities are [1]:

- Nonlinearity
- No prior knowledge about the problem (black box problem)
- Large dimensions
- Non-differentiation
- Non-convex
- Highly multimodal
- Multiple objectives
- NP-Hard
- Uncertainties in decision and problem parameters
- Mixed-types decision variables
- Discontinuity
- Epistasis (complex variable |relationship)
- Many-to-one mapping

## 1.1 Current Trends in Multi-Objective Research

Typically, due to the conflicting relationship among the objectives, there is no single optimal solution for all the objectives as for a single objective problem. Rather, for non-trivial MOPs, the generated solutions involve trade-offs. By compromising one objective, it is possible to improve another or other objective(s). For practical reasons, especially in real-world problems, decision makers are interested in having a variety of solutions in order to choose the most appropriate one based on their needs. The optimal solutions are called *Pareto optimal set*. The solutions belonging to a Pareto Optimal Set are called *non-dominated* solutions. The combination of the Pareto optimal sets are collectively known as the *Pareto front* (PF). There are two main objectives when using metaheuristics to solve MOPs. First, the solutions should be as close as possible to the PF. Second, the solutions should be uniformly distributed (diverse) so that the user can have a variety of choices [2]. Ideally, the Pareto set should capture the *complete spectrum* of the PF. Figure 1 illustrates three types of PF approximations. The first plot located in the left shows a well distributed front but the convergence is low. This front is deficient because it does not provide precise Pareto optimal solutions. The second plot located in the center shows strong convergence to the PF with a missing portion which could be critical for decision making and therefore is a deficient front. Finally, the last plot located in right has both desirable properties of strong convergence and good distribution which is the ideal front for decision making.

Several challenges in MOMs are still undergoing research. For example, convergence speed, solutions precision, solutions distribution, and scalable problems are some of the aspects that are the current focus of the MOO community. These criteria are further detailed below.

**Convergence speed:** A challenging issue in MOO is the design of metaheuristics for reaching optimal solutions with a low number of function evaluations. State-of-the-art MOMs might require thousands to millions of function evaluations (FCs) to achieve high accuracy levels. Therefore, researchers are proposing strategies to speed-up the convergence towards the Pareto front [3], [4].

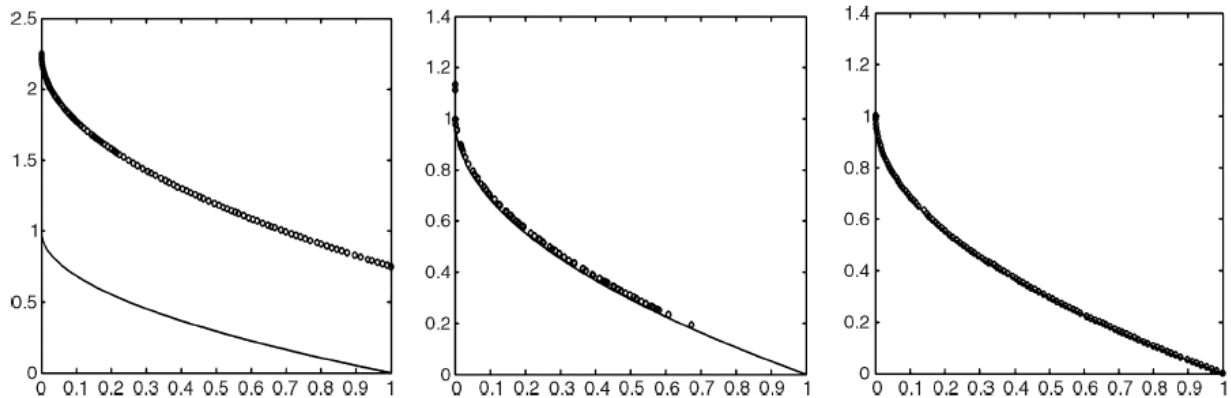


Figure 1: Examples of Pareto fronts for minimization bi-objective problems: poor convergence and good-distribution (left), strong convergence and poor distribution (center), strong convergence and uniform-distribution (accuracy) (right) [5].

**Convergence:** The convergence of solutions determines how close they are from the PF. The convergence is critical because a metaheuristic does not guarantee optimality; therefore, a solution should be as close as possible to the PF. Also, the accuracy level of a metaheuristic

depends on the complexity of problems. Some researchers are focusing on internal mechanisms of MOMs in order to enhance their convergence. For example in [4], authors studied the impact of the metaheuristic population size on the results' convergence. Also, [6] and [7] studied the precision of MOMs when solving complex MOPs.

**Distribution:** In a MOO context, the distribution (variety) of solutions is important. MOM might generate a set of solutions that belong to the Pareto front; however, they might converge to only a specific portion of the PF. Consequently, the generated set of solutions will not provide the required variety of solutions which is often necessary in most real-life problems [8].

**Scalability:** In MOO context, a scalable problem can have two meanings: a problem having a large number of objectives or large number of decision variables. For example, most benchmarking problems have a limited number of variables lower than 30 variables. Some researchers have studied the extension of MO Metaheuristics (MOM) methods to handle large scale decision variables problems [9].

There are other open research problems that interest the MOM research community, such as interactive optimization, robust optimization, and computationally expensive optimization problems. More information about current MOM research trends can be found in [10], [1].



## 1.2 Thesis Scope

The scope of the thesis focuses on the acceleration of *convergence speed* of MOMs while preserving a good accuracy, i.e., good *precision and distribution* of solutions. Different taxonomies have been proposed for classifying optimization methods [11]. However, based on the suggested taxonomy proposed by Feoktistov [12] in Figure 2, as shown in dark grey the scope of this work is the acceleration of population-based non-linear continuous global optimization metaheuristics but with multi-objectives.

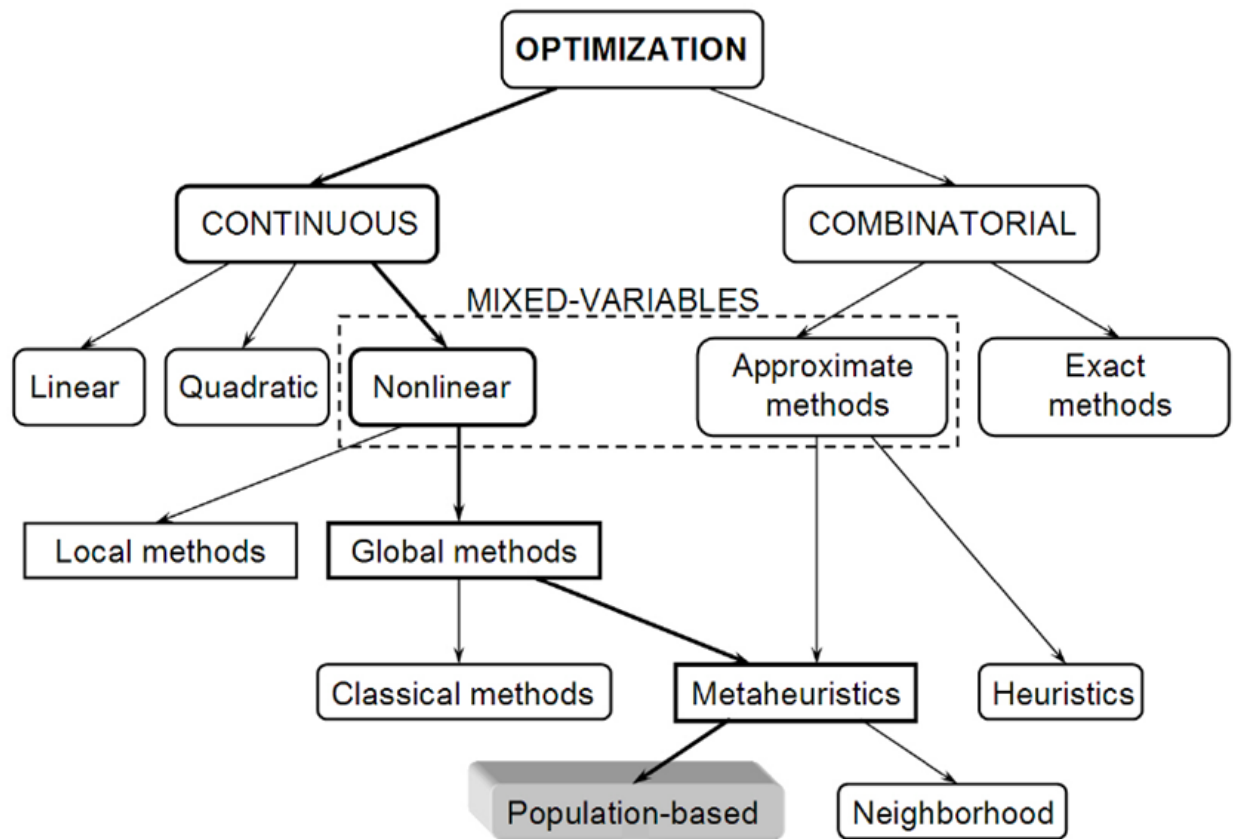


Figure 2: Classification of optimization methods.  
The grey box is the focus of the current work.

### 1.3 Thesis Objective

The objective of this thesis is to achieve fastest convergence of MO variants of DE and PSO by using the concepts of leadership. To evaluate the performance of the proposed methods, they are compared with state-of-the-art MOMs using comprehensive bi-objective benchmark problems. In addition, two real-life and complex case studies of optimal design of energy systems are used for the assessment of the proposed methods.

By conducting a comparative study, it was found that a MO variant of PSO named SMPSO is faster than other MOMs, especially for two-objective problems. One of the particularities of SMPSO over other MOMs is the use of leadership which seems be the main reason of its fast convergence. As says an Arabic proverb "don't ask the one who failed how did he fail?, but ask the one who succeed how did he succeed ?". The selection of a leader is trivial in single objective space, but the generalization of the concept of leader selection for MOO is complex [13]. When leaders are not appropriately selected, e.g. there is a high concentration of leaders in a specific region of the objective space, particles (candidate solutions) might be pulled to that region which results in a poor distribution (diversity). The particles will prematurely converge towards a specific region of objective space where these groups of leaders are located; so, the MOM will be either trapped in local optima or will require additional computational overhead to redistribute the particles along the PF. Therefore, one objective of this thesis is the development of new leader selection mechanisms in order to select leaders in a more representative manner. For example, the use the sum of weighted ratios (SWR) for leader selection is incorporated into SMPSO as an additional selection mechanism. Furthermore, the

leadership concept is also incorporated into a MO variant of DE called GDE3. Another avenue that is considered for the acceleration of MOMs is the use of opposition-based learning (OBL) with incorporation of leadership concept. OBL was successfully incorporated into DE for single objective problems [14]. The straight forward incorporation of OBL into GDE3 did not show the expected improvements; however, by utilizing a self-adaptive scheme of OBL with leadership, GDE3 was improved; the proposed method was called opposition-based third evolution step of generalized DE (OGDE3) [15].

Another objective of this thesis is the demonstration of MOMs practicality by solving real-world problems. One of the engineering fields that involve complex optimization problems is design of renewable energy systems. Two of the proposed MOMs, namely, LSMPSO and MODEL have been successfully used to solve respectively an optimal farm design problem and optimal design of a hydrogen network across Ontario. Both problems were highly complex because of mixed type variables, multimodality, constraints, and other complexities which challenge the efficiency of MOMs in general and the proposed methods in particular.

## **1.4 Thesis Contributions**

The contributions of this thesis are as follows.

- Conducting a comprehensive comparative study of state-of-the-art MOMs to select the most appropriate one and further enhance.
- Conducting a survey of optimization methods applied to RESs, with a particular focus on MOMs.

- Proposition of three MOMs which are enhancements of MO variants of PSO (SMPSO) and DE (GDE3) using leadership concepts.
  - LSMPSO: Application of leadership to SMPSO
  - OGDE3: Application leadership and OBL to GDE3
  - MODEL: Application of leadership to GDE3
- Case studies of optimal design of renewable energy systems.
  - Optimal MO design of a photovoltaic farm in Toronto, Canada area
  - Optimal MO design of a hydrogen distribution infrastructure across Ontario with consideration of electricity distribution network constraints

## **1.5 Outline of Thesis**

The thesis is organized in ten chapters and three appendices. The first two chapters describe fundamental concepts of MOMs to facilitate the understanding of this work. Chapters three and four present literature review of optimization methods applied to RESs, and a comparative study of MOMs. Chapters five, seven and eight are dedicated to the description of the proposed MOMs. Chapters six and nine are devoted to the proposed case studies. Finally, the last chapter is dedicated to conclusions and recommendations. So, the detailed organization of the remainder of the document is as follows.

Chapter 2 introduces the fundamental concepts of multi-objective optimization and the advantages of MOMs over classical optimization methods.

Chapter 3 presents a comprehensive comparative study of seven state-of-the-art MOMs using 53 well-known bi-objective and three-objective benchmark problems characterized by variant complexities. The robustness of the compared MOMs was the main focus of this study; the results are presented and discussed in detail. This study serves to find the most promising MOMs to be further improved in this thesis.

Chapter 4 is a survey of applications of optimization methods to renewable energy systems. The survey describes previous works, findings, future perspectives, and potential applications in this thesis.

Chapter 5 describes a proposed leader selection mechanism based on Weighted Sum Ratio method applied to a MO variant of PSO.

Chapter 6 presents the first multi-objective optimization case study. It presents findings for optimal designs of a photovoltaic farm in Toronto, Canada area. LSMPSO is compared with four others MOMs.

Chapter 7 describes the proposed OGDE3 MOM which uses a self-adaptive version of OBL that uses leadership for MO variant of DE.

Chapter 8 explains the proposed MODEL algorithm. Leadership concept has been successfully incorporated into a MO variant of DE. The leadership concept serves to accelerate the convergence speed and improve the accuracy of MODEL.

Chapter 9 presents a case study of optimal design of a hydrogen distribution network across Ontario considering current and future plans of electricity network in Ontario. The problem is complex due to multimodality, and mixed-type variables. The proposed MODEL

algorithm was compared to four other MOMs and the results, which are promising, are discussed in detail.

Chapter 10 concludes this thesis with regards to the main contributions. Future perspectives and recommendations are also discussed.

Appendix A provides details about multi-objective optimization benchmark problems used in the comparative study of Chapter 3.

Appendix B describes the meteorological data of Toronto used in the photovoltaic design case study presented in Chapter 6.

Appendix C contains electricity import/export information between Ontario zones and other provinces/states used in Chapter 9.

## **Chapter 2**

### **Multi-Objective Optimization: A Background Review**

This chapter introduces the reader to basic concepts related to MOO and MOMs. The chapter also covers definitions, notations, and concepts used in the remainder of this thesis.

## 2.1 Global Multi-Objective Optimization

A MOP consists of multiple functions (problems) to be minimized or maximized. However, for the sake of simplicity without loss of generality, in this thesis, it is assumed that all problems are minimization ones Chapters except if stated otherwise. Also, a MOP can be subject to equality and inequality constraints and variable boundaries (sometimes called box-constraints). A MOP is formulated as follows:

$$\text{Min } F(x) = [f_1(x), f_2(x), \dots, f_k(x)], \quad (1)$$

*s.t.*

$$g_i(x) \geq 0, \quad i = 1, 2, \dots, m \quad (2)$$

$$h_j(x) = 0, \quad i = 1, 2, \dots, p \quad (3)$$

where  $x$  is a vector of decision variables for the optimization problem,  $f_k(x)$  is  $k^{\text{th}}$  objective function,  $g_i(x)$  is  $i^{\text{th}}$  inequality constraint, and  $h_j(x)$  is  $i^{\text{th}}$  equality constraint. The constraints (2) and (3) determine the *feasible region*  $\Omega \subseteq \mathbb{R}^n$ .

## 2.2 Concept of Optimality in Multi-Objective Space

Some fundamental definitions related to Pareto-optimality are provided as follows.



**Definition 1: Pareto dominance**

Given two candidate solutions  $x, y \in \Omega$ ,  $x$  *dominates*  $y$  (denoted by  $x \prec y$ ) iff  $\forall i = 1, \dots, k$   $f_i(x) \leq f_i(y)$  and  $\exists$  one  $i = 1, \dots, k$  where  $f_i(x) < f_i(y)$ .

i.e., a solution  $x$  Pareto dominates solution  $y$ , if  $x$  is at least as good as  $y$  in every objective and better than  $y$  in at least one objective.

**Definition 2: Pareto optimality**

Given a solution  $x^* \in \Omega$ ,  $x^*$  is *Pareto Optimal* solution if  $\nexists y \in \Omega$  such that  $y \prec x^*$ .

$x^*$  is Pareto optimal if it is not dominated by any other solution.

**Definition 3: Pareto optimal set**

A *Pareto optimal set* is defined by  $PS = \{x \in \Omega \mid x \text{ is a Pareto optimal solution}\}$

i.e., a Pareto set  $PS$  is a set of non-dominated solutions.

**Definition 4: Pareto optimal front**

A *Pareto optimal front* is defined by  $PF^* = \{F(x) = [f_1(x), f_2(x), \dots, f_k(x)] \mid x \in PS\}$

i.e., non-dominated solutions make up a Pareto-optimal front when *visualized* in the objective space.

As shown in Figure 3, for example, an energy system design might involve two objectives, such as cost minimization and pollution minimization. One solution might be inexpensive but very polluting such as the solution  $f$ , while another solution can be affordable but more polluting such as the solutions  $c$ ,  $d$ , or  $e$ . A last solution can be very expensive but with

very low level of pollution such as the solution *a*. The optimal solutions which are *non-dominated* (*a,b,c,d,e,f*) represent the *Pareto optimal set*. The combined plot of Pareto optimal solutions in the objective space forms the *Pareto front*.

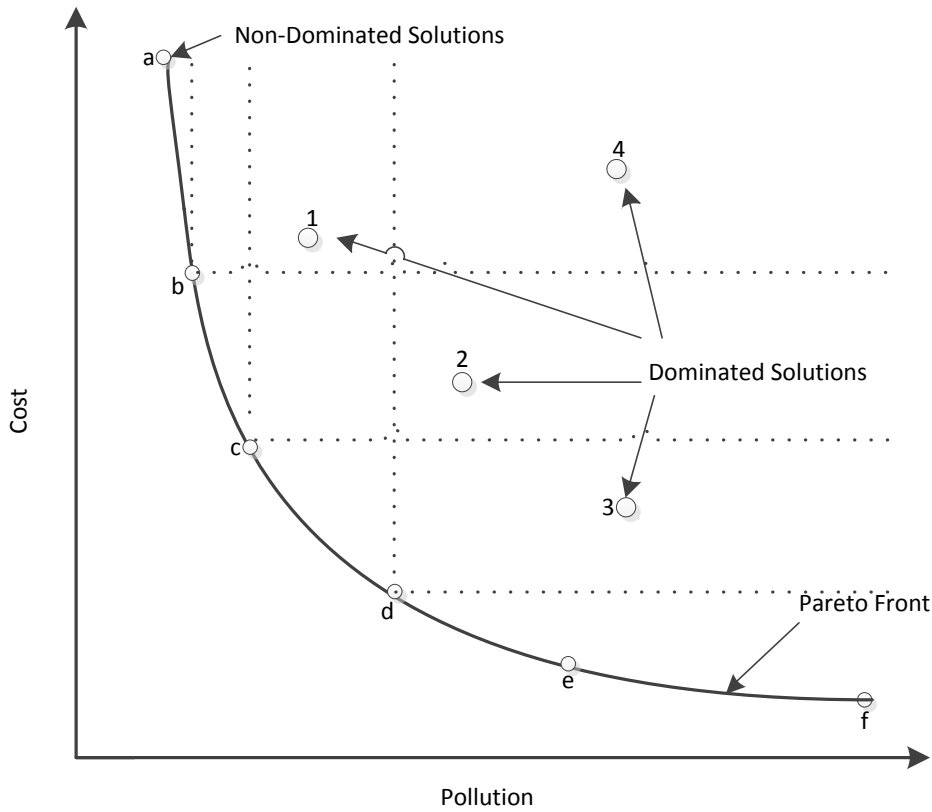


Figure 3: Pareto front schematic

In real-life, MOMs are executed for a certain number of function evaluations predefined by the user [9]. As illustrated in Figure 3, there are two main targets when using MOM to solve MOPs. First, the solutions should be as close as possible to Pareto front of the MOP. Second, the solutions should be uniformly distributed (diverse) to cover the entire Pareto front so that the user can have a variety of choices [2]. Ideally, the Pareto set should capture the *complete*

*spectrum* of the Pareto front. However, despite the advantages of population-based metaheuristics, they can be computationally expensive for solving complex problems due to the slow nature of their iterative process. State-of-the-art algorithms may require thousands to million function evaluations to find the PF. In brief, an efficient MOM should cover these three aspects: strong convergence, good sparsity (diversity), and fast convergence.

Another important quality of a MOM is that it should be robust enough in order to solve different types of problems. There are several benchmark problems known by the MOM community for comparing algorithms. The landscape has a major impact on the complexity of the problem. Figures 4 and 5 present some types of single objective optimization problems. For example, the *De Jong* function is convex and a relatively easy to solve problem even by a classical approach; while *Griewangk* function is a more complex problem because of its high multimodality feature.

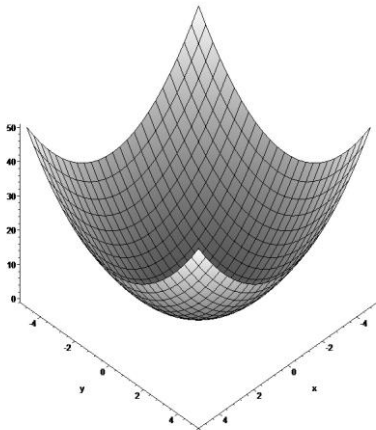


Figure 4: De Jong is unimodal, scalable, convex, and relatively easy function [16].

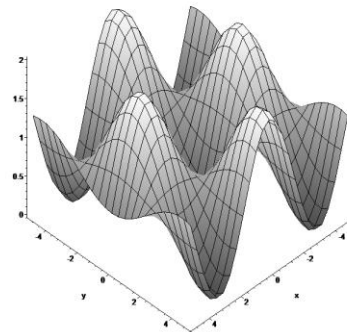


Figure 5: Griewangk's function has many, regularly distributed local minima and hard to locate global minimum [16].

## 2.3 Particularities of Multi-Objective Metaheuristics Over Single Objective Optimization Metaheuristics

There are several differences between single and multi-objective optimization [17]. For instance, in single objective optimization, the decision space consists of relationship between variables and objectives which can be visualized as a landscape for low dimensions (if  $D < 3$ ) in a single graph as shown in Figures 4, 5 and 6. But, in MOO the decision space consists of relationship among the variables themselves as shown in Figure 7. For example, one of the most complex benchmark MOPs are due to complex relationships among variables [18]. The objective space refers to relationship among objectives. For example, it is possible to have multimodal PFs shape and it is possible to have a multimodal relationship between a variable and an objective. So, visualization is an important challenge in MOO and it gets more challenging as the scalability of the problem increases. For example the visualization of scalable problems is an open problem when the number of variables or objectives is more than three.

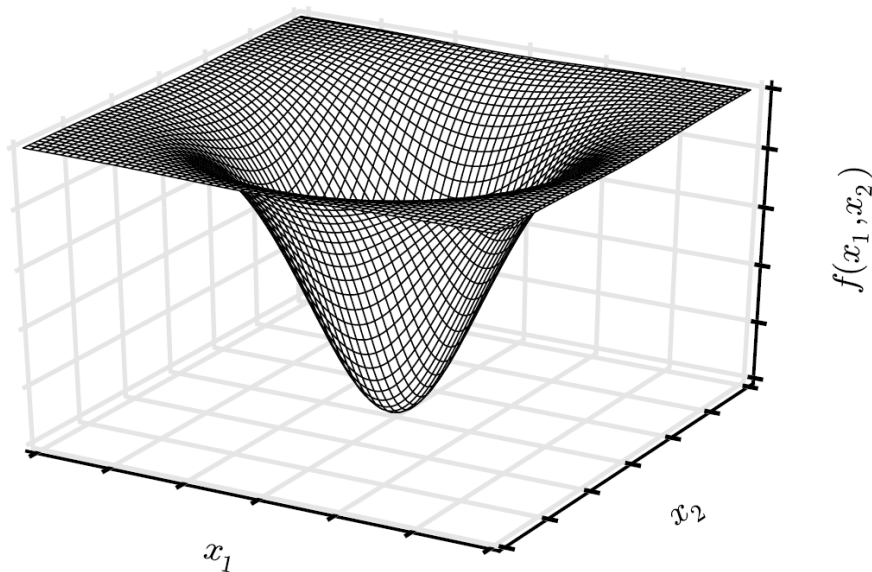


Figure 6: Illustration of relationships between variables and objectives in single objective space.

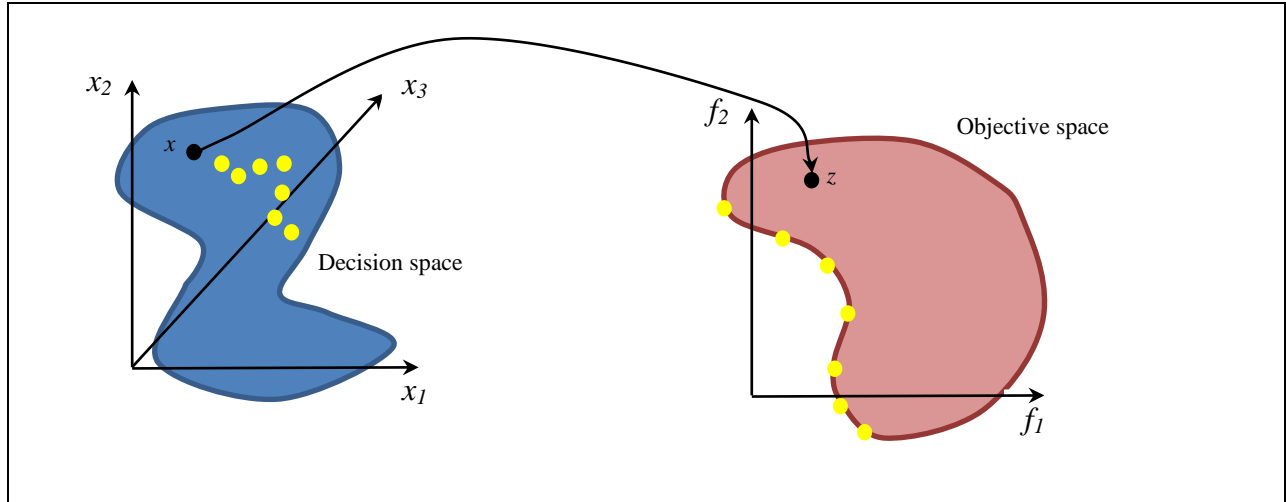


Figure 7: Illustration of relationships between variables and objectives in MO space.

## 2.4 Problems with Transforming Multi-Objective Optimization Problem into Single Objective Problem

Before the development of MOO methods, the classical approach consists of transforming a MOP into a single objective problem which is solved using a single objective metaheuristic. The main problem is that none of these single objective methods can generate a set of solutions to cover the PF in a single run. Generally speaking, several runs are required to generate the solutions. In addition, for every run some configuration parameters need to be modified to find a different solution which requires prior knowledge about the optimized MOP, that is not easy to apply to black-box problems. And, even then, a good distribution of the solutions is not guaranteed [18]. The following subsections explain these problems in detail by utilizing two well-known classical optimization methods: Weighted Sum Method and  $\epsilon$ -Constraint method.

### 2.4.1 Weighted Sum Method (WSM)

The most common way to handle multi-objective optimization problems as single objective ones is the use of the WSM method. It consists in summing weighted and usually normalized objective fitness values as follows.

$$F_{w_1, w_2} = w_1 f_1(x) + w_2 f_2(x), \quad (4)$$

where  $w_1, w_2 \in \mathbb{R}$  and they are supplied by the user and  $w_1 + w_2 = 1$ .

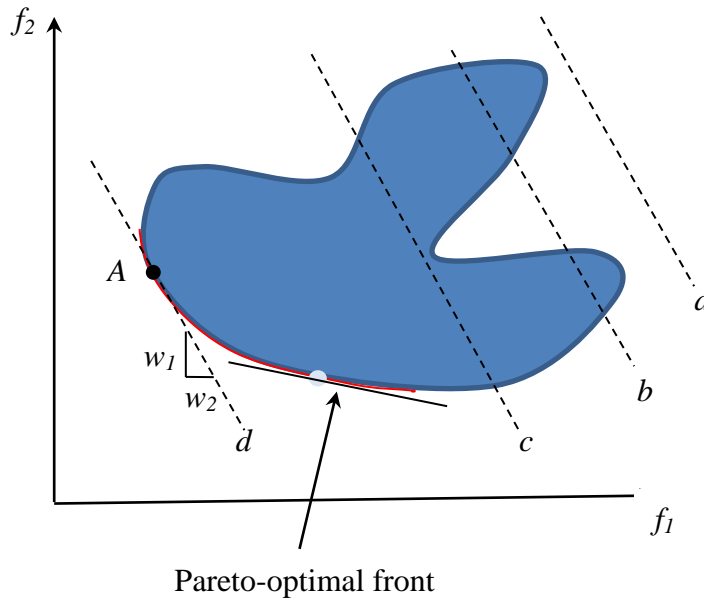


Figure 8: Weighted Sum Method. This example shows the importance of giving the right weights to find Pareto-optimal solutions.

As shown in Figure 8, the use of WSM requires providing the weights. In other words, the user needs to have prior knowledge about the MOP; which is not available for a black-box problem and multiple runs are needed. There are other difficulties such as non-uniformity found in Pareto optimal solutions. In addition, as shown in Figure 9, the WSMs are unable to find

Pareto optimal solutions located in non-convex region of the PF [18]. Nevertheless, a solution of a WSM approach is always Pareto optimal.

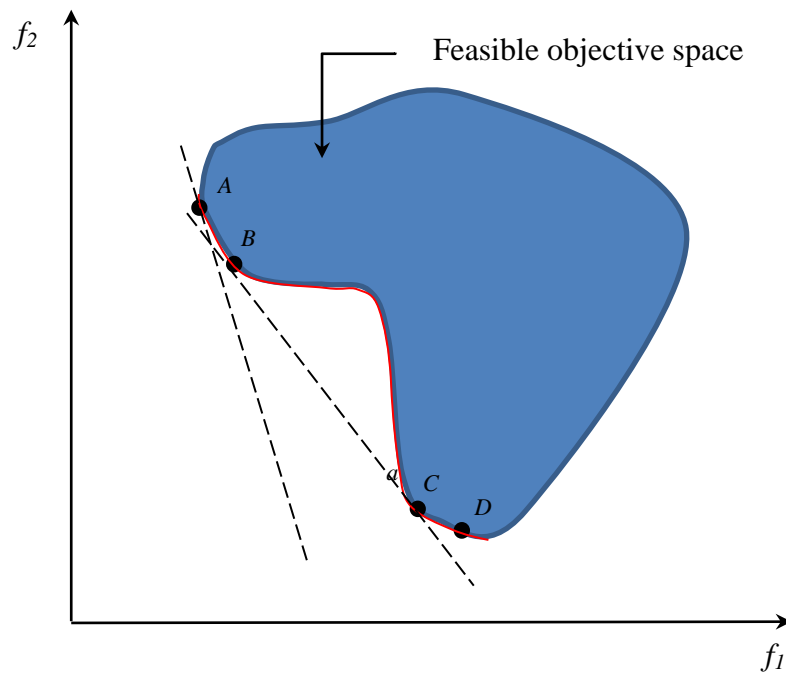


Figure 9: Difficulties associated with the WSM method such as not finding solutions in non-convex region of the PF

## 2.4.2 $\epsilon$ -Constraint method

Another popular method for handling a MOP is to transform all the objectives except one into constraints. So, the problem is formulated as follows:

$$\text{Min } f_{\mu}(x) \tag{5}$$

s.t.

$$f_m(x) \leq \epsilon_m, m \neq \mu \tag{6}$$

As for the WSM method, the  $\epsilon$ -Constraint method requires several runs because the MOP is converted into a single objective problem,  $\epsilon$  vectors need to be known (apriori), and the generated solutions are usually not well-distributed.

There are other types of problems with other variants of classical method which are discussed in [2].

Overall, classical methods have multiple deficiencies when solving MOP. They require multiple runs to generate optimal solutions, parameter tuning for every run, and usually do not generate well distributed solutions.

## **2.5 Summary**

This chapter covered important concepts related to MOO such as non-dominance relations, Pareto optimality, and Pareto fronts. In addition, the challenges of multi-objective optimization were discussed and compared to single objective optimization. Furthermore, the problems of transforming a multi-objective problem into a single objective were described.

Now that these fundamental concepts are reviewed, it is important to perform a comparative study among MOMs for the selection of the most promising MOMs for further improvement of speed convergence and accuracy using leadership concept.



## **Chapter 3**

### **Multi-Objective Optimization: A Comparative Study**

This chapter presents a comprehensive comparative study of state-of-the-art MOMs in order to select the most promising MOMs for further improvement of convergence speed and accuracy. This study compares the robustness of seven state-of-the-art multi-objective optimization metaheuristics, namely, NSGA-II, SPEA2, GDE3, SMPSO, AbYSS, MOCeLL, and MOEA/D. For simulation experiments, five well-known test suites are used, namely, ZDT, DTLZ, WFG, Van Veldhuizen's test problems, and LZ\_09 problems for a total of 53 benchmark problems including 33 bi-objective and 20 three-objective functions. This comparative study is the most comprehensive study of MOMs where they are compared using variant complexities such as complex Pareto front shapes, complex variable relationships shapes, and other complexities. In addition, an important number of three-objective functions are used whereas most previous studies focused on bi-objective problems. The benchmarking settings are similar to a practical environment, i.e. the number of function evaluations are fixed to low limits for each test case in order to find the most robust and the fastest MOM. The IGD indicator is used for ranking the accuracy of the compared MO methods, and as a complement, the hypervolume ratio indicator and boxplots were also utilized for a comprehensive comparison. In total, 371 experiments have been conducted with 100 independent runs per algorithm per problem for a total of 37,100 runs. The results are presented and discussed in detail.

### **3.1 Introduction**

The aim of this chapter is to perform an analysis of state-of-the-art MOMs in term of solving various types of MOPs. Putting aside the No Free Lunch Theorem [19] which says that "any two algorithms are similar when their performance is averaged across all possible problems" [20], a robust MOM should be able to generate accurate Pareto front approximations of variant types of problems in a timely manner. Two and three objective problems are the most common MO

problems [21]. Therefore, this chapter studies seven state-of-the-art MOMs in solving 53 well-known two and three objective benchmark problems. Other works which focused on more than three objective problems can be found in [22]. In this chapter, the stopping criteria is set to 10,000 function evaluations for two-objective problems with a population size of 100, and because three-objective problems are more complex, the number of function evaluations is increased to 30,000 with a larger population size of 200. The Pareto fronts are known beforehand which allows the utilization of variant comparison measures. The inverse generational distance (IGD) [23] measure is used for comparing the generated solutions by the seven state-of-the-art MOMs. As complementary performance assessment measures, the hypervolume ratio (HVR) [24] based on the hypervolume measure [25] and boxplots are employed [26].

In this comparative study, the selected seven MOMs consisted of genetic algorithms (NSGA-II [27] and SPEA2 [28]), a differential evolution algorithm (GDE3 [29]), a scatter search method (AbYSS [30]), a cellular genetic algorithm (MOCcell [31]), a particle swarm algorithm (SMPSO) [32], and an evolutionary algorithm based on decomposition (MOEA/D) [6].

The benchmark problems were composed of 33 bi-objective problems and 20 three-objective problems. These problems are taken from the Zitzler-Deb-Thiele (ZDT) problem family [33], the Deb-Thiele-Laumanns-Zitzler (DTLZ) problem family [34], the Walking-Fish-Group (WFG) problem family [35], the Li-Zhang problem family (LZ\_09) [7], and the Van Veldhuizen test suite [36]. These problems have variant complexities which are described in Section 3.3.

Overall, 53 multi-objective problems are utilized for the robustness and convergence comparison of seven state-of-the-art MOMs in solving complex MOPs using a low number of function evaluations. Every algorithm was executed independently 100 times for each problem.

### 3.2 Previous Comparative Studies: A Literature Review

There have been several comparative studies on MOMs. Due to the rapid progress in MOMs developments, some of them are already outdated such as [25]. Some others focused on specific types of problems, for example [37] focused on shortest-path problems. Some other comparative studies were too specific such as [38] which focused on a selection of an investment portfolio. This section surveys only the recent (last decade: 2003-2013) unconstrained continuous MO comparative studies.

Nebro et al. [3] studied the convergence speed of NSGA-II, SPEA2, PAES, OMOPSO [13], AbYSS, and MOCeII. For their comparison, they used a benchmark of three well-known problem families: Zitzler-Deb-Thiele (ZDT) test suite, the Deb-Thiele-Laumanns-Zitzler (DTLZ) problem family [34], and the Walking-Fish-Group (WFG) test problems. The population was set to 100 and a stopping condition was based on the hypervolume rate (HVR) being equal to 98%. However, in this study only bi-objective problems have been considered. The results showed the last three metaheuristics (MOCeII, OMOPSO, and AbYSS) achieved in average the fastest convergence speed. For ranking purposes, two aspects were considered: convergence speed and hit rate. The convergence speed refers to the number of evaluations required to obtain an accurate Pareto front. The hit rate was calculated at over 100 independent runs; it calculates the percentage of successful executions. An execution is considered successful if a metaheuristic reaches the HVR=98% before reaching  $10^6$  function evaluations.

In a more recent comparative study conducted by Durillo et al. [4], seven multi-objective metaheuristics were compared: two genetic algorithms (NSGA-II and SPEA2), an Evolution Strategy (PAES), a Scatter Search method (AbYSS), a cellular Genetic Algorithm (MOCeII), a Differential Evolution algorithm (GDE3), and a particle swarm method (SMPSO). The tests were

conducted on ZDT and DTLZ bi-objective benchmarks for a total of 12 problems. The population size for all methods was set to 100. The convergence speed was the focus of this study. Three different types of stopping conditions were utilized: HVR equal to 98% and 99% of the Pareto front, the Epsilon measure equal to 0.1, 0.05 and 0.01, and a certain number of Pareto front approximation should belong to the Pareto front (1, 5, 10, 20, 50 and 100). The numbers of function evaluations were counted for each test case. The SMPSO version of the MO PSO appeared to be the fastest overall. In contrast, NSGA-II and SPEA2 were found to provide the lowest performance among the seven compared methods for the studied bi-objective problems.

Durillo et al. [9] did a comparative study with a focus on the scalability of the compared MO methods. Five unconstrained ZDT problems were used by varying the number of variables from (8, 16, ..., 2048 variables). The stopping condition was set to HVR=98%; otherwise, the MO method is stopped after a maximum of  $10^6$  function evaluations. The compared methods were NSGA-II, SPEA2, PAES, PESA-II, OMOPSO, GDE3, AbYSS, and MOCcell. OMOPSO and GDE3 showed the highest accuracy.

In CEC 2009 competition [39], 13 unconstrained and 7 constrained MO problems were used to compare 13 MOMs. The variables of these problems had complex relationships (high epistasis); some of them were taken from LZ\_09. GDE3 and MOEA/D algorithms used in this chapter were also among the compared methods in the competitions. The maximum number of function evaluations was set to 300,000. The population size was set to 100 for bi-objective problems, 150 for three-objective problems, and 500 for five-objective problems. The IGD measure was used for results comparison. The results showed that MOEA/D followed by GDE3 were the most accurate methods among the compared ones.

The conducted comparative study in this thesis is the most comprehensive one in the MO field. It uses the largest number of MOPs (53 problems) with variant complexities. For example, the studies [3], [9] focused only on bi-objective problems. In addition, they did not have problems with complex variable relationship landscape due to high epistasis as in [39]. On the other hand, the CEC competition [39] focused only on MOP with high epistasis, whereas other complexities such as complex shapes of Pareto fronts were not included. In addition, only seven unconstrained benchmark problems were used to compare MO methods in 2-objective, 3-objective, and 5-objective spaces. This study incorporates large variant complexities in a single study. In addition, the most recent state-of-the-art methods are used such as MOEA/D and SMPSO. Finally, this study focuses on both the robustness and convergence speed of MO methods whereas, the previous studies focused only on the acceleration speed of MOMs. Based on [3] and [9], it has been shown that a good approximation of the real Pareto front is equal to HVR=98% and on average  $10^4$  function evaluations are sufficient to find relatively simple Pareto front with such a precision for two-objective problems. That is why the number of function evaluations has been limited to  $10^4$  which is more stringent. Let's assume that a function call requires one minute which is reasonable for a real world problem, so  $10^4$  function evaluations will require almost a week of computation time. For three objective problems which are more complex, the stopping condition has been increased to  $3*10^4$  function evaluations.

### **3.3 Problems Description**

In order to analyze the robustness of the selected state-of-the-art MOMs in this section, 53 well-known benchmark unconstrained continuous problems have been employed. These problems are composed of two and three objectives problems. Problems with a larger number of objectives (i.e., more than 3), are called many-objective problems and require significant modifications to

solve such problems. In fact, most existing MOMs face difficulties in solving many-objective problems [40]. It is known that the use of the concept of Pareto dominance for comparing candidate solutions loses its effectiveness when dealing with many-objective problems, because in such cases, the selection pressure gets quickly diluted and solutions are then selected at random. In order to deal with many-objective optimization problems, different techniques are required, such as, dimensionality reduction or relaxed forms of Pareto dominance. Some density estimators such as the crowding operator of the NSGA-II are unable to maintain a diverse set of solutions in the objective space when dealing with many-objective problems. Among the selected problems, 33 problems are bi-objective problems and 20 are three objective problems. Several families of problems are used. The bi-objective family of problems are composed of Zitzler-Deb-Thiele (ZDT) problem family [33], the Deb-Thiele-Laumanns-Zitzler (DTLZ) problem family [34], the Walking-Fish-Group (WFG) problem family [35], Li-Zhang problem family (LZ09) [7], and some problems are taken from Van Veldhuizen test suite [36], namely, Poloni [41], Kursawe [42], Schaffer [43], and Fonseca [44]. Three objective problems are composed of three Viennet [45] problems taken from the Van Veldhuizen test suite, DTLZ, and WFG family problems, and the LZ09\_06 problem is taken from LZ\_09 test suite.

### **3.3.1 Variant problem complexities**

A detailed explanation of MO problems can be found in [35]. First, as shown in Figure 10, the geometry of a Pareto front of a MO problem can be convex, concave, mixed (convex, concave), degenerate (Pareto of lower number of dimensions than the number of objectives), connected, and discontinuous (disconnected).

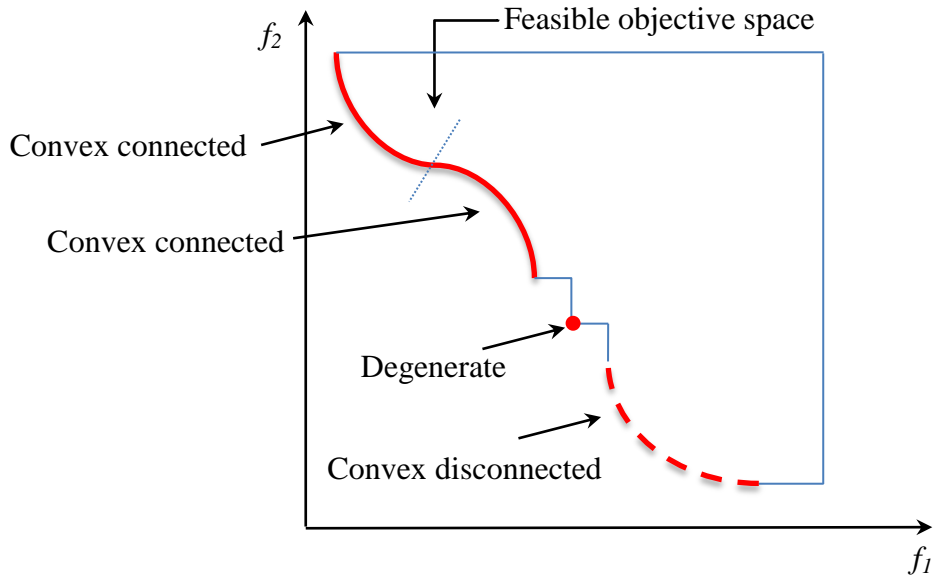


Figure 10: Pareto front geometries. The Pareto front is composed of mixed components, namely, convex, concave, connected, disconnected, and degenerate components. Degenerate is when the PF is of a dimension  $D - 1$ , e.g. for two objectives the solution is a single point.

Furthermore, there are other complexities related to functions and parameters [35]. A problem having parameters which are extremal or medial are easier to solve. Extremal means the parameter is located at the extreme of the definition domain; whereas medial means the parameter is located in the middle of the definition domain. Also, similar parameters domain or similar trade-off ranges are easier to solve. The objective functions can be separable and non-separable; non-separable functions are more complex to solve. Bias consists of having a higher concentration of solutions in a certain region of the objective space which makes the problem more complex. Also, a one-to-many or many-to-one mappings, flat regions, and isolated optima make a MO problem more difficult to solve. A multimodal objective function makes a MO problem more complex.

All the described complexities are part of the selected problems as detailed in the following subsections.



### 3.3.2 The ZDT problems

As shown in Table 35 (Appendix A), the ZDT [33] test suite is composed of five problems. The ZDT5 problem has been omitted because it is a binary encoded problem. This test suite is one of the most popular ones. However, the ZDT test suite offers an average complexity because none of the ZDT problems is deceptive, non-separable, or degenerate. In addition, all the parameters are either distance or position parameters, and most of them are extremal. Furthermore, the parameters have all the same definition domain with the exception of one variable in the problem ZDT4.

Figure 11 is an example of deceptive single objective problems with a single variable. It can be seen that most neighboring areas of the global optimum are deceiving optimization algorithms because they provide wrong information ( $f$  increases) as the algorithms get closer to the global optima. Deceptive problems are one of the most difficult features of an optimization problem which require strong exploration characteristics of an optimizer.

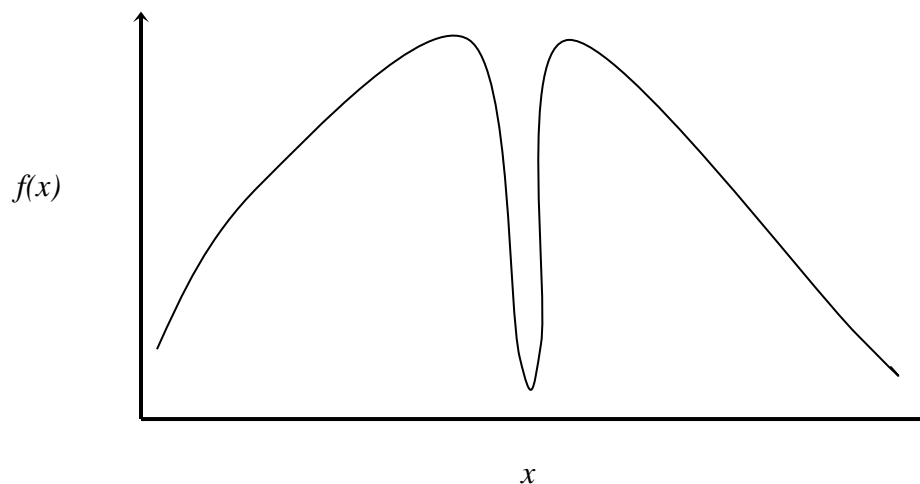


Figure 11: Example of a deceptive function for single objective minimization problem

### **3.3.3 The DTLZ problems**

The DTLZ test suite was developed by Deb et al. [34]; it is the second most commonly used test sets in the scientific literature. DTLZ is more complex than ZDT because all the objective functions are affected by both distance and distribution parameters; whereas, in ZDT only the second objective function is affected by both parameters, and the first one is affected only by a distance parameter. As shown in Table 36 (Appendix B), DTLZ is composed of nine problems having a scalable number of objectives. Therefore, in this study, the DTLZ problems have been used for both two and three objectives. Only seven problems have been used in this study; the DTLZ8 and DTLZ9 problems are omitted because they have side constraints.

DTLZ1 is linear and DTLZ2 and DTLZ3 are concave. DTLZ4, DTLZ5 and DTLZ6 are concave and degenerate when the number of objectives is greater than two. DTLZ7 is mixed convex/concave disconnected. Some limitations of this test suite are that none of the DTLZ problems have a flat fitness landscape region and none of them is deceptive or non-separable.

### **3.3.4 The Van Veldhuizen's test suite**

The Van Veldhuizen test suite [36] is a compilation of different benchmark multi-objective problems.

Van Veldhuizen test suite is composed of seven problems, namely, Schaffer [43], Fonseca [44], Poloni [41], Kursawe [42], one problem taken from the Deb's test suite [46], and two problems taken from Viennet [45]. In this study, the bi-objective problem taken from the Deb's test suite has been replaced by the three-objective problem Viennet4 from Ref. [45]. The geometries of the problems are described in Table 37 (Appendix A).

Most Van Veldhuizen problems are composed of mixed parameters; i.e. very few parameters are either distance or position parameters, the number of parameters is small (1, 3), none of the problems is deceptive, has a flat region, or a many-to-one problem. However, some problems are of special interest such as Poloni and Viennet3 because both are non-separable and multimodal which makes them more representative of real-world problems [35]. It is worth mentioning the geometry of Viennet3 is complex and composed of mixed convex/concave curves.

### **3.3.5 The WFG problems**

WFG [33] is composed of nine problems and it is overall more complex than the previous family of problems (ZDT and DTLZ). WFG incorporates non-separable problems that have multimodal objective functions. As shown in Table 38 (Appendix A), all variant geometrical shapes of a Pareto front are represented in WFG problems, namely, linear, convex, concave, mixed, and disconnected shapes. Furthermore, all the parameters are non-medial and non-extremal which makes the WFG problems more difficult to solve. All the other parameter transformations such as linearity, deceptivity, flat region and others are also part of WFG problem and are presented in Table 39.

Overall, WFG is a more complex family of problems due to the integration of variant complexities. Also, they are scalable parameter-wise and objective-wise. The description of the nine WFG problems can be found in Table 38 , 40, and 41 (Appendix A).

### 3.3.6 The LZ\_09 problems

The LZ\_09 [7] is another complex family of problems. It emphasises mainly the Pareto set shape. The Pareto sets refer to the *parameters* of a solution. For example, ZDT and DTLZ are relatively simple problems in this sense. For ZDT, all the parameters of a solution, except for the first, are in origin (0.0). For DTLZ, all the parameters of a solution, except for the two first, are equal:  $x_3 = \dots = x_n = 0.5$ . Such simple relationships are not usually really representative of real-world problems. That is why WFG have been designed with a higher complexity, especially the parameters features. However, the Pareto set shapes are not the emphasis of WFG; therefore, the shapes are difficult to describe due to the dynamic nature of the WFG problems which can be updated using variant shape functions (see Table 40 in Appendix A). The LZ\_09 problems have complex Pareto set shapes (high epistasis) which makes it amongst the most difficult family of problems to be solved. As shown in Figure 12 the Pareto set shapes are complex, however, the geometry of the Pareto fronts are simple as shown Table 41. Furthermore, not much attention has been given to other parameter complexities such as deceptiveness and flat regions.

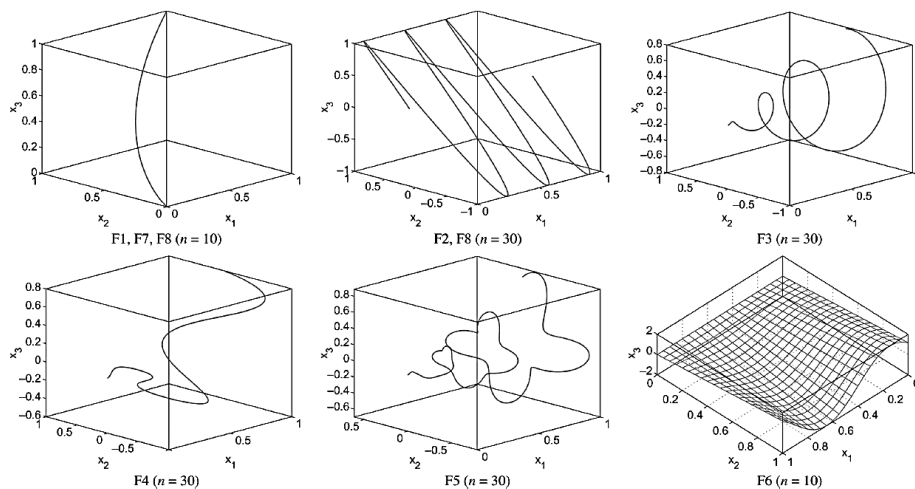


Figure 12: Projections of Pareto sets of F1–F9 onto the  $x_1, x_2, x_3$  space [7].

### 3.4 Compared State-Of-The-Art Multi-Objective Metaheuristics

This section describes the seven selected state-of-the-art MOMs for the current comparative study. The jMetal [47] multi-objective optimization framework has been used for conducting all the experiments.

The Non-dominated Sorting Genetic Algorithm (NSGA-II) was proposed by Deb et al. [27] in 2002. This genetic algorithm consists in generating new populations from the original population by the use of classical genetic operators such as selection, crossover, and mutation. The individuals of the two populations are sorted according to their ranking. Then, the best solutions are recombined for the generation of the next population. In the case of having solutions with the same rank, a density estimation (crowding distance) is calculated with regards to the surrounding solutions for the selection of the most promising solutions.

The Strength Pareto Evolutionary Algorithm (SPEA2) was proposed by Zitzler et al. [28] in 2002. In this MOEA, every candidate solution has a fitness value which equals to the sum of its strength raw fitness (solutions that dominates it) plus density estimation. SPEA2 uses the selection, crossover, and mutation operators for generating an archive of individuals. The non-dominated solutions of both the original population and the archive are copied into a new population. In case the number of non-dominated solutions is larger to the population size, a truncation operator is used by calculating the distances among solutions. The most similar solutions are removed.

The Speed Constrained Particle Swarm Optimization (SMPSO) algorithm was proposed by Nebro et al. in 2009. It is a particle swarm optimization algorithm for solving MO problems. This approach is based on OMOPSO [13], whose main features are the use of the crowding distance concept adopted by NSGA-II for filtering leader solutions that are stored in an archive.

The SMPSO uses mutation operators for swarm speed convergence acceleration, and it uses the  $\epsilon$ -Dominance when generating new candidate solutions. Its main difference with respect to OMOPSO is that SMPSO incorporates a mechanism for velocity limitation and a polynomial mutation operator.

The third version of the Generalized Differential Evolution algorithm (GDE3) was proposed by Kukkonen and Lampinen in [29]. GDE3 is an improved version of the GDE algorithm [46], which was originally proposed in 2005. It starts with a random solution population. In every iteration, a new offspring population is generated using the differential evolution operator. Both populations are combined; then, the size of the population is reduced using non-dominated sorting and a pruning method for diversity preservation as in NSGA-II. However, the GDE3 pruning method modifies the NSGA-II crowding distance in order to solve some GDE3 drawbacks when dealing with problems with more than two objectives.

The cellular genetic algorithm (MOCeLL) was introduced by Nebro et al. [31] in 2006. Being a genetic algorithm, it uses selection, crossover, and mutation operators. Similar to many multi-objective metaheuristics, it includes an external archive for storing non-dominated solutions found so far. This archive is bounded by using NSGA-II's crowding distance in order to maintain diversity in the Pareto front. The selection is achieved by selecting a solution from the neighborhood of the current solution (called cell in cGAs) and another solution selected randomly from the archive. Then, the genetic crossover and mutation operators are applied for generating a new offspring which is compared to the current one. If the offspring is better, it replaces the current one. Otherwise, if both solutions are non-dominated, then the worst solution in the neighborhood is replaced by the current one and inserted into the archive.

AbYSS was introduced by Nebro et al. [30] in 2008; it is a multi-objective version of *scatter search*. It has an external archive similar to MoCell. AbYSS uses evolutionary operators such as polynomial mutation, binary crossover and solution combination.

The Multi-objective Evolutionary Algorithm based on Decomposition (MOEA/D) [6] was proposed in 2007 and it consists of decomposing a MO problem into scalar sub-problems which are optimized in parallel. Each sub-problem is transformed into a scalar aggregation problem and is optimized using only neighborhood information. These neighborhood relations are determined by the calculation of distances among coefficient vectors.

### **3.5 Parameter Settings**

The section covers the parameter settings for simulation experiments which include the algorithms parameter settings, the stopping conditions, and the performance measures for comparison of the MOMs.

#### **3.5.1 Stopping criteria**

In this chapter, the performances of the selected seven state-of-the-art MOMs are studied using 53 well-known unconstrained benchmark problems. Every multi-objective optimizer was run independently 100 times to minimize the effect of stochastic behavior of the algorithms on the reported results. For every run, the maximum function evaluations are, respectively, 10,000 and 30,000 for two-objective and three-objective problems, respectively. In order to assess the quality of a Pareto front generated by a MO metaheuristic, the average of the Inverse Generational Distance (IGD) [23] is utilized. The IGD indicator can measure both the spread and convergence of an approximation of a Pareto front. It is commonly used as in the CEC competitions [39]. Other measures are also used as a complement for our analysis such as

Hypervolume (HV) indicator [25], hypervolume ratio (HVR) [24] and boxplots [26]. The Wilcoxon statistical procedure was based on [49] to present results at a 0.05 significance level.

Table 1: Control parameter settings (L= Number decision variables)

<b>NSGA-II</b>	
Population size	100 / 200 Individuals
Selection of parents	Binary tournament + binary tournament
Recombination	Simulated binary, $p_c = 0.9$
Mutation	Polynomial, $p_m = 1.0/L$
<b>SPEA2</b>	
Population size	100 / 200 Individuals
Selection of parents	Binary tournament + binary tournament
Recombination	Simulated binary, $p_c = 0.9$
Mutation	Polynomial, $p_m = 1.0/L$
<b>MOCeII</b>	
Population size	100 individuals ( $10 \times 10$ ) / 196 individuals ( $14 \times 14$ ) /
Neighborhood	1-hop neighbors (8 surrounding solutions)
Selection of parents	Binary tournament + binary tournament
Recombination	Simulated binary, $p_c = 0.9$
Mutation	Polynomial, $p_m = 1.0/L$
Archive size	100 individuals
<b>SMPSO</b>	
Particles/Leaders	100 / 200 particles
Mutation	Polynomial
<b>GDE3</b>	
Population size	100 / 200
Recombination	Differential evolution, $CR = 0.1, F = 0.5$
<b>MOEA/D</b>	
Population size	100 / 500
Recombination	Differential evolution,
Mutation	Polynomial
<b>AbYSS</b>	
Population size	100 individuals
Reference set size	10 + 10
Recombination	Simulated binary, $p_c = 1.0$
Mutation	Polynomial, $p_m = 1.0/L$
Archive size	100 individuals



### **3.5.2 Parameters settings**

Table 1 presents the parameters used for this comparative study. These parameters settings have been taken from the Refs. [9], [3] and [6]. NSGA-II, SPEA2, MOCell, AbYSS and GDE3 have a population size of 100 for bi-objective problems and 200 for three-objective problems (MOCell was set with a population size of 196 for the 3 objective problems). In the same manner, SMPSO has a configuration of 100 particles for the bi-objective, and 200 particles for three-objective problems, respectively. MOEA/D was used with a population size of 100 for bi-objective problems and 500 for three-objective problems. However, only the 200 most representative solutions are selected for each Pareto front approximation. The metaheuristics having an archive (SMPSO, GDE3, OGDE3, and MOCell) have also a maximum size of 100 and 200, respectively.

### **3.5.3 Performance measures**

Variants measures can be utilized for evaluating the performance of MOMs. For example, some researchers have compared MOMs by examining how long (in terms of number of function evaluations) it takes to a MOM to produce an accurate approximation of the Pareto front [3]. Some other researchers examined the accuracy of metaheuristics with scalable parameter problems (high variables dimension) [9]. However, a desirable set of solutions, in the MOO context, should have high convergence, good diversity, and should be found in a timely manner. High convergence means the solutions should be as close as possible to the true Pareto front. Diversity means the solution should be distributed in a uniform pattern such that they completely cover the Pareto Front.

A very common quality indicator that takes into consideration both the convergence of a solution set and the distribution of solutions along the Pareto front is the inverse generational

distance (IGD) indicator. IGD consists in measuring the average Euclidean distance between the true Pareto front and the approximation obtained by a multi-objective algorithm. Let's assume that  $P$  is a set of points representing the true Pareto front and  $S$  is a set of points representing the approximation obtained by a MOM. The average Euclidean distance in the objective space is calculated as follows:

$$IGD(S, P) = \frac{\sum_{v \in P} d(v, s)}{|P|} \quad (7)$$

where  $d(v, s)$  is the minimum Euclidean distance between a point  $v$  belonging the true Pareto front and a point  $s$  belonging to the approximation obtained.  $|P|$  is the number of selected points used to represent the Pareto front. When the value of the IGD is lower, a better approximation is achieved.

HV, HVR, and boxplots are used as complementary information. HV is obtained by computing the volume of the non-dominated set of solutions  $Q$  for MO minimization problems. For every solution  $i \in Q$ , a hypercube  $v_i$  is generated with a reference point  $W$  and the solution  $i$  as its diagonal corner. The reference point  $W$  can be generated by building a vector of worst possible objective function values. Then, HV is computed as a union of all the found hypercube as follows:

$$HV = volume \left( \bigcup_{i=1}^{|Q|} v_i \right) \quad (8)$$

The lower are the HV values, the better are the corresponding solutions because they are more precise and diverse for MO minimization problems.

HVR is the ratio of the approximation's HV ( $HV_S$ ) with regards to the true Pareto front's HV ( $HV_{PF}$ ) as follows.

$$HVR = \frac{HV_S}{HV_{PF}} \quad (9)$$

An ideal HVR is equal to 1, so the higher the value the better is the approximation obtained.

Finally, the boxplots [26] are used to show graphically the found solutions using five number summaries: the minimum, lower quartile (Q1), median (Q2), upper quartile (Q3), and the maximum. Also, boxplots indicate solutions as outliers, i.e., solutions that are numerically distant from the rest of the data.

### 3.6 Results

An efficient multi-objective optimization metaheuristic method should generate accurate and diverse solutions in a timely manner. The aim of this section is to see which method is the most robust to solve benchmark problems in a timely manner.

To facilitate the analysis of the results, they have been divided into three groups: the bi-objective problems, the three-objective problems, and the LZ\_09 problems. The LZ\_09 problems have been grouped in Table 7 because their particularity from the rest of problems; the LZ\_09 problems emphasize on complex relationships among the variables. All the results are discussed in the following subsections. In order to compare the MO algorithms, a ranking system is proposed. Two points are given for the most accurate MO algorithm per problem and one point is given to the second most accurate algorithm. Then, the MO algorithms are ranked based on

their points. It is important to mention that the results are presented with a 0.05 confidence, and the boxplots can be found in Figures 57-63 of the Annex A.

### **3.6.1 Bi-objective problems**

All the bi-objective problems results (IGD measures) have been grouped in

Table 3. Complementary results can be found in Tables 42-43 (HV and HVR), Figures 59-60 (IGD boxplots) of the Annex A. The selected bi-objective problems have variant complexities as detailed before. The stopping condition is set to 10,000 function evaluations with a population size of 100. First, Van Veldhuizen's bi-objective problems are Schaffer, Fonseca, Poloni, and Kursawe. These problems have a small number (i.e., 1 and 3) of mixed decision variables: distance and position. MOEA/D generated the most accurate solutions for Poloni's problem which is among the most difficult from this set because it is both non-separable and multimodal. Also, MOEA/D is the fastest for Fonseca's problem followed by SMPSO. SMPSO generated the most accurate solutions for the convex Schaffer problem followed closely by GDE3 and AbYSS. Finally, Kursawe's problem is a mixed, disconnected and degenerate problem that is best solved by MOCeLL followed by GDE3.

In regards to the ZDT problems which are simpler than most of the other problems, GDE3 was the most accurate for ZDT1, ZDT3, ZDT6 and the second most accurate for ZDT2. MOCeLL and SMPSO were the most accurate for ZDT2 and ZDT4. NSGA-II, SMPSO, MOCeLL were the second best for ZDT3, ZDT6, ZDT4. There is no apparent pattern to explain the performance of the algorithms; for example, GDE3 is performing very well with four ZDT problems having completely different characteristics.

In regards to the DTLZ test suite, contrary to the ZDT problems, these problems have variables of mixed distance and position type which make the problems more difficult to solve. AbYSS has been the most accurate for DTLZ2, DTLZ4, DTLZ5, followed by SMPSO which has been the most accurate for DTLZ3, DTLZ7, followed by GDE3 which has been the most accurate for DTLZ1, DTLZ6. The second most accurate algorithm was MOCeII with DTLZ2, DTLZ3, DTLZ5 followed by GDE3 which has been the second most accurate for DTLZ7, DTLZ4, followed by MOEA/D for DTLZ6.

The WFG test suite is composed of nine bi-objective problems. The WFG problems are composed of both non-separable and multimodal objective functions. In addition, all the parameters are non-medial and non-extremal, so, they are more difficult to solve. GDE3 achieved the highest accuracy by being the most accurate for 11 problems and the second most accurate for 6 problems. GDE3 offered a lower performance for WFG3 and WFG8 which are respectively linear degenerate and concave. Then, AbYSS was the best for WFG4 and WFG7, and it was second best for WFG3. Finally, SMPSO and MOEA/D presented the highest accuracy for WFG3 and WFG8.

Table 2: Scores for bi-objective problems (1 point for the 2<sup>nd</sup> position and 3 points for the 1<sup>st</sup> position)

	NSGA-II		SPEA2		GDE3		SMPSO		AbYSS		MOCeII		MOEA/D	
First	0	0	0	0	11	22	5	10	5	10	2	4	3	6
Second	3	3	2	6	6	6	6	6	1	1	5	5	2	2
Overall	3		6		28		16		11		9		8	

Based on the 25 bi-objective problems used in this section, GDE3 was the most accurate algorithm. SMPSO was the second most accurate algorithm. After them, close to each other, come AbYSS, MOCell and MOEA/D. The worst performances were achieved by SPEA2 and NSGA-II.

By looking at the standard deviation and boxplots, it can be seen that GDE3's performance is relatively consistent. Also, SMPSO is consistent except for two problems namely WFG7 and DTLZ6 where there is a medium dispersion.

In regards to HVR, a ratio equal to 98% of the real Pareto front is considered high accuracy [9]. It can be seen that in most cases, GDE3 achieved an HVR close to 98% except for Poloni, DTLZ3, ZDT3, DTLZ4 and WFG5. Among these bi-objective problems, Poloni and DTLZ3 are the most complex problems because they are not solved by most MOMs. In regards to ZDT4 and DTLZ3, although GDE3 had a low score, SMPSO achieved a high and relatively good accuracy. WFG8 is also relatively complex because the MOMs that achieved the highest average HVR reached a value of only 71%.



### 3.6.2 Three-objective problems

All three-objective problems except one (LZ\_06) have been grouped in Table 4 in which are shown the values corresponding to IGD performance. Complementary measures such as IGD boxplots can be found in Figures 61-63, HVR in Table 44, and HV in Table 45. There are 19 problems of different complexities composed of DTLZ, WFG, and Veldhuizen test suites. However, only the three-objective problems are taken from the Veldhuizen test suite namely the Viennet2, Viennet3 and Viennet4 problems. The stopping conditions are set to 30,000 function evaluations with a population size of 200.

As shown in Table 4, there is no best MO method; different DTLZ problems are solved by different algorithms. The highest accuracy in terms of the IGD measure is achieved by GDE3 (DTLZ1, DTLZ3, DTLZ7), AbYSS (DTLZ4, DTLZ5), SMPSO (DTLZ6), and SPEA2 (DTLZ2). Overall, the two most accurate algorithms to solve the DTLZ three-objective benchmark problems are respectively GDE3 and SMPSO. There is no apparent pattern of problems that these two MO algorithms can solve.

For the WFG and Viennet problems, SPEA2 clearly achieved the highest accuracy by having the best IGD for nine out of 12 problems. GDE3 achieved the second best performance. The most difficult problems were DTLZ6 and DTLZ3; however, DTLZ6 has been well solved by GDE3 and SMPSO. Then, the second most difficult problems were WFG8, WFG1, WFG5, DTLZ2, and DTLZ3. Table 5 confirms these rankings. By looking at the boxplots, it can be seen that SPEA2 is always consistent. It performs very well although it is not among the top two for the entire set of three-objective problems. It seems that the ranking scheme of SPEA2 is more efficient for three-objective problems than that of the NSGA-II which is used by most multi-objective evolutionary algorithms.



Table 4: IGD mmeasure, mean and standard deviation for three-objective problems taken from DTLZ, WFG, and Van Veldhuizen test suites after  $10^4$  function evaluations. Dark grey is the algorithm having the best IGD results followed by a lighter grey indicating the second best IGD score.

	NSGAI	SPEA2	GDE3	SMP	SO	AbySS	MOCe	l	MOEAD
DTLZ1	$3.07e - 03_{3.2e-03}$	$1.11e - 03_{1.1e-03}$	$3.76e - 04_{1.0e-05}$	$4.48e - 04_{1.8e-05}$	$1.59e - 03_{2.4e-03}$	$6.45e - 03_{9.3e-03}$	$2.09e - 03_{3.2e-03}$		
DTLZ2	$5.54e - 04_{2.7e-05}$	$4.12e - 04_{5.8e-06}$	$4.88e - 04_{1.3e-05}$	$5.57e - 04_{2.5e-05}$	$5.84e - 04_{3.2e-05}$	$5.65e - 04_{2.5e-05}$	$4.87e - 04_{1.4e-05}$		
DTLZ3	$1.67e - 01_{6.3e-02}$	$1.57e - 01_{5.2e-02}$	$7.81e - 04_{2.3e-05}$	$1.14e - 03_{1.1e-03}$	$7.42e - 02_{5.3e-02}$	$1.36e - 01_{8.2e-02}$	$7.32e - 02_{1.2e-01}$		
DTLZ4	$8.83e - 04_{9.2e-05}$	$1.22e - 03_{1.9e-03}$	$8.86e - 04_{8.6e-05}$	$8.99e - 04_{1.2e-04}$	$8.16e - 04_{6.6e-05}$	$1.38e - 03_{2.0e-03}$	$1.26e - 03_{2.2e-04}$		
DTLZ5	$1.02e - 05_{5.1e-07}$	$8.46e - 06_{3.4e-07}$	$7.18e - 06_{1.0e-07}$	$7.12e - 06_{1.4e-07}$	$7.09e - 06_{1.1e-07}$	$7.20e - 06_{1.5e-07}$	$9.84e - 06_{5.3e-07}$		
DTLZ6	$9.30e - 03_{4.5e-04}$	$1.04e - 02_{4.4e-04}$	$1.74e - 05_{8.5e-07}$	$1.68e - 05_{8.1e-07}$	$2.62e - 03_{8.5e-04}$	$1.80e - 02_{1.0e-03}$	$1.70e - 05_{7.7e-07}$		
DTLZ7	$1.59e - 03_{7.4e-05}$	$1.53e - 03_{1.4e-03}$	$1.50e - 03_{9.1e-05}$	$1.80e - 03_{1.8e-04}$	$1.48e - 02_{8.0e-03}$	$3.22e - 03_{4.3e-03}$	$7.61e - 03_{6.2e-03}$		
WFG1	$4.48e - 03_{8.7e-04}$	$7.87e - 03_{1.0e-03}$	$4.60e - 03_{3.4e-04}$	$1.32e - 02_{1.5e-04}$	$3.46e - 03_{1.7e-03}$	$3.80e - 03_{6.7e-04}$	$1.15e - 02_{2.7e-04}$		
WFG2	$6.38e - 04_{3.8e-05}$	$5.54e - 04_{4.3e-05}$	$6.33e - 04_{3.7e-05}$	$7.03e - 04_{4.0e-05}$	$7.32e - 04_{6.9e-05}$	$6.60e - 04_{4.4e-05}$	$1.04e - 03_{8.0e-05}$		
WFG3	$2.88e - 04_{5.5e-05}$	$3.16e - 04_{2.6e-05}$	$2.46e - 04_{6.5e-05}$	$3.95e - 04_{6.9e-05}$	$1.97e - 04_{3.9e-05}$	$2.52e - 04_{5.0e-05}$	$1.22e - 04_{1.1e-05}$		
WFG4	$5.28e - 04_{3.8e-05}$	$5.06e - 04_{2.1e-05}$	$4.65e - 04_{2.3e-05}$	$5.64e - 04_{2.3e-05}$	$5.09e - 04_{3.3e-05}$	$5.18e - 04_{3.9e-05}$	$5.56e - 04_{2.3e-05}$		
WFG5	$5.92e - 04_{1.5e-05}$	$5.30e - 04_{1.2e-05}$	$5.32e - 04_{1.3e-05}$	$5.69e - 04_{1.5e-05}$	$5.90e - 04_{2.5e-05}$	$5.79e - 04_{1.8e-05}$	$5.49e - 04_{1.1e-05}$		
WFG6	$5.60e - 04_{2.5e-05}$	$4.79e - 04_{1.6e-05}$	$4.86e - 04_{1.2e-05}$	$5.86e - 04_{2.1e-05}$	$6.63e - 04_{1.1e-04}$	$5.71e - 04_{5.6e-05}$	$5.24e - 04_{1.8e-05}$		
WFG7	$5.37e - 04_{1.9e-05}$	$4.61e - 04_{2.3e-05}$	$4.74e - 04_{1.3e-05}$	$5.49e - 04_{1.9e-05}$	$5.53e - 04_{2.6e-05}$	$5.27e - 04_{2.1e-05}$	$4.75e - 04_{1.1e-05}$		
WFG8	$1.29e - 03_{1.4e-04}$	$1.09e - 03_{1.7e-04}$	$1.26e - 03_{1.1e-04}$	$1.35e - 03_{3.9e-05}$	$1.26e - 03_{1.4e-04}$	$1.31e - 03_{1.1e-04}$	$1.08e - 03_{2.2e-04}$		
WFG9	$5.40e - 04_{2.4e-05}$	$4.73e - 04_{1.3e-05}$	$5.19e - 04_{1.8e-05}$	$5.11e - 04_{1.9e-05}$	$5.75e - 04_{3.5e-05}$	$5.43e - 04_{2.8e-05}$	$5.02e - 04_{1.3e-05}$		
Viennet2	$2.33e - 04_{2.3e-05}$	$1.08e - 04_{2.6e-06}$	$2.12e - 04_{1.7e-05}$	$2.14e - 04_{1.6e-05}$	$2.21e - 04_{1.8e-05}$	$2.12e - 04_{1.6e-05}$	$2.76e - 04_{6.7e-05}$		
Viennet3	$1.08e - 04_{1.2e-05}$	$8.20e - 05_{4.9e-06}$	$1.04e - 04_{7.6e-06}$	$1.10e - 04_{8.9e-06}$	$1.16e - 04_{9.7e-06}$	$1.09e - 04_{7.9e-06}$	$5.34e - 04_{2.6e-04}$		
Viennet4	$2.13e - 04_{1.6e-05}$	$1.30e - 04_{2.2e-06}$	$2.38e - 04_{2.2e-05}$	$5.07e - 04_{5.4e-05}$	$2.94e - 04_{2.3e-05}$	$2.86e - 04_{3.3e-05}$	$5.72e - 04_{5.7e-05}$		

The most difficult problems were DTLZ6 and DTLZ3; however, DTLZ6 has been well solved by GDE3 and SMPSO. Then, the second most difficult problems were WFG8, WFG1, WFG5, DTLZ2, and DTLZ3.

Table 5: Scores for three-objective problems (1 point for the 2<sup>nd</sup> position and 3 points for the 1<sup>st</sup> position)

	NSGA-II		SPEA2		GDE3		SMPSO		AbYSS		MOCeII		MOEA/D	
First	0	0	10	20	4	8	1	2	3	6	0	0	2	4
Second	2	2	2	2	7	7	3	3	1	1	2	2	1	1
Overall	2		22		15		5		7		2		5	

### 3.6.3 LZ\_09 problems

The LZ\_09 test suite consists of nine problems composed mainly of two-objective functions except for F6 which is a three-objective problem. The main challenges of the LZ\_09 problems reside in the complex relationships among the decision variables (high epistasis). They have different complex shapes as shown before. The results for the LZ\_09 problems are compiled in Tables 6 and 7. Complementary results can be found in Annex A: HVR in Table 46, HV in Table 47, and IGD boxplots in Figure 64. The MO algorithms that achieved the highest accuracy are NSGA-II and GDE3. Although SPEA2 is not ranked among top two for the LZ\_09 problems, by looking at the boxplots, its performance is still close to the top two.

Based on the HVR results, LZ\_06 to LZ\_09 are the most difficult problems whereas the remaining LZ\_09 problems have average complexity. Overall, the LZ\_09 test suite is among the most difficult problems because it has the highest number (four) of complex problems.

Table 6: Scores for LZ\_09 objective problems (1 point for the 2<sup>nd</sup> position and 3 points for the 1<sup>st</sup> position)

	NSGA-II		SPEA2		GDE3		SMPSO		AbYSS		MOCeII		MOEA/D	
First	4	8	0	0	4	8	0	0	0	0	0	0	1	2
Second	3	3	3	3	2	2	0	0	0	0	0	0	0	0
Overall	11		3		10		0		0		0		2	

Table 7: IGD, mean and standard deviation LZ\_09 Problems.

	NSGAI	SPEA2	GDE3	SMPSO	AbYSS	MOCeII	MOEAD
LZ09F1	$4.47e-03_{1.7e-03}$	$6.32e-03_{1.9e-03}$	$4.13e-03_{9.5e-04}$	$4.57e-03_{2.0e-03}$	$7.50e-03_{2.3e-03}$	$6.34e-03_{2.2e-03}$	$4.22e-03_{1.1e-03}$
LZ09F2	$5.95e-03_{2.2e-03}$	$6.40e-03_{2.5e-03}$	$5.10e-03_{1.2e-03}$	$1.33e-02_{1.8e-03}$	$1.02e-02_{2.1e-03}$	$1.42e-02_{6.3e-03}$	$1.12e-02_{3.1e-03}$
LZ09F3	$4.57e-03_{1.3e-03}$	$5.09e-03_{1.6e-03}$	$4.50e-03_{6.7e-04}$	$1.51e-02_{6.0e-03}$	$7.68e-03_{3.3e-03}$	$9.77e-03_{5.6e-03}$	$1.03e-02_{1.8e-03}$
LZ09F4	$4.58e-03_{9.7e-04}$	$5.16e-03_{1.4e-03}$	$4.65e-03_{4.2e-04}$	$1.30e-02_{4.0e-03}$	$5.99e-03_{3.2e-03}$	$7.93e-03_{4.4e-03}$	$1.06e-02_{1.4e-03}$
LZ09F5	$3.64e-03_{8.3e-04}$	$4.40e-03_{1.7e-03}$	$3.68e-03_{4.0e-04}$	$1.27e-02_{5.2e-03}$	$6.82e-03_{3.1e-03}$	$8.29e-03_{5.1e-03}$	$1.05e-02_{1.7e-03}$
LZ09F6	$6.64e-03_{2.2e-03}$	$4.99e-03_{1.7e-03}$	$5.20e-03_{1.3e-03}$	$3.94e-02_{2.3e-02}$	$1.14e-02_{3.7e-03}$	$1.13e-02_{4.8e-03}$	$2.86e-03_{4.1e-04}$
LZ09F7	$1.20e-02_{3.8e-03}$	$1.23e-02_{4.1e-03}$	$1.57e-02_{2.1e-03}$	$2.00e-02_{3.5e-03}$	$1.96e-02_{6.7e-03}$	$1.81e-02_{6.1e-03}$	$1.97e-02_{5.0e-03}$
LZ09F8	$1.31e-02_{2.5e-03}$	$1.34e-02_{2.9e-03}$	$1.83e-02_{1.9e-03}$	$2.07e-02_{3.9e-03}$	$1.80e-02_{6.1e-03}$	$1.71e-02_{6.3e-03}$	$2.01e-02_{4.3e-03}$
LZ09F9	$7.59e-03_{2.1e-03}$	$8.01e-03_{2.1e-03}$	$5.65e-03_{2.6e-04}$	$1.60e-02_{2.3e-03}$	$1.13e-02_{2.9e-03}$	$1.35e-02_{6.9e-03}$	$1.22e-02_{4.0e-03}$

### 3.6.4 Overall results

All the results are compiled in this subsection. All the bi-objective problems are examined first, followed by all the three-objective problems, followed by the entire 53 problems used in this comparative study.

Table 8 shows that GDE3 is clearly the most accurate method for bi-objective problems followed by the SMPSO and NSGA-II methods. It is of interest to mention that SMPSO was capable of solving accurately very complex problems such as ZDT4 and DTLZ3 that were unsolved with good accuracy by any other method. NSGA-II had good performance with bi-objective problems with complex relationships among the variables such as LZ\_09.

As shown in Table 9, the most accurate MOMs for solving three-objective problems was the SPEA2 method followed by GDE3. All the remaining MO methods had a lower accuracy. Consequently, it can be said that SPEA2 is the most accurate in solving three-objective problems, followed by GDE3.

Overall, as shown in Table 10, GDE3 is the most robust method for solving MO problems in a timely manner. It is very accurate for two-objective problems and offers good accuracy for three-objective problems with some weaknesses. In the second position, SPEA2 offers high accuracy with three-objective problems; however, its accuracy drops when it comes to bi-objective problems. SMPSO is in the third position. SMPSO offers good accuracy for bi-objective problems; however, its accuracy drops when it comes to solving three objective problems. It is important to mention that SMPSO was the only method capable of solving accurately the ZDT4 and DTLZ3 problems. The other methods ranked based on accuracy are AbYSS, NSGA-II, MOEA/D and MOCcell.

Table 8: Overall score for all the bi-objective problems

	NSGA-II	SPEA2	GDE3	SMPSO	AbYSS	MOCeII	MOEA/D
Overall	14	8	38	16	11	9	8

Table 9: Overall score for all the three-objective problems

	NSGA-II	SPEA2	GDE3	SMPSO	AbYSS	MOCeII	MOEA/D
Overall	2	23	15	5	7	2	7

Table 10: Overall score for all the bi-objective and three-objective problems

	NSGA-II	SPEA2	GDE3	SMPSO	AbYSS	MOCeII	MOEA/D
Overall	16	31	53	21	18	11	15

### 3.7 Conclusions

This chapter presented an extensive comparative study of multi-objective unconstrained continuous optimization using metaheuristics. In total, 53 well-known benchmark problems (33 bi-objectives and 20 three-objectives) have been used to compare seven state-of-the-art MOMs. The benchmark problems were composed of five test suites namely ZDT, DTLZ, WFG, Van Veldhuizen and LZ\_09. The metaheuristics were composed of NSGA-II, SPEA2, GDE3, SMPSO, AbYSS, MOCeII and MOEA/D. In total, 371 experiments have been conducted with 100 independent runs per function per problem for a total of 37,100 runs. For comparison purposes, this study used the Inverse Generational Distance (IGD) measure with complementary analysis from boxplots and a hypervolume ratio measure.

For the bi-objective problems, GDE3, clearly outperformed the other MO methods followed by SMPSO. SMPSO was capable of solving accurately very complex problems such as

ZDT4 and DTLZ3 that were unsolved with a good accuracy by any other algorithm. It is important to mention that NSGA-II achieved a good accuracy with bi-objective problems with complex variable relationships such as LZ\_09. In regards to three-objective problems, the most accurate MO metaheuristic was SPEA2 followed by GDE3.

Overall, the results showed that GDE3 is the most robust method for solving MO problems in a timely manner. Its performance is very accurate for two-objective problems and offers good accuracy for three-objective problems with some weaknesses. In the second position, SPEA2 offers high accuracy for three-objective problems; however, its accuracy drops when it comes to solving bi-objective problems. SMPSO is in third position. SMPSO offers good accuracy for bi-objective problems; however, its accuracy drops when it comes to solving three objective problems.

When examining the problem complexity, several of them appeared to be very complex because the HVR of all the MO methods was very low. Within the bi-objective problems, Poloni, DTLZ3, WFG1, WFG8 and ZDT4 are the most difficult to solve. Within the three-objective problems, DTLZ6, DTLZ3, LZ6, LZ7, LZ8 and LZ9 are the most difficult to solve.

The purpose of this comparative study was to find the most robust MOMs in solving variant bi-objective problems in timely manner. This thesis focuses on multi-objective problems in general and on bi-objective problems in specific as both utilized case studies in this thesis are bi-objective problems. Consequently, based on the results presented in this chapter, GDE3 and SMPSO, the most robust MOM for bi-objective problems, and are selected for further improvement in the remaining chapters of this thesis. Now, to determine an unexplored applicative niche of MOMs in renewable energy systems design, the next chapter conducts a literature review of optimization applications for renewable energy systems design.

## **Chapter 4**

# **Optimal Design of Hybrid Renewable Energy Systems**

Design of optimal renewable energy systems (RESs) is a very active research field. The aim of this chapter is the review of previous RESs-related works in order to find RESs-related sub-areas where state-of-the-art MOMs were not used so far. Then, contribute to RES research community by proposing innovative RESs applications.

## **4.1 Introduction**

Renewable and hybrid energy systems (HESs) are expanding due to environmental concerns of climate change, air pollution, and depleting fossil fuels. Moreover, HESs can be cost-effective in comparison with conventional power plants. This chapter reviews current methods for designing optimal HESs. The survey shows that these systems are often developed on a medium scale in remote areas and standalone, but there is a global growing interest for larger scale deployments that are grid-connected. Examples of hybrid energy systems are PV-Wind-Battery and PV-Diesel-Battery. PV and wind energy sources are the most widely adopted. Diesel and batteries are often used but hydrogen is increasing as a clean energy carrier. The design of an efficient HES is challenging because HES models are non-linear, non-convex, and composed of mixed-type variables which cannot be solved by traditional optimization methods. Alternatively, two types of approaches are typically used for designing optimal HESs: simulation-based optimization and metaheuristic optimization methods. Simulation-based optimization methods are limited in view of human intervention which makes them tedious, time consuming, and error-prone. Metaheuristics are more efficient because they can handle automatically a range of complexities. In particular, MOMs are the most appropriate for optimal HES because HES models involves multiple objectives at the same time such as cost, performance, supply / demand management, grid limitations, and so forth. This chapter shows that the energy research



community has not fully utilized state-of-the-art MOMs. More recent MOMs could be used such as robust and interactive optimizations.

## **4.2 Types Renewable Hybrid Energy System**

Renewable energy systems are in expansion around the world because of the environmental concerns due to global warming, new carbon pricing regulations arising out of these concerns, and nuclear safety concerns especially after the Fukushima nuclear accident. For example, Germany declared that it plans to shut down the nuclear plants by 2022. In addition, the supply of fossil fuels is decreasing while the demand for energy is rapidly increasing. Consequently, energy systems such as photovoltaic (PV), wind, and fuel-cells are attractive alternatives because they are profuse, clean, and decentralized. A challenge with solar and wind resources is that they are intermittent and not constantly available. The combination of multiple RESs is a sustainable solution for developing *persistent* hybrid stand-alone energy systems, and also more reliable and lower cost systems [50], [51].

Several renewable energy projects have proven to be efficient and economically viable on a smaller scale, especially in remote areas such as: islands [52], [53] or desert areas [54], [55]. Usually, these energy systems are not fully implemented from RESs. Challenges include the high cost of the RES plants and storage [56], [57]. However, the RES-based systems are still being expanded faster than expected; by 2020, it is expected to be over 20% of Europe energy supply originating from pure RESs [58]. As the RES market grows, the prices of the components will decrease as a consequence of higher demand and technological advancements. Currently, RESs are still often combined with other conventional energy systems to form hybrid energy systems such as PV-Diesel-Battery or PV-Wind-Battery [57].

Designing *optimal* hybrid energy systems is a complex task because of the difficulty of accurately predicting the output of these hybrid energy systems. This optimization complexity arises for several reasons. First, there are a high number of variables involved in the energy design optimization problem. Second, there are conflicting objectives which make the optimization problem complex such as cost, performance, supply / demand management, grid limitations, and so forth. Also, coupled non-linearities, non-convexities, and mixed-type variables, often eliminate the possibility of using conventional optimization methods to solve such problems. This paper reviews the simulation and optimization techniques applied to RES-based systems with a particular focus on renewable energy sources.

### **4.3 Modeling Renewable Energy Systems**

The following subsections describe variant types of RESs commonly modeled such as photovoltaic (PV), wind, and Fuel-Cells.

#### **4.3.1 Modeling of photovoltaic systems**

Understanding factors that affect the performance of PV modules is of great importance in order to achieve a precise anticipation of the PV module performance under variable climatic conditions. Many researchers worked in this direction. Overstraeten and Mertens [59] developed the fundamental model of PV cells. Borowy and Salameh [60] introduced a simplified model that calculates the maximum power output for a PV module based on the solar radiation and the ambient temperature. Jones and Underwood [61] proposed a more complete model by calculating the PV power output efficiency model. Kerr and Cuevas [62] introduced a model for calculating current–voltage (I–V) of PV modules by measuring open-circuit voltage under variable light intensity. Nishioka et al. [63] studied the temperature impact on the PV system

annual output; it appears that the annual energy output of the PV system increases by about 1% for every 0.1%/C° improvement in temperature coefficient of the conversion efficiency. Stamenic et al. [64] examined low irradiance efficiency of PV modules installed on buildings. Zhou et al. [65] introduced a "simple" simulation model for PV array performance predictions under operating conditions, with limited data available from PV module manufacturers. Mondol et al. [66] developed a simulator for building integrated photovoltaic; the monthly average error between measured and predicted PV output was estimated to be 6.79%.

### **4.3.2 Modeling of wind systems**

The modeling of wind energy systems includes wind turbine specifications and generator modeling. One of the simplest models to simulate the power output of a wind turbine was proposed by Ghali et al [67]; they used a probabilistic approach to simulate a hybrid PV-wind-battery energy system. Borowy and Salameh [60], [68] used a statistical method for calculating the power output from a wind turbine; they assumed the wind speed distribution to be a Weibull distribution. Karaki et al. [69] proposed a probabilistic model to simulate an autonomous wind energy conversion system composed of several turbines connected to a battery. Lu et al. Nehrir et al. [70] developed an algorithm that simulates the power output from the wind turbine based on wind average speed, the electrical load, and the power curve. The wind turbine power curves do not always represent wind turbine power output with exactitude because they neglect instantaneous wind speed variations, and therefore, undermine the wind turbine performance [71]. Therefore, Zamani and Riahy [72] introduced a new way for calculating the wind turbine output power by taking into consideration the wind speed variations.

### 4.3.3 Modeling of hydrogen fuel cells

The hydrogen offers variant advantages when integrated to hybrid RESs because of several reasons [73]. It is decentralized and intermittent supply in similar fashion as the wind and PV RESs. Also, It can become economically more viable the predominant steam-methane reforming technology if merged properly with other RESs. In addition, the hydrogen can be reused as backup power generator, for regenerating electricity during peak hours, or used as is for transportation or other purposes.

Once the hydrogen is generated, it can be reconverted to electricity using fuel-cell technology. A fuel-cell is an electrochemical mechanism to generate electrical DC current from hydrogen and oxygen. Initially, Vanhanen et al. proposed a simulation PV-hydrogen system that generates hydrogen for PV panels, and then it reconverts it back to electricity [74]. Then, Amphlett et al. [75], Kim et al. [76], and Lee et al. [77] worked on modeling of proton exchange membrane fuel-cell stack. Mann and Amphlett [78] [79] continued to work on more precise models such as the degradation effect on the fuel-cell performance. Later, Cheddie and Munroe [80] presented a review of on proton exchange membrane fuel cell modeling. In this review, they categorized the fuel-cell models as analytical, semi-empirical, and mechanistic. More recently, Mann and Amphlett [81] [82] emphasized on activation and concentration polarization.

Another aspect regarding hydrogen that needs to be addressed is its storage. The hydrogen storage is even more critical in hybrid energy system because Solar and Wind energy sources are inconsistent. Deshmukh and Boehm [83] categorize current available hydrogen storage technologies as compressed hydrogen, liquid hydrogen, metal hydrides, and carbon-based materials (fullerenes, carbon nanotubes, activated carbons). An extensive literature review of PV, wind, and FC models can be found in [84].

#### 4.4 Simulation-Based Optimization of Energy System Components

Currently, researchers working on RESs are mainly focusing on solar and wind energy sources. The photovoltaic array area, the specificities of wind turbines, and the storage capacity have an important role in operation of hybrid PV-wind energy systems, while satisfying load [85]. The most common renewable standalone hybrid energy systems are: PV-Wind-Battery, PV-Diesel-Battery, and Hydroelectric-PV-Wind-Battery. None of these are *completely benign* renewable energy systems because of the battery component. The solar and wind systems are intermittent sources of energy which require storage like a battery to form a PV-wind-battery system [57], or a backup energy source such as diesel to form PV-wind-diesel systems [57]. In both cases, the hybrid energy system is not completely renewable. The most common RES-based systems are not completely sufficient by themselves because of the intermittence of the wind and solar sources. Hydrogen is a cleaner alternative for energy storage, and it can be used for regenerating electricity by using fuel-cells.

The hybrid energy system designs are mainly dependent on the performance of their respective components. In order to forecast the system's performance, these components should be modeled and simulated. Then their combination could be evaluated to determine if it satisfies the demand load. If the power output estimation from these individual components is accurate enough, their combination can deliver power at the lowest cost.

Most of the simulation papers for hybrid energy systems use the HOMER (Hybrid Optimization Model for Electric Renewables) tool [86], developed by NREL (National Renewable Energy Laboratory, USA) because of its capabilities and flexibility. It can optimize a wide range of energy components: photovoltaic generator, batteries, wind turbines, hydraulic turbines, AC generators, fuel cells, electrolyzers, hydrogen tanks, AC-DC bidirectional

converters, and boilers. The loads can be different types: AC, DC, and/or hydrogen or thermal loads. In addition, the tool is available free of charge.

#### **4.4.1 Simulation-based optimization of photovoltaic systems**

Shaahid and Elhadidy [87] used the HOMER tool for cost optimization of a PV–Diesel–Battery system to supply a shopping center in a desert area. The hybrid energy system reduced the diesel consumption and pollution by 27%. Shaahid and El-Amin [100] used HOMER for finding an optimal design of a PV–Diesel–Battery hybrid energy system, rather than diesel-only, for supplying a remote village in Saudi Arabia. The study examined the effect of PV/battery penetration on the cost of electricity, the unmet load, the electricity excess generation, percentage of fuel savings, and reduction in carbon emissions. The results showed that the optimal combination is the PV-Diesel-Battery rather than Diesel-only or PV-Diesel. The percentage of fuel savings by using a hybrid PV–diesel–battery energy system (2.5 MW PV, 4.5 MW diesel system, 1 h storage, and 27% PV penetration) is 27% less than using diesel only. In addition, the carbon emissions decrease by 24% (1,005 tons/year) as compared to the diesel-only scenario. Li et al. [89] used simulation methods for the development of a standalone PV system. Due to the intermittent nature of the solar energy, they considered batteries and/or fuel cells (FC) for energy storage. The hybrid PV-battery-FC energy system appeared to be the cheapest, most efficient, and least demanding in terms of PV module numbers as compared to either single storage system.

Wies et al. [90] simulated, with Simulink and HOMER, a real hybrid PV–Diesel–Battery energy system located in Alaska. They compared it with a system with only a diesel generator, and another Diesel–Battery system to supply energy for the same load. The results indicated that

the system with only a diesel generator had a lower installation cost, but higher operation and maintenance costs.

#### **4.4.2 Simulation-based optimization of wind systems**

Himri et al. [91] used the HOMER software tool for the optimization of energy production, life cycle cost, and the greenhouse gas emissions of a hybrid energy system. The hybrid wind-diesel energy system is a grid-connected power plant supplying energy to a remote village. The results show that the wind–diesel hybrid system becomes feasible when the wind speed reaches 5.48 m/s and the fuel price is \$0.162/L or more. The maximum annual capacity shortage did not impact in any way on the system optimization. Lu et al. [92] used probabilistic models to select the optimal (maximum power output) turbine characteristics, depending on the yearly wind properties. They found that hub height is an important factor. At 37 m, the wind turbine can function for 6,820 hours (77.85%) a year and generate 32,400 kWh with a capacity factor of 0.387 for Waglan Island.

#### **4.4.3 Simulation-based optimization of fuel-cell systems**

The hydrogen FCs fit well with hybrid energy systems for several reasons [73]. First, FCs provide a decentralized supply in a similar fashion to wind and solar RESs. Second, hydrogen can be generated during off-peak periods where electricity prices are low. Third, the hydrogen FC can be reused as a backup power source; it can be used for regenerating electricity during peak hours. The FC mechanism generates Direct Current (DC) from hydrogen and oxygen.

As mentioned previously, Li et al. [89] examined on a combination of FCs with PV-battery systems.

#### **4.4.4 Simulation-based optimization of PV-wind systems**

McGowan and Manwell [93] discussed PV–Wind–Diesel–Batteries hybrid energy systems in different locations in the world using the HYBRID2 tool [94]. They concluded that hybrid energy-related research should further examine the reliability of components and systems, improve the documentation and monitoring of system performance, and reduce the cost of the renewable energy components. Furthermore, they designed PV–Wind–Diesel–Battery systems for different locations in South America [95]. They found by comparing HYBRID2 and SOMES tools that they provide similar results, and they can be used to design and analyze such systems. However, there is no universal tool yet, and different types of problems need to be solved through the use of different approaches and tools. Karaki et al. [69] examine simulation algorithms for PV–Wind–Battery systems. They report on economics of hybrid PV–Wind–Battery energy systems. However, the battery capacity is limited, depending on the required charging/discharging cycle time. Elhadidy [96], [55] studied the performance of possible variances of PV-wind-diesel systems. It has been found that PV panels are economically not yet viable for desert areas in Saudi Arabia. Nfah et al. [97] proposed a design for a PV–Wind–Diesel–Battery system located in a remote area in the north of Cameroon. They demonstrated that the hybrid energy system can generate in a range of 70 – 2,585 kWh/year rather than extending the grid.

Diaf et al. [98] studied the optimization of economic and technical performance of a stand-alone hybrid PV-wind-battery energy system on Corsica Island. They compared the optimum dimensions of the system in five sites on the island. The results showed the hybrid energy system offers a better performance than a single source system. The PV system was not



affected by changing sites; however, the wind system dropped from 40% power generation to 20%, depending on site location.

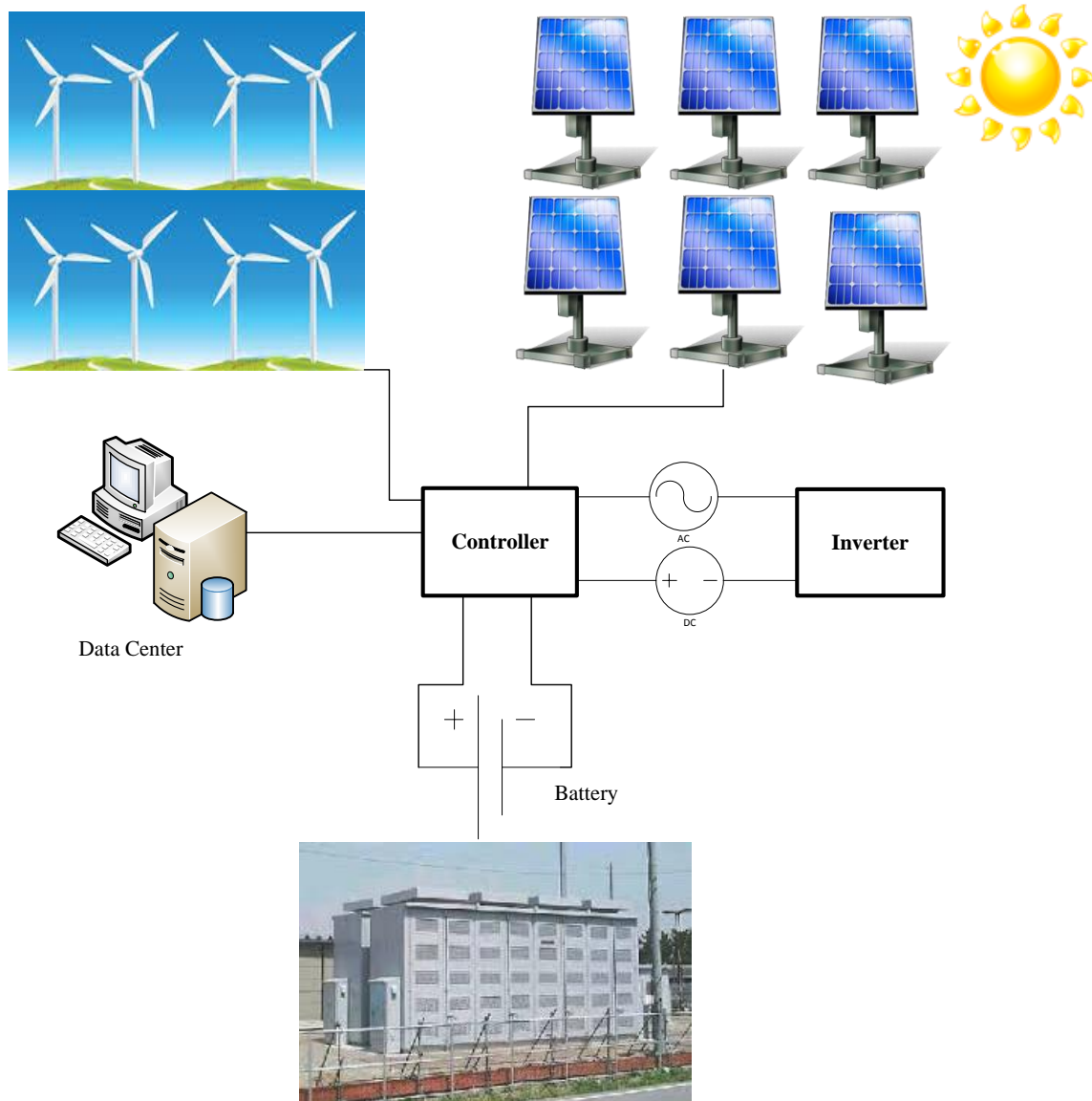


Figure 13: Example of a hybrid PV-wind energy system

Figure 13 presents an example of a hybrid PV-Wind system model with a battery to store electricity.

Dalton et al. [99] worked on the design optimization of a standalone renewable energy PV-Wind-battery-Diesel system, using HOMER and HYBRIDS tools, for a large hotel (4,100 beds) located in a subtropical coastal area in Australia. More specifically, they compared diesel generator-only, PV-Wind-Battery, and PV-Wind-Battery-Diesel hybrid technologies. Three objectives were considered: the Net Present Cost (NPC), renewable fraction (RF), and payback time. The result showed that it is possible to build a completely RES that meets the demand load. However, a hybrid diesel-Wind-battery configuration provides the lowest NPC result with a resultant RF of 76%. The NPC is reduced by 50%, and the greenhouse gas emissions by 65%.

Mondal and Denich [100] studied the potential of PV, Wind, Biomass, and Hydro energy sources in Bangladesh. The results showed that PV grid-connected sources have the highest potential for the country. Prodromidis and Coutelieris [101] examined an existing RES installed in Leicestershire, UK. The system is a standalone PV-Wind-FC. By using the HOMER tool, it was determined how to optimize the use of the system and the cost impact of connecting the RES system to the grid. Results showed that in the long term, the connection to the grid will be costly.

Balamurugan et al. [102] used the HOMER tool for designing an HES composed of biomass-PV-Wind-battery in a remote area. The objective was a combined maximization of the supply of energy to the loads and minimization of the supply of energy from the sources. A sensitivity analysis was performed for the load, wind speed, and solar radiation. The proposed system satisfied the load demand, nonlinear seasonal variations, and equipment constraints of three different typical villages in India.

#### **4.4.5 Simulation-based optimization of solar-wind-fuel-cell systems**

Dufo-López et al. [103] worked firstly (case A) on the design and economic analysis of hybrid PV-Wind energy systems. In addition (case B), they considered the use of these systems for generating hydrogen when the amount of electricity is not needed by the demand load. Finally (case C), the reuse of hydrogen was considered for regenerating back electricity when the demand is high. The results (case A) showed that hybrid PV-Wind energy systems match well and they are more economical than the use of a unique energy source. For case B, the generation of hydrogen for selling purposes appeared to be economically viable only for locations having a high average wind speed ( $> 4.66$  m/s). For case C, the use of hydrogen for regenerating electricity by fuel cells was not economically viable based on the electricity prices in Spain. The authors attribute this to a low energetic efficiency rate of the electricity-hydrogen-electricity process. However, if the electricity prices were higher or the energetic efficiency rate improved, the model would become viable.

Figure 14 is an example of a PV-FC (hydrogen) model.

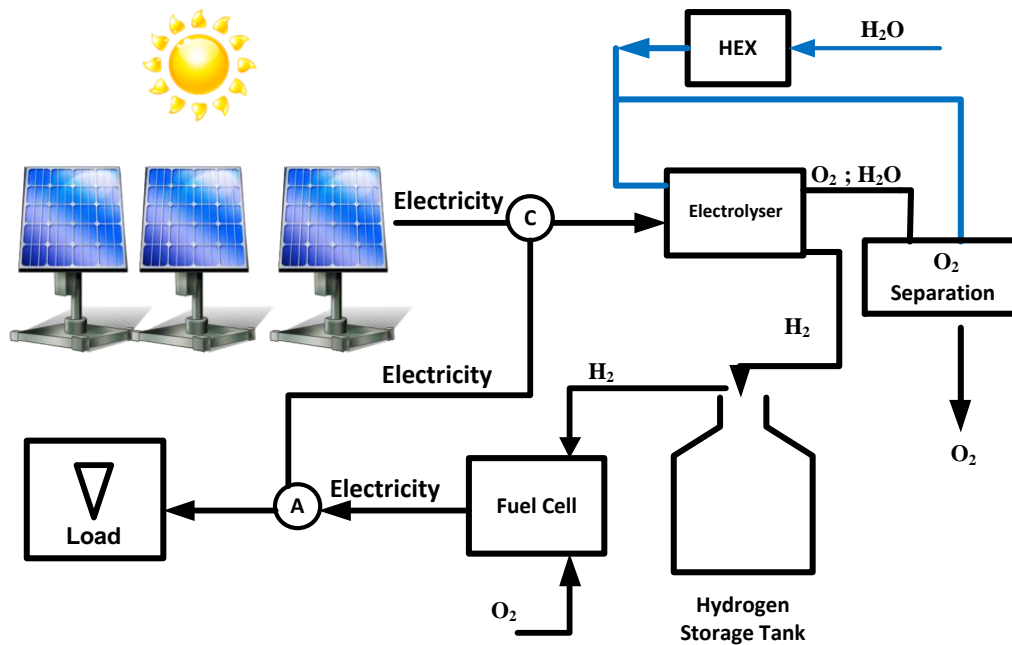


Figure 14: Example of modeling of a PV-hydrogen FC energy system

Zervas et al. [104] developed a framework for HES that used hydrogen for energy storage. Thus, they tested the framework with a PV-FC system connected to a grid in Greece. The proposed tool is especially useful for HES that incorporate hydrogen systems.

#### 4.5 Optimization of Energy System Components

Several papers have been published regarding the optimization of hybrid energy sources. However, this thesis focuses on recent studies published in the last decade. Usually, an optimum combination of hybrid energy sources needs to address several objectives. Among them, the system and the production costs should be minimal, the load demand should be met, and the power should be reliable. Sometimes, HES is optimized by taking all the objectives at the same

time. And sometimes, one objective is optimized whereas other objectives are transformed into constraints. Both approaches are described in the next subsections.

#### **4.5.1 Mono objective optimization for hybrid energy systems design**

Koutroulis et al. [105] worked on designing a standalone hybrid PV-wind-battery energy system by focusing on the minimization of a 20-year total system cost. This cost is the sum of the components of capital and the maintenance fees. In addition, the solution is constrained by the load energy requirements that need to be completely covered, i.e., a zero load rejection. A genetic algorithm (GA) was used and it attained the global optimum faster than conventional optimization methods such as dynamic programming and gradient techniques. In addition, the result showed that a standalone hybrid PV-Wind energy system is lower cost than the exclusive usage of one energy source.

Sequential Quadratic Programming was used for the optimization of solar field design [106]. The system was divided into three sub-problems: energy maximization, minimization of the area field, and maximization of the solar unit area. They found that it is possible to increase the yearly energy by about 20% and a decrease of about 15% of the field area, compared to the current industrial standards in their area.

Ashok [107] used Non-Linear optimization for the design of a PV-Wind-Micro-Hydro-Diesel-battery system. They have found that a micro-hydro/wind hybrid energy system to be the most optimal combination from the cost perspective. In addition, it is the cleanest combination because of no diesel in the system. The system is tested in India (Western Ghats - Kerala).

Yang et al. [108] studied the design of hybrid solar-wind-battery energy systems. It was possible to calculate the system's optimum configurations while minimizing the annualized cost of the system, with respect to the required loss of power supply probability (LPSP). Five

decision variables were considered in the optimization process: PV module number, PV module slope angle, wind turbine number, wind turbine installation height, and battery capacity. The results showed that it was possible for GA to attain the global optimum with relative computational simplicity. The proposed hybrid energy system served as a power supply for a telecommunication relay station located in the southeastern coast of China.

Tina et al. [109] used a probabilistic approach based on a convolution technique for assessing long-term performance of a hybrid grid-connected PV-wind energy system. The system permitted the evaluation of different economic objectives such as electric contract demand, expected values of annual total cost, annual energy consumption, and others. The results of the analysis were not used only for the index of reliability calculation, but also allowed the documentation of other relationships among system parameters of interest.

Dufo-López and Bernal-Agustín used Genetic Algorithms (GAs) for designing an optimal PV-Diesel-battery system [110]. GAs were used because of mixed type variables: Boolean, integer, discrete. One GA served for selecting the components, while the second served for handling electric dispatch strategy (Cycle Charging or Combined). They integrated the GAs into the HOGA tool. It appeared that the GA algorithm offered more precision than traditional methods because it was possible to get the number of PV panels, as well as their type, and the number of batteries in parallel, and their type. Also, HOGA was compared to the HOMER modeling tool [86], which they mentioned to be the best tool available. In addition, the tool is available free of charge. After the comparison, HOGA appeared to be faster and more precise than HOMER. This performance is attributed to the use of GAs by HOGA.

Glover et al. [111] worked on the design of PV systems which are connected to storage units (compressed-air-energy-storage and super-capacitors), and also grid connected. They have

used the *OptQuest* [112] tool for the design, which incorporates two metaheuristics Scatter Search, Tabu Search, and Neural Networks. They successfully obtained an optimal mixture of required capacities of the systems.

Giannakoudis et al. [113] used the stochastic annealing optimization method for designing a PV-Wind-FC-Diesel system with consideration of the uncertainties. The resulting systems have a more robust response to external or system-inherent variations. Kaabeche et al. [114] performed a case study on a PV-Wind-Battery system in Algeria. They have used a GA for system optimization. Zhao et al. [115] proposed a GA for designing a wind farm by optimizing the production cost and system reliability. Senjyu et al. [116] used a GA for the design of a PV-Wind-battery-diesel system in Japanese islands. The results showed that HES systems reduce the cost by 10% in comparison with diesel generators.

Kaviani et al. [117] used the Particle Swarm optimizer for the design of a PV-Wind-FC system. They demonstrated the importance of considering outage scenarios in the design. Hakimi et al. [118] used a PSO algorithm to optimize the design of a wind-FC system in a remote area in Iran. The designed system was sufficient to cover the demand of that area.

A limitation of the previous studies is that all of these tools optimize a single objective. They consider other objectives as constraints or use weighted sum approach. Nevertheless, the design of hybrid energy systems (HESs) is a multi-objective problem, and it should be modeled accordingly. The next section reviews multi-objective optimization methods applied to the design of HES.

#### **4.5.2 Multi-Objective optimization for hybrid energy systems design**

Dufo-Lopez et al. were the first and only research group to the best our knowledge that have used multi-objective optimization (MO) metaheuristic methods for HES design [119], [120],

[121]. They developed a tool called HOGA [122]. According to their survey [57], it appears that this is the only tool that uses a MO metaheuristic for HESs. It supports, according to the user manual, the following objectives: total cost (Net Present Cost (NPC)) versus CO<sub>2</sub> Emissions, or total cost (NPC) versus unmet energy. It can handle various components: photovoltaic generator, batteries, wind turbines, hydraulic turbine, AC generators, fuel cells, electrolyzers, hydrogen tanks, rectifiers, and inverters. The loads can be AC, DC, and/or hydrogen.

First, Dufo-Lopez et al. [119] worked on the design of PV–wind–diesel–battery using MO metaheuristic for the first time. The problem was composed of two objectives: minimization of cost through the useful life of the installation and the pollutant emissions while guaranteeing electrical energy supply at all times. The system generated a Pareto front composed of 50 solutions. The designer could choose the most appropriate solution, considering the costs and pollutant emissions, which demonstrate the practicality of using MO methods.

Then, they [120] used the same algorithm (SPEA) for the same problem by adding more real-world complexity. They used a GA for a control strategy. Also, they added unmet load as a third objective and Hydrogen-based Fuel-Cells as an additional type of storage component. They developed a triple multi-objective design of a standalone PV-Wind-Diesel-Hydrogen-Battery hybrid energy system. The system was located in Zaragoza, Spain. The SPEA algorithm was used for the simultaneous minimization of three objectives: the total net present cost, pollutant emissions (CO<sub>2</sub>), and the unmet load. The processing resulted in a Pareto front of 35 solutions from which the designer could select. Most of these solutions integrate Wind and PV panels, and batteries for storage. Due to the high cost of a hydrogen storage component at that time, most of the solutions incorporated the exclusive use of batteries. The diesel fuel is highly priced in that location, which is why it was not part of the solutions.



There are some past studies applied to HES design. Dipama et al. proposed a new variant of a GA for the optimization of two different power plant problems [123]. First, they worked on the design of a Cogeneration thermal plant. The objectives were the maximization of exergy efficiency and minimization of cost rate. Second, they worked on the design of an advanced steam power station. The objectives were the maximization of both, the efficiency and the net power output of the plant. For both designs, the proposed GA has appeared to be reliable, powerful, and robust when compared to previous research studies.

Meza et al. [124] examined a power generation expansion planning optimization problem. They proposed a multi-objective evolutionary programming algorithm (MEPA) for determining which, when, and where new generation units should be installed. A unit can be any one of the following: conventional steam units, coal units, combined cycle modules, nuclear plants, gas turbines, wind farms, and geothermal and hydro units. First, two objectives were considered: the minimization of investment, operation costs, and the environmental impact. Then, they added two other types (imports of fuel, and fuel price risks of the whole system) for a total of four objectives. The problem was nonlinear, mixed-integer, and considered NP-Hard. They concluded that the system offered good quality solutions (close to the real Pareto set) when optimizing two objectives. Furthermore, the system was able to provide solutions when handling four objectives. However, it was not possible to compare the results with previous works because no past studies considered more than two objectives for these kinds of problems.

Niknam et al. [125] proposed a new multi-objective modified honey bee mating optimization algorithm for the design of a PV-Wind-FC grid connected system. The proposed method showed better results than uni-objective optimization methods.

Ould e t al. [126] used a multi-objective GA for analyzing a hybrid PV–wind-battery energy system by minimizing the annualized cost system and the loss of power supply probability in remote areas in Senagal. They compared three configurations in their study.

Katsigiannis [127] used the NSGA-II multi-objective algorithm to design a PV-Wind-FC-Diesel-Battery system. The results showed that PV-Wind-Battery is the most attractive combination from the cost and environmental point of view in Greece.

## **4.6 Summary and Future Trends**

### **4.6.1 Energy system-related observations**

As shown in Table 11, most of the systems are composed of PV and wind energy sources. These two energy sources match well together because both are intermittent and they complement each other. For example, sometimes there is no wind, but the weather is sunny and vice versa; PVs will compensate for such trends. However, their complementary roles are sometimes deficient especially at night-time because PV panels do not generate electricity. As a third component, hydrogen fuel cells are becoming more common within a standalone energy system framework. Previously, diesel and battery systems have been used, but fuel cells gained more popularity in the last couple of years because these are becoming more affordable, as well the technology is improving, and are more environmentally friendly than batteries and diesel. The unused electricity generated from PV-wind is converted into hydrogen as an energy storage medium, which serves for operating FCs to regenerate electricity when needed (e.g. night-time). Moreover, hydrogen surplus can be directly used for industrial or transportation purposes. Thus, PV and wind systems are the most common renewable systems; however, hydrogen systems are increasingly used in hybrid energy systems.

Almost all of the HES projects involved a PV component to convert the solar energy source into electricity. But PV has a lower conversion efficiency than solar thermal systems in high temperature areas. PV systems become less efficient in hot areas like deserts because of the high temperature. Consequently, studies should consider the use of solar thermal systems as an alternative to PV systems to benefit from solar energy sources in such areas. Another interesting observation is that previously HES was typically designed as standalone systems in remote areas. Currently, HES tends to be integrated into existing grids which requires more complex models.

Table 11 summarizes the simulation and optimization methods found for the design of HES.

#### **4.6.2 Optimization-related observations**

As shown in Table 11, simulation-based optimizations are declining because they require manual intervention for every run which is very time consuming, tedious, and error prone. On the other hand, metaheuristics such as genetic algorithms are more attractive for the design of HES for several reasons. They are intelligent and autonomous, can generate results in a much shorter time, and can handle complex non-linear models in an automated manner.

The energy research community has not fully utilized the most recent discoveries in the optimization field. There is a gap among the energy and optimization communities that should be bridged. This bridging will have several positive impacts as follows when designing HES: First, HESs involve very complex optimization problems because of mixed type variables, non-linearity, and non-convexity, which make them difficult to solve with classical optimization methods; consequently, optimization metaheuristics such as genetic algorithms are more appropriate for optimal design of HESs.

All HES design projects involve multi-objectives such as cost and pollution minimization, efficiency maximization, to name a few. Thus, multi-objective metaheuristics are more promising for these types of problems. Despite these advantages, only few studies have been completed with MOO metaheuristics methods for energy systems design. Even most of the state-of-the-art multi-objective optimization methods have not been fully utilized yet. Comparative studies of state-of-the-art multi-objective optimization methods can be found in [4] and [3]. Moreover, multi-objective metaheuristics offer HES designers multiple tradeoff solutions which are more practical and attractive for real-world engineering systems. The decision makers can select the solutions that best fit their needs.

Table 11: Résumé of reviewed HESs-related works

Research	Year	Solar	Wind	Fuel Cell	Diesel	Battery	Other	Standalone	Grid connected	Simulation Only	Multi-Objective	Unique Objective	Optimization	Tools	Optimization Methods
Borowy and Salameh	1996	X	X			X		X		X					
McGowan and Manwell	1999	X	X		X	X		X		X				Hybrid 2	
Karaki SH et al.	1999	X	X			X		X		X				Probabilistic model	
Elhadidy MA	2002	X	X		X			X		X					
Weinstock and Appelbaum	2004	X						X				X	X		SQP
Wies et al.	2005	X			X	X				X				Simulink, HOMER	
Dufo-López and Bernal-Agustín	2005	X			X	X		X				X	X	HOGA, HOMER	GA
Koutroulis E et al.	2006	X	X			X		X				X	X	HOMER	GA
Tina et al.	2006	X	X						X			X	X		probabilistic
Nfah EM et al.	2007	X	X		X	X		X		X					
Shaahid SM and Elhadidy MA	2007	X			X	X		X		X				HOMER	
Ashok	2007	X	X		X	X	Hydro	X				X	X		NL
Senjyu	2007	X	X	X	X			X				X	X		GA
Diaf S et al.	2008	X	X			X		X		X					
Dalton et al.	2008	X	X		X	X		X		X				HOMER and HYBRIDS	
Himri et al.	2008		X		X				X	X				HOMER	
Dufo-López	2008	X	X	X	X			X			X		X		GA, evol. Strategy
Li et al.	2008	X		X		X		X			X		X	HOGA	GA
Yang et al.	2009	X	X			X		X				X	X		GA
Shaahid and El-Amin	2009	X			X	X		X		X				HOMER	
Dufo-López and al	2009	X	X	X					X	X					
Meza et al.	2009		X				X	X			X		X		Evolutionary (PEAS)
Zhao et al.	2009		X					X				X	X		GA
Kaviani et al	2009	X	X	X				X	X						PSO
Hakimi et al.	2009		X	X				X				X	X		
Mondal and Denich	2010	X	X				Hydro		X	X				HOMER	
Prodromidis and Coutelieris	2010	X	X	X			Hydro	X	X	X				HOMER	
Katsigiannis	2010	X	X	X	X	X		X			X				NSGA-II
Glover et al.	2011	X					X		X			X	X	OptQuest	Scatter search, tabu, NN
Giannakoudis et al.	2011	X	X	X	X				X			X	X		Stochastic Annealing
Kaabeche et al.	2011	X	X			X		X				X	X		GA
Niknam et al.	2011	X	X	X					X		X		X		modified honey bee mating
Balamurugan et al.	2011	X	X			X	Biomass	X		X				HOMER	

Furthermore, there are other newer MOO metaheuristics. For example, decision makers can be involved in the multi-objective optimization process by selecting intermediate solutions or adding prior knowledge to an HES problem. Consequently, the metaheuristic will converge faster, and generate solutions which will be more ad hoc to the needs of the decision makers. Such methods are called *interactive optimization* methods; more details can be found in [128]. Also, most past studies have not presented a comprehensive sensitivity analysis.

HES designs involve several uncertainties such as weather conditions, variations in the demand, and others. Therefore, HES design should always incorporate a sensitivity study to test the robustness of the HES. Alternatively, robust optimization methods can be used; these methods look for the most *robust* and optimal solutions at the same time. An extensive study of such methods can be found in [129].

## **4.7 Conclusions**

Hybrid energy systems are attracting greater attention because they can become more economical, environmentally cleaner, and can be installed in a distributed fashion. This literature review shows that most HESs are based on PV and wind energy sources because of their complementary roles. A challenge with solar and wind resources is their intermittency; usually, they are complemented by energy sources or carriers such as diesel or batteries. However, diesel and batteries are decreasing while hydrogen systems are increasing. Hydrogen is cleaner than diesel and batteries, is becoming cheaper, can be reused for energy storage and can regenerate electricity when needed. Another conclusion is that previous studies focused on standalone systems usually installed in remote areas. Currently, the tendency is to have grid-connected HES. The simulation tools are more mature. However, several HES systems connected to the grid can generate grid congestion during peak hours. These congestion issues should be also considered

when integrating multiple HES systems into a grid. Finding the optimal design of a hybrid energy system is a complex task because it involves multiple objectives, a large number of variables, heterogeneous energy technologies, uncertainties such as weather, demand, and other factors.

This chapter has reviewed the current trends to designing optimal hybrid energy systems. There are two main approaches for designing optimal hybrid energy systems. The first is simulation-based optimization. It permits the variation of different variables or parameters of hybrid energy systems in order to find an "optimal solution". These approaches require a designer's interaction for setting the parameters in order to find an "optimal" design. Therefore, this approach is arduous and time consuming. Moreover, every simulation generates only one solution. Furthermore, there is no automated support for helping or guiding the designer towards the optimum solution. The second approach uses optimization methods for designing hybrid energy systems. The current trend is the use of metaheuristic algorithms for HES optimization design because they obtain automatically optimal or close to optimal solutions. They can handle a high number of mixed type variables (i.e., real vs. discrete variables). Furthermore, metaheuristics can handle complex problems such as energy design systems which are not linear, nor convex. Therefore, metaheuristics are more suitable for solving hybrid design energy problems. In addition, all HES involve multiple competing objectives such as cost minimization and energy maximization which can be solved by multi-objective optimization metaheuristics. MOO metaheuristics generate multiple tradeoff solutions that are more practical and attractive for real-world engineering systems. Despite these advantages, this literature review has shown that very limited work has been conducted in the past with multi-objective optimization metaheuristics for energy systems design. Furthermore, the used multi-objective optimization

metaheuristics were not state-of-the-art. Therefore, the design of optimal HESs requires more interaction between both energy and multi-objective optimization research communities to fill this gap. Other more recent MOO metaheuristics methods should be explored such as MOO robust optimization and MOO interactive optimization methods. Robust optimization targets optimal and robust solutions at the same time, while interactive optimization takes input from decision makers while searching optimal solutions.

Based on the conclusions of this chapter, it is proposed to develop new MOMs with applications in RES. This way, state state-of-the-art MOMs can be used to solve RESs and demonstrate further their benefit for such applications. In addition, such proposed work can contribute to bridge the gap between MOM and RES research communities. In the following chapters, two models will be proposed for the reasons mentioned above. One of them should be related to optimal design of a grid-connected hydrogen energy system. Such a project will be very innovative and will demonstrate the efficiency of MOMs in solving even complex grid connected RES problems.



## **Chapter 5**

# **Leaders and Speed Constraint Multi-Objective Particle Swarm Optimization**

Now that the base (parent) MOMs are determined, and renewable energy problems to be solved have been selected, it is proposed, as first fundamental contribution in this thesis, to improve leader selection mechanism in a multi-objective variant of particle swarm optimizer (PSO).

Selection of representative particle swarm leaders in multi-objective optimization (MO) is a critical task because they influence the progress quality of the entire population. Most MO variants of PSOs use the concept of non-dominance to select leaders. The problem occurs when all or majority of leaders (non-dominated individuals) are concentrated in a specific region of the objective space. The leaders attract the particles to that specific area which impacts the uniform distribution of the population and leads to a slower explorative algorithmic ability. In this chapter, a second discriminative mechanism is proposed to support a more representative (well-distributed) selection of leaders. The proposed algorithm, called leaders, and speed constrained multi-objective PSO (LSMPSO), is an extension of SMPSO. The convergence speed of LSMPSO is compared with seven state-of-the-art MOMs using the ZDT and DTLZ bi-objective benchmark family problems.



Figure 15: Example of flock of birds [130]



Figure 16: Example of fish schools [131]

## 5.1 Particle Swarm Optimization

Particle swarm optimization (PSO) is a population-based metaheuristic that has been very successful in many fields. PSO is a nature inspired metaheuristic simulating the social behavior of flock of birds or school of fish as shown in Figure 15 and 16. It was proposed by Kennedy and Eberhart [132] in 1995; Since then, PSO has been cited in over 20,000 papers. The description of PSO is provided in the remainder of this subsection.

In PSOs, the movement of candidate solutions, called particles, is influenced by leaders. The entire population of particles is called a swarm. In PSO, a particle  $x_i(t)$  is updated at a generation  $t$  as follows:

$$x_i(t) = x_i(t - 1) + v_i(t), \quad (10)$$

where the  $v_i(t)$  is the particle's velocity which is calculated as follows:

$$v_i(t) = w \cdot v_i(t - 1) + r_1 C_1 \times (p_i - x_i(t - 1)) + r_2 C_2 \times (p_g - x_i(t - 1)), \quad (11)$$

where  $p_i$  is the personal best found by candidate solution  $x_i$ ,  $p_g$  is the global best found particle in the entire swarm, called leader.  $w$  is the particle inertia weight which controls exploration and exploitation (fine tuning) stages,  $r_1$  and  $r_2$  are random vector variables in the range  $[0,1]$ ,  $C_1$  and  $C_2$  are learning factors towards the particle's personal success and its neighbors success.

Figure 17 illustrates the movement of a particle which is affected by its own best found solution and global best solution among the particles.

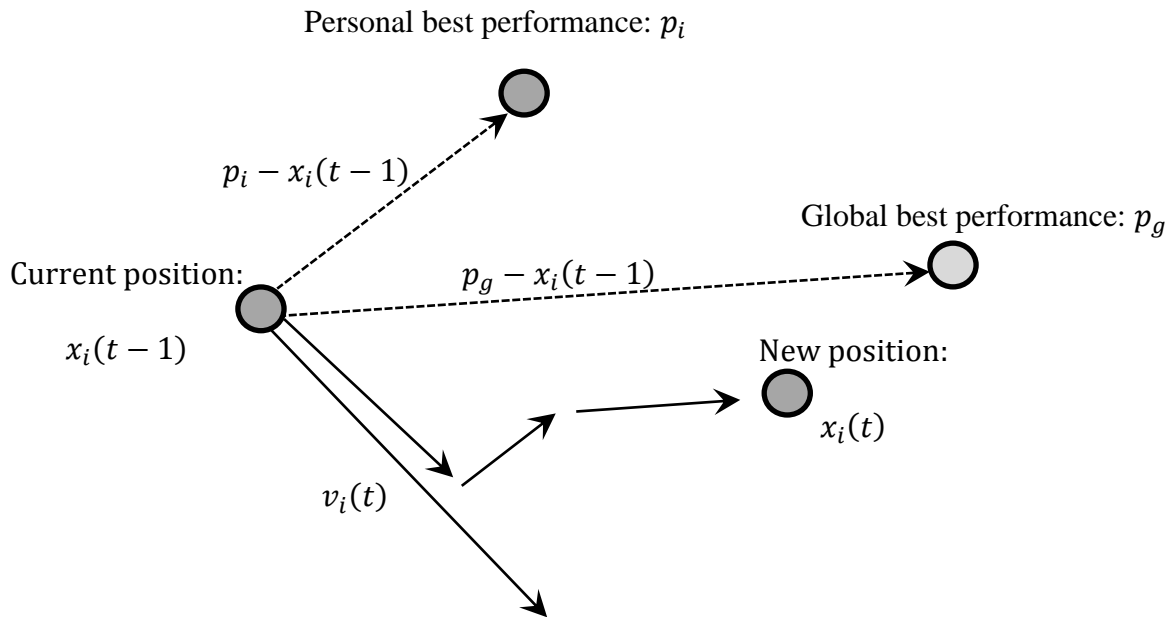


Figure 17: Movement of a particle and the velocity update.

### PSO Algorithm

```

Random initialization of the whole swarm (uniform random distribution);
repeat
  for all particles  $i$  do
    Update velocities:

$$\vec{v}_i(t) = w \cdot \vec{v}_i(t-1) + C_1 \cdot r_1(\vec{x}_{p_i} - \vec{x}_i) + C_2 \cdot r_2(\vec{x}_{G_i} - \vec{x}_i)$$

    Move to the new position:  $\vec{x}_i(t) = \vec{x}_i(t-1) + \vec{v}_i(t)$ ;
    if  $f(\vec{x}_i) < f(\vec{x}_{p_i})$  then
       $\vec{x}_{p_i} = \vec{x}_i$ 
    end if
    if  $f(\vec{x}_i) < f(\vec{x}_{G_i})$  then
       $\vec{x}_{G_i} = \vec{x}_i$ 
    end if
    Update( $\vec{x}_i, \vec{v}_i$ )
  end for
until Stopping Criteria

```

## 5.2 Speed Constraints Multi-objective Particle Swarm Optimizer

Since the invention of PSO, over 30 multi-objective variants of PSO have been proposed [32]. However, the most salient one is SMPSO [32]. SMPSO is an extension of OMOPSO [13]. Its main difference with respect to OMOPSO is the incorporation of a mechanism for velocity limitation and the introduction of a polynomial mutation operator.

SMPSO has shown a high accuracy for MO optimization problems as reported in [32] and a high convergence speed as demonstrated in [4]. In PSOs, the movement of candidate solutions, called particles, is influenced by the leaders. However, our observations show that if the leaders are not appropriately selected, the particles might be attracted by a concentration of leaders in certain region of the objective space. Consequently, the entire particles movement will prematurely converge towards that specific objective space region where these groups of leaders are located. Additional computation overhead would be required to find the entire Pareto front or even worse, the SMPSO can be trapped in a local optimum.

## 5.3 Leadership in PSO Related Work

This section describes the most relevant PSO-based multi-objective algorithms work focused mainly on global leader selection mechanisms. Other types of surveys about MO versions of PSO can be found in Ref. [133].

The first MO variant of PSO has been proposed by Moore et al. [134]. The selection of leaders was scalar as in single objective optimization; however, the details of scalar ranking are not provided. Most MO variants of PSO use the non-dominance ranking similar to NSGA-II for selecting their leaders to the archive. Then, different selection schemes are used to select them from the archive as described in the remainder of this subsection.

In [135], a leader is *randomly* selected from the archive. The work focused essentially on the incorporation of an elitist-mutation to PSO. The proposed MO PSO-based algorithm showed promising results; however, it was compared only to NSGA-II using only the ZDT problems in addition to another problem for a total of six problems.

Other approaches used the roulette-wheel which consists in prioritizing certain leaders over others assigning a probability of selection to every leader. In [136], a roulette-wheel and crowding distance were used to select a leader. The proposed algorithm outperformed four other MO PSOs; however, only the ZDT family of problems has been used. In [137], it was proposed to hybridize PSO with differential evolution (DE). PSO served to accelerate the convergence speed whereas DE mutation properties were used for diversity maintenance. The selection of leaders is done using the non-dominance scheme. Thereafter, the centroid point of leaders is calculated and a roulette wheel mechanism is used to select leaders. The probability of a leader to be selected is proportional to the distance from the centroid; the further is a leader from the centroid point, the higher are the chances to be selected to encourage diversity. The proposed algorithm was compared with OMOPSO, SMPSO, NSGA-II and DEMO using the ZDT problems, and it converged faster for two problems out of five, namely, ZDT1 and ZDT2. Another approach consists in prioritizing leaders based on their previous performance. An initial proposal suggested giving points to leaders when they lead the generation of fitter new particles. The more points a leader accumulates, the chances of selection become higher [138]. A more recent contribution consisted in giving preference (roulette wheel) to leaders having lowest average distance to  $K$ -neighbors in the objective space [139].

Other approaches such as in [140] used a grid structure; the proposed method outperformed PAES and NSGA-II using two test functions. In [141], the sigma method is

proposed, which consists in selecting for every particle the closest leader in the objective space. The results were promising; however, the number of particles had to be increased to maintain a good distribution of particles and a turbulence parameter was added to do some abrupt changes in the population.

In [142], five leader selection strategies have been compared using a multi-objective PSO namely, the random strategy, the sigma strategy, the nearest strategy, the grid strategy, and the non-dominated strategy. The WFG family problems were used for comparison purposes. The results showed that the classical non-dominance strategy generates the highest accuracy.

Other leaders selection methods have been investigated for many-objective optimization (more than 3 objectives) problems in [143].

#### **5.4 Description of the Proposed Leader Selection Approach**

In order to better understand the purpose of leader selection process, let us review the relationship among leaders and particles and how leaders influence particles movement during a convergence process.

The main challenge of extending the PSO algorithm to MO space resides in the generalization of the concept of leader [13]. The most common approach consists in considering the non-dominated solutions as leaders. If the number of leaders exceeds the maximum size of an archive, then the crowding factor is used as a second discriminant, as in the NSGA-II [27]. As shown in Figure 18, the non-dominance discriminant can affect the distribution of the particles especially at early exploration stage. Sometimes, it is possible to have a concentration of leaders which are non-dominated, in a certain region of the objective space; consequently, the entire swarm movement will be predominantly affected by these leaders as shown in Figure 19. The particles will be covering a certain portion of the Pareto front rather than the entire Pareto front

(PF). So, additional computational overhead would be required to find the remaining portion of the PF or even worst a portion of the PF which can be valuable in decision making will not be found because no leaders are located in the missing part of the PF.

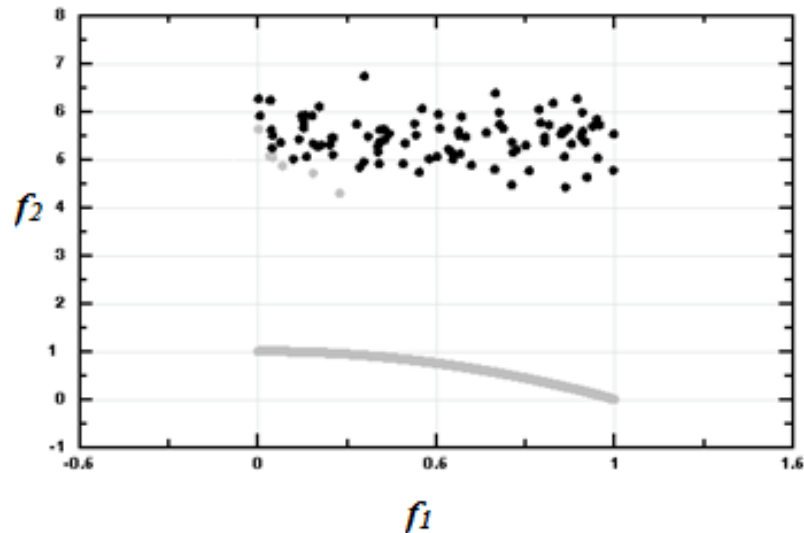


Figure 18: First iteration for the ZDT2 problem - The grey particles are leaders (non-dominated solutions), the black particles are the dominated particles and the grey curve represents the PF.

In order to maintain a sound distribution of particles, especially during the early stages of the search process (i.e., exploration), it is proposed to select leaders in a more representative manner. Let us call these leaders in PSO context *deputies*. The number of deputies is restricted and they should be representative of the swarms by being more diversified (well-distributed). The selection of leaders is done using the classical non-dominance ranking. Thereafter, it is proposed to select deputies using the sum of weighted ratios (SWR) explained in the next section.



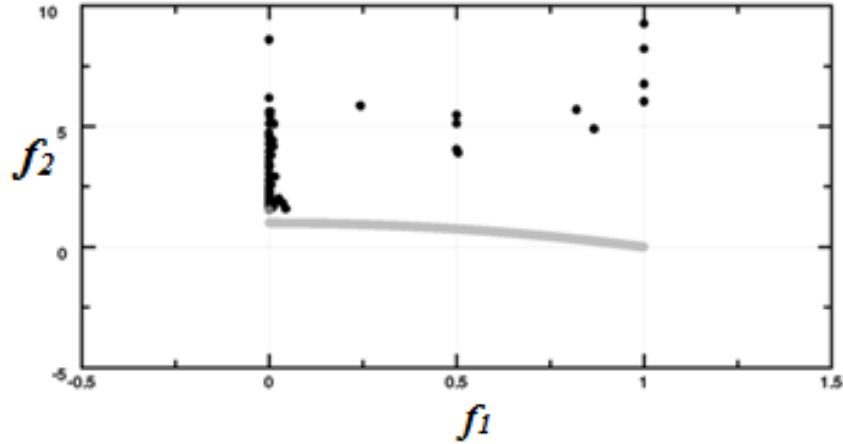


Figure 19: Iteration 15<sup>th</sup> (1500 FCs) for the ZDT2 problem – One grey particle is a leader (non-dominated solution), black markers are the remaining particles (dominated); and the grey line is the PF.

## 5.5 Representative Non-Dominance Concept

The SMPSO archive is the same used by NSGA-II which is commonly utilized by other MOMs. However, the proposed archive selects a more representative number of leaders using SWR, which are then used for the calculation of particle velocity. In SMPSO, in every iteration two leaders are selected randomly. The less crowded between the two leaders is selected for the calculation of the particle velocity. For the proposed LSMPSO algorithm, only the  $p\%$  of the most representative leaders, to be referred as deputy leaders, are selected and used for particles velocity update as described in the next sub-section. Thereafter, in every iteration a deputy leader is selected randomly for the calculation of the particle velocity.

For better clarity, the pseudocode of SMPSO algorithm is given next. As shown in bold, only the calculation of the particles speed has been modified.

## SMPSO Algorithm

```
1: initializeSwarm()
2: initializeLeadersArchive()
3: generation = 0
4: while generation < maxGenerations do
5:   computeSpeed() // MODIFIED
6:   updatePosition() // Eq. 1
7:   mutation() // Turbulence
8:   evaluation()
9:   updateLeadersArchive()
10:  updateParticlesMemory()
11:  generation ++
12: end while
13: returnLeadersArchive()
```

### 5.6 Selection Scheme of Deputy Leaders

The selection of deputy leaders is based on the sum of weighted ratios (SWR). The fitness value of every objective  $f_i$  is converted into a ratio  $r_i$  in  $[0,1]$  range as follows:

$$r_i = \frac{f_i - \min_i}{\max_i - \min_i}, \quad (12)$$

where  $\min_i$  and  $\max_i$  are the minimum and maximum values of the objective  $i$ .

Then, the scaled fitness  $F_x$  of the particle  $x$  is calculated by summing all  $r_i$ s:

$$F_x = \sum_1^D r_{i_x}, i = 1, 2, \dots, D, \quad (13)$$

where  $D$  is the number of objectives, and  $x$  is the current particle for whom  $F_x$  is calculated.

It should be noted that the lower the value of  $F_x$ , the closer is the point to the Pareto front. The lower values are selected rather than the larger among the leaders to promote a good distribution of solutions. The fitness values of extreme points of a Pareto front are usually equal to 1.0. Therefore,  $D$  extreme solutions are always kept among deputy leaders where  $D$  is the number of objectives.

#### Deputies Selection Procedure

```

Begin
maxDeputies=%p * MaxArchiveSize;
i=0;

If (ArchiveSize == 1) // There only one leader
  Deputies=Leaders

Else if (ArchiveSize ≤ maxDeputies) //Nb. leaders < Max. allowed deputies

  For each Leader
    Deputies.add(Leader)
  EndFor

Else ArchiveSize > maxDeputies
  Sort (Leaders) // ascending sorting based on F measure

  While Deputies not full and still Leaders

    If (Leader.F < 1.0 Or Leader.Crowding == Infinity and Leader.F ==1.0 )
      Deputies.add(Leader)
    EndIf

  EndWhile
EndIF

```

In every iteration, before the calculation of the particles' velocity, the SWR of the leaders are calculated. Thereafter, deputy leaders are determined as shown in the upper deputy selection. To

clarify the proposed approach, assume there are eight leaders as described in Table 12 and Figure 20, and the maximum number of deputies allowed is four. The SWR measure is used to select representative deputies: two extreme leaders because the problem has two objectives and two other deputies located in the middle of the PF

Table 12: Example of eight leaders in two-objective space  
In bold are the selected deputies.

Objective 1	Objective 2	F
<b>2.2109</b>	<b>15.989</b>	<b>1.0</b>
3.7248	13.997	0.9681
<b>5.5071</b>	<b>9.3777</b>	<b>0.7640</b>
9.0128	6.2587	0.7997
<b>10.749</b>	<b>4.4470</b>	<b>0.7978</b>
12.0744	3.7935	0.8498
13.6567	3.2865	0.9319
<b>15.4774</b>	<b>2.3427</b>	<b>1.0</b>

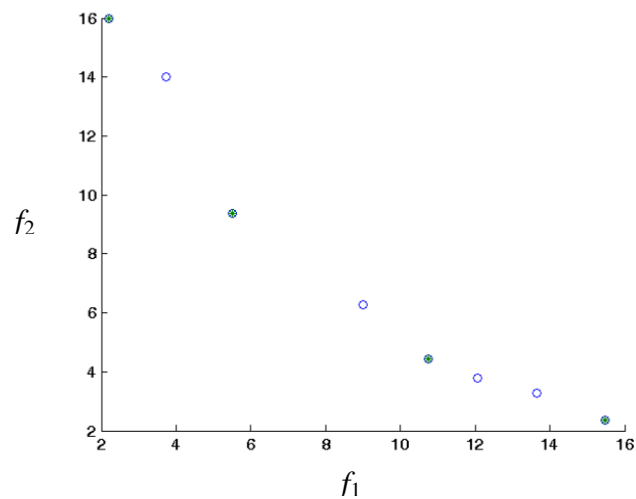


Figure 20: Example of four selected deputies (full particles) based on the SWR measure.

The same leaders are plotted in Figure 20. As shown in bold in Table 12, two leaders having the lowest fitness value and two extreme leaders are selected. These deputies are represented in the graph with plain points whereas the other leaders are represented with empty points. It can be seen that the selected deputies represent well the full spectrum of the leaders. In addition, it can be seen that there is no concentration of leaders in a specific region of the objective space which affects particles distribution.

## 5.7 Experiments Settings

This section describes the settings for the experiments used in this chapter, namely, the description of the used benchmark problems, the compared MOMs with the proposed LSMPSO algorithm, and parameter settings such as population size and stopping criteria.

### 5.7.1 Benchmark problems

Table 13: Utilized bi-objective problems in LSMPSO comparison

<b>Problem</b>	<b>Number Variables</b>	<b>Geometries</b>
ZDT1	30	Convex
ZDT2	30	Concave
ZDT3	30	Convex, disconnected
ZDT4	10	Convex
ZDT6	10	Concave, non-uniformly spaced
DTLZ1	7	Linear
DTLZ2	12	Concave
DTLZ3	12	Concave
DTLZ4	12	Concave
DTLZ5	12	Concave
DTLZ6	12	Concave
DTLZ7	22	Disconnected

As shown in Table 13 two well-known families of problems are used for comparison purposes: the ZDT [33] and the DTLZ [34] family. These two families are the most commonly used ones

and are composed of different PF geometries, namely, convex, concave, disconnected, linear, and non-uniformly spaced. A more detailed description can be found in Tables 35 and 36 (Appendix A).

### 5.7.2 Comparison of LSMPSO with other MOO algorithms

The proposed LSMPSO is compared with seven state-of-the-art MOMs which have been described earlier in Chapter 3. They are briefly presented in Table 14.

Table 14: Algorithms compared with LSMPSO

Algorithm	Type	Inventors	Year
SPEA2	Genetic Algorithm (GA)	Zitzler et al. [28]	2001
NSGA-II	GA	Deb et al. [27]	2002
GDE3	Differential Evolution (DE)	Kukkonen and Lampinen [29]	2005
MOCeII	Cellular GA	Nebro et al. [31]	2007
AbySS	Scatter Search	Nebro et al. [30]	2008
MOEAD	Evolutionary based on Decomposition	Zhang and Li [6]	2008
SMPSO	Particle Swarm Optimization (PSO)	Nebro et al. [32]	2009

### 5.7.3 Parameters settings

The parameters settings are the same for every MO metaheuristic. These parameter settings were taken from [9] and the same as in the comparative study presented in Chapter 3.

NSGA-II, SPEA2, MOCeII, AbySS and GDE3 and MOEA/D have a population size of 100. In the same manner, LSMPSO and SMPSO have a configuration of 100 particles. The metaheuristics having an archive such as NSGA-II, SPEA2 and others, have also a maximum size of 100.

In regards to the number of deputies set for LSMPSO, it is fixed to 10. In other words, only 10% of the maximum archive size can be used as deputies.

Given that the Pareto fronts of the problems used in this study are known beforehand, the algorithms are executed until sufficient approximation of the real Pareto fronts (i.e.  $HVR \geq 98\%$ ) is reached as shown in Figure 21.

Finding the Pareto front might not always be possible for some algorithms depending on the problem's complexity. In other words, some algorithms might perform well with some specific problems, but not able to find the Pareto front for other types of problems, or it might take too long to produce the Pareto front. Consequently, another stopping condition is added by allowing every metaheuristic to perform at most  $10^6$  function evaluations as in [4].

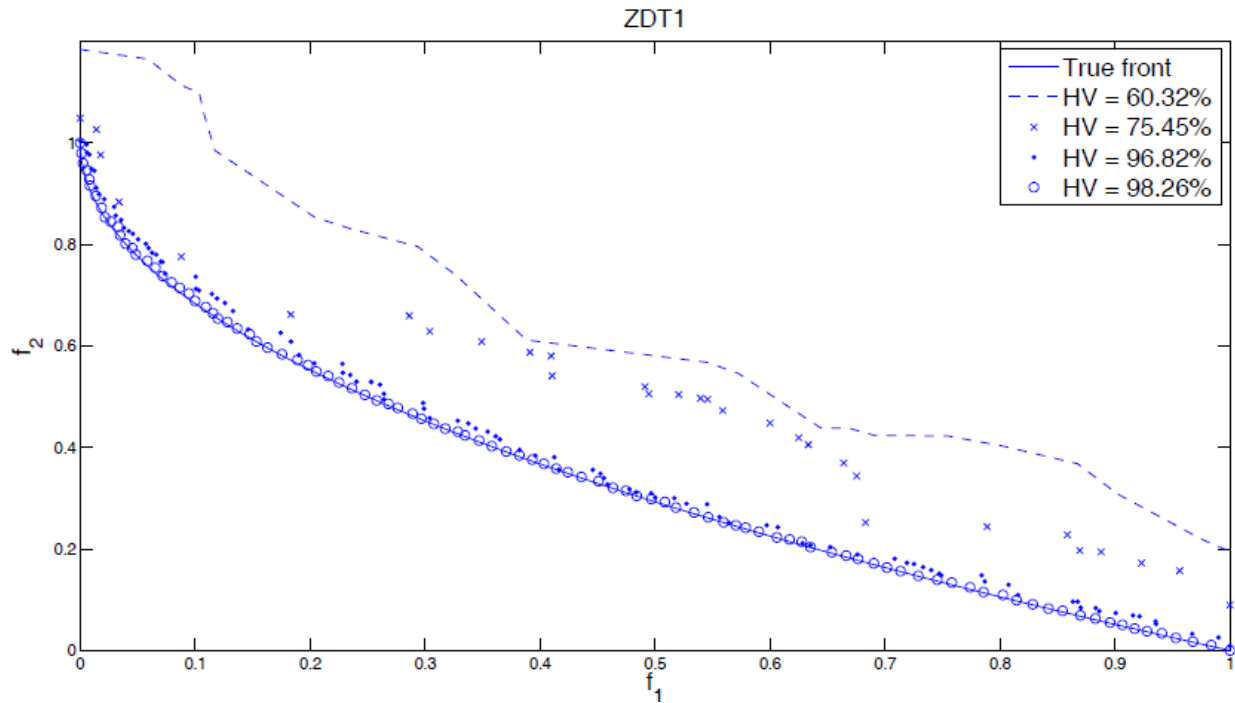


Figure 21: Pareto fronts with different HV values obtained for the ZDT1 problem [3].

## 5.8 Result Analysis

Due to the stochastic nature of metaheuristics, every algorithm was run 100 times independently. The results are reported in Table 15. The dark grey shows the fastest algorithm, while lighter grey shows the second fastest algorithm.

The Wilcoxon statistical test is employed based on [49], to present results at a 0.05 significance level. However, whenever the statistical test does not show a statistical difference between the two fastest algorithms, both of them are ranked first. For example, for the problems ZDT3, ZDT4, ZDT6 and DTLZ1 there was no significant statistical difference between the two fastest algorithms. So, the two fastest MOMs were ranked first for these specific cases.

The hit rate means the number of runs where a MOM was able to find an accurate approximation of the Pareto front ( $HVR \geq 98\%$ ). For example, 100 means an accurate approximation was found 100 out of 100 runs. A lower rate than 100 automatically disqualifies the algorithm from the comparison process for that specific optimization problem.

It can be seen in Table 15 that the proposed algorithm LSMPSO, was on average, the fastest algorithm among all the compared algorithms for 10 out of 12 problems. The LSMPSO was the fastest algorithm for all the ZDT and DTLZ problems except for the DTLZ4 and DTLZ6 problems. In addition, it achieved a hit rate of 100% for all the problems.

When LSMPSO was compared to its parent algorithm the SMPSO, it is found that LSMPSO improved the convergence speed of SMPSO for 7 problems out of 12 namely for ZDT1, ZDT2, ZDT3, DTLZ2, DTLZ3, DTLZ5 and DTLZ7. LSMPSO had the same performance as SMPSO for the three problems ZDT4, ZDT6 and DTLZ1. And LSMPSO achieved a lower performance than SMPSO for only two problems DTLZ4 and DTLZ6. However, it is worth mentioning that SMPSO was not the fastest algorithm for the following two



problems: DTLZ4 and DTLZ6. Overall, LSMPSO improved SMPSO for 58.66% of the problems, they had both the same fastest performance for 25% of the problems, and LSMPSO had a lower performance than SMPSO for 16.33% of the problems. In brief, it can be said that LSMPSO improved the convergence speed of SMPSO algorithm to make it the fastest algorithm while maintaining consistently a high accuracy.

The second performance was achieved by SMPSO. It was the fastest algorithm for three problems namely ZDT4, ZDT6 and DTLZ1 and the second fastest algorithm for six problems, namely, ZDT1, ZDT2, DTLZ3, DTLZ4, DTLZ6 and DTLZ7. SMPSO had a hit rate of 100% for all the problems. So, overall SMPSO offered the second best convergence speed.

The third performance was achieved by GDE3. It was the fastest algorithm only for two problems ZDT3 and DTLZ6. GDE3 had a hit rate of 100% for all the problems. Overall, it had a good performance except for the problems ZDT2, ZDT4 and DTLZ2 where GDE3 had serious difficulties as compared to other fastest algorithms.

Furthermore, only LSMPSO, SMPSO and GDE3 achieved a hit rate of 100% for all the compared problems which demonstrate their consistency in the results as well as the robustness of these three algorithms.

AbYSS comes in fourth position. AbYSS has been the fastest optimization algorithm for the DTLZ4 problem and the second fastest for two problems, namely, DTLZ2 and DTLZ5. However, AbYSS had difficulties with DTLZ6 and especially with DTLZ7 by having a hit rate of only 1%.

Table 15: Median and interquartile range (IQR) of the number of evaluations for reaching the Pareto front ( $HV \geq 98\%$ ). The dark grey area shows the fastest algorithm, while the lighter grey area shows the second fastest algorithm.

	LSMPSO	SPEA2	NSGAI	GDE3	SMPSO	AbYSS	MOCcell	MOEAD
ZDT1	7.40e + 03 <sub>2.3e+03</sub>	1.61e + 04 <sub>9.0e+02</sub>	1.41e + 04 <sub>8.0e+02</sub>	9.60e + 03 <sub>5.0e+02</sub>	9.55e + 03 <sub>2.9e+03</sub>	1.31e + 04 <sub>1.4e+03</sub>	1.30e + 04 <sub>1.0e+03</sub>	5.24e + 04 <sub>6.1e+03</sub>
ZDT2	8.05e + 03 <sub>2.8e+03</sub>	2.46e + 04 <sub>1.7e+03</sub>	2.22e + 04 <sub>1.2e+03</sub>	1.12e + 04 <sub>6.0e+02</sub>	8.90e + 03 <sub>2.8e+03</sub>	1.71e + 04 <sub>2.7e+03</sub>	1.53e + 04 <sub>6.0e+03</sub>	7.03e + 04 <sub>9.1e+03</sub>
ZDT3	1.05e + 04 <sub>3.0e+03</sub>	1.54e + 04 <sub>1.2e+03</sub>	1.27e + 04 <sub>1.2e+03</sub>	1.02e + 04 <sub>5.0e+02</sub>	1.33e + 04 <sub>4.4e+03</sub>	1.24e + 04 <sub>2.5e+03</sub>	1.28e + 04 <sub>1.2e+03</sub>	5.60e + 04 <sub>6.4e+03</sub>
ZDT4	4.95e + 03 <sub>1.6e+03</sub>	2.60e + 04 <sub>4.8e+03</sub>	2.19e + 04 <sub>5.1e+03</sub>	1.63e + 04 <sub>9.0e+02</sub>	4.95e + 03 <sub>1.3e+03</sub>	2.10e + 04 <sub>9.7e+03</sub>	1.67e + 04 <sub>5.2e+03</sub>	7.06e + 04 <sub>1.3e+04</sub>
ZDT6	3.95e + 03 <sub>1.8e+03</sub>	3.33e + 04 <sub>1.2e+03</sub>	2.84e + 04 <sub>1.3e+03</sub>	4.50e + 03 <sub>7.0e+02</sub>	4.40e + 03 <sub>2.2e+03</sub>	1.54e + 04 <sub>1.2e+03</sub>	2.16e + 04 <sub>1.2e+03</sub>	2.00e + 04 <sub>8.1e+03</sub>
DTLZ1	5.70e + 03 <sub>2.0e+03</sub>	2.53e + 04 <sub>7.1e+03</sub>	2.56e + 04 <sub>8.4e+03</sub>	1.03e + 04 <sub>6.0e+02</sub>	5.90e + 03 <sub>2.6e+03</sub>	2.64e + 04 <sub>1.4e+04</sub>	1.99e + 04 <sub>6.2e+03</sub>	2.71e + 04 <sub>1.5e+04</sub>
DTLZ2	2.80e + 03 <sub>7.5e+02</sub>	7.20e + 03 <sub>8.0e+02</sub>	6.70e + 03 <sub>8.5e+02</sub>	6.40e + 03 <sub>3.5e+02</sub>	5.30e + 03 <sub>2.0e+03</sub>	4.69e + 03 <sub>8.0e+02</sub>	5.90e + 03 <sub>9.0e+02</sub>	9.70e + 03 <sub>1.0e+03</sub>
DTLZ3	8.55e + 03 <sub>1.4e+04</sub>	1.01e + 05 <sub>4.3e+04</sub>	1.09e + 05 <sub>4.4e+04</sub>	2.24e + 04 <sub>1.5e+03</sub>	1.15e + 04 <sub>2.9e+04</sub>	1.23e + 05 <sub>6.2e+04</sub>	6.69e + 04 <sub>2.2e+04</sub>	1.17e + 05 <sub>5.9e+04</sub>
DTLZ4	1.01e + 04 <sub>3.0e+03</sub>	7.80e + 03 <sub>2.4e+05</sub>	7.30e + 03 <sub>1.2e+03</sub>	8.05e + 03 <sub>1.3e+03</sub>	5.75e + 03 <sub>1.5e+03</sub>	4.80e + 03 <sub>8.1e+02</sub>	1.00e + 06 <sub>9.9e+05</sub>	1.46e + 04 <sub>2.1e+03</sub>
DTLZ5	2.85e + 03 <sub>8.5e+02</sub>	7.40e + 03 <sub>8.0e+02</sub>	6.70e + 03 <sub>8.5e+02</sub>	6.30e + 03 <sub>3.0e+02</sub>	5.15e + 03 <sub>1.9e+03</sub>	4.56e + 03 <sub>8.6e+02</sub>	5.70e + 03 <sub>9.0e+02</sub>	9.80e + 03 <sub>1.0e+03</sub>
DTLZ6	2.02e + 04 <sub>9.6e+03</sub>	2.50e + 05 <sub>2.2e+05</sub>	2.50e + 05 <sub>2.2e+05</sub>	3.70e + 03 <sub>2.0e+02</sub>	9.15e + 03 <sub>3.9e+03</sub>	1.00e + 06 <sub>2.0e+01</sub>	1.00e + 06 <sub>0.0e+00</sub>	9.50e + 03 <sub>1.8e+03</sub>
DTLZ7	5.75e + 03 <sub>1.5e+03</sub>	1.69e + 04 <sub>1.1e+03</sub>	1.38e + 04 <sub>1.0e+03</sub>	8.50e + 03 <sub>5.0e+02</sub>	6.80e + 03 <sub>2.3e+03</sub>	1.07e + 04 <sub>1.8e+03</sub>	1.17e + 04 <sub>1.6e+03</sub>	4.58e + 04 <sub>2.8e+05</sub>

Table 16: Average hit rate of the compared MO optimization algorithms.  
 In bold are low hit rate (low accuracy)

	LSMPSO	SPEA2	NSGAII	GDE3	SMP SO	AbYSS	MOCeII	MOEAD
ZDT1	100	100	100	100	100	100	100	100
ZDT2	100	100	100	100	100	100	100	100
ZDT3	100	100	100	100	100	100	100	100
ZDT4	100	100	100	100	100	100	100	100
ZDT6	100	100	100	100	100	100	100	100
DTLZ1	100	100	100	100	100	100	100	100
DTLZ2	100	100	100	100	100	100	100	100
DTLZ3	100	100	100	100	100	100	100	100
DTLZ4	100	<b>72</b>	<b>82</b>	100	100	100	<b>44</b>	100
DTLZ5	100	100	100	100	100	100	100	100
DTLZ6	100	<b>48</b>	<b>34</b>	100	100	<b>1</b>	<b>9</b>	100
DTLZ7	100	100	100	100	100	<b>82</b>	<b>88</b>	<b>76</b>

In order to rank the remaining multi-objective optimization algorithms, boxplots [26] are used. The boxplots allow a graphical analysis of the found solutions and show the consistency of the results by examining the IQR visually.

In boxplots the conducted experiments are compiled respectively in Figure 22 for the ZDT family problems and in Figure 23 for the DTLZ family problems. It can be seen from the boxplots that MOCeII achieves usually the fourth performance most of the time, followed by NSGA-II, followed by SPEA2, then finally by MOEA/D. As shown in Table 16, it is worth

mentioning that MOEA/D achieved a low hit rate only for one problem whereas the NSGA-II and SPEA2 algorithms achieved a low rate for two problems and MOCcell achieved a low rate for three problems.

By examining the boxplots, another interesting observation is that the proposed algorithm, LSMPSO, offered a consistent performance which for most of the time is better than its parent algorithm SMPSO. However, GDE3 achieved the highest consistency in the results. It might be interesting to analyze why GDE3 has a higher consistency in comparison with the other algorithms. Thus, LSMPSO could be further enhanced not only to be the fastest one but also to provide more consistent results.

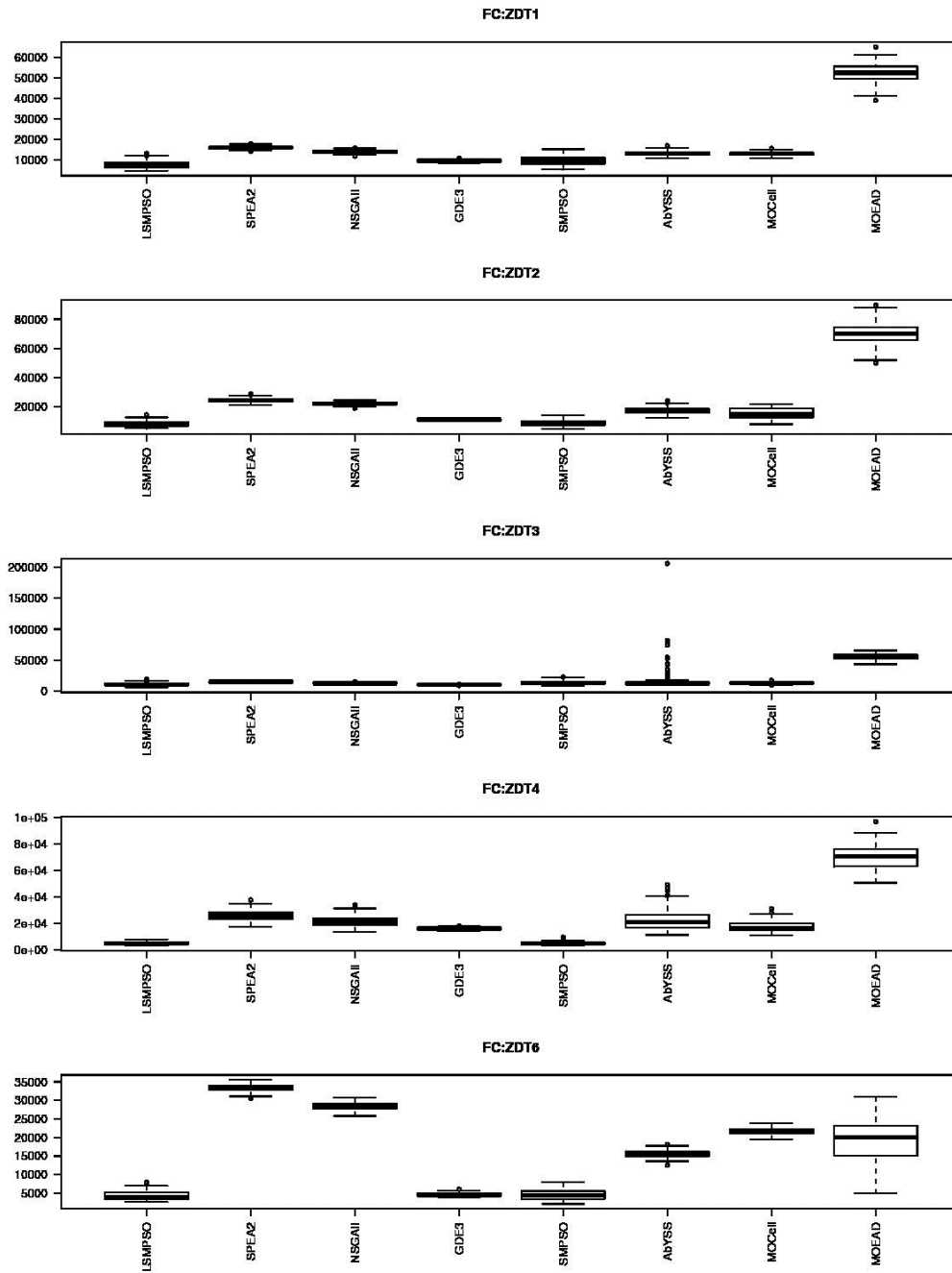


Figure 22: Boxplots of the number of function evaluations to find the real Pareto front for the ZDT bi-objective problems.

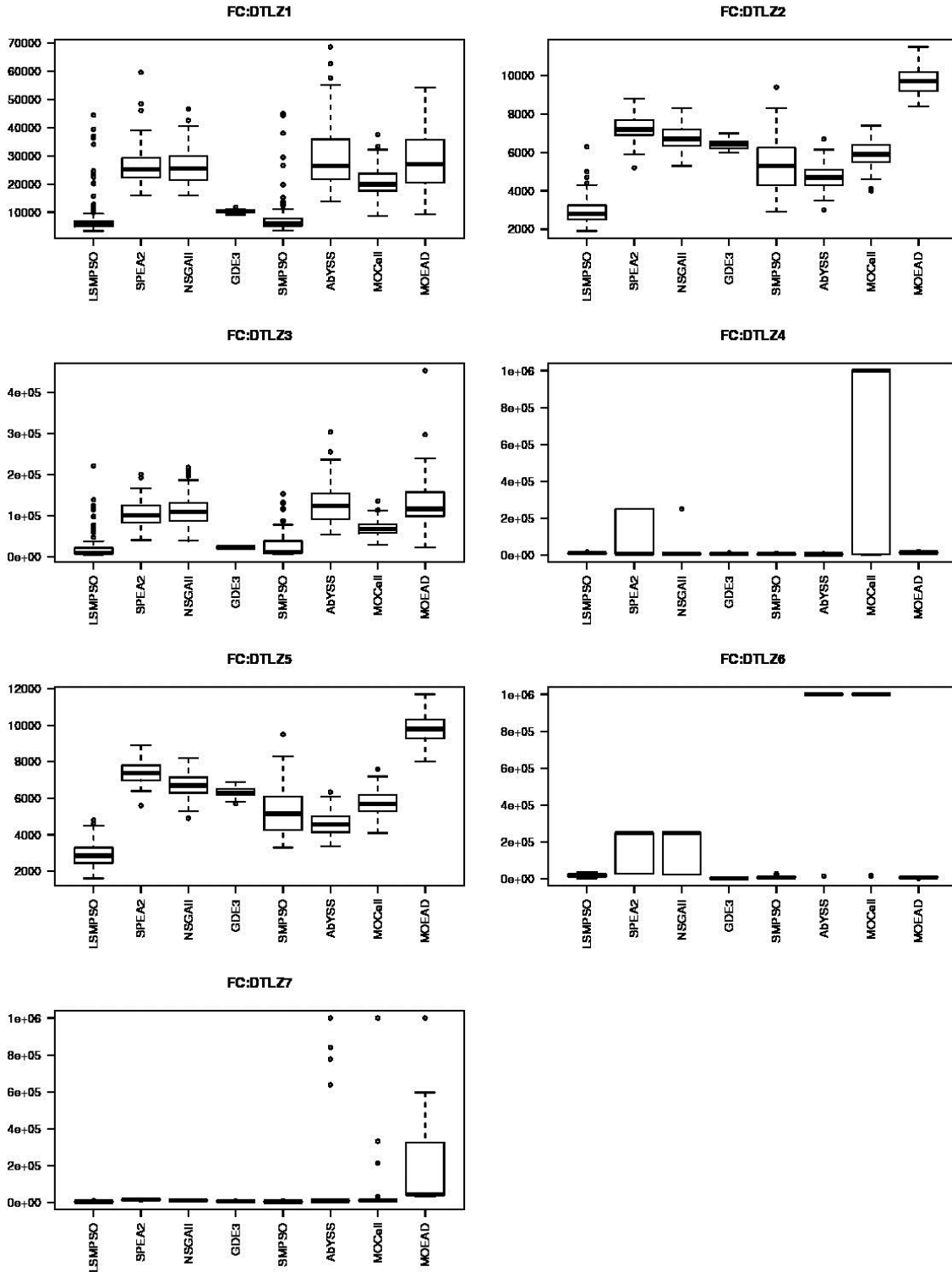


Figure 23: Boxplots of the number of function evaluations to find the real Pareto front for the DTLZ bi-objective problems

## 5.9 Summary

This chapter proposed an enhanced variant of multi-objective particle swarm optimization in order to accelerate its convergence speed. The proposed algorithm called LSMPSO incorporated a restriction mechanism on the leaders that are used for particle velocity calculation. Only the  $p\%$  most representative leaders, called deputies, are selected using the SWR algorithm, for the particle velocity calculation. The proposed algorithm LSMPSO was compared to seven state-of-the-art metaheuristics, namely, NSGA-II, SPEA2, GDE3, SMPSO, AbYSS, MOCell and MOEA/D using the ZDT and DTLZ family problems. The convergence speed of these algorithms was compared by counting the number of function evaluations required to find an accurate approximate of the Pareto front ( $HV \geq 98\%$ ) with a maximum of  $10^6$  function evaluations allowed.

The proposed LSMPSO algorithm was overall the fastest algorithm to find an accurate approximation of the Pareto front for 10 out of 12 studied problems. In addition to its high convergence speed, LSMPSO achieved a hit rate of 100% for all the studied problems.

In future work, we would like to study the proposed selection method on other multi-objective metaheuristics. Also, it is proposed to utilize the proposed LSMPSO to solve a real MOP. In the next chapter, LSMPSO performance is compared with other MOMs to solve a photovoltaic farm design.

## **Chapter 6**

### **Case Study I: Optimal Photovoltaic System Design**

#### **Using LSMPSO**



It was found in the survey of optimal design of RESs presented in Chapter 4 that most MOPs related to RESs did not use recent state-of-the-art metaheuristics; there is a gap between the research communities of MOMs and RESs. This chapter tries to bridge between the two research communities by using state-of-the-art MOMs. In addition, this chapter serves to demonstrate the use of the proposed LSMPSO method presented in the previous chapter and compares it with four other MOMs to solve a MO photovoltaic farm design problem.

## **6.1 Introduction**

Recently, several parts of the world suffered from electrical black-outs due to high electrical demands during peak hours. Stationary photovoltaic (PV) collector arrays produce clean and sustainable energy, especially if sunny, which is usually during peak hours. In addition, PVs do not emit any waste or emissions except during their production or disposal, and are silent in operation. The incident energy collected by PVs is mainly dependent on the number of collector rows, distance between collector rows, dimension of collectors, collectors angle of inclination, and collectors azimuth, which are all involved in the proposed modeling in this chapter. The objective is to achieve optimal design of a PV farm yielding two conflicting objectives, namely, maximum field incident energy and minimum cost of deployment. The proposed LSMPSO algorithm is compared with four state-of-the-art multi-objective evolutionary algorithms MOMs namely, GDE3, MOCcell, AbYSS, and SMPSO to solve a PV farm design problem in Toronto, Canada area. These four algorithms have been selected because they showed the highest accuracy with identical experiment settings in the comparative study presented in Chapter 3. Simulation results are presented and discussed to illustrate the advantage of utilizing MOMs in PV farms design and other energy related real-world problems.

Solar energy systems are popular renewable energy systems because they are emission free and easily deployable. Multiple sun-based energy systems exist such as photovoltaic collectors (PV), concentrated solar power plants, and solar thermal electricity plants. These systems can be used for meeting the global energy crisis due to rising world-wide demands and insufficient supply of electricity throughout the world by deploying the appropriate systems in the required areas. For example, PV systems are inefficient in very hot areas, such as desert, but are more efficient in mild to cold areas. In this chapter, PV panels are selected because of mild-cold weather conditions in the area of Toronto, Canada. Although Canada produces enough electricity to fulfill the national demand, nevertheless solar energy is of special interest due to PV non-polluting properties.

There are several solar-related energy systems. Concentrated solar systems like the parabolic trough heat transfer fluid/steam systems can typically generate full rated electrical output for 10-12 hours a day [144]. Other solar power generation systems include large solar updraft towers which can produce large amounts of electricity via utilizing air flow created by heated air which drives pressure staged turbines [145].

In spite of the above available large-scale technologies, photovoltaic panels are the most popular method for harvesting solar energy, because they directly convert the Sun's rays into electrical power. In addition, photovoltaic panels can be deployed anywhere and can provide a relatively stable electrical output. However, there are several drawbacks; they are subject to changing output efficiencies based on external factors such as shade, cloudy weather, covered by sands, and others.

There are two types of solar radiations on the Earth: direct and diffuse radiation. The sunlight is filtered through the Earth's atmosphere. The solar radiation is received directly from

the Sun without having been dispersed by the atmosphere is called *direct* radiation. When the sun's radiation is changed by the atmosphere due to clouds, water vapour, and other molecules, it is called *diffuse* radiation. Therefore energy absorbed by the PV panels is the sum of the amount of direct and diffuse radiations received in a given day.

In this case study, comparison is made between LSMPSO and the four fastest and most accurate found MOMs in the previous comparative study, namely, GDE3, MOCcell, AbYSS and SMPSO, to optimize the deployment of solar PV farms.

The objective is to maximize the total incident solar energy and minimize the cost of PV panel deployment in a specific field. As in [146] and [5] the cost was limited to initial investment because the papers focused only on the PV configuration setup. However, a real PV farm requires overhead costs such as maintenance costs, residual fees, and energy storage component fee. Six decision variables compose the optimization problem, namely, the number of collector rows, the distance among collector rows, the dimension of collectors, the collectors inclination angle, the collectors azimuth angle, and collector's clearance above ground.

## **6.2 Related Works**

This section presents the most recent optimization works applied to design of solar energy systems.

Varun [147] implemented a genetic algorithm for maximizing the thermal performance of flat plate solar air heaters to optimize various systems, and operating parameters. The basic values like number of glass covers, Irradiance and Reynolds, plate tilt angle, and emissivity of plate are optimized for maximizing thermal performance.

Thiaux et al. [148] applied the NSGA-II algorithm to optimize the load profile impact on stand-alone photovoltaic system gross energy requirement. Yang et al. [149] developed a hybrid

optimized solar-wind system. They optimized the components' capacity sizes of hybrid solar-wind power generation systems which employs a battery tank. Chang [150] attempted to maximize the electrical energy output of photovoltaic modules using a hybrid heuristic method. They combined PSO with nonlinear time-varying evolution to determine the optimal tilt angle of the modules.

Recently, Deb et al. [40] have attempted to solve a four-objective optimization model of a solar thermal power plant operation system. The four objectives were profit, total investment costs, internal rate of return, and pollution. First, they have used clustered NSGA-II algorithm to find set of trade-off solutions over the entire Pareto-optimal front. Then, they used a reference point based on Multiple Criterion Decision Making (MCDM) approach with the clustered NSGA-II to find preferred solutions on some parts of the Pareto-optimal front. They have demonstrated the benefits of using multi-objective optimization procedure with user decision making interaction to find a single preferred solution.

In a related study, the shading among solar panels was modeled and a simulation-based algorithm was developed to predict the loss of energy due to shade in three individual locations in Arizona [151]. Myers et al. [152] have proposed and simulated a theoretical solar cell by using a modified genetic optimization algorithm for shaping solar cells. The result of the optimization process is a 3D shape which fits within the area and volume of a conventional solar cell but it is drastically more efficient than regular rectangular shapes.

O. Ekren and Y. Ekren [153] have used simulation and single-solution based metaheuristic algorithm, called simulated annealing (SA), for optimizing the size of a PV-wind integrated hybrid energy system with battery storage. The objective was to minimize of the hybrid energy system's total cost. They have demonstrated that the optimum result obtained by

the SA algorithm showed a 10.13% improvement on the objective value as compared to their simulation model.

Appelbaum and Weinstock [154] worked on electrical output maximization for photovoltaic by concentrating on shading and spacing issues. They used Sequential Quadratic Programming for optimization. More recently, they [155] added the azimuth angle of a solar panel as variable to the problem. However, the variable is manipulated in a manual fashion, the system is optimized automatically. They reached 12% enhancement for a small scale photovoltaic array by reducing the amount of shading in order to increase the efficiency of array. Bourennani et al. [156] utilized Differential Evolution (DE) and simulation-based optimization methods to compare the maximum annual incident energy captured by solar collectors. The captured energy was close to the simulation approach and DE algorithm. This problem has been converted into a MOP and GDE3 and NSGA-II MOMs have been used to solve it [157]. NSGA-II showed more accurate results than GDE3.

### **6.3 Physical System Model**

The modelling of this case study is taken from our previous work in [157]; however, several additional algorithms have been tested, the PF has been generated and a more objective evaluation measure (IGD) has been utilized for comparison purposes. There has been a very limited use of multi-objective optimization methods in PV field. Thiaux et al. [148] used MO but they focused on the optimization of the entire solar farm assuming a certain static setup whereas this work focuses on the setup of PV panels which is composed of six decision variables namely, the number of collector rows (a discrete variable), distance among the collector rows, the inclination of the PV panels, the height of a PV panel, collector's azimuth due south, and collector's clearance above ground. Five MOMs are compared to solve this problem, namely

LSMPSO, SMP SO, GDE3, AbYSS and MOCe ll. The results are compared and discussed in detail in Section 6.4.

The model to be optimized is composed of stationary PV panels. The objective is to capture the maximum solar radiation with minimal cost investment. The PV collectors are fixed in the field as shown in Figure 24. As it can be seen, the collectors are inclined at an angle  $\beta$  facing roughly the south because they are located in the north hemisphere of the globe. The dimension of the collectors is referred as length  $L$  and as height  $H$ . The length of the collectors is fixed  $L$  and is equal to the length of the field whereas the width of field is  $W$ . There should be a minimum clearance of  $E$  above the ground to minimize the accumulation of dust, debris, or snow on the collectors.

### 6.3.1 Solar collector model

Collector maintenance requires the height above the ground  $E$  to be limited. The minimum distance  $D$  between two rows is limited to allow easy access between PV panels. Moreover, the height  $H$  of the collectors themselves is constrained by the manufacturer [154] [155]. Thus,

$$H' + E \leq A_{max}, \quad (14)$$

$$H \leq H_{max}, \quad (15)$$

where  $H' = H \sin \beta$ .

The configuration factors for un-shaded and shaded collectors are given by as follow, respectively:

$$F_d = \cos^2 \left( \frac{\beta}{2} \right), \quad (16)$$

$$F_d^{sh} = F_d - \left[ (d^2 + 1)^{\frac{1}{2}} - d \right] \sin \beta, \quad (17)$$

where  $d$  is the normalized distance between two rows given by  $d = D/H'$ .

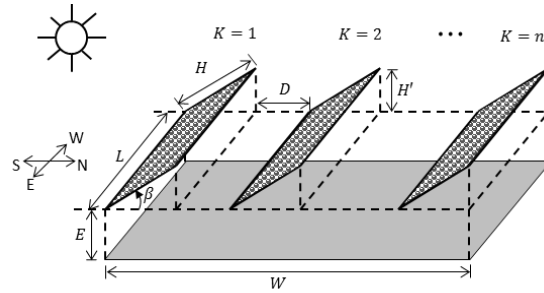


Figure 24: Collectors arrangement in a stationary solar field, K indicates row number, L indicates length of PV, W indicates the width of the solar field, D indicates the distance between collector rows,  $\beta$  indicates PVs' inclination angle, and  $H'$  indicates the perpendicular distance created by the PVs.

The angle of incidence  $\theta$  is the angle between a normal to the collector face and the incoming solar beam, it depends on the solar angles (altitude and azimuth) and collector angles (azimuth and tilt, Figure 25).

$$\cos \theta = \cos(\beta) \sin(\alpha) + \sin(\beta) \cos(\alpha) \cos(\gamma) \quad (18)$$

where  $\alpha$  is the sun elevation angle;  $\beta$  is the collector inclination angle and  $\gamma = \gamma_s - \gamma_c$  is the difference between the sun and collector azimuth with respect to south.

The relative shaded area is calculated as follows:

$$a_s = \frac{l_s}{L} \times \frac{h_s}{H} \quad (19)$$

where,

$$l_s = 1 - \frac{d \sin\beta + \cos\beta}{l} \times \frac{|\sin\gamma|}{\cos\beta \sin\alpha + \sin\beta \cos\gamma} \quad (20)$$

and

$$h_s = \frac{d \sin\beta + \cos\beta}{\cos\beta + \frac{\sin\beta \cos\gamma}{\tan\alpha}} \quad (21)$$

$l = L/H'$  is the normalized collector length.

The yearly direct ( $q_b$ ) and diffuse ( $q_d$ ) beam irradiances per unit area of an un-shaded collector (first row) are calculated as follows:

$$q_b = \sum_{n=1}^{n=365} \sum_{T_R}^{T_S} G_b \cos\theta \Delta T \quad (22)$$

and

$$q_d = F_d \sum_{n=1}^{n=365} \sum_{T_R}^{T_S} G_{dh} \Delta T \quad (23)$$



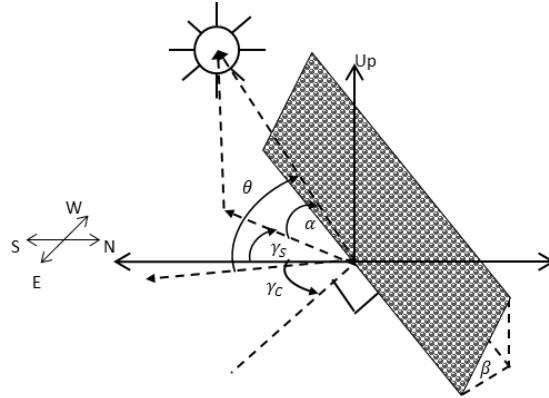


Figure 25. Angle of incidence  $\theta$ : angle between a normal to the collector face and the incoming solar beam.

The average yearly direct ( $q_b^{sh}$ ) and diffuse ( $q_d^{sh}$ ) beam irradiances per unit area of an un-shaded collector ( $(K - 1)$  row) are given by:

$$q_b^{sh} = \sum_{n=1}^{n=365} \sum_{T_R}^{T_S} G_b \cos \theta (1 - a_s) \Delta T, \quad (24)$$

and

$$q_d^{sh} = F_d^{sh} \sum_{n=1}^{n=365} \sum_{T_{SR}}^{T_{SS}} G_{dh} \Delta T, \quad (25)$$

where  $\Delta T$  is the summation time interval from sun rise  $T_R$  to sunset  $T_S$  on the collector for the beam irradiance, and from sun rise  $T_{SR}$  to sun set  $T_{SS}$  for the diffuse irradiance. The outer

summation represents one year term from January 1<sup>st</sup> ( $n = 1$ ) to December 31<sup>st</sup> ( $n = 365$ ). Figure 26 shows the sixth decision variable ( $\gamma_C$ ); collectors azimuth with respect to the south and limited to  $[-45^\circ, 45^\circ]$ .

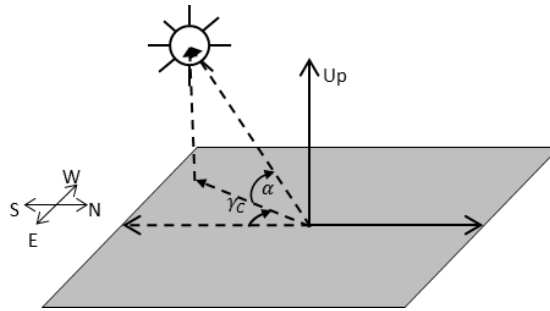


Figure 26: Collector azimuth with respect to south ( $\gamma_C$ ).

### 6.3.2 System complexities

The current multi-objective optimization PV farm design is composed of several complexities that make it hard to solve. It is composed of mixed-type integer (number of PV collector rows) and continuous variables. The first objective is multimodal because it encompasses trigonometric functions which are hard to solve. The Pareto front geometry is linear. Some variables take widely different ranges of values, thereby making it difficult for the solvers to provide adequate emphasis to correct variable combinations.

Despite the existence of only six variables (6D), this problem exhibits a wide and non-uniform range of variable values. In addition, the non-dominated solutions' variables are composed of other complexities which are a) non-extremal, b) non-medial, having c) dissimilar parameter domains, and d) many-to-one mappings which make the problem more complicated to solve [35].

Dissimilar parameter domains consists of variables with heterogeneous parameters bounds; for example, the heterogeneous domains of height and inclination angle are defined respectively as follows  $0.2 \leq H \leq 2$  and  $0^\circ \leq \beta \leq 90^\circ$ .

Non-extremal and non-medial means the variables are neither located in the extreme nor middle of parameter domains. For example,  $H \neq 0.2$ ,  $H \neq 2$  and  $H \neq 0.9$  (middle).

Many-to-one mappings imply that different combination of parameters can generate exactly the same solutions (same fitness values). For example, two similar solutions on the PF have completely different parameter settings. One solution has six rows of PV panels with small dimensions, and another solution can have only two rows with very large panel dimensions. Both cases result roughly in the same cost and energy generation.

### **6.3.3 Objectives, variables, and constraints**

As mentioned previously, the PV design optimization problem is composed of two objectives, six variables, and two constraints. A final optimal solution is composed of the following variables: the number of collector rows, distance between collector rows, dimension of collectors, collectors inclination angle, and collectors azimuth angle. The objectives, constraints, and variable domains are described in Equations 26-35.

The two objectives are the maximization of incident energy and minimization of the installation and material cost.

- 1) Incident energy: the yearly absorbed incident energy should be maximized in order to generate the maximum possible electricity.
- 2) Cost: the cost of PV array collectors installation should be as low as possible.

The mathematical formulation of the optimization problem is defined as follows:

$$\max Q = K \times L \times [q_b + q_d + (K - 1)(q_b^{sh} + q_d^{sh})], \quad (26)$$

$$\min C = K \times L \times H \times P, \quad (27)$$

s. t.

$$K \times H \times \cos\beta + (K - 1) \times D \leq W, \quad (28)$$

$$H + E \leq A_{max}, \quad (29)$$

Variable bounds:

$$2 \leq K \leq 10 \quad (30)$$

$$0.2 \leq H \leq 2 \quad (31)$$

$$0^\circ \leq \beta \leq 90^\circ \quad (32)$$

$$0.8 \leq D \leq 2.5 \quad (33)$$

$$-45^\circ \leq \gamma_c \leq 45^\circ \quad (34)$$

$$0.5 \leq E \leq 2 \quad (35)$$

Where:

$$K \in Z^+$$

$$H, \beta, D, \gamma, E \in R$$

- $P$  is the price of PV panel per square meter.
- $q_b$  is the yearly beam irradiation per unit area of an un-shaded collector (first row).
- $q_d$  is the yearly diffuse irradiation per unit area of an un-shaded collector (first row).
- $q_b^{sh}$  is the average yearly beam irradiation per unit area of shaded collectors ( $n - 1$  rows).
- $q_d^{sh}$  is the average yearly diffuse irradiation per unit area of shaded collectors ( $n - 1$  rows).

### **6.3.4 Climate information**

The location selected for all the simulations is Toronto, Ontario, Canada (Latitude  $43.45^{\circ}$ / Longitude  $-79.25^{\circ}$ ). Table 48 (Appendix B), show 30 years of monthly averaged hourly direct normal beam irradiance and horizontal diffuse irradiance in  $\text{KWh/m}^2$  [158]. These datasets were generated by joining twelve Typical Meteorological Months taken from a database of 30 years of Canadian Weather Energy and Engineering Datasets (CWEEDS) data. Table 49 (Appendix B) shows the monthly average hourly diffuse irradiance (used in equations 9 to 12) and Table 51 (Appendix B) shows 22 years monthly average hourly solar angles relative to the horizon, and Table 50 (Appendix B) solar azimuth angles due south in degrees (used in Equations 12 and 14). The solar datasets were taken from the NASA GEOS-4 [159].

### **6.3.5 PV panel specification**

There are numerous types of PV panels in the market. PV panels are priced based on their electrical characteristics (Rated power, Voltage, Current, Module efficiency, Short-circuit current, Open-circuit voltage, Maximum series fuse rating, Maximum system voltage) and mechanical characteristics (Dimensions, Weight, Frame, number of Solar Cells). In this case study, Ameresco Solar BP 90 Watt has been used, 12V solar panel priced at  $\$616.59/\text{m}^2$  [160]. Please note that even though this specific solar panel was utilized for the experiments, the solution outcome would not necessarily be affected if other panels are used. Overall, the current PV panels' average price in Ontario is  $\$4.50$  per Kwh including all installation fees and required material.

## 6.4 Experimental simulations

The parameter settings of the compared MOMs are the same as in the presented comparative study (Section 3.5.2). Due to the stochastic nature of MOMs, they were executed 100 times independently. The stopping criterion for all the algorithms was set to  $10^4$  function evaluations. Their best and median solutions were compared graphically. In addition, the inverse generational distance (IGD) [23] measure was used for complementarity; the Wilcoxon statistical procedure was used to present the IGD results at a 0.05 significance level. In order to generate the IGD measure, the solution needs to be known beforehand. Therefore, all the algorithms have been executed for  $10^6$  function evaluations several times; then, all the combined non-dominated solutions have been used to establish an approximation of the Pareto front which is linear and described as follows:

$$y = -0.4476x - 212.63, \quad (36)$$

where  $x$  is the first objective and  $y$  is the second objective,  $x \in [2096.86, 206820.5]$ ,  $y \in [725.93, 92360.22]$ .

The synthetic solutions have been generated in such a way to be well distributed and equidistant from each other in the objective space.

## 6.5 Discussion of the results

The results can be divided into two groups. The first group is composed of GDE3, MOCell and AbYSS. They roughly found half of the Pareto front as shown respectively in Figure 27, 28, and 29. The second group detected the full Pareto front and is composed of SMPSO and the proposed LSMPSO as shown in Figure 30 and 31. It is obvious that the second group generated more

accurate solutions than the first. The performance of the first group of algorithms over the second is confirmed by the respective compilation of the 100 runs in Tables 17 and 18. The mean and standard deviation of LSMPSO and SMPSO are clearly superior to GDE3, MOCcell, and AbYSS. And, the results of LSMPSO and SMPSO have a high similarity to pass the statistical validation. Therefore LSMPSO and SMPSO are declared as equally the most accurate.

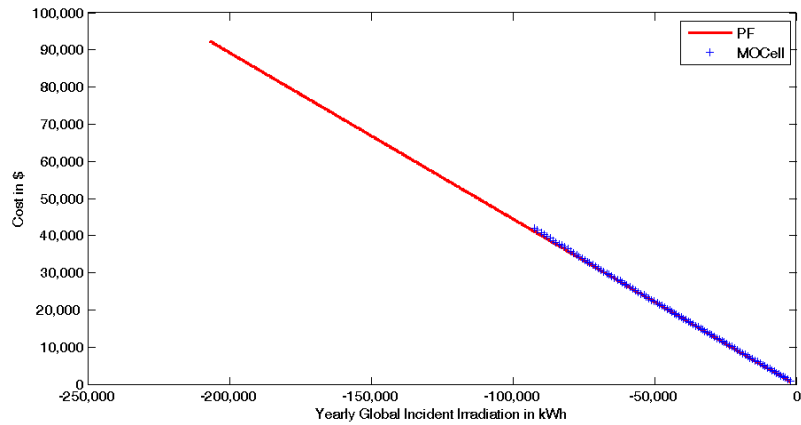


Figure 27: Median (IGD) solutions found by MOCcell

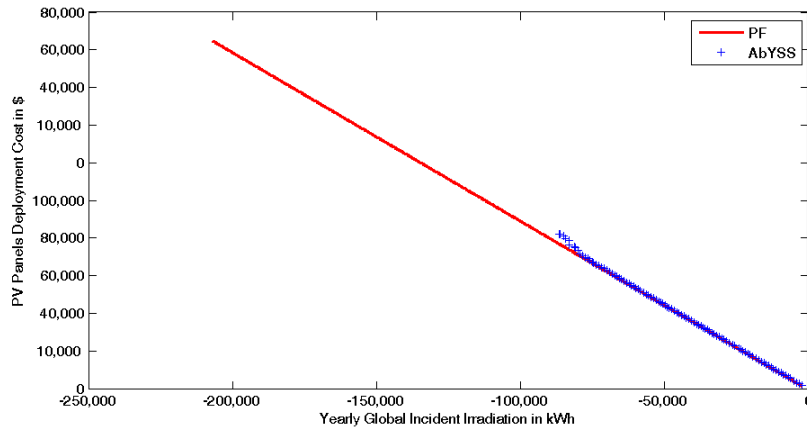


Figure 28: Median (IGD) solutions found by AbYSS

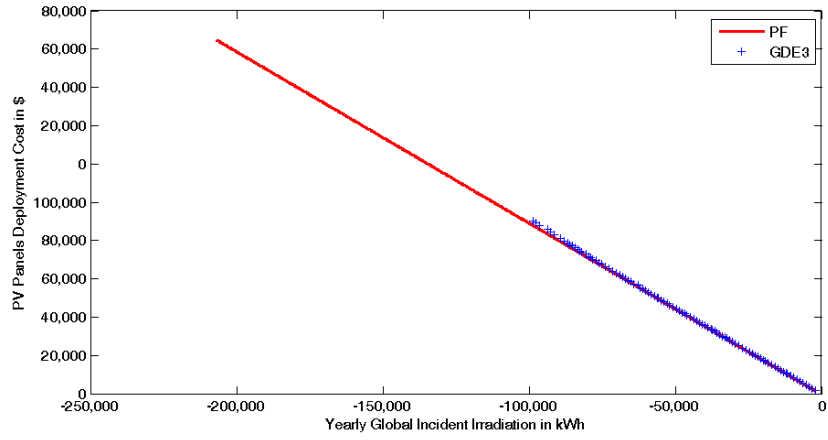


Figure 29: Median (IGD) Solutions found by GDE3

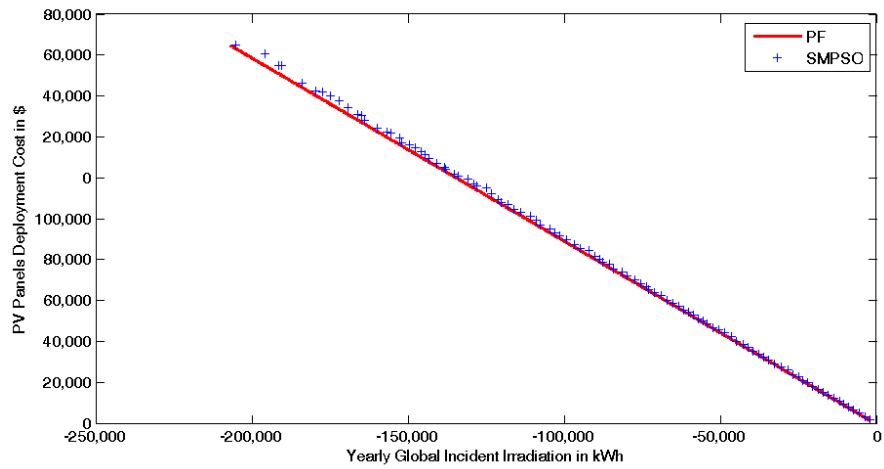


Figure 30: Median (IGD) Solutions found by SMPSO



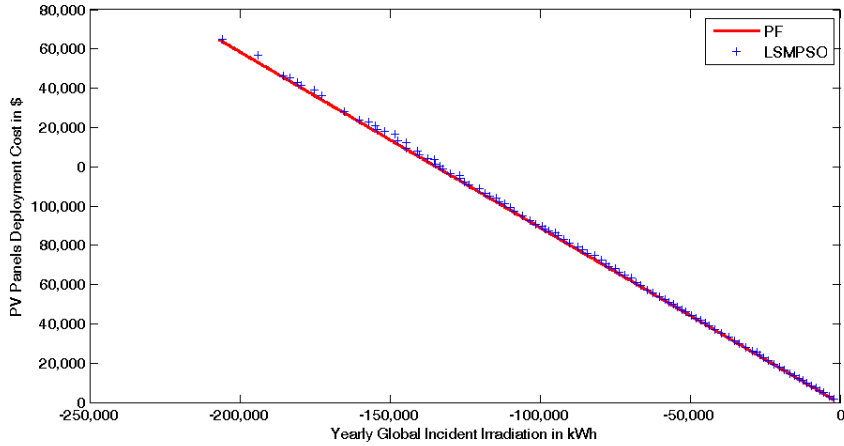


Figure 31: Median (IGD) solutions found by LSMPSO

The boxplots of the 100 runs are presented in Figure 32. It can be seen again that LSMPSO and SMPSO occupy the first position and have both similar accuracy with a high consistency which is confirmed by a low standard deviation. The second position is occupied by GDE3, followed by MoCell and AbYSS.

It is important to mention that the proposed LSMPSO achieved a lower IGD median and a lower IQR than SMPSO but not sufficient to pass the Wilcoxon statistical test. In addition, the lowest IGD among all the compared MOMs is achieved by LSMPSO, the details of the solutions are shown in Table 52 in Appendix B.

Table 17: IGD mean and standard deviation

	LSMPSO	GDE3	MoCell	AbYSS	SMP SO
PV	$3.42e-04_{1.0e-04}$	$1.03-02_{7.9e-04}$	$1.11-02_{1.2e-03}$	$1.13-02_{1.3e-03}$	$3.42e-04_{1.1e-04}$

Table 18: IGD median and IQR

	LSMPSO	GDE3	MoCell	AbYSS	SMP SO
PV	$3.26e-04_{1.3e-04}$	$1.02-02_{9.0e-04}$	$1.07-02_{2.1e-03}$	$1.14-02_{2.0e-03}$	$3.29e-04_{1.5e-04}$

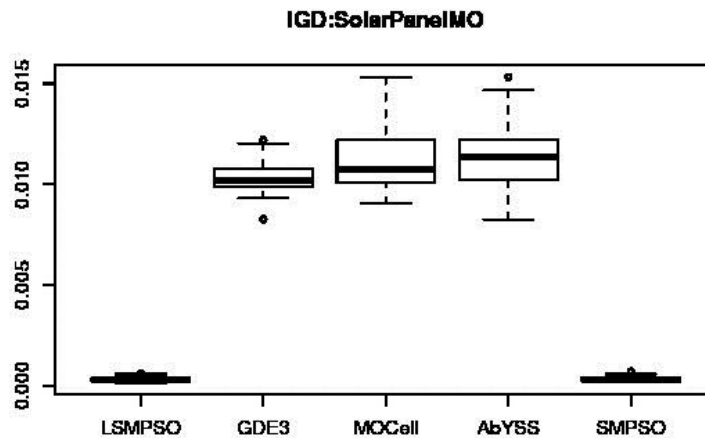


Figure 32: Boxplots of LSMPSO, SMPSO, GDE3, MOCcell, and AbYSS over 100 runs to solve PV design problem

One question needs to be addressed based on the results. Why GDE3, AbYSS and MOCcell performed poorly when compared with SMPSO and LSMPSO? A possible answer is that the PV farm design problem can be classified as a many-to-one problem. It means that the same solutions in the objective space might be generated with different variables. For example, two rows of *large* PV panels might have the same cost and energy output as five rows of PV panels but of small size. So, when two heterogeneous solutions in the variable space and homogeneous in the objective space are combined, using evolutionary operators such crossover and mutation, the resulting new solutions might be of poor quality because of the high heterogeneity in the variable space.

The first group of algorithms (GDE3, AbYSS and MOCcell) found solutions varying from one to six rows which can generate up 100,000 MWh. The second group (LSMPSO and SMPSO) found solutions that cover the full spectrum: from one to ten rows that can generate up to 184,676 MWh. So, the lowest cost is of \$925 which allows to absorb 2096 MWh per year with one row of solar panel having the smallest possible dimensions (0.2 m x 0.8 m) an inclination of

28° towards south-east direction (-5.6°). The maximum energy that could be generated is 184,676 MWh per year with a cost of \$88,116. This is the only solution with 10 rows collectors having a dimension of 1.91 m x 14.42 m with an inclination of 16.13° towards the south.

## 6.6 Summary

In this chapter, five state-of-the art MOMs, namely the proposed LSMPSO, the parent algorithm SMPSO, and AbYSS, MOCeII and GDE3, were used for optimal design of solar farm in Toronto, Canada. These MOMs have been selected because they showed the highest accuracy in the previous comparative study. The objectives were the maximization of the total incident solar energy and the minimization of the cost of deployment for a specific field. The decision variables consisted in number of collector rows, distance between collector rows, dimension of collectors, collectors' inclination angle, collectors azimuth, and elevation above ground.

The use of MOMs permitted to find a variety of optimal PV farm design solutions which would not be found using single objective solutions. For example, some intermediate solutions could be of interest with regards to other non-expressed objectives or secondary objectives such as space between solar panels or other technical aspects. Based on our result the maximum energy was  $Q = 108$  MWh/year when the number of rows  $K = 8$ , the PV panel height  $H = 1.69$  m, the PV inclination angle  $\beta = 61.2^\circ$ , the distance between subsequent panels  $D = 80$  cm, and the PV clearance above the ground  $E = 51$  cm.

The results showed that overall the LSMPSO and SMPSO algorithms achieved more accurate performance based on the IGD measure than GDE3, AbYSS and MOCeII by discovering broader spectrum of the Pareto front. LSMPSO and SMPSO found a portion of the Pareto front that was not found by GDE3, AbYSS and MOCeII because of the many-to-one mapping properties. For example, solutions having a number of rows from 7 to 10 were found

only by LSMPSO and SMPSO. Also, LSMPSO showed slightly better results than SMPSO by achieving a lower IGD median and IQR but that was not statistically significant.

The generated solutions demonstrated the practicality of MOMs which generated interesting solutions with a higher ROI in the middle of the Pareto front which won't be generated using a single objective optimization method.

As future work, we would like to extend the deployment of solar farms with tracking capability as supposed to stationary solar farms discussed in this chapter. Also, we would like to investigate gradual linear land inclination between rows to minimize the shadow on subsequent rows. Finally we would like investigate the use of ray focusing mirrors to direct the radiation when the sun's ray is not in the direction of the solar panels.

This case study demonstrated the performance of MO variants PSO in solving a real-world problem. This performance is due to leadership selection mechanism as all the other MOMs (GDE3, Abyss and MOCcell) do not use the leadership concept. Since GDE3 showed the highest accuracy in the comparative study; it would be valuable to incorporate the concept of leadership into GDE3.

## **Chapter 7**

# **Opposition-Based Third Generalized Differential Evolution (OGDE3)**

This chapter presents the second fundamental algorithmic contribution of this thesis. As shown in the comparative study presented in Chapter 3, the most accurate MOM is GDE3 which is a MO variant of DE. Opposition-based learning (OBL) has been successfully used in the past for acceleration of single-objective metaheuristics, especially DE. The most successful example in this regard is the opposition-based differential evolution (ODE) [14]. However, OBL was not fully explored for MOMs. Therefore, in this chapter, for the first time, OBL is successfully adapted for a MOM by using a single population (no coevolution) [15]. The proposed MOM is based on the GDE3 method and is called opposition-based GDE3 (OGDE3). OGDE3 utilizes OBL for opposition-based population initialization and self-adaptive opposition-based generation jumping. Also, the concept of leadership is incorporated into OBL for faster convergence. The proposed OGDE3 algorithm is compared with seven state-of-the-art MOMs using the ZDT test suite. OGDE3 outperformed the other algorithms; the results are presented and discussed in detail.

## 7.1 Introduction

It is common to use MOMs to solve complex optimization problems which can take over million function evaluations to find the real front [9]. One reason for this convergence problem is due to metaheuristics generating initially *random* solutions. Then, they try to converge towards optimal solutions. If random points are generated close to the optimal solutions, it can result in a fast convergence. Otherwise, if random points are generated far from an existing solution, in a worst case, in the opposite location, then the convergence will become much slower or even intractable. Overall, in the absence of any *prior* knowledge

about the problem to optimize, it is not possible to make a good initial guess. Therefore, all directions should be considered simultaneously, or more practically, the opposite direction should be considered, based on *opposition-based learning* (OBL) concept. Rahnamayan et al. [161], [162] proved mathematically and experimentally that the use of opposite points is more efficient than a pure random point.

In this chapter, OBL with leadership are applied to a state-of-the-art MOM called third generalized differentiation evolution (GDE3) to accelerate its convergence speed. The proposed algorithm, called an opposition-based third generalized differentiation evolution algorithm (OGDE3), is compared with seven state-of-the-art MOMs including its parent algorithm GDE3 using the ZDT test suite [33]. The results are promising and they are presented and discussed in detail in this chapter.

## **7.2 Opposition-Based Learning (OBL)**

Opposition concepts have been used for decades in many fields. The following list gives some examples [16]:

- Opposite particles/elements (physics)
- Antonyms (language)
- Antithetic variables (simulation)
- Opposite proverbs (culture)
- Complements (set theory)
- Opposition party (politics)
- Inverter (digital design)

- Dualism (philosophy and religion)
- Classical elements (archetype)
- If-then-else (algorithm)
- Complement of an event (probability)
- Revolution (social-political)

In a similar way, the concept of OBL has been introduced by Tizhoosh [163] as a new concept in computational intelligence. Often a machine learning algorithm starts with initial random points then, the algorithm tries to enhance the candidate solution, hopefully, towards an existing optimum. For example, weights in neural networks, and initial population in genetic algorithms, are generated randomly.

### 7.2.1 Variants of opposition-based Schemes

There are several variants of opposition schemes [164]. The main types are described below:

**Definition (Type-I Opposite Points)** [164]: Let  $x$  be a real number defined in the interval  $[a, b]$ . The opposite number  $\check{x}$ , as illustrated in Figure 33, is defined as follows:

$$\check{x} = a + b - x, \quad (37)$$

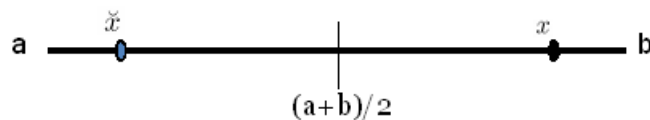


Figure 33: An opposite point in a one-dimensional search space



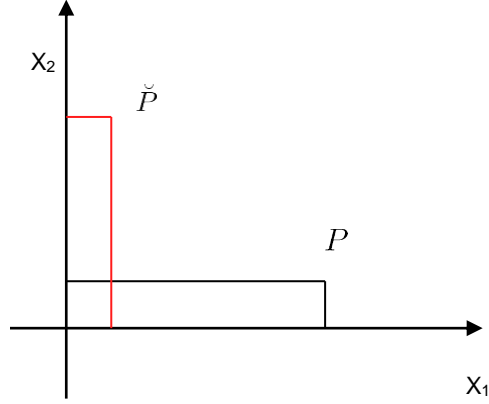


Figure 34: Illustration of an opposite point in 2D search space.

Similarly, the opposite of  $x$  in a multidimensional search space can be defined as follows. Let  $P = (x_1, x_2, \dots, x_n)$  be a point in an  $n$ -dimensional system with  $x_1, \dots, x_n \in \mathbb{R}$ , and  $x_i \in [a_i, b_i]$ . The opposite point  $\check{P}$  is defined by its coordinates  $\check{x}_1, \dots, \check{x}_n$  where

$$\check{x}_i = a_i + b_i - x_i, \quad i = 1, \dots, n \quad (38)$$

**Definition (Type-I Super-Opposite Points)** [157]: Let  $P = (x_1, x_2, \dots, x_n)$  be a point defined in  $n$ -dimensional space with  $x_i \in [X_{min}^i, X_{max}^i]$  and  $\check{P} = (\check{x}_1, \check{x}_2, \dots, \check{x}_n)$  is its opposite point in the same space. Then, any point  $\check{P}^s$  is a type-I super-opposite of  $P$  if  $d(\check{P}^s, P) > d(\check{P}, P)$ , where  $d(\dots)$  denotes a distance metric such as the Euclidean distance.

**Definition (Type-I Quasi-Opposite Points)** [157]: Let  $P = (x_1, x_2, \dots, x_n)$  be a point defined in  $n$ -dimensional space with  $x_i \in [X_{min}^i, X_{max}^i]$  and  $\check{P} = (\check{x}_1, \check{x}_2, \dots, \check{x}_n)$  are the opposite points in the same space. Then, any point  $\check{P}^q$  is a type-I super-opposite of  $P$  if  $d(\check{P}^q, P) < d(\check{P}, P)$ , where  $d(\dots)$  denotes a metric such as the Euclidean distance. An illustration of the difference between the type-I super-opposite and quasi-opposite is shown in Figure 35.

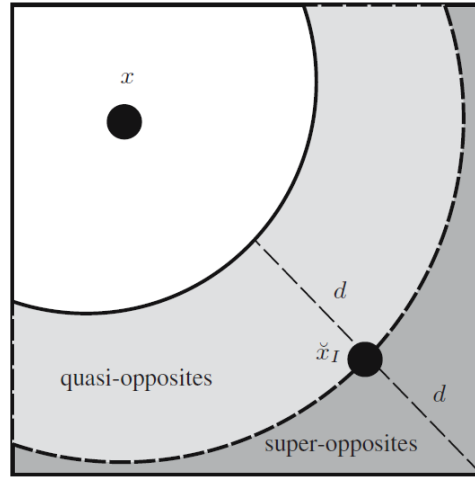


Figure 35: Simplified representation of quasi-opposites and super-opposites in 2D search space [164]

**Definition (Type-II Opposite Points)** [164]: Assume  $f(x_1, x_2, \dots, x_n)$  is a known function, and  $y_{min}, y_{max}$  are given or they can be estimated. Let  $y = f(x_1, x_2, \dots, x_n) \in \mathbb{R}$  be an arbitrary function with  $y \in [y_{min}, y_{max}]$ . For every point  $P = (a_1, a_2, \dots, a_n)$ , define the type-II opposite point  $\check{P} = (\check{a}_1, \check{a}_2, \dots, \check{a}_n)$  under the following condition.

$$\check{P} = \{a \mid \check{y} = y_{min} + y_{max} - y\}, \quad (39)$$

An illustration of the difference between the type-I opposite and type-II opposite is shown in Figure 36. The type-I opposition points are calculated based on the input points, while the type-II opposition points are calculated based on fitness values. For example, the opposite (type-I) of the point  $x$  is  $\check{x}_I$ ; but the opposite (type-II) of  $x$  is  $\check{x}_{II}$  because  $f(\check{x}_{II})$  is the opposite of  $f(\check{x}_I)$ .

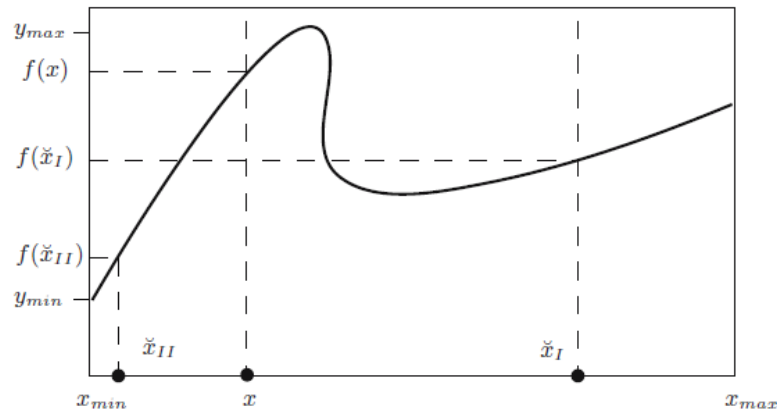


Figure 36: Type-I versus type-II opposition

## 7.2.2 Opposition-based learning: Applications in optimization

Rahnamayan et al. [165] presented pioneering work in using the opposition-based learning concept in optimization. More specifically, the authors applied OBL to accelerate the differential evolution algorithm and called the new enhanced variant of the algorithm

opposition-based differential evolution (ODE) [14]. First, it enhanced the initial population, rather than only using a random initial population  $P(n)$ , the algorithm generates also the corresponding opposite population  $OP(n)$ . Thereafter, the fittest candidate solutions are selected from the union set of the two populations  $P(n)$  and  $OP(n)$ . Furthermore, during the optimization process, an opposite population is generated for the current population, and the fittest candidate solutions are selected for the next generation. However, a jumping rate is used for controlling the number of times the opposition population is generated, and the interval of the search space is recalculated for opposition-based generation jumping. The proposed methods were tested extensively on 58 benchmarking functions for a comparison of DE, ODE, and FADE [166]. The results showed that ODE achieved superior results for high dimensional problems. The use of opposition points during the learning process accelerates the convergence rate by 57%. The jumping rate should be within the range of [0.1, 0.3] for unknown problems.

Rahnamayan and Wang [167] studied the use of ODE for large scale optimization problems. ODE and DE were compared by using seven large scale benchmark functions (500 and 1,000 dimensions). The results showed that ODE achieved higher accuracy and convergence speed compared to its parent algorithm, DE. Even an ODE variant was proposed for solving noisy problems efficiently [168].

Rahnamayan et al. [169] enhanced ODE by using quasi-opposite points rather than opposite points with a lower generation jumping rate. They proved that quasi-opposite points have a higher probability of being closer to the real solution than opposite points. The

proposed method (QODE) was compared to ODE and DE methods by using 15 benchmarking functions with two different dimensions for a total of 30 problems. The results showed that QODE required a lower number of function evaluations than DE and ODE, and achieved a higher success performance than DE and ODE. However, DE achieved a slightly higher average success rate than QODE and ODE.

In the previous methods, the jumping rate was constant ( $J_r=0.3$  for ODE and  $J_r=0.05$  for QODE). Rahnamayan et al. [170] studied two varying jumping rates based on a linearly increasing or decreasing function. The latter has a higher jumping rate during exploration and lower jumping rate during exploitation, and vice-versa for the former. The tests were based on 15 benchmark problems; the results showed that the linearly decreasing jumping rate achieves better performance than constant or linearly increasing jumping rates because OBL is more useful in the exploration phase.

Lin and Xingshi [18] developed an opposition particle swarm optimization (OPSO) algorithm by utilizing an OBL concept for the swarm initialization, and generation jumping for the best member during exploration phase. The swarms are initialized with random positions and velocities. The opposite swarms are calculated by computing their respective opposite positions and velocities. The fittest swarms are selected for the exploration phase. Then, the opposite of the current generation is generated using a jumping rate and a dynamic constriction factor (CF) as follows:

$$ox_{ij} = L_j + U_j - C F_{ij} \cdot x_{ij}, \quad (40)$$

where

$$C F_{ij} = 1 - \lambda r_{ij}, \quad (41)$$

where  $r_{ij}$  is a Cauchy random number, and  $\lambda$  starts at 1.0 and decreases every 50 generations. OPSO was compared to the PSO algorithm by using six benchmarking problems. OPSO achieved, on average, a faster convergence speed and stronger global search ability by escaping from local optima.

Omran and al-Sharhan [171] introduced three variants of opposition-based PSO which are OPSO, iOPSO, and iPSO. OPSO used opposition concepts for population initialization similar to [166]. An improved OPSO named iOPSO used opposition for every iteration by replacing the particle with the lowest fitness value by its opposite. iPSO is similar to iOPSO but without opposition-based population initialization. The performance of the three proposed opposition variants of the PSO algorithm were compared with PSO using eight benchmark problems. The results showed that iOPSO and iPSO achieved better performance than PSO and OPSO in both accuracy and convergence speed. The results of iOPSO and iPSO were very close.

A more extensive survey of the OBL applications to other machine learning methods can be found in Ref. [172]. Most of the papers related to opposition-based optimization have selected DE for their experiments, which appeared very efficient.

### 7.3 Opposition-based Learning for Multi-Objective Optimization

Opposition-based multiobjective optimization (OB-MO) is a new research direction. OB-MO methods have been inspired from the Opposition Differential Evolution (ODE) algorithm [165]. This section reviews MOMs-related work that used the OBL concept.

Peng et al. [173] developed an OB-MO algorithm inspired from ODE named the Opposition-based Multi-Objective Differential Evolution algorithm (OMODE). OMODE uses OBL for the generation of the initial population. Both the initial population and its opposite population are combined then sorted using the non-dominance sorting and crowding distance mechanisms. OMODE was compared to several MOMs such as NSGA-II [27] (real-code), NSGA-II (binary-code), PAES [174], SPEA2 [28], IBEA [175], and IBEAHD. The benchmarking problems ZDT1, ZDT2, ZDT3, ZDT4, ZDT6 [33] were used for algorithms comparison in terms of convergence and diversity measures [27]. Furthermore, a space rendezvous problem was utilized for comparing OMODE and NSGA-II methods. The results showed that the OMODE Pareto solutions offered the best convergence and distribution (diversity) for all benchmarking problems. Regarding the space rendezvous problem, OMODE also performed better than NSGA-II. However, it is important to note that OMODE was not compared to GDE3.

Dong and Wang [176] proposed a similar algorithm called Multi-objective Differential Evolution-based on Opposite Operations (MDEOO). MDEOO generates an opposite-based initial population in the same fashion as the OMDE optimization method described earlier. However, at every iteration, opposite offspring points are generated only

for the new non-dominated solutions. The new solutions are then filtered based on the non-dominance sorting and crowding distance mechanisms in order to respect the population size limit. A plotting comparison was done with respect to PDE, SPEA, DEMO, RM-MEDA MOM methods using ZDT1, ZDT2, ZDT3, ZDT6 [33], and F1 [170] benchmarking problems. The authors concluded that the comparison confirmed the effectiveness of the algorithm in terms of precision and distribution. However, it is also important to note that MDEOO was not compared to GDE3.

Coevolution is the simultaneous evolution of two or more species (populations) with a coupled fitness. Every species involves a number of individuals working together to solve the problem. Competitive coevolution involves individuals that compete against each other for dominance in the population. Tan and Teo [178] proposed two new opposition-based competitive coevolution algorithms for MOO called SPEA2-CE-HOF and SPEA2-CE-KR. These hybrid algorithms are the combination of SPEA2 [28] with two types of competitive fitness strategies, which are Hall of Fame (HOF) and K-Random Opponents (KR). The original algorithm (SPEA2) was compared with the two new proposed algorithms using the DTLZ [34] benchmark problems with three to five objectives. Three measures used for the experiments are generational distance [23] (closeness), distribution [179] (diversity) and coverage metrics [33]. The results showed that SPEA2-CE-KR produced better results in terms of generational distance, spacing and coverage in almost all of the test problems. It significantly improved the results as the number of objectives increased. Therefore, SPEA2-CE-KR has an enhanced capability of escaping sub-optimal local solutions during



exploration phase which results in more accurate Pareto optimal solutions. SPEA2-CE-HOF improved the performance of SPEA2 in some of the problems. Therefore, the use of opposition-based competitive coevolution for SPEA2 improved its performance for solving multi-objective optimization problems.

In brief, as shown in this literature review, very little work related to MOM and OBL has been conducted. Also, based on a literature review, even the studies which combined MOM methods and OBL are relatively deficient, because they have not demonstrated that the opposition version of the MOM was better than the original MOM (parent algorithm). Rather, the opposition version of MOM was always compared with other metaheuristics such as NSGA-II which does not demonstrate any improvement of OBL to MOM. Based on our experience, classical OBL does not improve nor worsen the GDE3 performance. Therefore, this proposed research aims to develop a new opposition-based MOM with high accuracy that outperforms even GDE3

#### **7.4 Proposed Algorithm: Opposition-Based Third Generalized Differential Evolution Algorithm (OGDE3)**

This section describes the proposed MOM called opposition-based third generalized differential evolution algorithm (OGDE3). OGD3 utilizes OBL with leadership to enhance GDE3 proposed by Kukkonen and Lampinen [29]. GDE3 is one of the most efficient MOO algorithms as shown in the comparative study in Chapter 3 and other references such as [9].

OBL was applied successfully with DE for single-objective problems as mentioned in section 7.2.2. It starts with an initial random population and in each iteration a new offspring population is generated using the differential evolution operator. Both populations are combined, then, the size of the population is reduced using the non-dominance sorting and a pruning method for diversity preservation as in NSGA-II. However, the GDE3 pruning method modifies the NSGA-II crowding distance in order to solve some GDE3 drawbacks when dealing with problems having more than two objectives.

As shown in the pseudo code below, the proposed OGDE3 works similarly to GDE3, but during the exploration phase it generates the opposite population (with  $NP$  individuals); then, all candidate solutions ( $NP \cup OP$ ) are sorted, and the best candidate solutions are selected based on the non-dominance sorting. The opposite candidate solution is calculated based on dynamic variation of variables, called dynamic opposition. The range (variable definition domain) of opposite variables shrinks for every iteration using the three best solutions (leaders) of the population. The following is a description of the procedure for updating the variable definition domain. Let  $p = (x_1, x_2, \dots, x_n)$  be a point in an  $n$ -dimensional system with  $x_1, \dots, x_n \in \mathbb{R}$ , and  $x_i \in [a_i, b_i]$ . The opposite point  $\check{p}$  is defined by its coordinates  $\check{x}_1, \dots, \check{x}_n$  where

$$\check{x}_i = a_{i\_min3} + b_{i\_max3} - x_i, \quad i = 1, \dots, n \quad (42)$$

where  $a_{i\_min3}$  and  $b_{i\_max3}$  are the minimum and maximum variables for the three best solutions (leaders) in the population, respectively.

OGDE3's Min and Max update based on three leader solutions at every iteration

```

While  $j < 3$  //  $j$  is position of the leader
  While  $i < n$  //  $n$  is maximum number of variables.
    if ( $a_{i\_min3} > x_{ji}$ )  $a_{i\_min3} = x_{ji}$ 
    if ( $b_{i\_max3} < x_{ji}$ )  $b_{i\_max3} = x_{ji}$ 

```

The following is the pseudocode of OGDE3 algorithm; the added portions to GDE3 are highlighted by bold face.

#### OGDE3 Algorithm

1. Evaluate the initial population  $P$  of random individuals.
2. While stopping criterion not met, do:
  - 2.1. For each individual  $P_i$  ( $i = 1, \dots, popSize$ ) from  $P$  repeat:
    - (a) Generate candidate  $C$  from parent  $P_i$
    - (b) Evaluate the candidate  $C$ .
    - (c) If the candidate dominates the parent, the candidate replaces the parent.  
If the parent dominates the candidate, the candidate is discarded. Otherwise, the candidate is added in the population.
  - 2.2. If the population has more than  $popSize$  individuals, truncate it.
  - 2.3. Randomly enumerate the individuals in  $P$ .
  - Opposition-based added section:**
  - 2.4. If ( $\text{random}(0,1) < \text{JumpingRate}$ ) //  $\text{JumpingRate} = 0.15$** 
    - (a) Calculate  $\check{C} = a_{i\_min3} + b_{i\_max3} - x_i$**
    - (b) Generate candidates  $\check{C}$  for active candidate solutions  $p_i$  to form  $\check{P}$ .**
    - (c) Discard identical solutions from  $P \cup \check{P}$ .**
    - (d) Select best  $popSize$  solutions from  $P \cup \check{P}$ .**

## 7.5 Self-Adaptive Selection of Candidate Solutions for Opposition

It should be noted that OBL-based acceleration scheme is not necessarily always beneficial; it is more beneficial during the exploration phase. The opposite of all candidate solutions will not necessarily generate better solutions for all of the population. Consequently, these observations generate some questions. When should the OBL mechanism be applied or stopped? Which candidate solutions should be selected as candidate for opposition? To answer these questions, a self adaptive version of OBL will be proposed. But, first, the definitions are given with regards to adaptivity.

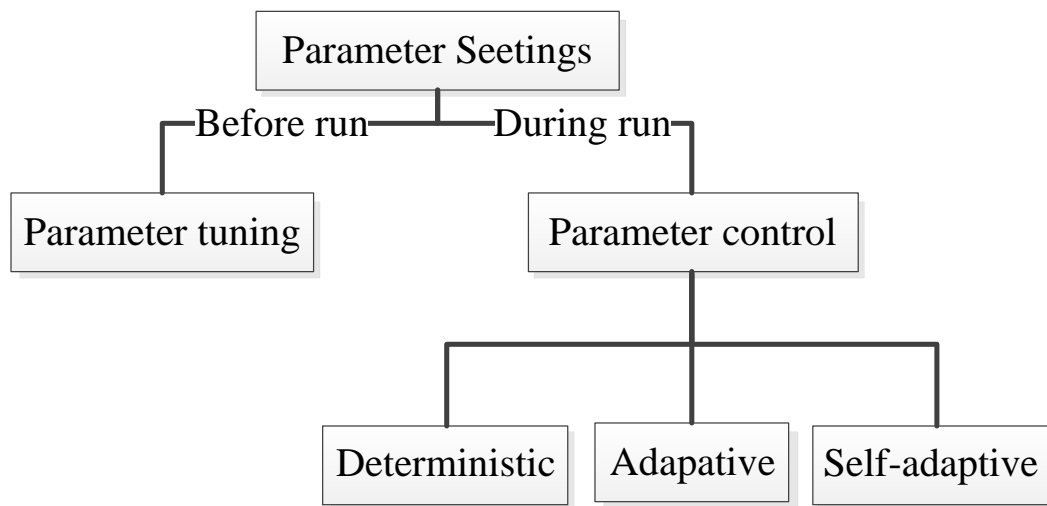


Figure 37: Taxonomy of parameter control for metaheuristics

As shown in Figure 37, Eiben and Schut [180] classified the parameter setting methods into parameters tuning and control. *Parameter tuning* is defining parameter values *before* the execution of an algorithm. These values remain the same during the entire

execution of the algorithm. For example, the jumping rate is fixed at 0.15 for OGDE3. This is the simplest and most common form of parameter settings. However, it does not take into consideration the progress of an algorithm (e.g. exploration versus exploitation). Also, it does not consider any feedback such as the landscape or the progress of candidate solutions. Parameter control consists of modifying parameter values using a rule. This rule can be based on deterministic, adaptive, or self-adaptive approach. The deterministic approach modifies variables using a specific mechanism such as linear or any schedule-based mechanism. Conceptually, the deterministic approach is better than the parameter tuning approach because there is an adaptation depending on the progress of the algorithm. It is commonly used in machine learning algorithms such as PSO or self-organizing maps. However, some optimization problems are more complex and require more computational time than others. Use of the exact same deterministic approach for such different cases becomes inefficient. The adaptive and self-adaptive controls modify the parameter values based on some feedback. But the difference between them is that the adaptive control modifies *one* parameter for *all* of the population. The self-adaptive control modifies independent parameter values for *every* individual of the population. Usually, this parameter(s) is (are) encoded into chromosomes of solutions. Both the adaptive and self-adaptive approaches are computationally more expensive than the deterministic and parameter tuning approaches because the feedback values need to be compiled and analyzed. However, these adaptive and self-adaptive approaches make optimization algorithms more generic to different problems due to the adaptive mechanisms. In addition, there is no need to tune algorithms as with the

parameter tuning approach. Intuitively, the self-adaptive approach can be more efficient because every candidate solution is analyzed independently but it can be computationally much more expensive than the adaptive approach if not designed appropriately.

In this chapter, self-adaptive control is used for the determination of candidate solutions which are used for opposition-based generation. Also, it determines when a candidate solution is inactive, which means it is ineligible for opposition-based generation. Therefore, every individual has an integer variable initialized to two, i.e., every individual can fail at most twice consecutively before being inactive. If the opposite of a candidate solution does not improve the parent candidate solution *two times in a row*, then this candidate solution becomes ineligible (inactive) to generate opposite solutions. Finally, when all candidates are inactive, the OBL mechanism is completely stopped.

As shown in Figure 38, OBL has been incorporated into GDE3 after the evolutionary process, i.e., the population has been generated. Then, at every iteration, the jumping rate condition is checked for every candidate solution to see whether to proceed with OBL or no. If the condition is positive, the opposition individuals are generated only for the individuals where the OBL is still active using the self-adaptive scheme. In the experiments, the condition of keeping OBL active is that an opposite candidate solution should not be dominated two times in a row by the parent candidate solution.

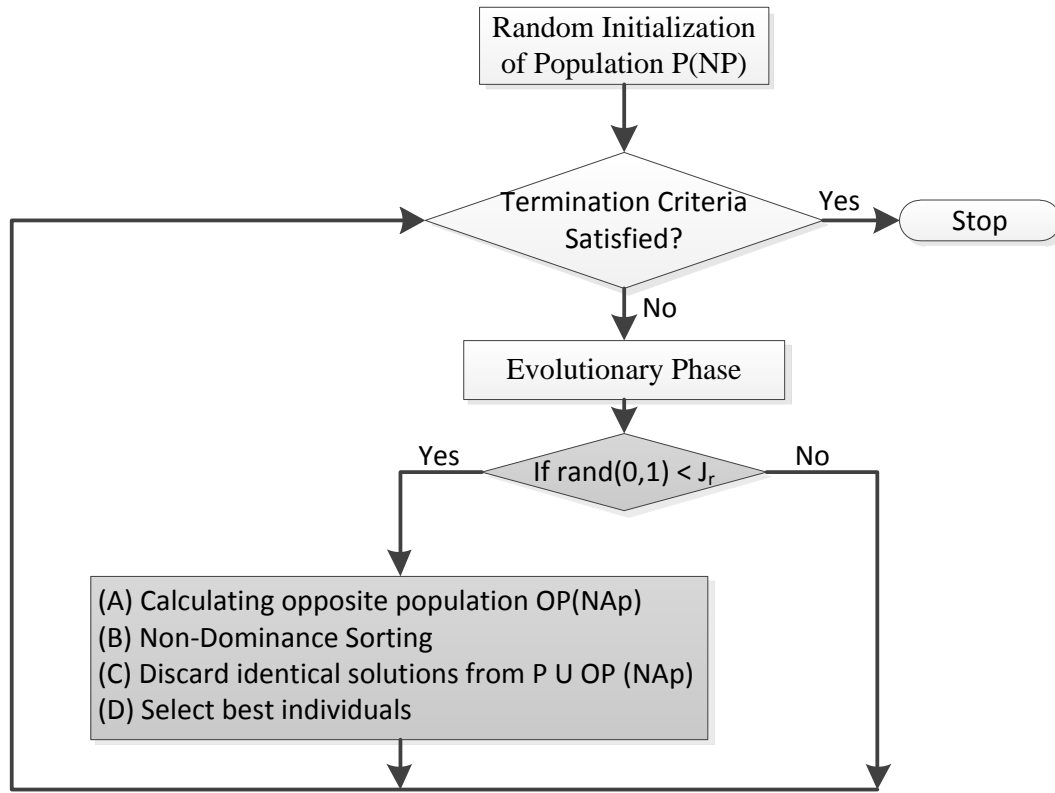


Figure 38: Incorporation of opposition based learning into GDE3.

The grey boxes show where OBL has been applied,  $N_p$  is the population size and  $N_{Ap}$  is the number of individuals where opposition is still active.

## 7.6 Experiments

This section describes the configuration of the simulation experiments, namely, the benchmark problems, the used MOMs, the evaluation methods, and the results.

### **7.6.1 Benchmarking problems**

The well-known Zitzler-Deb-Thiele (ZDT) test suite [33] was selected for the tests. These problems are commonly used for comparative studies such as Ref. [9]. Their description can be found in Table 36 (Appendix A).

### **7.6.2 Metaheuristics parameter settings**

The parameter settings for the experiments are the same as the comparative study of Chapter 3; they can be found in Table 1. These parameters have been taken from Refs. [3] and [9]. All of the genetic algorithms (NSGA-II, SPEA2, and MOCell) and evolutionary algorithms (GDE3 and OGDE3) have a population size of 100. In the same fashion, SMPSO has a configuration of 100 particles. The metaheuristics having an archive (SMPSO, NSGA-II, SPEA2, and MOCell) also have a maximum size of 100.

In order to perform a fair comparison between OGDE3 and GDE3, it should be emphasized that OGDE3 and GDE3 have exactly the same configuration ( $CR = 0.1$  and  $F = 0.5$ ). In this way, any improvement or degradation of OGDE3 over GDE3 will be attributed to the addition of the self-adaptive OBL mechanism with leadership to GDE3.

### **7.6.3 Evaluation measure**

The convergence speed of OGDE and the seven state-of-the-art MOMs are analyzed for five well-known benchmark problems. In order to assess the quality of a Pareto front generated by a MO metaheuristic, the number of function evaluations is counted. The hypervolume rate (HVR) indicator [33] is used as stopping criteria. The stopping condition was fixed to



HVR $\geq$ 98% or when reaching a maximum number of  $10^6$  function evaluations, a criterion commonly used as per Ref. [9]. Every MO algorithm is independently executed 100 times for every problem. The algorithm requiring the lower number of function evaluations to find the real Pareto front is considered the fastest algorithm. The hit rate is then compiled, which refers to the number of times the algorithm was able to find (approximate with HVR $\geq$ 98%) the real Pareto front.

Given that the Pareto fronts of the problems used in this study are known beforehand, the algorithms are executed until approximating reasonably well the real Pareto fronts (HVR  $\geq$  98%). However, finding the Pareto front might not be always possible for some algorithms, depending on the problem complexity. In other words, some algorithms might perform well with some specific problems, but not able to find the Pareto front for other types of problems. Or it might take too long to produce the Pareto Front. Consequently, another stopping condition is added by allowing every metaheuristic to perform at most  $10^6$  function evaluations.

For every problem, the metaheuristic is executed 100 times independently. The comparison of stochastic algorithms requires statistical analysis so that the results can be presented with a certain level of confidence. The Wilcoxon statistical test based on Ref. [181] is used to present results at a 0.05 significance level.

#### **7.6.4 Experimental simulation results**

As explained earlier, every algorithm has been executed 100 times per problem. Table 19 shows the median of the number of function evaluations required to achieve an HVR=98%.

The dark grey area shows the fastest algorithm, while the light grey area indicates the second fastest algorithm. For the case where the fastest algorithm does not pass the statistical test with the subsequent algorithms, then all of them will be ranked equally. It can be seen that OGDE3 was the fastest algorithm for all the ZDT problems.

Table 19: Median and IQR of the number of function evaluations for reaching the PF

Problem	NSGA-II	SPEA2	PAES	OGDE3	GDE3	OMOPSO	AbYSS	MOCcell
ZDT1	1.43e4 <sub>9.0e2</sub>	1.61e4 <sub>1.0e3</sub>	1.25e4 <sub>8.1e3</sub>	6.82e3 <sub>1.7e3</sub>	9.50e3 <sub>5.0e2</sub>	4.09e5 <sub>4.3e5</sub>	1.33e4 <sub>1.3e3</sub>	1.29e4 <sub>1.0e3</sub>
ZDT2	2.43e4 <sub>1.6e3</sub>	2.49e4 <sub>1.8e3</sub>	1.03e5 <sub>1.2e5</sub>	1.26e4 <sub>9.9e5</sub>	1.13e4 <sub>6.0e2</sub>	5.35e5 <sub>5.6e5</sub>	1.76e4 <sub>1.8e3</sub>	1.40e4 <sub>5.1e3</sub>
ZDT3	1.28e4 <sub>7.0e2</sub>	1.53e4 <sub>1.3e3</sub>	2.56e4 <sub>2.7e4</sub>	7.81e3 <sub>1.3e3</sub>	1.02e4 <sub>5.0e2</sub>	6.14e5 <sub>6.3e5</sub>	1.23e4 <sub>2.5e3</sub>	1.28e4 <sub>1.4e3</sub>
ZDT4	2.24e4 <sub>5.7e3</sub>	2.61e4 <sub>5.7e3</sub>	4.41e4 <sub>1.9e4</sub>	1.62e4 <sub>1.2e3</sub>	1.63e4 <sub>1.0e3</sub>	–	2.11e4 <sub>9.2e3</sub>	1.72e4 <sub>4.6e3</sub>
ZDT6	2.92e4 <sub>1.7e3</sub>	3.34e4 <sub>1.3e3</sub>	9.06e3 <sub>1.0e4</sub>	3.29e3 <sub>1.1e3</sub>	4.50e3 <sub>5.0e2</sub>	2.17e5 <sub>2.1e5</sub>	1.55e4 <sub>1.6e3</sub>	2.17e4 <sub>1.3e3</sub>

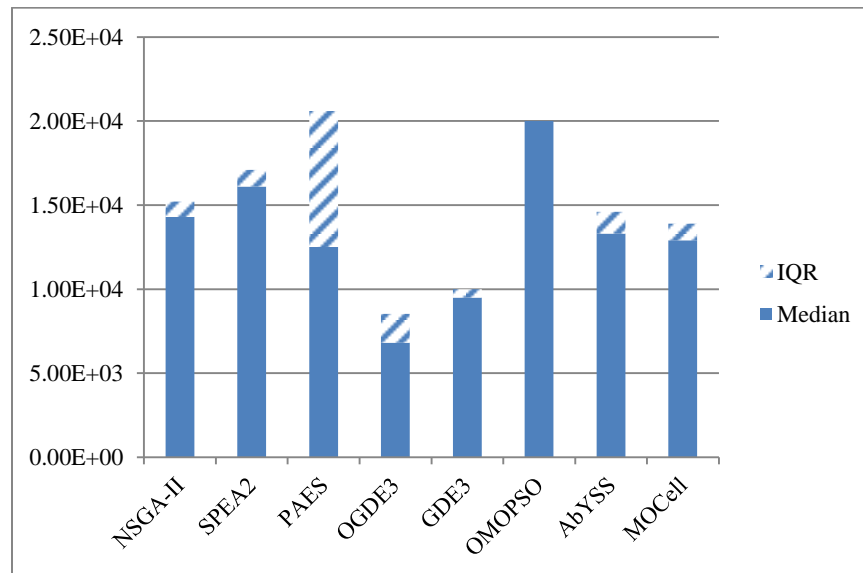


Figure 39: Median and IQR of the number of function evaluations for ZDT1. OMOPSO IQR intentionally omitted for a better clarity of the figure.

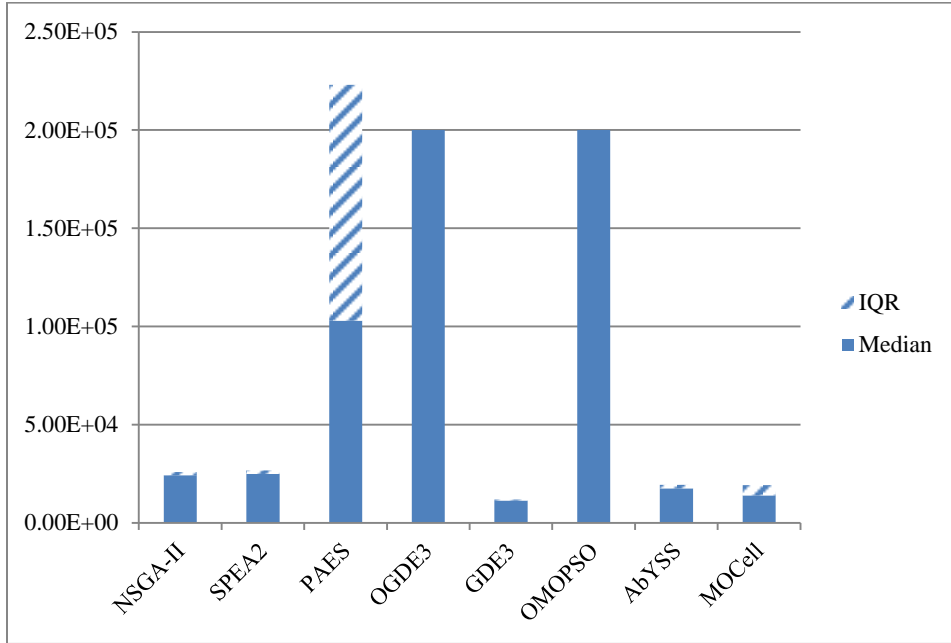


Figure 40: Median and IQR of the number of function evaluations for ZDT2. OGDE3 and OMOPSO intentionally omitted for a better clarity of the figure

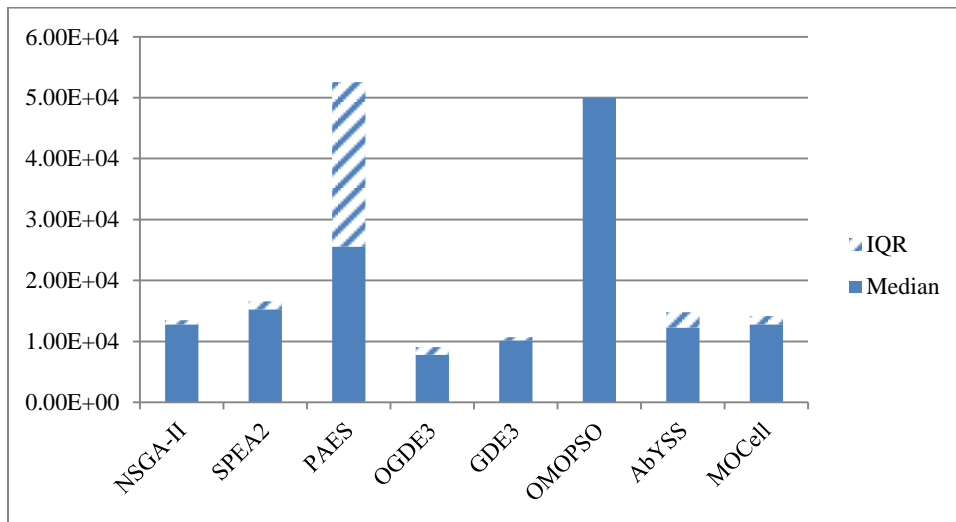


Figure 41: Median and IQR of the number of function evaluations for ZDT3.

OMOPSO IQR intentionally omitted for a better clarity of the figure

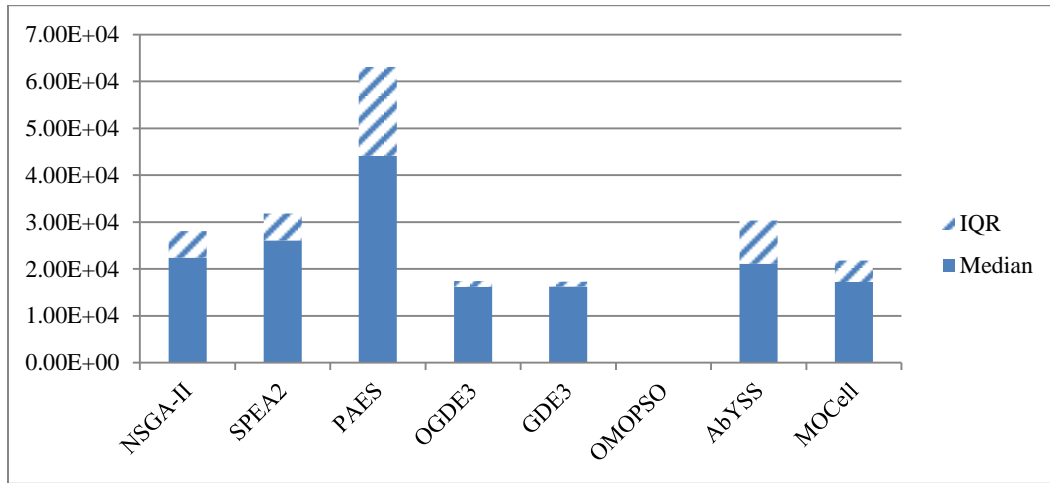


Figure 42: Median and IQR for ZDT4

OMOPSO intentionally omitted because it did not find the PF

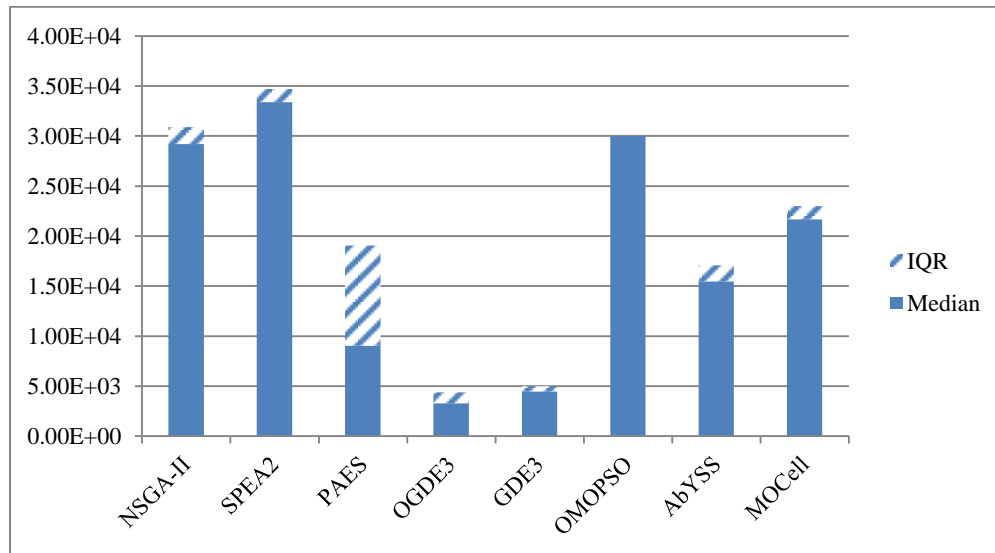


Figure 43: Median and IQR for ZDT6

OMOPSO IQR intentionally omitted for a better clarity of the figure

The results were plotted graphically for every benchmarking problem as shown in Figure 39 to 43. To make the graphs clearer, the histogram (median) of algorithms with a significantly higher median than the others were omitted for a better clarity of the graphs. The solid color in the histogram represents the median and the dashed portion of the histogram represents the interquartile (IQR).

As shown in the results, OGDE3 was the fastest algorithm for 80% of the problems. OGDE3 was also faster than its parent algorithm. As shown in Table 20, on average, OGDE3 was faster than the other seven algorithms by 50%. OGDE3 required only half of the function evaluations required by the average of all state-of-the-art algorithms and was 76% faster than the average algorithms for ZDT6. Average, OGDE3 was 26% to 76% faster than the average metaheuristics for solving the ZDT problems. It was especially (27% and 28%) faster than its parent algorithm (GDE3) for the problems ZDT1 and ZDT6.

When OGDE3 is compared to its parent algorithm GDE3, it is found that OGDE3 improved GDE by 13% on average for the ZDT problems. As explained earlier, the OGDE3 had a high IQR for ZDT2 because of a lower hit rate (54%). The hit rates show how many times out of one hundred the metaheuristic was able to find the real Pareto front. If ZDT2 is excluded, OGDE3 is on average 20 % faster than GDE3 for the remaining ZDT problems. Also, it is important to mention that for ZDT4, the statistical test did not pass between GDE3 and OGDE3; however, the test passed OGDE3 and the rest of the algorithms and GDE3 and the rest.

Table 20: Relative difference of the convergence speed between OGDE3 with the other MOMs

e.g. OGDE3 required in average 50% less number of function evaluation to find the PF of ZD1

	NSGAI	SPEA2	PAES	GDE3	OMOPSO	AbYSS	MOCcell	Average
ZDT1	-52%	-58%	-45%	-28%	-98%	-49%	-47%	-54%
ZDT2	-48%	-49%	-88%	+12%	-98%	-28%	-10%	-44%
ZDT3	-39%	-49%	-69%	-23%	-99%	-37%	-39%	-51%
ZDT4	-28%	-38%	-63%	-1%	-	-23%	-6%	-26%
ZDT6	-89%	-90%	-64%	-27%	-98%	-79%	-85%	-76%
							<b>Total Average</b>	<b>50%</b>

As mentioned earlier, OGDE3 performed well except for the problem ZDT2, where it came out as second best. OGDE3 had actually a very high IQR because of its low hit rate as shown in Table 21. OGDE3 was able to find the Pareto front of ZDT2 only 54% of the times. ZDT2 is a non-convex problem, but ZDT 4 and 6 are also non-convex. Therefore, the characteristics of the problem are not likely causing a lower rate. Also, it can be seen that for about 1% to 2% of the time, OGDE3 is unable to find the Pareto front. It is likely the same anomaly that causes OGDE3 to not converge is also contributing to the low hit rate for the ZDT2 problem. It might be the consequence of using only the three leaders to reduce the OBL domain of definition which might be located close to each other. This anomaly should be further investigated to eliminate this hit rate-related problem.

Table 21: Hit Rate of the compared MOMs

	NSGA-II	SPEA2	PAES	OGDE3	GDE3	OMOPSO	AbYSS	MOCeII
<b>ZDT1</b>	100%	100%	100%	98%	100%	100%	100%	100%
<b>ZDT2</b>	100%	100%	100%	54%	100%	90%	100%	100%
<b>ZDT3</b>	100%	100%	100%	99%	100%	78%	100%	100%
<b>ZDT4</b>	100%	100%	100%	100%	99%	0%	100%	100%
<b>ZDT6</b>	100%	100%	100%	99%	100%	100%	100%	100%

## 7.7 Conclusions

This chapter has shown the first successful application of an opposition-based learning scheme to a multi-objective metaheuristic with a single population (no coevolution). The OBL was used for opposition-based initial population generation and opposition-based jumping generation. The OBL with leadership was applied to the differential evolution algorithm in a MO objective space for the acceleration of its convergence speed. The new proposed algorithm (OGDE3) uses a self-adaptive scheme for OBL activation/deactivation. In addition, the leadership concept is incorporated into OBL by using the three best solutions to calculate the respective minimum and maximum thresholds of every variable.

The convergence speed of the OGDE3 was compared to seven state-of-the-art multiobjective metaheuristics, namely, NSGA-II, SPEA2, PAES, PESA-II, GDE3, OMOPSO, MoCell, and AbYSS. The ZDT benchmark test suite was used for the experimental verifications. Every metaheuristic was executed 100 times independently per

problem. The metaheuristics stopping criterion was fixed to 98% of the real hypervolume or a maximum of  $10^6$  functions evaluations.

This study also showed that the proposed OGDE3 was faster than all the metaheuristics in most of the cases. Hence, on average, OGDE3 required only half of the average number of function evaluations as compared to the other MOMs to find the Pareto front. OGDE3 required 26% to 76% less function evaluations than the average state-of-the-art metaheuristics to converge towards the Pareto front, depending on the problem. In comparison with its parent and second best algorithm GDE3, OGDE3 was 20% faster than GDE3 excluding the ZDT2 problem.

Although, OBL has shown promising results in this chapter, nevertheless, it required complex adjustments of OBL such as self-adaptive selection and leadership.

One of the OBL paths that remain unexplored in both single objective and multi-objective fields is the use of OBL at operation level which might be more beneficial for multi-objective optimization algorithms. In the next chapter, it is proposed to explore the utilization of leadership without OBL with GDE3.



## **Chapter 8**

# **Multi-Objective Differential Evolution with Leadership Enhancement (MODEL)**

In the comparative study of Chapter 3, GDE3 achieved highest robustness among all the compared state-of-the-art MOMs. Therefore, this chapter proposes to improve GDE3 with the use of leadership as detailed in the next sections.

## 8.1 Introduction

It has been observed in the comparative study (Chapter 3), that GDE3 shows distributed movement of individuals compared to SMPSO. Usually, GDE3 preserves a uniform distribution of particles during the entire search process but does not converge as fast as the SMPSO. A probable reason is that PSOs use leaders to direct particles into most promising directions. Therefore, in this chapter it is proposed to incorporate the concept of leadership into the mutation operator because DE mutation operator is one of the main strengths of DE in single and multi-objective search space. However, the incorporation of leadership into MO-DE's mutation operator causes sometimes premature convergence. In order to solve this problem, it is proposed to change the sign of the control parameter  $F$  with a certain probability (prob=0.3) of DE which makes MODEL more robust and strengthens its capabilities to avoid premature convergence due to local optima.

This chapter proposes the following contributions related to the differential mutation operator of GDE3.

- Incorporation of leader selection mechanisms into GDE3.
- Selection of more representative leaders, using stringent Non-dominance sorting.
- Adaptation of single objective mutation scheme DE/best/1 to MOO providing GDE3/deputy/1 where deputy is a deputy leader.
- Implementation of the non-dominance sorting in the difference vector.
- Utilization of negation of control of parameter  $F$  with a certain probability.

## 8.2 Proposed Mutation Scheme

The general convention used to represent mutation schemes in DE is DE/x/y/z, where x stands for the base vector to be perturbed, y is the number of difference vectors used for one perturbation of x, and z represents the type of crossover being used (exp: exponential; bin: binomial) [182].

The classical scheme in the single objective version of DE is DE/rand/1 [183]. "rand" means the three vectors used for mutation are randomly selected from population, "1" means there is only one difference vector. So, the mutation is done as follows:

$$\vec{V}_t = \vec{X}_a + F \times (\vec{X}_c - \vec{X}_b), \quad (43)$$

where  $\vec{X}_a, \vec{X}_b, \vec{X}_c$  are randomly selected vectors from the current population and  $i \neq a \neq b \neq c, i$  is the current vector.

### 8.2.1 Use of leadership in the mutation (GDE3/best/1)

In single objective optimization, the DE/best/1 scheme works as follows

$$\vec{V}_t = \vec{X}_{best} + F \times (\vec{X}_c - \vec{X}_b), \quad (44)$$

where  $\vec{X}_{best}$  is the best found solution.

The purpose of using the best solution is to achieve a faster convergence of the population as in PSO where the global best solution is used to update the velocity of every particle. Now, the issue is that there is no best (fittest) solution in MOPs. A possible and logical alternative would be to select randomly one of the non-dominated solutions as in SMPSO. However, it has been shown recently [184] and in the previous chapter that if non-dominated solutions are located in the same area in the objective space

they will pull the entire population towards that specific region which affects the well-distribution of the population. Consequently, the population will end-up either by a slower convergence speed or a premature convergence. As a solution, it is proposed to select more representative leaders, called deputy leaders, in a more representative (well-distributed) manner as in [184]. So, it is proposed to use the GDE3/best/1 scheme where "best" are deputy leaders. This proposed scheme is the main cause of GDE3 performance improvement. But, the deputy leaders are selected differently than in LSMPSO which used the WSM for leader selection. Actually,  $p\%$  of deputy leaders are selected using the classical non-dominance sorting which uses the non-dominance and crowding distance discriminants as follows:

$$\vec{V}_t = \vec{X}_{deputy} + F \times (\vec{X}_c - \vec{X}_b), \quad (45)$$

where  $\vec{X}_{deputy}$  is a  $p\%$  "best" solutions selected using the Non-Dominance sorting. In this chapter,  $p = 10\%$ .

### **8.2.2 Non-dominance sorting for the difference vector**

To further accelerate the convergence speed; it is proposed to apply the same non-dominance sorting between the vectors used to generate the difference vector. Intuitively, the difference vector should be, as in PSO, from a better solution to a lower quality solution to converge towards optimum. So, the proposed mutation scheme GDE3/best/1 is described below. The bold sections are the modified portions of the difference vector.

Proposed (in bold) Difference Vector

**If**  $\left( (\vec{X}_c < \vec{X}_b) \text{ OR } \left( (\vec{X}_c \leq \vec{X}_b) \text{ and } (CD(\vec{X}_c) < CD(\vec{X}_b)) \right) \right)$

$$\vec{V}_t = \vec{X}_{deputy} + F \times (\vec{X}_c - \vec{X}_b)$$

**Else**

$$\vec{V}_t = \vec{X}_{deputy} + F \times (\vec{X}_b - \vec{X}_c)$$

**EndIf**

where  $\vec{X}_{deputy}$  is randomly selected among deputy leaders, and  $\vec{X}_c$  and  $\vec{X}_b$  are randomly selected from the population,  $i \neq deputy \neq a \neq b$ .

*CD*: crowding distance.

### 8.2.3 Negation of Control Parameter F

The earlier proposed schemes, namely, the use of deputies and the use of non-dominance ranking in differential mutation serve to increase the convergence speed while preserving a uniform distribution [15]. However, our observations show in specific cases these modifications can lead to premature convergence. For example, the experiments show that premature convergence might happen when the search space is very large, i.e. there is a large distance between the initial population and the real Pareto optimal solutions in the objective space as illustrated in Figure 44 and 45.

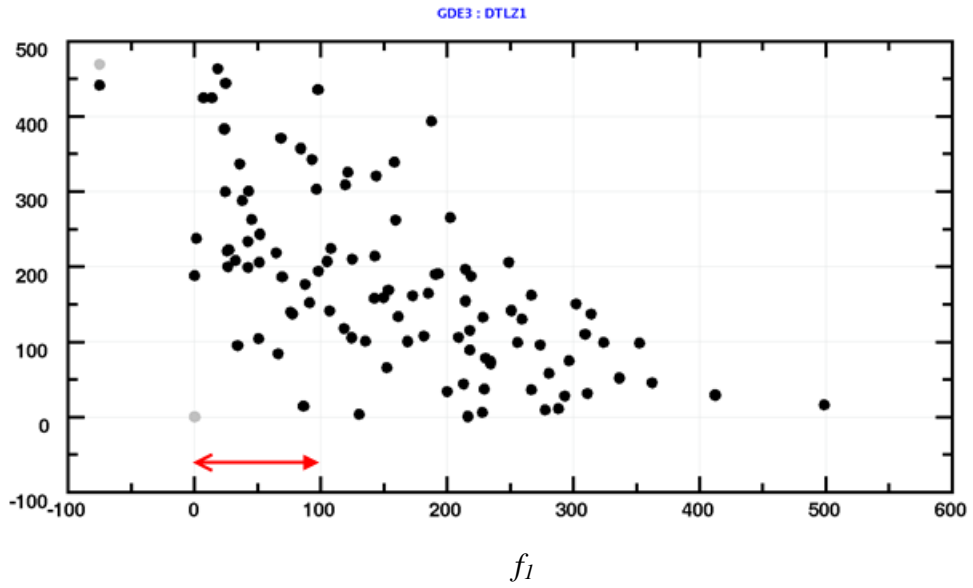


Figure 44: Example of a problem where the distance between the initial population and the PF is reasonable

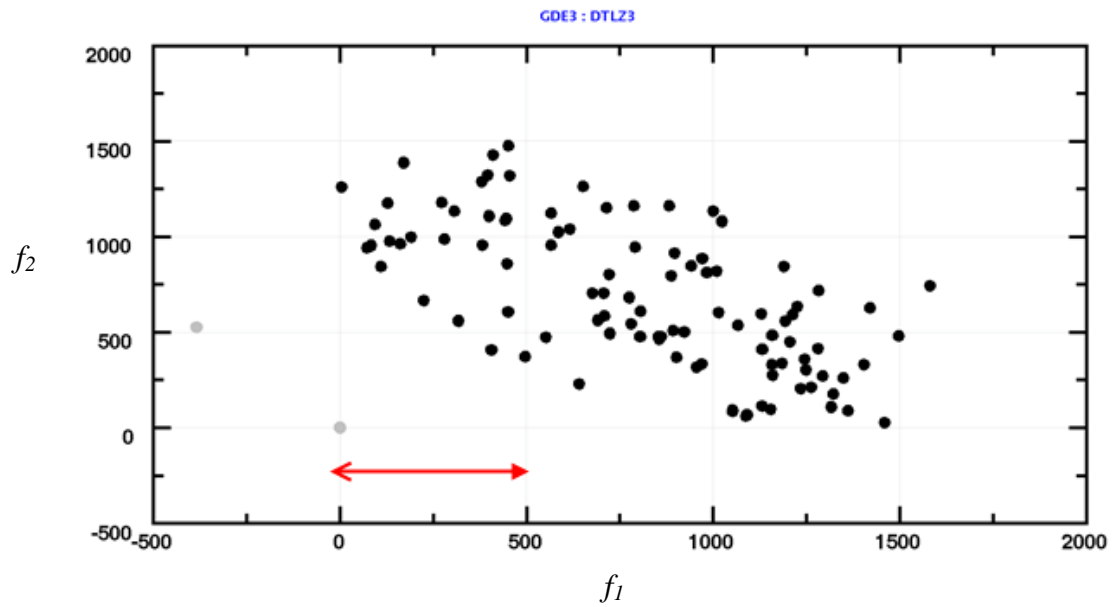


Figure 45: Example of a problem where the distance between the initial population and the PF is large

Therefore to solve this problem, it is proposed to use the negative of control parameter F with a certain probability which is fixed to 0.3 in our experiments similar to the jumping rate used in ODE [14]. Changing the sign of F serves to relax the convergence speed and maintain diversity in variable space to avoid premature convergence.

#### Negation of the F Factor with Jumping

Modified sections for inverse factor F are in red.

```
If (rand(0, 1) < p) { //p=0.3
```

$$\vec{V}_t = \vec{X}_{deputy} - F \times (\vec{X}_b - \vec{X}_c)$$

```
}
```

```
where  $(\vec{X}_c < \vec{X}_b)$  OR  $((\vec{X}_c \leq \vec{X}_b)$  and  $(CD(\vec{X}_c) < CD(\vec{X}_b))$ )
```

### 8.3 Multi-Objective Differential Evolution with Leadership

By integrating the proposed mutation modifications, presented in previous section, into GDE3, a new MOM is proposed, called Multi-objective Differential Evolution with Leadership enhancement (MODEL). The details are described in the pseudocode.

MODEL Algorithm. In bold, the modification added to GDE3.

1. Evaluate the initial population  $P$  of random individuals.
2. While stopping criterion not met, do:
  - 2.1. For each individual  $P_i$  ( $i = 1, \dots, popSize$ ) from  $P$  repeat:
    - (a) Generate candidate  $t$  from parent  $P_i$  as follows.
 
$$\mathbf{If} \left( (\vec{X}_c < \vec{X}_b) \mathbf{OR} \left( (\vec{X}_c \leq \vec{X}_b) \mathbf{and} (CD(\vec{X}_c) < CD(\vec{X}_b)) \right) \right)$$

$$\vec{X}_d = (\vec{X}_c - \vec{X}_b)$$

$$\mathbf{]Else\{}$$

$$\vec{X}_d = (\vec{X}_b - \vec{X}_c)$$

$$\mathbf{\}}$$

$$\mathbf{If} (rand(0,1) < p) \{ \mathbf{//change sign of } F$$

$$\vec{V}_t = \vec{X}_{deputy} - F \times \vec{X}_d$$

$$\mathbf{\}else\{}$$

$$\vec{V}_t = \vec{X}_{deputy} + F \times \vec{X}_d$$

$$\mathbf{\}}$$

And  $i \neq deputy \neq a \neq b$
    - (b) Evaluate the candidate solution.
    - (c) If the candidate dominates the parent, the candidate replaces the parent.  
 If the parent dominates the candidate, the candidate is discarded.  
 Otherwise, the candidate is added in the population.
  - 2.2. If the population has more than  $popSize$  individuals, truncate it.



## 8.4 Experimental Results

MODEL is compared to seven state-of-the-art metaheuristics, namely, SPEA2, NSGA-II, GDE3, SMPSO, AbYSS, MOCeLL and MOEAD as in all the previous studies in this thesis. The algorithms settings are similar to the comparative study in Chapter 3. The stopping criterion of MOMs is set  $10^4$  functions evaluations for bi-objective problems and  $3 \times 10^4$  functions calls for three-objective problems. The population and archive sizes are set to 100. The IGD measure is used as comparative measure for rankings the algorithms. The bi-objective ZDT, DTLZ, WFG and LZ\_09 problems are used for comparison purposes.

### 8.4.1 ZDT, DTLZ, and WFG problems

All the problems in Table 22 are bi-objective problems. It can be clearly seen that the proposed MODEL algorithm outperformed all the other state-of-the-art MOMs, followed by its parent algorithm GDE3.

As shown in Table 23, MODEL is the most accurate for 12 problems (ZDT1-ZDT3, ZDT6, DTLZ6-DTLZ7, WFG1-WFG2, WFG4, WFG6 and WFG9) and second most accurate for 3 problems (DTLZ1, DTLZ3 and WFG7). Overall, MODEL is in top two positions 15 out of 21 problems i.e. 71.5%. The second position is occupied by GDE3 which is the most accurate for four problems (ZDT6, DTLZ1, DTLZ6, and WFG4) and the second most accurate for nine problems (ZDT1, ZDT3, DTLZ4, WFG1-WFG2, WFG5-WFG7, and WFG9). In addition, MODEL was more accurate or equivalently accurate to its parent algorithm GDE3 for 20 out 21 problems with the

exception of the DTLZ1 problem, which is a linear problem. Therefore, MODEL proves to be consistently outperforming GDE3 in variant complex problems. It can be seen from Table 22 that MODEL was not among the top two MOMs for the WFG3 which is also a linear problem; however, its performance was similar to GDE3. The performance of MODEL with linear problems needs to be further investigated.

Table 22: IGD, mean and standard deviation for bi-objective problems  
 Dark grey is the algorithm having the best IGD results followed by light grey in the second position.

	MODEL	SPEA2	NSGAI1	GDE3	SMPSO	AbYSS	MOCcell	MOEAD
ZDT1	1.62e-04 <sub>8.6e-06</sub>	9.74e-04 <sub>3.0e-04</sub>	6.09e-04 <sub>1.3e-04</sub>	2.23e-04 <sub>5.2e-05</sub>	2.10e-04 <sub>9.9e-04</sub>	7.75e-04 <sub>6.8e-04</sub>	4.37e-04 <sub>9.8e-05</sub>	2.69e-02 <sub>7.1e-03</sub>
ZDT2	1.80e-04 <sub>2.3e-05</sub>	2.73e-03 <sub>1.6e-02</sub>	9.84e-04 <sub>3.0e-04</sub>	3.47e-04 <sub>1.1e-04</sub>	1.52e-04 <sub>1.1e-04</sub>	7.31e-04 <sub>1.5e-03</sub>	2.28e-04 <sub>1.9e-04</sub>	4.95e-02 <sub>8.5e-03</sub>
ZDT3	3.83e-04 <sub>6.2e-05</sub>	1.35e-03 <sub>4.9e-04</sub>	7.33e-04 <sub>1.6e-04</sub>	5.71e-04 <sub>1.2e-04</sub>	3.72e-03 <sub>5.2e-03</sub>	5.23e-03 <sub>4.5e-03</sub>	7.96e-04 <sub>6.0e-04</sub>	3.42e-02 <sub>4.9e-03</sub>
ZDT4	1.62e-02 <sub>8.3e-03</sub>	4.26e-02 <sub>2.0e-02</sub>	1.76e-02 <sub>1.2e-02</sub>	3.20e-02 <sub>1.3e-02</sub>	1.54e-04 <sub>1.1e-05</sub>	1.37e-02 <sub>1.1e-02</sub>	4.59e-03 <sub>5.4e-03</sub>	4.21e-01 <sub>2.8e-01</sub>
ZDT6	1.17e-04 <sub>7.2e-06</sub>	2.08e-02 <sub>4.5e-03</sub>	1.23e-02 <sub>2.3e-03</sub>	1.17e-04 <sub>7.8e-06</sub>	1.20e-04 <sub>1.1e-05</sub>	1.22e-03 <sub>4.5e-04</sub>	1.45e-03 <sub>3.5e-04</sub>	6.98e-03 <sub>3.8e-02</sub>
DTLZ1	3.40e-04 <sub>4.2e-05</sub>	1.33e-01 <sub>1.1e-01</sub>	1.19e-01 <sub>1.0e-01</sub>	6.64e-04 <sub>4.7e-04</sub>	3.31e-04 <sub>3.8e-05</sub>	1.02e-01 <sub>1.0e-01</sub>	5.42e-02 <sub>8.9e-02</sub>	1.72e-01 <sub>4.7e-01</sub>
DTLZ2	3.49e-04 <sub>9.4e-06</sub>	3.58e-04 <sub>1.3e-05</sub>	4.43e-04 <sub>3.4e-05</sub>	3.51e-04 <sub>9.1e-06</sub>	3.62e-04 <sub>1.8e-05</sub>	3.44e-04 <sub>6.9e-06</sub>	3.46e-04 <sub>8.6e-06</sub>	3.58e-04 <sub>7.0e-06</sub>
DTLZ3	5.78e-01 <sub>3.0e-01</sub>	1.42e+00 <sub>7.7e-01</sub>	1.21e+00 <sub>6.6e-01</sub>	8.61e-01 <sub>2.9e-01</sub>	8.46e-04 <sub>3.1e-02</sub>	1.51e+00 <sub>9.1e-01</sub>	7.85e-01 <sub>5.6e-01</sub>	1.49e+00 <sub>2.9e+00</sub>
DTLZ4	1.66e-04 <sub>4.6e-05</sub>	1.11e-04 <sub>6.6e-03</sub>	1.11e-04 <sub>2.6e-05</sub>	9.60e-05 <sub>2.0e-05</sub>	1.02e-04 <sub>2.5e-05</sub>	8.69e-05 <sub>7.4e-06</sub>	6.70e-03 <sub>6.6e-03</sub>	3.28e-04 <sub>1.4e-04</sub>
DTLZ5	3.48e-04 <sub>7.8e-06</sub>	3.58e-04 <sub>1.1e-05</sub>	4.45e-04 <sub>2.5e-05</sub>	3.53e-04 <sub>1.1e-05</sub>	3.58e-04 <sub>2.1e-05</sub>	3.43e-04 <sub>7.5e-06</sub>	3.46e-04 <sub>8.8e-06</sub>	3.58e-04 <sub>7.8e-06</sub>
DTLZ6	3.49e-04 <sub>6.9e-06</sub>	1.68e-01 <sub>1.1e-02</sub>	1.25e-01 <sub>9.5e-03</sub>	3.49e-04 <sub>5.4e-06</sub>	4.20e-04 <sub>6.1e-02</sub>	5.16e-02 <sub>1.4e-02</sub>	4.40e-02 <sub>9.2e-03</sub>	4.07e-04 <sub>9.7e-04</sub>
DTLZ7	2.00e-04 <sub>1.7e-05</sub>	8.78e-04 <sub>2.8e-04</sub>	4.69e-04 <sub>9.6e-05</sub>	2.22e-04 <sub>2.3e-05</sub>	1.79e-04 <sub>1.4e-05</sub>	2.88e-04 <sub>2.0e-04</sub>	2.73e-04 <sub>5.8e-05</sub>	4.25e-02 <sub>1.4e-02</sub>
WFG1	7.15e-04 <sub>2.8e-04</sub>	5.22e-03 <sub>9.6e-04</sub>	4.29e-03 <sub>8.4e-04</sub>	9.66e-04 <sub>1.9e-04</sub>	4.79e-03 <sub>6.2e-05</sub>	5.70e-03 <sub>1.2e-03</sub>	4.15e-03 <sub>9.0e-04</sub>	4.37e-03 <sub>7.4e-04</sub>
WFG2	5.32e-05 <sub>6.1e-06</sub>	3.48e-04 <sub>2.8e-04</sub>	3.48e-04 <sub>2.8e-04</sub>	5.60e-05 <sub>7.4e-06</sub>	1.44e-04 <sub>3.8e-05</sub>	3.49e-04 <sub>4.0e-06</sub>	3.48e-04 <sub>1.5e-06</sub>	2.54e-04 <sub>4.1e-05</sub>
WFG3	6.84e-04 <sub>8.4e-08</sub>	6.86e-04 <sub>6.9e-06</sub>	6.84e-04 <sub>1.6e-06</sub>	6.84e-04 <sub>1.1e-07</sub>	6.82e-04 <sub>1.3e-06</sub>	6.83e-04 <sub>1.2e-06</sub>	6.83e-04 <sub>9.7e-07</sub>	6.83e-04 <sub>4.5e-07</sub>
WFG4	9.16e-05 <sub>2.5e-06</sub>	1.15e-04 <sub>6.5e-06</sub>	1.25e-04 <sub>1.3e-05</sub>	9.21e-05 <sub>3.0e-06</sub>	3.46e-04 <sub>3.1e-05</sub>	9.19e-05 <sub>2.6e-06</sub>	9.46e-05 <sub>3.8e-06</sub>	3.86e-04 <sub>4.0e-05</sub>
WFG5	5.38e-04 <sub>5.6e-07</sub>	5.45e-04 <sub>2.2e-06</sub>	5.51e-04 <sub>4.8e-06</sub>	5.38e-04 <sub>4.9e-07</sub>	5.38e-04 <sub>1.2e-06</sub>	5.39e-04 <sub>9.5e-07</sub>	5.40e-04 <sub>1.1e-06</sub>	5.48e-04 <sub>2.2e-06</sub>
WFG6	9.56e-05 <sub>1.3e-05</sub>	1.70e-04 <sub>1.3e-04</sub>	1.93e-04 <sub>1.5e-04</sub>	9.73e-05 <sub>1.5e-05</sub>	1.29e-04 <sub>1.7e-05</sub>	6.86e-04 <sub>7.3e-04</sub>	3.92e-04 <sub>6.4e-04</sub>	1.31e-04 <sub>9.2e-06</sub>
WFG7	8.73e-05 <sub>2.4e-06</sub>	9.66e-05 <sub>4.1e-06</sub>	1.22e-04 <sub>1.3e-05</sub>	8.72e-05 <sub>2.0e-06</sub>	1.12e-04 <sub>1.2e-05</sub>	8.65e-05 <sub>2.0e-06</sub>	8.69e-05 <sub>2.4e-06</sub>	1.31e-04 <sub>4.3e-06</sub>
WFG8	1.07e-03 <sub>2.3e-05</sub>	1.06e-03 <sub>1.2e-04</sub>	9.40e-04 <sub>1.4e-04</sub>	1.07e-03 <sub>4.1e-05</sub>	1.01e-03 <sub>6.8e-05</sub>	1.07e-03 <sub>3.7e-05</sub>	1.06e-03 <sub>3.8e-05</sub>	8.95e-04 <sub>1.6e-04</sub>
WFG9	1.09e-04 <sub>1.4e-05</sub>	1.25e-04 <sub>1.8e-05</sub>	1.51e-04 <sub>1.8e-05</sub>	1.13e-04 <sub>1.6e-05</sub>	1.59e-04 <sub>8.3e-06</sub>	1.35e-04 <sub>4.2e-05</sub>	1.22e-04 <sub>2.4e-05</sub>	1.79e-04 <sub>7.6e-06</sub>

The third most robust MOM is AbYSS. It is the most accurate for five problems; which were all concave problems, although there are also several other problems characterized by concavity where AbYSS was not accurate. In brief, AbYSS seems to be advantageous when dealing with certain types of MO optimization concave problems.

Table 23: Scores for bi-objective problems (1 point for the 2<sup>nd</sup> position and 3 points for the 1<sup>st</sup> position)

	MODEL		NSGA-II		SPEA2		GDE3		SMPSO		AbYSS		MOCeII		MOEA/D	
1 <sup>st</sup>	12	36	0	0	0	0	4	12	3	9	5	15	0	0	1	3
2 <sup>nd</sup>	3	3	1	1	2	6	9	9	1	1	1	1	1	5	0	0
Total	39		1		6		21		10		16		5		3	

As shown in Figure 46, 47, 48 the MODEL algorithm is very consistent across variant problems in terms of accuracy using limited number of function evaluations. In addition, it can be seen that MODEL accuracy was significantly better than all other MOMs with the WFG problems which are known to be the most complex family of MOPs after LZ\_09.

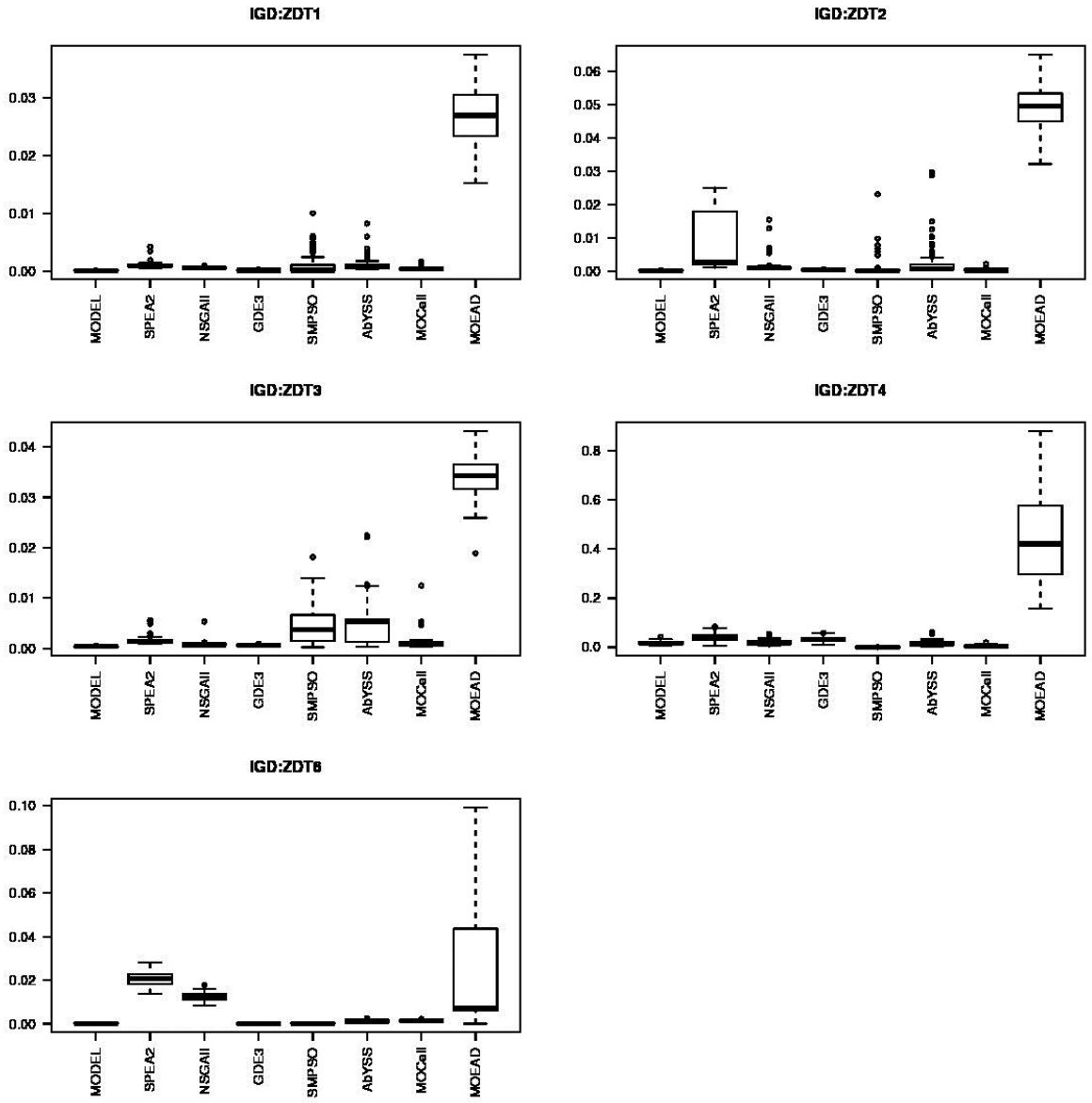


Figure 46: IGD boxplots for ZDT bi-objective problems

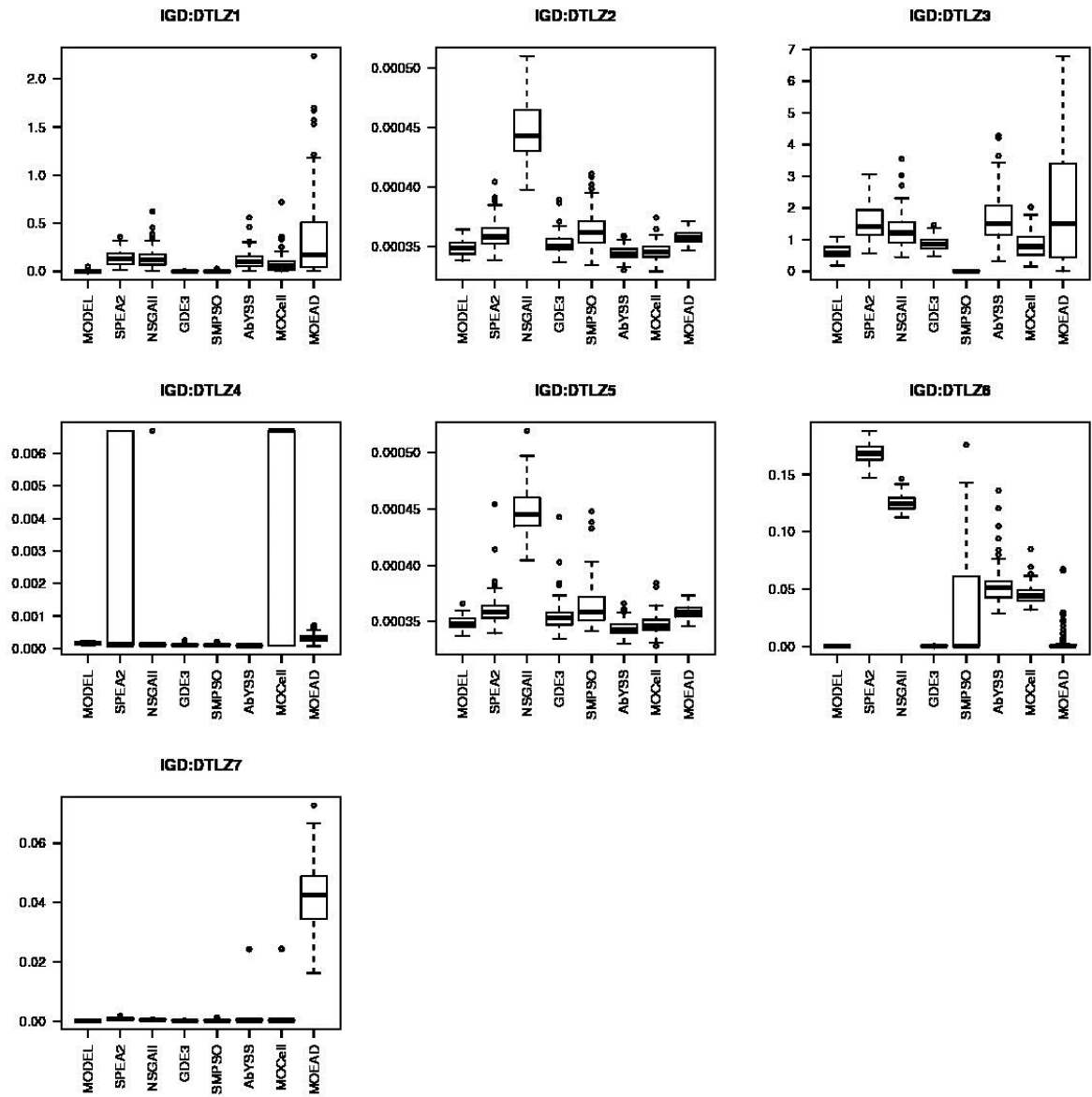


Figure 47: IGD boxplots for DTLZ bi-objective problems

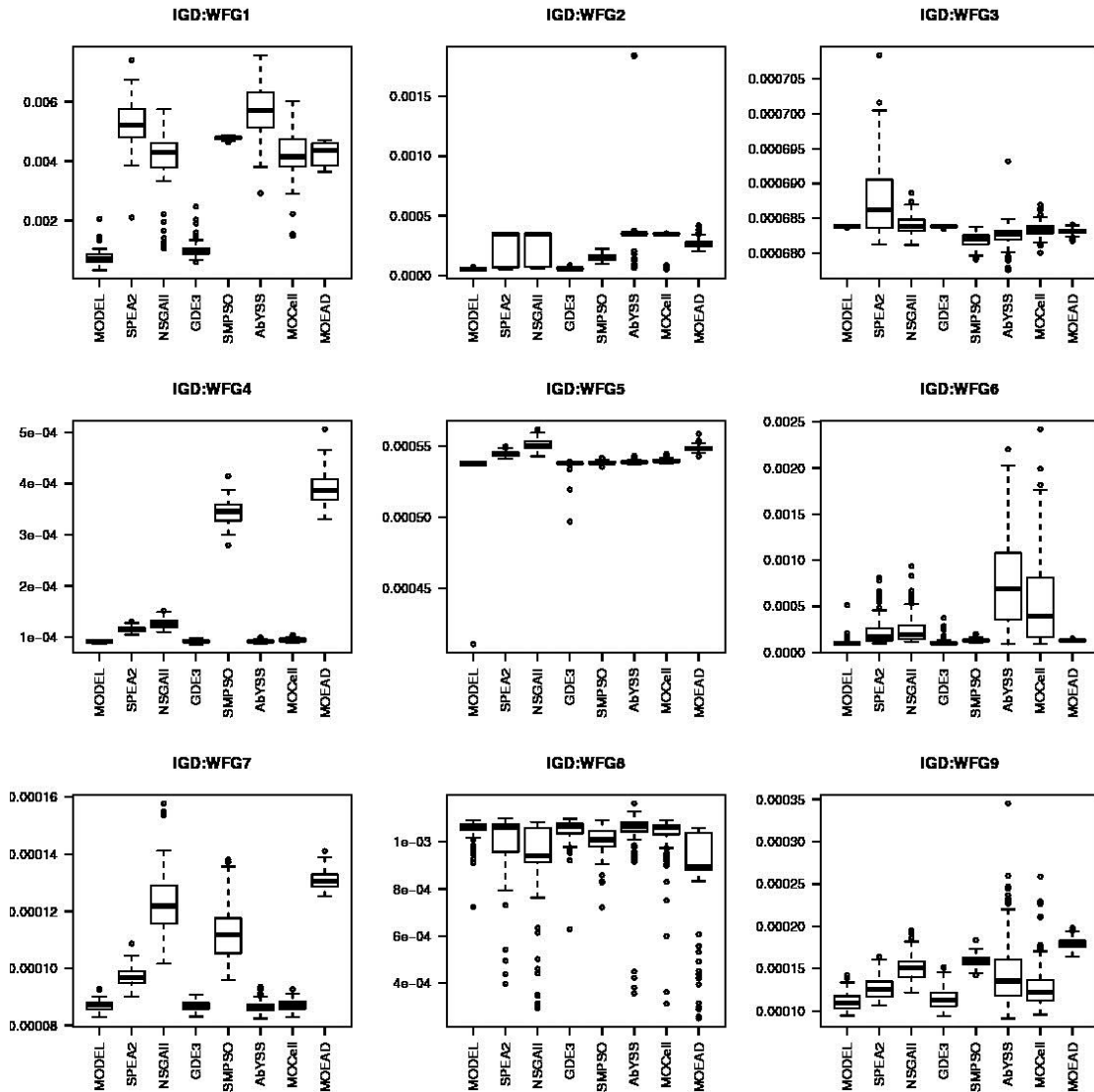


Figure 48: IGD boxplots for WFG bi-objective problems

### 8.4.2 LZ\_09 problems

The LZ\_09 are the most complex family of problems. As shown in Figure 49: IGD boxplots for LZ\_09 bi-objective problems, the proposed MODEL in six out of nine problems (F1-F4, F6 and F9) the most accurate MOM, and it occupies only once second position for F5. Overall, it is among top two most accurate MOMs seven out of nine problems i.e. 77.7%.

Table 24: IGD, mean and standard deviation for bi-objective problems.

Dark grey is the algorithm having the best IGD results followed by light grey in the second position.

MODEL	SPEA2	NSGAI	GDE3	SMP	AbYSS	MOCe	MOEA	
LZ09F1	3.46e-03 <sub>8.5e-04</sub>	5.95e-03 <sub>2.9e-03</sub>	3.59e-03 <sub>2.0e-03</sub>	3.84e-03 <sub>1.3e-03</sub>	5.35e-03 <sub>2.1e-03</sub>	6.86e-03 <sub>3.1e-03</sub>	6.02e-03 <sub>2.8e-03</sub>	4.29e-03 <sub>1.4e-03</sub>
LZ09F2	4.98e-03 <sub>5.5e-04</sub>	5.36e-03 <sub>9.6e-04</sub>	5.18e-03 <sub>2.8e-03</sub>	4.95e-03 <sub>5.5e-04</sub>	1.29e-02 <sub>1.5e-03</sub>	1.00e-02 <sub>2.7e-03</sub>	1.11e-02 <sub>6.6e-03</sub>	1.21e-02 <sub>5.1e-03</sub>
LZ09F3	4.16e-03 <sub>5.6e-04</sub>	4.34e-03 <sub>8.6e-04</sub>	3.92e-03 <sub>4.9e-04</sub>	4.28e-03 <sub>5.4e-04</sub>	1.31e-02 <sub>7.2e-03</sub>	8.94e-03 <sub>6.3e-03</sub>	1.00e-02 <sub>7.8e-03</sub>	1.11e-02 <sub>2.1e-03</sub>
LZ09F4	4.38e-03 <sub>6.9e-04</sub>	4.76e-03 <sub>8.6e-04</sub>	4.39e-03 <sub>6.1e-04</sub>	4.46e-03 <sub>4.0e-04</sub>	1.22e-02 <sub>5.8e-03</sub>	4.65e-03 <sub>1.1e-03</sub>	4.57e-03 <sub>2.5e-03</sub>	1.04e-02 <sub>2.5e-03</sub>
LZ09F5	3.48e-03 <sub>4.7e-04</sub>	3.82e-03 <sub>6.3e-04</sub>	3.60e-03 <sub>6.8e-04</sub>	3.58e-03 <sub>3.4e-04</sub>	1.04e-02 <sub>5.5e-03</sub>	4.90e-03 <sub>5.9e-03</sub>	6.21e-03 <sub>6.9e-03</sub>	1.04e-02 <sub>2.2e-03</sub>
LZ09F6	5.27e-03 <sub>9.3e-04</sub>	7.23e-03 <sub>2.9e-03</sub>	1.21e-02 <sub>5.3e-03</sub>	5.17e-03 <sub>1.2e-03</sub>	2.76e-02 <sub>2.4e-02</sub>	1.48e-02 <sub>6.4e-03</sub>	1.68e-02 <sub>8.1e-03</sub>	2.05e-02 <sub>2.2e-03</sub>
LZ09F7	1.44e-02 <sub>3.1e-03</sub>	1.20e-02 <sub>5.9e-03</sub>	1.08e-02 <sub>3.8e-03</sub>	1.61e-02 <sub>3.0e-03</sub>	1.86e-02 <sub>1.1e-03</sub>	1.76e-02 <sub>8.6e-03</sub>	1.68e-02 <sub>7.2e-03</sub>	2.24e-02 <sub>8.7e-03</sub>
LZ09F8	1.82e-02 <sub>2.6e-03</sub>	1.26e-02 <sub>3.5e-03</sub>	1.29e-02 <sub>3.9e-03</sub>	1.82e-02 <sub>2.2e-03</sub>	1.97e-02 <sub>2.1e-03</sub>	1.73e-02 <sub>1.0e-02</sub>	1.56e-02 <sub>7.0e-03</sub>	2.01e-02 <sub>6.0e-03</sub>
LZ09F9	5.55e-03 <sub>4.8e-04</sub>	6.34e-03 <sub>4.1e-03</sub>	7.62e-03 <sub>3.4e-03</sub>	5.60e-03 <sub>4.3e-04</sub>	1.67e-02 <sub>3.2e-03</sub>	1.06e-02 <sub>1.4e-03</sub>	1.10e-02 <sub>8.4e-03</sub>	1.20e-02 <sub>5.8e-03</sub>



The second position is occupied by GDE3 which is the most accurate for five problems (F2, F4-F6 and F9) and second most accurate for one problem which was F1. The accuracy of MODEL and GDE3 is comparable for LZ\_09 family of problem. They both equally top one for four problems (F2, F4, F6 and F9), and MODEL achieved a higher accuracy than GDE3 for F3. Both MODEL and GDE3 did not perform well with F8 and F9 which have a simple curving shape relationship among the variables as shown in Figure 12 (Chapter 3), whereas all the other problems have a much more complex relationship. F1 has also a similar curvature but MODEL achieved the highest score.

It is interesting to note that NSGA-II achieved a good accuracy with LZ\_09 test suite by being thrice the most accurate (F4, F7 and F8) and the second most accurate (F1, F3 and F5). It seems that the cross-over of NSGA-II achieves better results with complex variable relationships. It would be interesting to investigate if by modifying the configuration parameters (CR and F), is it possible to enhance MODEL's accuracy.

Table 25: Scores for LZ\_09 problems (1 point for the 2<sup>nd</sup> position and 3 points for the 1<sup>st</sup> position)

	MODEL		SPEA2		NSGA-II		GDE3		SMP SO		AbYSS		MOCe ll		MOEA/D	
1 <sup>st</sup>	6	18	1	3	3	9	5	15	0	0	0	0	0	0	0	0
2 <sup>nd</sup>	1	1	1	1	3	3	1	1	0	0	0	0	0	0	1	1
Total	19		4		12		16		0		0		0		1	

As shown Figure 49, both MODEL and GDE3 provided consistent accuracy. Thus, based on the boxplots, there is four MOMs that achieved overall high accuracy which are: MODEL, SPEA2, NSGA-II and GDE3.

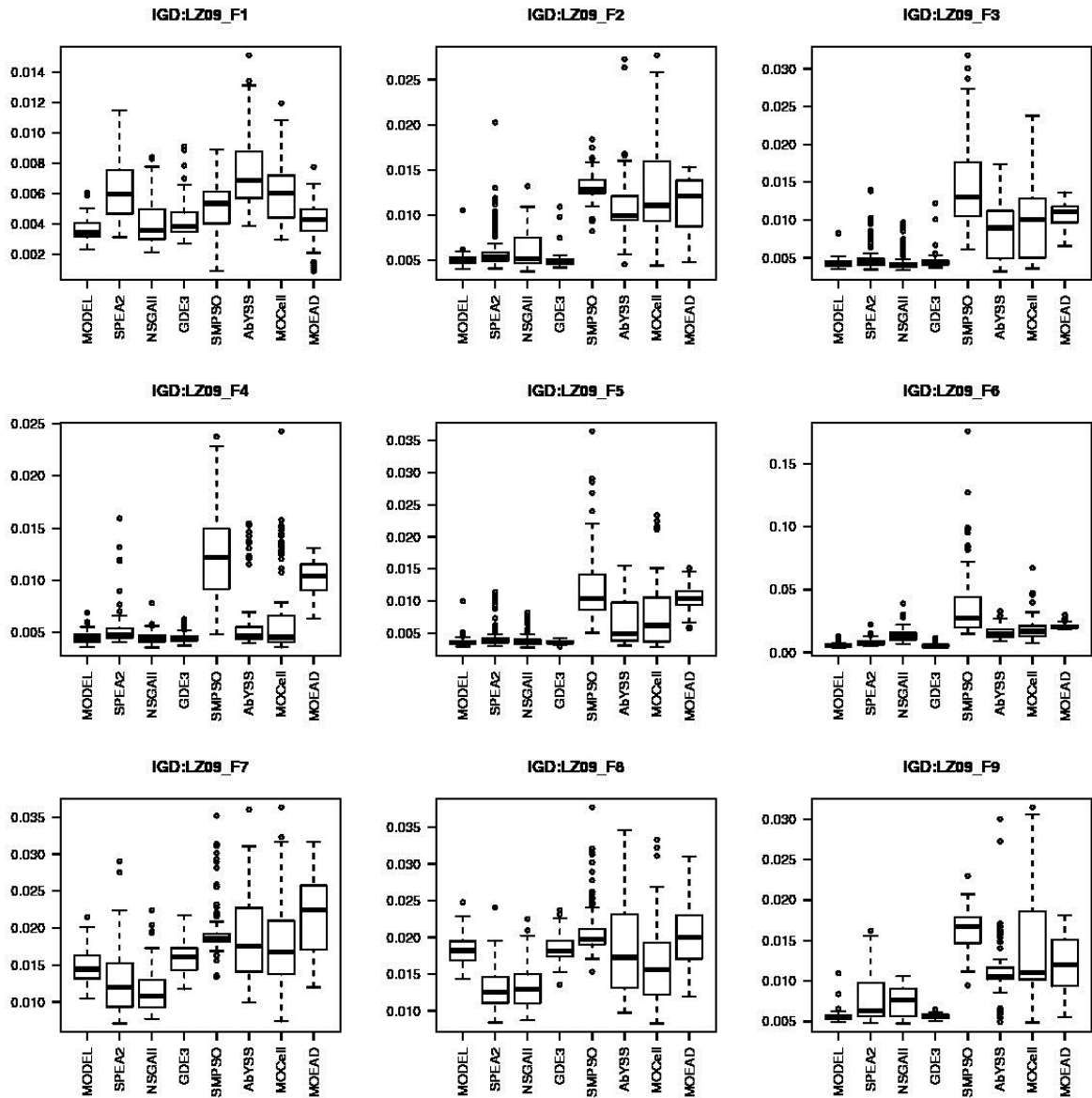


Figure 49: IGD boxplots for LZ\_09 bi-objective problems

## 8.5 Conclusions

This chapter proposed a new MOM named MODEL based on a MO version of DE. MODEL incorporated the leadership concept into DE's mutation operator. The leadership served to accelerate GDE3 by adapting the DE/best/1 mutation scheme to multi-objective space as GDE3/deputy/1. In addition, the non-dominance concept was used to determine the leader among the two vectors that generate the mutant vectors. Finally, the negation of the control factor  $F$  with probability was used to avoid premature convergence.

The proposed MODEL has been compared to seven state-of-the-art metaheuristics using 30 bi-objective problems taken from ZDT, DTLZ, WFG, and LZ\_09. It was the most accurate one for 18 out of 30 problems. For the first group of problems (ZDT, DTLZ, WFG), MODEL outperformed its parent algorithms most of the time and Abyss also showed good accuracy for certain concave problems. For the LZ\_09 problems which are considered to be among the most complex problems, MODEL was the most accurate MOM, performing slightly better than GDE3. Both of these algorithms seemed to have lower accuracy with problems having curvature landscape among variables. NSGA-II showed a good accuracy possibly because of the crossover mechanism.

In future, we would like to test the proposed method on many-objective problems. It is also important to examine the performance of MODEL by varying the configuration parameters for problems with high epistasis.

To demonstrate the performance of the proposed MODEL MOM, it would be valuable to apply the MODEL algorithm on a real case study. The next chapter presents a complex RES-related case study.

## **Chapter 9**

### **Case Study II: Optimization of Transition to Hydrogen-Fuelled Vehicles in Ontario, Canada Considering Electricity Grid Constraints**

For optimal design of RESs, as stated in Chapter 4, MOO methods are rarely used, and even when they are used, state-of-the-art MOMs are rarely utilized because of miscommunication between RES and MOM research communities. Also, most works focused on wind and solar RESs, and all the projects were standalone. Therefore, this case study addresses these challenges by utilizing state-of-the-art MOO methods to design a hydrogen energy system which is grid-connected. In reality, the proposed model in the case study consists of an integrated hydrogen infrastructure with the electrical grid in Ontario, Canada which has a larger superficies than any European country. The developed MODEL algorithm presented in the previous chapter is compared with four other MOMs to solve the proposed case study.

## **9.1 Introduction**

The rapidly increasing population and the booming economy of Canada are posing a serious challenge to its energy sector. The "Natural Resources Canada" estimates a projected growth of 1.3% per year for total energy demand and a 1.6% per year increase for transportation demand [185]. This challenge is exacerbated when factors such as environmental impact and global warming taken into consideration. To meet the future energy needs and environmental expectations, different levels of government in Canada are devising new policies and programs. To alleviate this future energy challenges, this chapter seeks to design optimal hydrogen distribution network for hydrogen-fuel vehicles (HFVs) that considers the Ontario's Integrated Power System Plan [186]. More specifically, this chapter investigates the development of electrolytic hydrogen production for HFVs during off-peak hours in the province of Ontario considering the existing and the future plan for the Ontario electricity transmission network between the

periods of 2008 to 2025. The model considers the effective generation capacity of every zone which contributes to base-load energy. The bi-objective hydrogen infrastructure model is optimized using the proposed MOM described in the previous chapter called MODEL, targeting the maximization of the HFVs penetration while minimizing the investments for hydrogen distribution network. The solutions provide the size of the hydrogen productions plans as well as the distribution network of hydrogen among the zones. This problem is innovative as it was found in RES-related literature reviews [187], [188] that state-of-the-art MOMs were not used in RESs and most RESs systems were standalone. The proposed case study uses a new MOM to optimize not only a grid connected energy system but two integrated systems: Electricity and Hydrogen distribution networks.

## **9.2 Hydrogen-Fueled Vehicles in Canada**

The world demand of energy is expected to increase by 50% in the next 25 years [189]. The combination of this important energy demand increase and fossil fuels decrease pose very serious problems for worldwide energy supply in general, and for transportation sector in particular. Transportation is the lifeblood of any economy. In Canada, 35% of the total energy demand is related to transportation, and it is the second largest contributor to greenhouse gases [190] [191]. Today's oil prices are also much higher and are expected to increase, placing additional burden on the energy and transportation demands [185]. Therefore, looking for alternative forms of energy sources is necessary from the economical and the pollution points of view. In comparison to 'zero-emission' electric vehicles, which are costly, and do not provide quick recharge solutions, with limited battery life, the hydrogen powered vehicles (HFVs) or fuel cell

vehicles provide the advantages of zero emission and rapid refueling. A switch to HFVs to a large extent would significantly reduce urban pollutants such as NO<sub>x</sub>, SO<sub>x</sub>, and CO<sub>2</sub> [192].

The concept of the hydrogen economy is not new, it was originally proposed in the early 1970s [193]. It reduces our dependence on the depleting wells of oil and makes a transition into an era of more environmentally friendly energy utilization. Hydrogen's ability to act as an energy carrier makes it even more favorable. Electrolysis, which is a non-spontaneous process of generating hydrogen from water using electricity, is approximately 80% efficient [193], [194] which allows hydrogen to be stored and transported as an alternative to electrical energy. However, currently the production of hydrogen is more expensive than oil. As an alternative, it is proposed to base hydrogen economy on exploiting the fluctuating prices of electricity generation plants that have on-peak and off-peak periods [186], [195]. All generators are rated, especially nuclear, at certain levels, where they perform optimally. However, during off-peak periods the rated levels may not be required, which results in reduced efficiency. Likewise, shutting down power plants for a few hours is not desirable either, as it could be quite costly in the case of nuclear plants [196] and thus be prohibitive.

In principle, during off-peak periods, when the electricity prices are low, electrical energy could be converted into hydrogen and used as an alternative emission-free fuel. This fuel could also be transported to other regions where hydrogen demand is high, eliminating losses due to congestion in the grid during on-peak hours. The goal of the present case study examines the feasibility of transitioning to a hydrogen economy in Ontario by extending the work in [197] but by targeting multiple objectives: 1) to

maximize the penetration of hydrogen vehicles in Ontario, and 2) to minimize the total cost of electricity generation, transportation and conversion. The optimization is done considering the constraints of existing and future plans of the electrical distribution network and hydrogen network constraints.

### 9.3 Electricity Model of Ontario

This section provides details about the electrical modeling in Ontario such as the power transmission system, the power generation sources, the possibilities of importations and exportations, the zonal electricity demand.

#### 9.3.1 Power Transmission

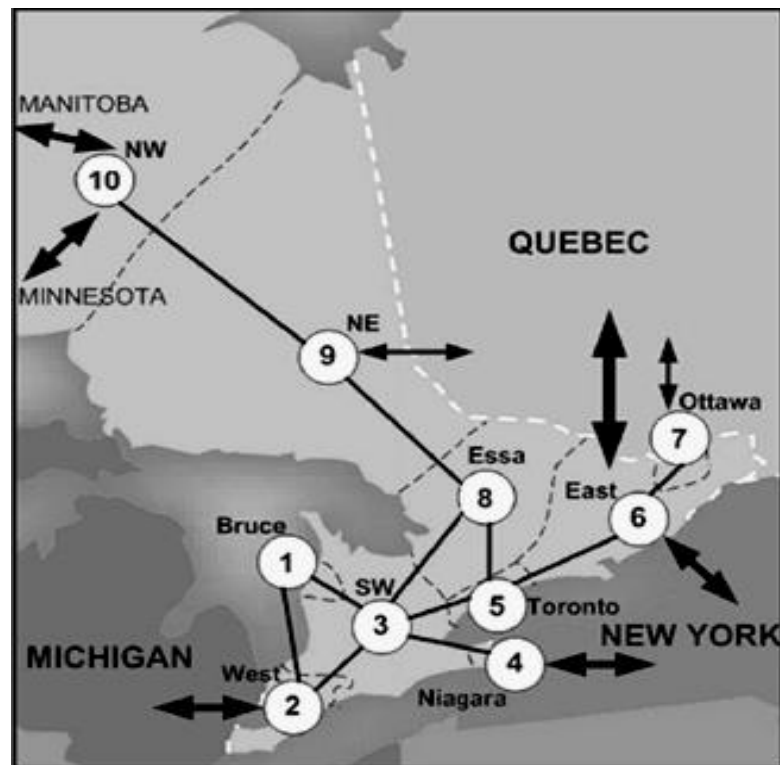


Figure 50: Simplified model of Ontario's grid zones



The Independent Electricity System Operator (IESO) has divided Ontario into ten zones that are significant for their electricity generation and demands.

Figure 50 depicts ten different zones and the power transmission grid of Ontario. It also shows the power sharing between Ontario and its neighboring regions. This grid is mainly composed of 500 kV electricity transportation networks, except for the NE-NW interconnection, which is a 230 kV network. The parameters used to model the electricity grid are determined using the typical values based on the distances among zones and transmission capacities as per the Independent Electricity System Operator [198] which specify the line loading limits for each corridor as summarized in Table 26. Moreover, these corridors are enhanced over the study period considered as outlined in Table 27 based on the data provided by OPA [198], [199].

Table 26: Line loading limits of the transmission grid

From Zone $i$	To Zone $j$	$\overline{Pd}_{ij}$ [MW]	$\overline{Pd}_{jy}$ [MW]
1	2	1940	9999
1	3	2560	9999
2	3	1560	1560
3	4	9999	1750
3	5	3212	9999
3	8	2488	9999
5	6	9999	9999
5	8	2000	1000
6	7	1900	9999
8	9	1900	1400
9	10	350	325

Table 27: Transmission corridor enhancements during the study period considered.

<b>Year</b>	<b>Corridor</b>	<b>Current MW</b>	<b>Planned MW</b>
<b>2012</b>	Bruce-SW (1-3)	2560	4560
<b>2012</b>	SW-Toronto (3-5)	3212	5212
<b>2013</b>	NE-NW (9-10)	350	550
<b>2015</b>	Bruce-West (1-2)	1940	2440
<b>2017</b>	Toronto-Essa (5-8)	2000	2500
<b>2017</b>	Essa-NE (8-9)	1900	2400

### **9.3.2 Power generation**

According to the latest directives from the Ministry of Energy to Ontario Power Authority (OPA), the Integrated Power System Plan (IPSP) [200], [197] contains several planned power generating units to the existing ones. The main energy resources in Ontario that are considered in this study are nuclear, wind, hydro, Combined Heat and Power (CHP) and coal. While natural gas is also important to satisfy Ontario electricity demands, it is ignored in this study because it only contributes during peak-loads as specified by the municipal government's 2006 Supply Mix Directive [200], [197]. Additionally, the conserved power over the study period from the Conservation and Demand Management (CDM) program is also considered as a resource in this study. Figure 51 gives an overview of the expected distribution of power capacity in different zones of Ontario.

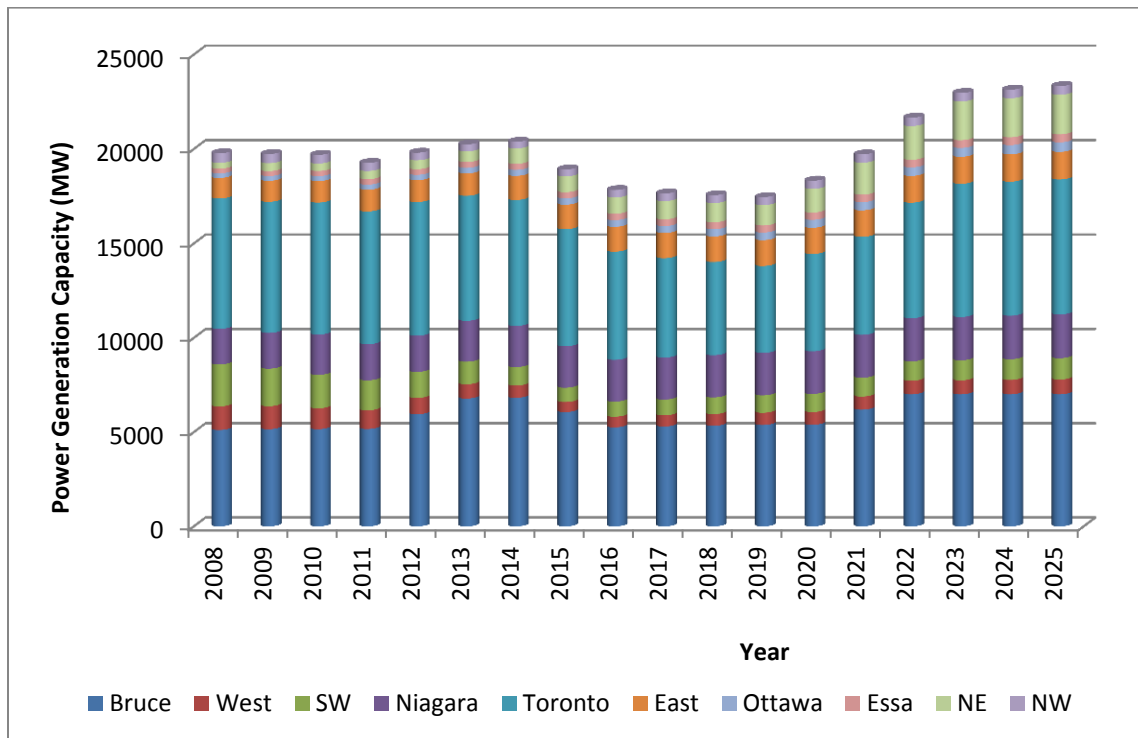


Figure 51: Overview of the expected distribution of power capacity in different zones of Ontario

### 9.3.3 Import and export of power

As mentioned previously, Ontario’s power transmission grid is interconnected with its neighboring regions from where it can import or export electricity. The excess of power in the Bruce zone makes it ideal to export electricity to Michigan via West zone. Likewise, imports are also considered from New York, Quebec, Manitoba and Minnesota. The maximum limits for imports and exports for each zone in Ontario are given in Table 53-54 (Appendix C), respectively.

### 9.3.4 Zonal electricity demand

The base-load demand for each zone was calculated using the zonal peak-load growth rate, given in Table 28, and Ontario’s overall base-load growth rate is 1.11% [201] [202], using the following equation:

$$\lambda_i = \lambda \left( \frac{\pi_i \sum_i b_i}{\sum_i \pi_i b_i} \right), \quad (46)$$

where  $\lambda_i$  is the base-load growth rate of zone  $i$ ,  $\pi_i$  is the peak-load growth rate of zone  $i$ ,  $\lambda$  is the annual overall base-load growth rate of Ontario, and  $b_i$  is the base-load value in zone as shown in Table 29.

Table 28: Estimated zonal peak-load growth rate

Zone	Bruce	West	SW	Niagara	Toronto	East	Ottawa	Essa	NE	NW
Ann. Growth %	0.78	1.14	1.28	0.41	0.77	0.71	1.42	1.17	-0.33	0.10

Table 29: Zonal base-load electricity demand [MWh]

Zone	Bruce	West	SW	Niagara	Toronto	East	Ottawa	Essa	NE	NW	Total
Weekdays 12 am - 7 am (8 h)	71.02	1667.65	2982.16	593.62	5038.52	943.34	1097.99	805.83	1353.97	634.05	15188.15
Weekdays 12 am-7 am (14 h)	71.63	1615.37	2915.64	558.82	4995.19	961.15	1156.18	845.11	1375.36	630.44	15124.88

## 9.4 Hydrogen Infrastructure Model

The following subsections provide details about the hydrogen infrastructure modeling such as hydrogen generation, hydrogen demand, and hydrogen transportation.

### 9.4.1 Hydrogen generation

During off-peak hours, demand for electricity falls. As a result, utility companies are forced to significantly reduce the consumer's 'Hourly Ontario Energy Price' (HOEP), because shutting down or switching a plant to standby mode is undesirable for its optimal performance [203]. IESO defines the on-peak hours from 7 am to 11 pm [204]. Therefore, off-peak hours, for this study, are considered to be between 12 am to 7 am for weekdays, and 12 am to 1 pm for weekends. HOEP was averaged for weekdays and weekends, at \$31.95 and \$32.73, respectively, for the first year of study. The following expressions capture the cost of electricity usage during off-peak hours in Ontario, when electricity could be utilized to produce hydrogen:

$$C_y^{d1} = \omega_y^{d1} \cdot 8 \times 261, \quad (47)$$

$$C_y^{d2} = \omega_y^{d2} \cdot 14 \times 104, \quad (48)$$

where  $C_y^{d1}$  and  $C_y^{d2}$  are the yearly electricity costs for weekdays and weekends, respectively. And  $\omega_y^{d1}$  and  $\omega_y^{d2}$  are the HOEP for weekdays and weekends.

Installing and operating hydrogen production plants (HPP) requires a large economic investment. The costs of HPP (electrolyzer) with 70% efficiency requires approximately \$1,736 CAD/KWe of investment which is calculated based on a unit of 60

Nm<sup>3</sup>/h (5.38kh/h): the cost of electrolyzer and compressor (\$84,500 CAD), \$4,500 CAD per kg/h of hydrogen flow, and \$600 CAD/kg for the storage, for a total of \$504,767 [190]. They also estimated 3% of this amount will be spent on the insurance, operations and maintenance costs of the plant [198] [199]. The resulting expression that accounts for all of the HPP costs is:

$$C_{i,y}^h = P_{i,y}^{HPP} \cdot 1736000 \cdot (1 + 0.03), \quad (49)$$

where  $C_{i,y}^h$  is the total yearly investment for HPP in zone i, and  $P_{i,y}^{HPP}$  is the size of the installed plant in megawatts (MW).

#### 9.4.2 Hydrogen demand

The demand for hydrogen was determined by estimating the number of HFVs expected to operate in Ontario each year. According to the Natural Resources of Canada, Ontario is estimated to have 0.55 vehicles per capita [207]. A reliable model of the hydrogen demand was developed by first studying the population size of each zone as posted by Statistics Canada [208], and then estimating the number of vehicles in each zone in Figure 53. These numbers were projected into the future, as the base-load growth was expected to increase over the period of study. A transition to HFVs over the study period is assumed to increase linearly as illustrated in percentage in Figure 52, with no HFV expected in the first year and K% expected in the last year. The expression that yield the expected number of zonal HFVs in a year is

$$N_{i,y}^{FCV} = 0.55 \cdot \mu_{i,y}^p \cdot \frac{K}{100} \cdot \frac{y - y_0}{y_f - y_0}, \quad (50)$$

where  $\mu_{i,y}^p$  represents the yearly population size of zone  $i$ ,  $K$  stands for the total penetration of hydrogen HFVs in the year  $y_f$ , the last year of study, and  $y_0$  stands for the first year of study.

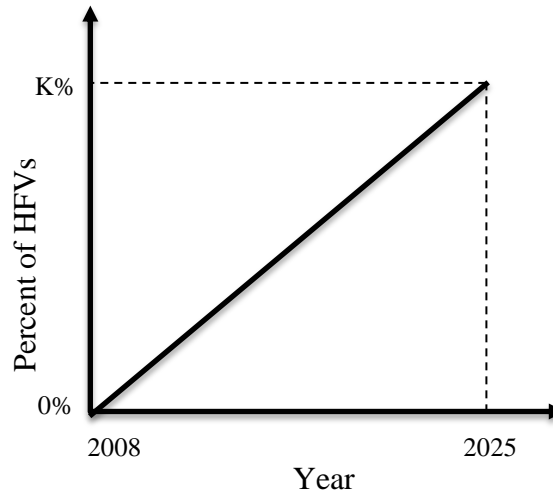


Figure 52: Estimated penetration of HFVs in Ontario

The fuel economy of HFVs is known to be around 100 km/kg [205], [209], with an average annual mileage of 20,000 km, the yearly demand for hydrogen was determined to be 200 kg/ HFV. The yearly total hydrogen demand of each zone  $i$  is therefore,  $200N_{i,y}^{HFV}$  (kg). The corresponding electrical capacity that could produce the required hydrogen during the off-peak duration of 68 hours a week was determined by relating the size of the HPP (in MW) to the amount of hydrogen production. Hajimiragha

et al. [197] suggested that a plant of size 5.8 MW is capable of producing one ton of hydrogen per day.

$$\varphi_{i,y}^{hpp} = 5.8 \cdot \frac{200 \cdot N_{i,y}^{FCV}}{365 \times 1000} = 3.178 \times 10^{-3} \cdot N_{i,y}^{FCV}, \quad (51)$$

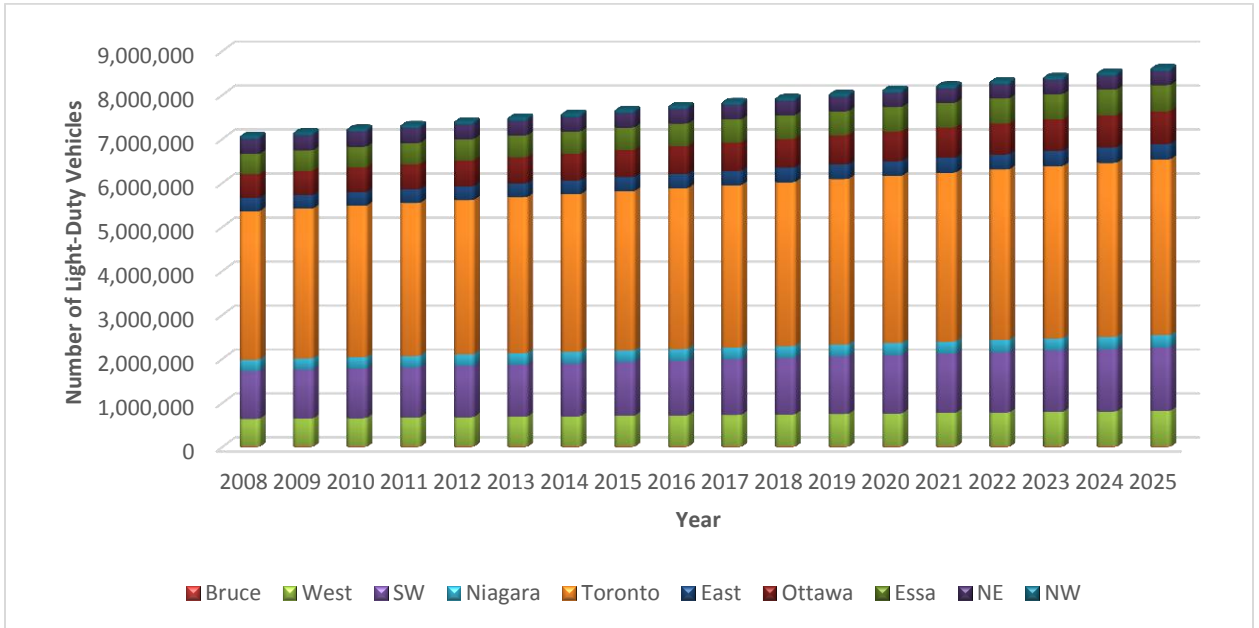


Figure 53: Projected number of light-duty vehicles in 18 years period in the ten zones of Ontario

### 9.4.3 Hydrogen transportation

Ideally, each zone should have a large enough HPP that could fulfill its own hydrogen demands. However, when the electricity capacity for a zone is low it may not be able to support its own HPP or the needed amount of hydrogen is not sufficient to justify the



installation of a new HPP. Under these circumstances, it may be favorable for the zone to import hydrogen from its neighbouring zones. Although this method eliminates the power loss due to power transfer in the grid, it does introduce additional costs associated with the investment and maintenance of the trucks used to transfer hydrogen. These costs include the capital costs of the trucks ( $C^{tube}$ ) and the truck tubes ( $C^{tube}$ ) over their lifetime ( $t$ ) at a discount rate ( $r$ ) of 8%. The initial operational costs ( $C_0^{ot}$ ) were estimated to be \$1.1212 CAD/km and expected to increase by 2.5% per year [206], [203]. The total costs related to the trucks could be expressed as follows:

$$C_y^t = \sum_{(i,j) \in \gamma} N_{ij,y}^t \cdot \left\{ C_0^{ot} \cdot [1 + 0.025 \cdot (y - y_0)] \cdot 2 \times d_{ij} + \frac{r \cdot C^{cab}}{1 - (1+r)^{-t_{cab}}} + \frac{r \cdot C^{tube}}{1 - (1+r)^{-t_{tube}}} \right\}, \quad (52)$$

where  $N_{ij,y}^t$  stands for the number of trucks required in year  $y$  between corridors ( $\gamma$ ) of zone  $i$  and  $j$ , and  $d_{ij}$  is the distance between them. The capacity ( $\sigma$ ) of each tube is 0.4 tons, and the number of trucks could be determined by the following equation:

$$N_{ij,y}^t = \text{ceil} \left( \frac{\sum_{i \neq j} P_{ij,y}^s}{\sigma} \right), \quad (53)$$

## 9.5 Optimization Model

The focus of the current study is to optimize the costs associated with power generation while maximizing the potential for HFVs in Ontario by the last year of the study. Costs associated with hydrogen production and installing HPP are considered above. However, the cost of power generation, import, and export require further scrutiny, since power loss

is an intrinsic property of power transmission that strongly depends on the amount of power transferred, and the physical properties of the grid lines. The task is further exacerbated because of the non-linear properties of power transmission and loss (equation 9 and 10). The power loss in the grid between zone  $i$  and  $j$  is expressed as follows [211]:

$$p_{ij,y}^{loss} = 2g_{ijy}[1 - \cos(\delta_i - \delta_j)], \quad (54)$$

where  $g_{ijy}$  is the conductance of the line between buses  $i$  and  $j$ , and  $\delta$  is the bus voltage angle in the corresponding zone. Therefore, the net power injected at the  $i^{\text{th}}$  zone is given by

$$P_{iy} = \sum_{(i,j) \in \Omega} [g_{ijy}[1 - \cos(\delta_i - \delta_j)] - b_{ijy} \sin(\delta_i - \delta_j)] \quad (55)$$

where  $b_{ijy}$  is the susceptance of line  $(i,j)$  in the year  $y$ , and  $\delta$  is the bus voltage angle in the corresponding zone.

Traditionally, optimization problems are simplified by using linear models to approximate non-linear behaviours, such as the piece-wise approximation of line losses and power transmission in [197]. These approximations could introduce several constraints on the optimizer, increasing the chances of misleading results. Metaheuristics, on the other hand, are capable of dealing with non-linear models, making it an attractive alternative to classical methods such as the Simplex method.

### 9.5.1 Objective Functions

In this chapter, the two considered objectives are inversely correlated. In other words, as the number of HFVs increases, it will require more capital investment and more power to operate the HPPs. Consequently, the cost of electricity, HPP installation, and most likely line losses and the cost of hydrogen transfer via trucks will also increase. The two objectives invested for the hydrogen economy are explicitly stated as follows:

- 1) Maximize the percentage of hydrogen vehicles in Ontario by the year 2025
- 2) Minimize the total cost of electricity generation, transportation and conversion

The first objective of maximizing hydrogen penetration of hydrogen economic is transformed into a minimization problem as follows:

$$\min f_1 = 100 - K, \quad (56)$$

where  $K$  is the percentage of HFVs in the last year of study as a measure of hydrogen penetration in the Ontario economy.

The second objective function consists of costs pertaining to power generation, export, and import, and hydrogen transportation between different zones ( $Z$ ) in all the years ( $Y$ ). It is expressed as follows:

$$\min f_2 = \sum_{y \in Y} \sum_{i \in Z} \left\{ \begin{array}{l} C_y^{d1} \cdot (P_{i,y}^{gen1} + P_{i,y}^{imp1} + P_{i,y}^{exp1}) \\ + C_y^{d2} \cdot (P_{i,y}^{gen2} + P_{i,y}^{imp2} + P_{i,y}^{exp2}) + C_y^t \end{array} \right\}, \quad (57)$$

where  $P_{i,y}^{gen1}$ ,  $P_{i,y}^{imp1}$ , and  $P_{i,y}^{exp1}$  are the components of the yearly power generated, imported and exported, respectively, in zone  $i$  during the weekdays. Likewise,  $P_{i,y}^{gen2}$ ,  $P_{i,y}^{imp2}$ , and  $P_{i,y}^{exp2}$  are the components of the yearly power generated, imported and exported, respectively, in zone  $i$  during the weekends.

### 9.5.2 Variable Bounds

The current problem is composed of 63 variables resumed in Table 30: 18 variables for bus angles, 44 for hydrogen transport, and HFV percentage. Each zone has a bus angle ( $\delta$ ) associated with it. However, one of the bus angles could be taken as a reference, leaving nine unknown angles for weekdays and nine for weekends in a year. Furthermore, each connected zone is restricted to be within 30 degrees of each other:

$$\Delta\delta_{ij} = |\delta_i - \delta_j| \leq 30^\circ, \quad (i, j) \in Z \quad (58)$$

Hydrogen Transport ( $P_{i,j}^s$ ) among corridors were restricted to a reasonable number to make sure an unrealistic number of trucks are not used in a certain corridor that could cause traffic congestion or produce other unfavorable consequences. For ten zones, 45 corridors exist that require optimizing 44 variables per year. A limit corresponding to ten trucks (23MW) per corridor was imposed on the hydrogen transport.

$$0 \leq P_{i,j,y}^s \leq 23 \text{ (MW)}, \quad (i, j) \in Z \quad (59)$$

Finally, a single continuous variable that represents the penetration of the hydrogen economy in Ontario by the year 2025 ( $K\%$ ) should also be optimized. The limits imposed on  $K$  are as follows:

$$0 \leq K \leq 10 \quad (60)$$

Table 30: Details of the case study model variables

<i>Variable</i>	<i>Number</i>	<i>Type</i>
Bus Angles ( $\delta$ )	18	Continuous
Hydrogen Transport ( $P_{ij}^s$ )	44	Continuous
Hydrogen Penetration ( $K\%$ )	1	Continuous
<b>Total</b>	<b>63</b>	

Hydrogen economy penetration is assumed to be a linear function of time, which allows the calculation of the cost of electricity in the previous years as a function of the cost of last year and the percentage of hydrogen penetration of the corresponding year. The following equation is used to calculate the total cost of electricity in 18 years:

$$C^{t'} = C^{18} \cdot \sum_{y \in Y} \left[ 1 - \frac{K}{100} \cdot \left( \frac{y_f - y}{y_f - y_0} \right) \right] \quad (61)$$

where  $C^{18}$  is the cost of electricity in the 18<sup>th</sup> year alone.

### 9.5.3 Constraints

Table 31: Case study model constraints description

Constraint	Equation Number	Quantity	Type
Power Balance	46	20	Equality
Power Generation	47	20	Inequality
Power Import	48	20	Inequality
Power Export	49	20	Inequality
Direct Transmission	50	22	Inequality
Reverse Transmission	51	22	Inequality
Hydrogen Balance	52	10	Equality
<b>Total</b>		134	

As shown Table 31, the problem composed of equality constraints which are more complex than inequality constraints. The constraints are described as follows: 20 constraints for power balance, 20 constraints for power generation, 20 constraints for import, 20 constraints for export, 22 constraints for direct and 22 constraints for reverse transmissions, and 10 constraints for hydrogen balance, making a total of 134 constraints summarized in Table 31. The power balance constraint is an equality constraint that ensures each zone meets its local needs after line losses and export, every year. It is expressed as:

$$P_{i,y}^{gen\mathcal{V}} - P_{i,y}^{HPP} - P_{i,y}^{\varphi\mathcal{V}} + P_{i,y}^{imp\mathcal{V}} - P_{i,y}^{exp\mathcal{V}} - \sum_{(i,j)} \left[ \frac{1}{2} p_{ijy}^{loss}(\delta_i, \delta_j) - b_{ijy} \sin(\delta_i - \delta_j) \right] = 0, \quad (62)$$

where  $\mathcal{V}$  is the set containing weekdays and weekends.

$P_{i,y}^{gen\forall}$ ,  $P_{i,y}^{imp\forall}$ , and  $P_{i,y}^{exp\forall}$  are also bounded:

$$0 \leq P_{i,y}^{gen\forall} \leq \overline{P_{i,y}^{gen}}, \quad (63)$$

$$0 \leq P_{i,y}^{imp\forall} \leq \overline{P_{i,y}^{imp}}, \quad (64)$$

$$0 \leq P_{i,y}^{exp\forall} \leq \overline{P_{i,y}^{exp}}, \quad (65)$$

where  $\overline{P_{i,y}^{gen}}$  is the maximum power generation capacity given in Figure 51, and  $\overline{P_{i,y}^{imp}}$  and  $\overline{P_{i,y}^{exp}}$  are the import and export upper limits, given in Table 53-54, respectively. Likewise, 11 transmission corridors have upper bounds that are applied to both, weekdays and weekends, in all the studied years:

$$-b_{ijy} \sin(\delta_i - \delta_j) + g_{ijy} [1 - \cos(\delta_i - \delta_j)] \leq \overline{P_{i,y}^d}, \quad (66)$$

$$+b_{ijy} \sin(\delta_i - \delta_j) + g_{ijy} [1 - \cos(\delta_i - \delta_j)] \leq \overline{P_{i,y}^r}, \quad (67)$$

where  $\overline{P_{i,y}^d}$  and  $\overline{P_{i,y}^r}$  are the maximum power allowed in the direct and reverse directions, respectively, given in Table 26. Note, these transmission upper bounds are increased over the years as mentioned previously in Table 27.

Finally, the total amount of hydrogen required ( $\varphi_{i,y}^h$ ) and exported ( $\sum_{i \neq j} P_{ij,y}^S$ ) by a zone must be fulfilled by the total installed plant capacity ( $\sum_{y'=0}^y P_{i,y'}^{HPP}$ ) and the imported hydrogen ( $\sum_{j \neq i} P_{ji,y}^S$ ). This constraint applied to each zone, and every year is expressed as:

$$\varphi_{i,y}^h = \sum_{y'=0}^y P_{i,y'}^{HPP} - \sum_{i \neq j} P_{ij,y}^S + \sum_{j \neq i} P_{ji,y}^S, \quad (68)$$

## 9.6 Experimental Simulations

This section describes the experimental simulation settings and the results of the hydrogen infrastructure design case study.

### 9.6.1 Parameter settings

For all the experiments, MODEL algorithm is compared with the four most accurate MOMs based on the comparative study conducted in Chapter 3, namely GDE3, SMPSO, AbYSS and MOCeII. The algorithms parameter settings are the same as in the comparative study, and the MODEL parameter settings are the same as its parent algorithm GDE3. The population sizes are set to 100 for all the compared MOMs. The stopping criterion (FCs) is increased to 50,000 function evaluations because this problem is a more complex problem due to large number of constraints. All the compared MOMs are executed 100 times independently. The IGD measure is used to compare the results.



## 9.6.2 Discussion of the results

As shown in Table 32, MODEL outperformed all the other MOMs. Figure 54 further shows that the accuracy of MODEL is better than the other compared MOMs for the hydrogen economy problem. Please note that the SMPSO was not plotted because none of the found solutions was feasible.

Table 32: Median and IQR IGD measures for the hydrogen economy problem  
Dark grey is the MOM with the best IGD results followed by light grey in the second position

MODEL	GDE3	SMPSO	AbYSS	MOCeII
2.54e-02 <sub>1.3e-02</sub>	2.88e- 02 <sub>1.6e-02</sub>	1.60e- 01 <sub>5.6e-02</sub>	3.99e - 02 <sub>2.2e-02</sub>	3.22e- 02 <sub>1.6e-02</sub>

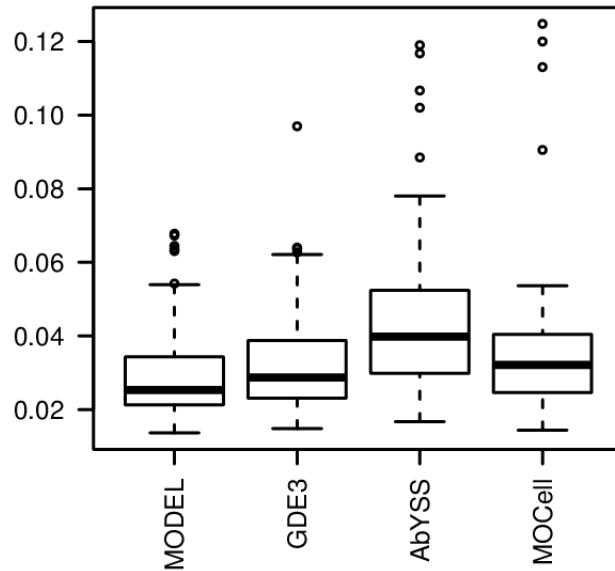


Figure 54: Boxplots for the IGD measures for the hydrogen economy problem.

The Pareto optimal sets achieving median IGDs of the compared MOMs are plotted in Figure 55. It can be seen that in reality AbYSS and MOCeII achieved

respectively the best and second best convergence. However, AbYSS and MOCeLL found approximately only a third and roughly a half of the PF compared to that of MODEL. Thus, MODEL achieved a significantly better distribution of solutions with a lower accuracy than both AbYSS and MOCeLL. Furthermore, MODEL achieved a better convergence compared to its parent algorithm GDE3. Overall, it can be stated that MODEL achieved the highest accuracy (strong convergence + uniform distribution). It would be interesting to investigate why AbYSS achieved a better convergence for this case study to try to further enhance MODEL properties.

To illustrate the advantage of variety of solutions provided by MOMs, the details of two solutions are provided in Table 33. It can be seen that it costs roughly \$250M to increase the ratio of HFVs by 1% per year. Overall, it can be seen that Toronto is has the largest hydrogen demand in Ontario with 46.36% of total demand as shown in Figure 52.

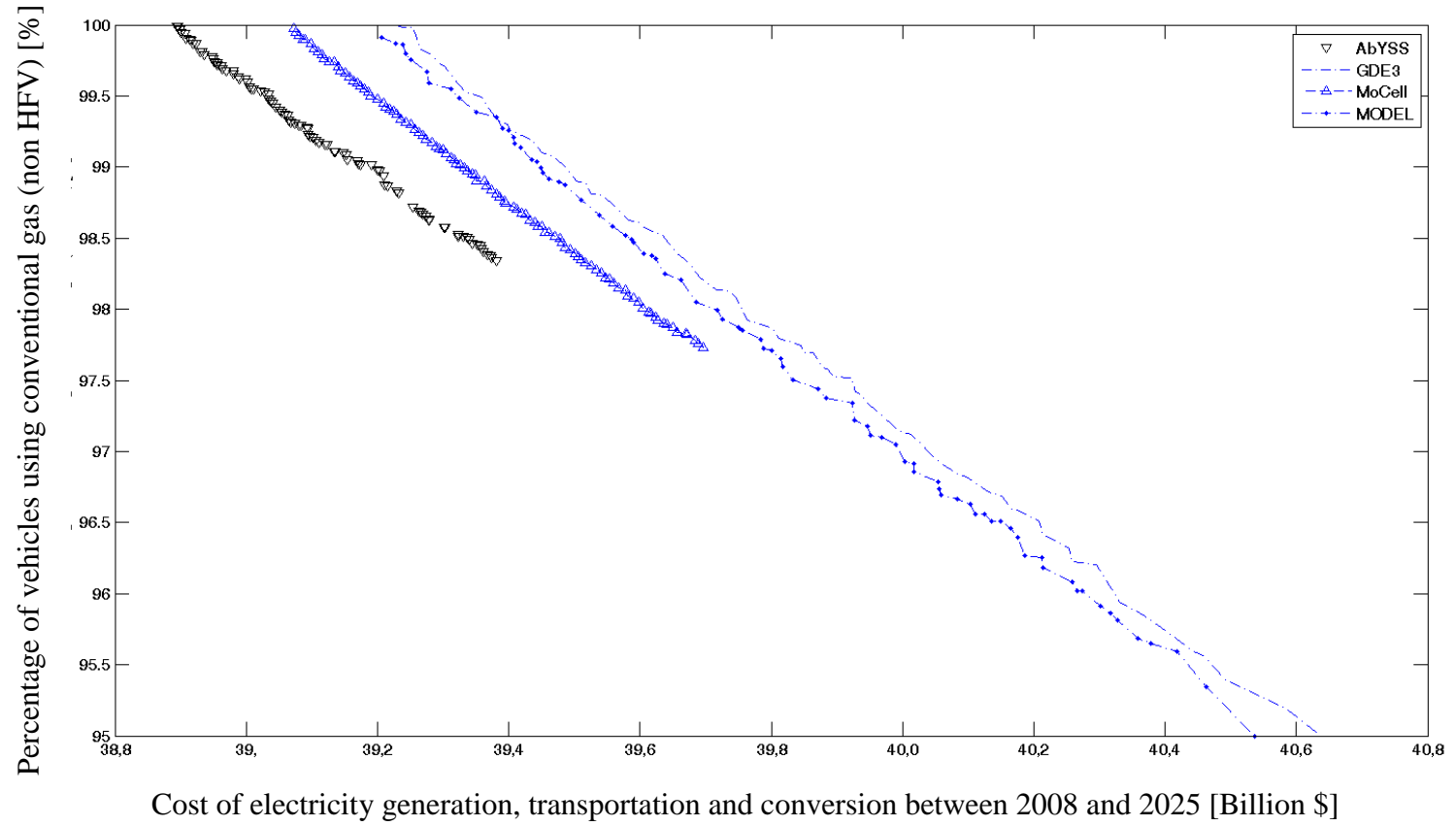
Table 33: Details of two optimal solutions found by the MODEL algorithm. The hydrogen is represented in [MW].

	Bruce	West	SW	Niagara	Toronto	East	Ottawa	Essa	NE	NW	Cost \$Millions	H <sub>2</sub> %
Production	6.55	126.37	231.59	25.17	640.44	78.04	113.67	90.35	49.17	13.18	40536	5%
Demand	2.96	127.77	230.37	44.62	637.18	56.44	118.34	94.81	50.20	11.85	-	-
Shipments	3.59	-1.40	1.23	-19.45	3.26	21.60	-4.68	-4.46	-1.03	1.33	-	-
Production	4.47	79.57	139.81	6.37	396.85	50.27	69.09	59.65	32.67	5.17	40003	3%
Demand	1.82	78.45	141.44	27.39	391.21	34.65	72.66	58.21	30.82	7.27	-	-
Shipments	2.65	1.13	-1.63	-21.03	5.64	15.62	-3.57	1.44	1.85	-2.10	-	-

In general, it can be seen that the optimizer tries to install the hydrogen power plants in the zones themselves to reduce hydrogen transportation. Zones such as the Niagara, which have limited electrical production capacities, become importation zones.

On the contrary, Bruce which has a large nuclear power plant with a small population becomes a hydrogen exportation zone. Other zones depend on their specific scenarios. For example, in the first case the West zone is importing hydrogen (-1.4 MW) and the SW zone is exporting (1.23 MW). In the second case, the West zone exports (1.13 MW) and SW imports (1.63 MW). These kinds of options can be advantageous to users because often certain decision factors are expressed by users and therefore not represented in the modeling.

Figure 55: Pareto optimal sets of median IGDs found for simplified version of the hydrogen economy problem



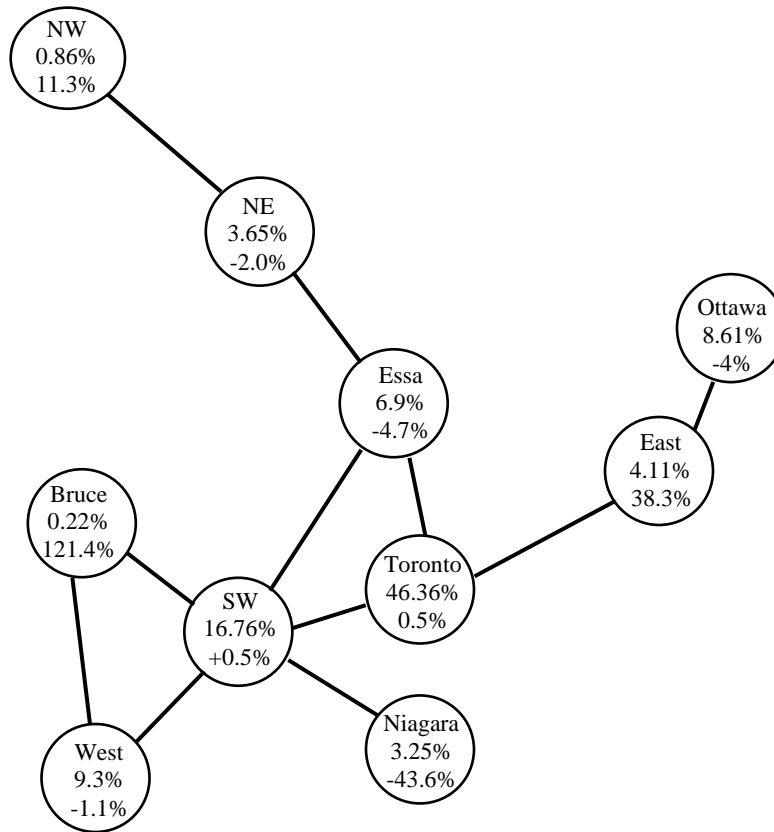


Figure 56: Details of an optimal solution found by MODEL with a cost of \$40.5 billion and 5% of hydrogen-fueled vehicles. The upper number represents the ratio of the respective demand in the zone whereas the second represents ratio of exportation with regards to zone production of hydrogen.

It can be seen from Figure 56 that most zones are self-sufficient with the exception of three zones: Bruce, East, and Niagara. Bruce and East zones export 121.4% (21.4% above self-consumption) and 38.3% of the hydrogen produced in their zones, respectively. The Niagara zone imports 43.6% of the hydrogen to fulfill its base-load hydrogen.

Table 34: Number of HFVs in every zone based on the solution with a cost of 40.536 \$Million and a ratio of 5% of HFVs.

	Bruce	West	SW	Niagara	Toronto	East	Ottawa	Essa	NE	NW	Total
NB. of HFVs	825	35620	64222	12439	177634	15734	32992	26432	13994	33037	<b>412929</b>

As shown in Table 34, it is possible to achieve up to 412929 light duty vehicles which represents 5% of total number of vehicles) running on hydrogen by 2025 based on the results.

## 9.7 Conclusions

This chapter studied an integrated model of electrolytic hydrogen production during off-peak hours considering the existing and planned electricity infrastructure in Ontario. To solve this problem five MOMs have been compared: the proposed MODEL, GDE3, AbYSS, SMP SO and MOCe ll. Two objectives were targeted, namely, the hydrogen production cost minimization and maximization of the number of HFV over a 18 year period. The optimization problem of 63 dimension with 134 equality and inequality constraints.

The proposed MODEL algorithm achieved overall the highest accuracy; however, by examining the Pareto fronts, it was found the AbYSS and MOCe ll found solutions with slightly higher convergence than MODEL, but MODEL achieved a much better Pareto set distribution. It would be interesting to investigate how to further improve the precision of the MODEL algorithm while preserving well-distributed solutions. In regards to the solutions, it was found that it is possible to have solutions between 5% of the vehicles running on hydrogen with a cost of \$40.5 billion and 0% of HFVs and a cost

of \$38.8 billion for just electricity productions. In general, the optimizer seemed to prefer to have self-sufficient zones in terms of hydrogen with the exception of two major exporters Bruce and East Zone, and a major importer Niagara zone.

There are certain limitations of the current model such as absence of the environmental impacts and their costs, the absence of industrial demand of hydrogen, and the assumption of a uniform price of electricity across the zones. Usually sensitivity analysis is performed, but since there is a multitude of solutions, it is more appropriate to perform the sensitivity analysis once a solution is selected. Furthermore a linear growth is assumed for increase of hydrogen economy; therefore optimizing just the last year was sufficient. In future, we would like to solve with more than 1000 variables and study the performance of MODEL algorithm with such large scale variables.

## **Chapter 10**

### **Conclusions and Recommendations**



This thesis made several contributions: conducted a multi-objective optimization comparative study, surveyed works related to optimization of renewable energy systems modeling, proposed three new multi-objective metaheuristics, and performed two cases studies where multi-objective optimization methods are applied to renewable energy systems design. The conclusions and recommendations of future works are described in the following subsections.

## **10.1 Conclusions**

Multi-Objective metaheuristics are powerful tools to solve complex multi-objective optimization problems. However, it is desirable to have faster and more accurate algorithms. This thesis focused on enhancement of state-of-the-art MOMs using leadership concepts. Both leadership and OBL approaches have been investigated for single objective problems, but their use in multi-objective optimization is not a trivial task. In this thesis, three new multi-objective metaheuristics (MOMs) are proposed based on these two concepts, for which findings are explained and discussed in detail. Furthermore, in addition to well-known benchmark problems, two energy-related case studies are utilized to demonstrate the performance of the presented methods to solve real-world problems. The main contributions of this thesis are as follows.

- This thesis conducted the most comprehensive comparative study ever in multi-objective optimization by focusing on robustness of MOMs under stringent number for function evaluations. As our case studies are bi-objective problems, the analysis of the results focused in particular on bi-objective problems. The highest performance for bi-objective problems was achieved respectively by multi-

objective versions of differential evolution (GDE3) and particle swarm optimization (SMPSO), although NSGA-II showed good performance with problems having high epistasis. Overall, it is impossible to design an algorithm that can handle variant complexities with a static mechanism, rather a dynamic mechanism needs to be considered. Example of such dynamic mechanisms is hybridization, adaptive parameter control, and self-adaptive parameter control. In regards to three-objective problems, SPEA2 showed the highest accuracy probably due to its different method of solution ranking. In this thesis, it has been shown that the non-dominance sorting has serious deficiencies, especially during the exploration phase and it seems to offer lower performance as the number of objectives increases.

- To demonstrate the performance of the proposed MOMs, complex optimal design problems of renewable energy systems had to be found. A survey of applications of optimization in design of energy systems has been conducted. The results showed that most previous works considered only standalone problems (not grid-connected), using single objective optimization algorithms, and focused mainly on solar and wind energy. Furthermore, the existing research conducted on MOPs did not use state-of-the-art MOMs. Therefore, one of the proposed case studies in this thesis focused on a complex multi-objective design of an original hydrogen energy infrastructure, which integrates two networks, namely, hydrogen and electrical, and uses a state-of-the-art MOM. Thus, the MOM field is growing fast but there is a gap between the MOM research community and other research

communities such as energy system design community. If this gap is bridged many real-world problems could be solved.

- The first proposed MOM consisted enhancing the leadership concept of SMPSO. It is proposed to select leaders using the Sum of Weighted Ratios (SWR) method. The purpose of using SWR is to make sure that the selected leaders remain well-distributed during the entire search process especially during the exploration phase. When leaders are concentrated in a narrow region of the objective space, it leads to either a premature convergence (trapped in local optima) or requires additional computational overhead to redistribute the particles across the PF once a portion of it is found. The proposed method called LSMPSO was compared to seven state-of-the-art metaheuristics, namely, NSGA-II, SPEA2, GDE3, SMPSO, AbYSS, MOCcell and MOEA/D using the ZDT and DTLZ bi-objective family problems. The convergence speed of these MOMS was compared and the proposed LSMPSO was found to be the fastest MOM for 10 out of 12 problems. The performance of LSMPSO is due to two particularities: use of leadership and the proposed enhanced leader ranking mechanism. Most algorithms do not take advantage of leadership concept to accelerate the convergence speed despite the available information. Further, the non-dominance mechanism needs to be seriously reviewed or enhanced especially at exploration phase. The use of SWR is an example of such enhancement as part of this thesis. LSMPSO is recommended for bi-objective energy designs problem or other real problems with two objectives, and limited time constraints as LSMPSO achieved the

highest performance for the compared problems MOM with a limited number of function evaluations ( $10^6$ ).

- As a demonstration of the performance for the proposed LSMPSO, it was compared to the four most accurate MOMs, based on the presented comparative study, for bi-objective problems, namely, SMPSO, AbYSS, MOCcell and GDE3 to solve a MO optimal photovoltaic farm design problem in Toronto, Ontario area yielding the objectives of total incident solar energy maximization and the cost of deployment minimization. Configuration variables consisted of number of collector rows, distance between collector rows, dimension of collectors, collectors' inclination angle, collectors' azimuth, and elevation above ground. The proposed problem is complex because of multimodality, mixed-type variables, and many-to-one mapping. Only LSMPSO and SMPSO were able to find the entire PF. Despite the appearance of this problem being of average complexity with five mixed-type variables and two inequality constraints, it was a complex problem especially due to the many-to-one mapping feature. Problems with complex variable relationship such as many-to-one should be given a special attention by the research community.
- The second proposed MOM consisted in using the opposition-based learning concept in multi-objective optimization metaheuristics. The proposed opposition-based GDE3 (OGDE3) was the first successful application of OBL into MOM with single population (no coevolution) due to leadership and self-adaptive

mechanism. The convergence speed of OGDE3 outperformed seven other state-of-the-art MOMs for ZDT problems by using a *self-adaptive* version of OBL. The use of OBL *when appropriate* can have important acceleration of the convergence speed of MOMs; for the studied problems OGDE3 required only half of function evaluations when compared with other MOMs. Other stochastic mechanisms for activation/deactivation of OBL should be explored for multi-objective problems.

- The third proposed MOM used the leadership concept for enhancing a multi-objective variant of DE (GDE3). The leadership improved both the convergence speed and the convergence of GDE3 by incorporating it into the mutation operator. Sometimes, when the search space in the objective space is very large, the proposed algorithm results in premature convergence. To avoid a premature convergence, the factor  $F$  was negated using probabilistic factor to maintain diversity in the variable space. The proposed MOM called MODEL achieved the highest accuracy with a low number of function evaluations when compared to seven other MOMs using 30 comprehensive benchmark problems. Therefore, the robustness and fast convergence speed of MODEL make it an attractive alternative MOM to solve bi-objective real world optimization problems. It should be further studied for larger dimensional problems in both objective and variable spaces.
- To demonstrate the performance of MODEL in solving real-world problems, MODEL has been compared with SMPSO, AbYSS, MOCcell and GDE3 MOMs

to solve a complex and large hydrogen design infrastructure integrated with existing and planned electrical network in the province of Ontario, Canada which is larger in superficies than any European country. MODEL outperformed the other MOMs by generating a larger variety of designs for the hydrogen infrastructure model.

## **10.2 Future Work and Recommendations**

This thesis proposed new MOMs based on the leadership concept which achieved promising results. In addition, this work contributed to share knowledge between the optimization and energy research communities. However, there are several promising avenues that remain to be explored; some of them are described as follows:

- Improving leadership selection.
  - The non-dominance ranking has serious deficiencies in maintaining a good diversity in the population especially at early stage which affects the performance of MOMs. So, new ranking methods should be investigated and this should be even more useful for larger dimension problems ( $> 3$  objectives). For example, it has been shown that SPEA2 achieved a better accuracy than the compared methods for three-objective problems due to its different ranking mechanism.
  - The ratio of leader selected among population was set to 10% in this thesis. This threshold should be further investigated. Another possibility

is the use of an adaptive/self-adaptive threshold depending on the progress of the algorithm.

- Examination of the performance of leadership selection on large scale problems with decision variables dimension set to more than a thousand should be studied.
- Extension of OBL.
  - Very limited work has been done with OBL in MOO field as a straightforward application is not efficient for MOMs. A successful self-adaptive variant of OBL was proposed which demonstrates OBL potential in MOO field. Adaptive and self-adaptive OBL is one interesting research direction. In general, adaptive and self-adaptive mechanisms should be the focus of future research works related to OBL.
- Extension to the proposed case studies models
  - Optimization of the hydrogen distribution infrastructure focused only on the last year. The consideration of the full 18 years would be a valuable attempt but it is a time consuming experiment due to large dimensionality.
  - The proposed case studies' design models can be used for energy systems design at macro level for the development of more integrated models such as wind / photovoltaic / hydrogen which can be grid-connected. Such designs were previously avoided buy the energy

research community due to lack of awareness with regards to the available algorithms. Therefore, stronger collaboration between MOO and other research communities such as energy design community is mandated.

- Use of MOM for optimal control of the energy power plants.
  - Test the proposed MOMs at micro level rather than macro level as it was done in the PV design problem.
  - More accurate and realistic models are required giving consideration to real life factors. For example, in the photovoltaic problem, the maintenance fees were not considered. In both proposed models, the price of the land used for power plants was again not considered. The incorporation of such variables makes the problem and the solutions more realistic and predictable.
- Other general recommendations
    - Based on the comparative study and the case studies conducted in this thesis, problems with complex variable relationship e.g. high epistasis, many-to-one mapping are the hardest to solve; therefore, the MOMs community should further focus on such problems as many real life problems have complex variable relationship.
    - Large scale optimization problems as the hydrogen problem are an important research direction which needs to be further investigated. For example, the performance of proposed MOMs should be further



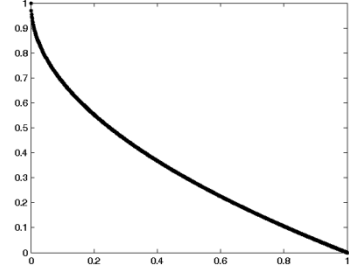
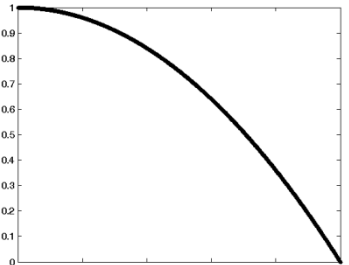
investigated when solving large scale problems, the development of parallel and distributed multi-objective optimization frameworks should be considered to encourage stronger collaboration among MOM research community, and also meta-modeling methods can be interesting avenues for large scale problems.

- In general multi-objective optimization problems can be composed of heterogeneous complexities. It is impossible to develop a robust metaheuristic implementation using static mechanisms; therefore, dynamic mechanisms should be further explored such as hybridization, adaptive and self-adaptive mechanisms.

## **Appendix A: Multi-Objective Benchmark Problems Description**

This appendix describes the benchmark functions used in the comparative study in Chapter 3. The details of the following problems are provided: Zitzler-Deb-Thiele (ZDT) problem family [33], the Deb-Thiele-Laumanns-Zitzler (DTLZ) problem family [34], the Walking-Fish-Group (WFG) problem family [35], the Li-Zhang problem family (LZ\_09) [7], and the Van Veldhuizen test suite [36]. Also, the IGD boxplots, the HV and HVR results of the experiments are presented as complementary information.

Table 35: ZDT test functions (all minimization problems)

Problem	Objective Functions	Variable Bounds	Number Objectives	Number Variables	Pareto Front Geometry	
ZDT1	$f_1(\vec{x}) = x_1$ $f_2(\vec{x}) = g(\vec{x}) \left[ 1 - \sqrt{x_1/g(\vec{x})} \right]$ $g(\vec{x}) = 1 + 9 \left( \sum_{i=2}^n x_i \right) / (n - 1)$	$0 \leq x_i \leq 1$	2	30	Convex	
ZDT2	$f_1(\vec{x}) = x_1$ $f_2(\vec{x}) = g(\vec{x}) \left[ 1 - (x_1/g(\vec{x}))^2 \right]$ $g(\vec{x}) = 1 + 9 \left( \sum_{i=2}^n x_i \right) / (n - 1)$	$0 \leq x_i \leq 1$	2	30	Concave	

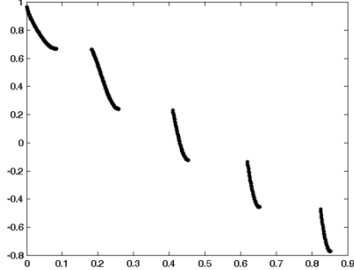
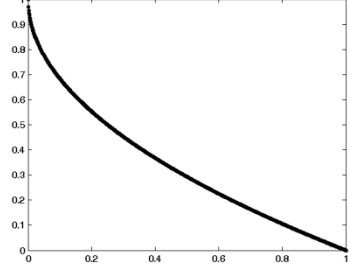
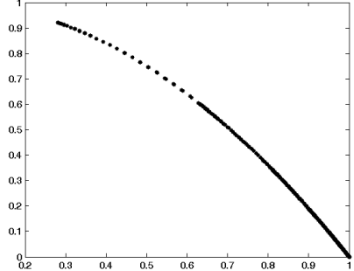
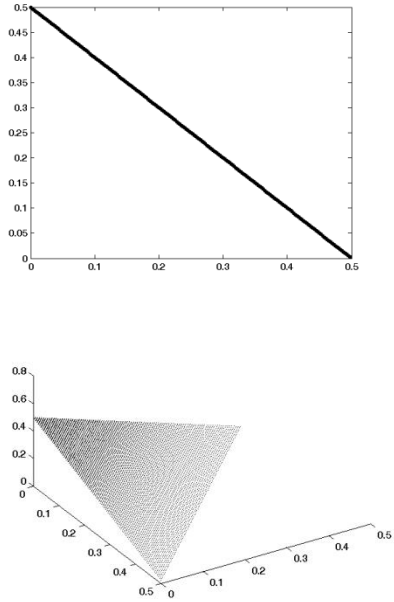
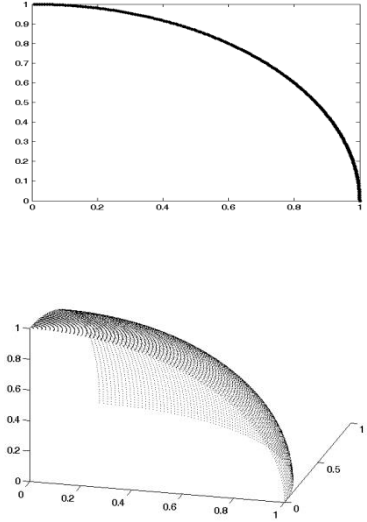
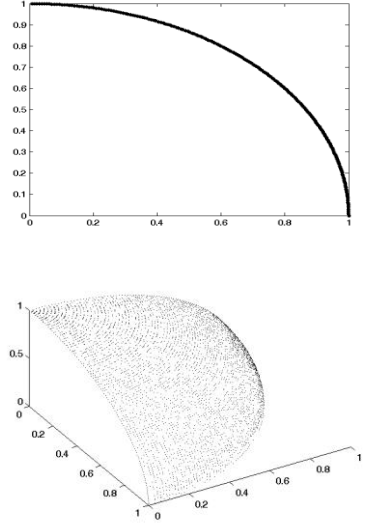
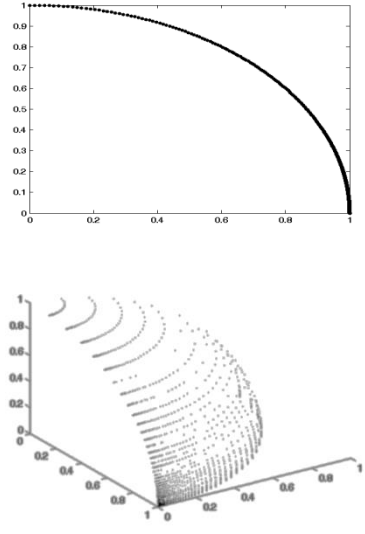
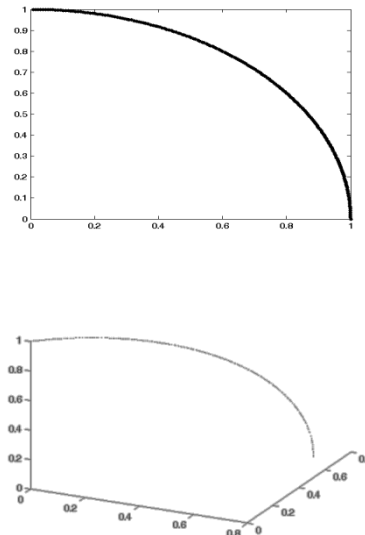
ZDT3	$f_1(\vec{x}) = x_1$ $f_2(\vec{x}) = g(\vec{x}) \left[ 1 - \sqrt{\frac{x_1}{g(\vec{x})}} - \frac{x_1}{g(\vec{x})} \sin(10\pi x_1) \right]$ $g(\vec{x}) = 1 + 9 \left( \sum_{i=2}^n x_i \right) / (n - 1)$	$0 \leq x_i \leq 1$	2	30	Convex Disconnected	
ZDT4	$f_1(\vec{x}) = x_1$ $f_2(\vec{x}) = g(\vec{x}) [1 - (x_1/g(\vec{x}))^2]$ $g(\vec{x}) = 1 + 10(n-1) + \sum_{i=2}^n [x_i^2 - 10 \cos(4\pi x_i)]$	$0 \leq x_1 \leq 1$ $-5 \leq x_i \leq 5$ $i = 2, \dots, n$	2	10	Convex	
ZDT6	$f_1(\vec{x}) = 1 - e^{-4x_1} \sin^6(6\pi x_1)$ $f_2(\vec{x}) = g(\vec{x}) [1 - (f_1(\vec{x})/g(\vec{x}))^2]$ $g(\vec{x}) = 1 + 9 \left[ \left( \sum_{i=2}^n x_i \right) / (n - 1) \right]^{0.25}$	$0 \leq x_i \leq 1$	2	10	Concave, Non-uniformly spaced	

Table 36: DTLZ M-objectives minimization problems

Problem	Objective Functions	Variable Bounds	No. objectives	No. variables	Pareto front geometry	
DTLZ1	$f_1(\vec{x}) = (1 + g(\vec{x}))0.5 \prod_{i=1}^{M-1} x_i$ $f_{m=2:M-1}(\vec{x}) = (1 + g(\vec{x}))0.5 \prod_{i=1}^{M-m} x_i (1 - x_{M-m+1})$ $f_M(\vec{x}) = (1 + g(\vec{x}))0.5(1 - x_1)$ $g(\vec{x}) = 100[k + \sum_{i=1}^k ((x_i - 0.5)^2 - \cos(20\pi(x_i - 0.5)))]$	$0 \leq x_i \leq 1$	2/3	7	Linear	

DTLZ2	$f_1(\vec{x}) = (1 + g(\vec{x})) \prod_{i=1}^{M-1} \cos(x_i \pi/2)$ $f_{m=2:M-1}(\vec{x}) = (1 + g(\vec{x})) \left( \prod_{i=1}^{M-m} \cos(x_i \pi/2) \right) \sin(x_{M-m+1} \pi/2)$ $f_M(\vec{x}) = (1 + g(\vec{x})) \sin(x_1 \pi/2)$ $g(\vec{x}) = \sum_{i=1}^k (x_i - 0.5)^2$	$0 \leq x_i \leq 1$	2/3	12	Concave	
DTLZ3	$f_1(\vec{x}), f_m(\vec{x}) \text{ and } f_M(\vec{x}) \text{ idem DTLZ2}$ $g(\vec{x}) = 100[k + \sum_{i=1}^k ((x_i - 0.5)^2 - \cos(20\pi(x_i - 0.5)))]$	$0 \leq x_i \leq 1$	2/3	12	Concave	

DTLZ4	$f_1(\vec{x}) = (1 + g(\vec{x})) \prod_{i=1}^{M-1} \cos(x_i^\alpha \pi/2)$ $f_{m=2:M-1}(\vec{x}) = (1 + g(\vec{x})) \left( \prod_{i=1}^{M-m} \cos(x_i^\alpha \pi/2) \right) \sin(x_{M-m+1}^\alpha \pi/2)$ $f_M(\vec{x}) = (1 + g(\vec{x})) \sin(x_1^\alpha \pi/2)$ $g(\vec{x}) = \sum_{i=1}^k (x_i - 0.5)^2$	$\alpha = 100$ $0 \leq x_i \leq 1$	2/3	12	Concave, degenerate when (M > 2)	
DTLZ5	<p>Idem DTLZ2, except <math>\forall x_2, \dots, x_{M-1} \in x</math> are replaced by <math>\frac{1+2g(\vec{x})x_i}{2(1+g)}</math></p>	$0 \leq x_i \leq 1$	2/3	12	Concave, degenerate when (M > 2)	

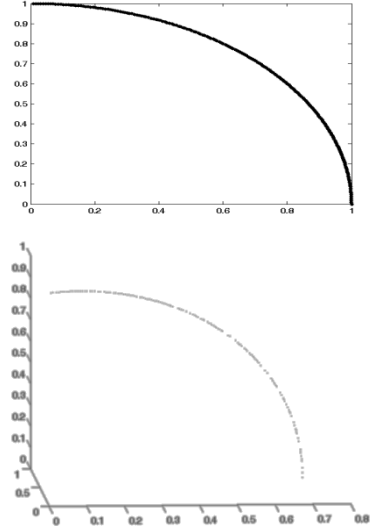
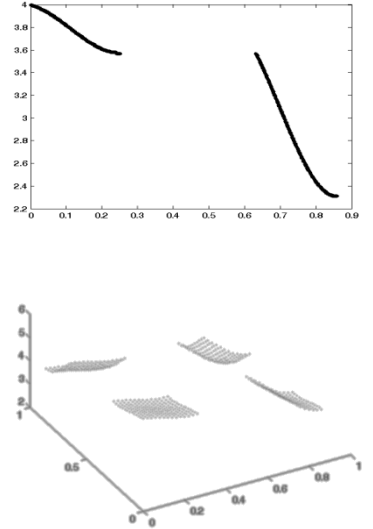
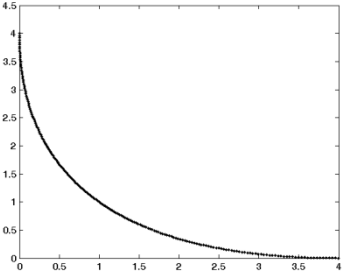
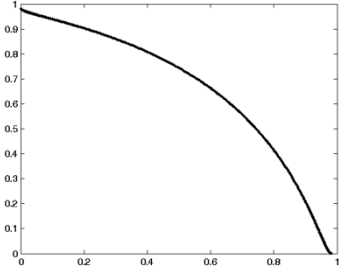
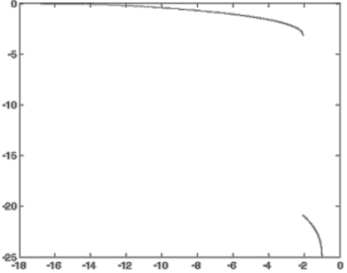
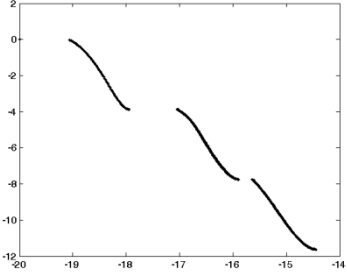
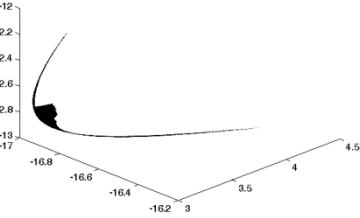
DTLZ6	Idem DTLZ5, except $g(\vec{x}) = \sum_{i=1}^k x_i^{0.1}$	$0 \leq x_i \leq 1$	2/3	12	Concave, Degenerate	
DTLZ7	$f_{m=1:M-1}(\vec{x}) = x_m$ $f_M(\vec{x}) = (1 + g(\vec{x})) \left( M - \sum_{i=1}^{M-1} \left[ \frac{f_i}{1+g} (1 + \sin(3\pi f_i)) \right] \right)$ $g(\vec{x}) = \sum_{i=1}^k (x_i - 0.5)^2$	$0 \leq x_i \leq 1$	2/3	22	Disconnected	



Table 37: Van Veldhuizen test suite (with Viennet4 added)

Problem	Objective Functions	Variable Bounds	No. objectives	No. variables	Pareto front geometry	
Schaffer	$f_1(\vec{x}) = x_i^2$ $f_2(\vec{x}) = (x_i - 2)^2$	$-10^5 \leq x_i \leq 10^5$	2	1	Convex	
Fonseca	$f_1(\vec{x}) = e^{-1.0 \sum_{i=1}^n (x_i - \frac{1}{\sqrt{n}})^2}$ $f_2(\vec{x}) = e^{-1.0 \sum_{i=1}^n (x_i + \frac{1}{\sqrt{n}})^2}$	$-4 \leq x_i \leq 4$	2	3	Concave	

Poloni	$\text{Max. } f_1(\vec{x}) = -1 - (A_1 - B_1)^2 - (A_2 - B_2)^2$ $f_2(\vec{x}) = -1 - (x_1 + 3)^2 - (x_2 + 1)^2$ $A_1 = 0.5 \sin 1 - 2 \cos 1 + \sin 2 - 1.5 \cos 2$ $A_2 = 1.5 \sin 1 - \cos 1 + 2 \sin 2 - 0.5 \cos 2$ $B_1 = 0.5 \sin x_1 - 2 \cos x_1 + \sin x_2 - 0.5 \cos x_2$ $B_2 = 1.5 \sin x_1 - \cos x_1 + 2 \sin x_2 - 0.5 \cos x_2$	$-\pi \leq x_i \leq \pi$	2	2	Disconnected, mixed	
Kursawe	$f_1(\vec{x}) = \sum_{i=1}^n (-10e^{-0.2} \sqrt{x_i^2 + x_{i+1}^2})$ $f_2(\vec{x}) = \sum_{i=1}^n ( x_i ^{0.8} + 5 \sin(x_i)^3)$	$-5 \leq x_i \leq 5$	2	3	Disconnected, mixed, degenerate	
Viennet2	$f_1(\vec{x}) = \frac{(x_1-2)^2}{2} + \frac{(x_2+1)^2}{13} + 3$ $f_2(\vec{x}) = \frac{(x_1+x_2-3)^2}{36} + \frac{(-x_1+x_2+2)^2}{8} - 17$ $f_3(\vec{x}) = \frac{((x_1+2)(x_2-1))^2}{175} + \frac{(2x_2-x_1)^2}{17} - 13$	$-4 \leq x_i \leq 4$	3	2	Convex, Disconnected	

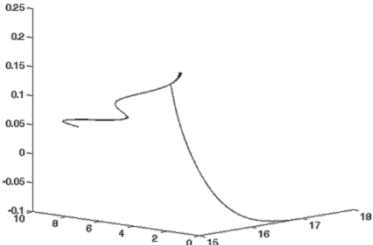
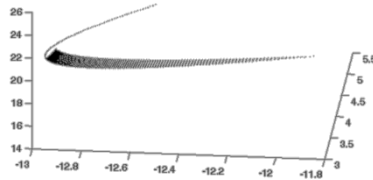
Viennet3	$f_1(\vec{x}) = (3x_1^2 + x_2^2) + \sin(x_1^2 + x_2^2)$ $f_2(\vec{x}) = \frac{(3x_1 - 2x_2 + 4)^2}{8} + \frac{(x_1 - 2x_2 + 1)^2}{27} + 15$ $f_3(\vec{x}) = \frac{1}{(x_1^2 + x_2^2 + 1)} - 1.1e^{-x_1^2 - x_2^2}$	$-3 \leq x_i \leq 3$	3	2	Disconnected, mixed	
Viennet4	$f_1(\vec{x}) = \frac{(x_1 - 2)^2}{2} + \frac{(x_2 + 1)^2}{13} + 3$ $f_2(\vec{x}) = \frac{(x_1 + x_2 - 3)^2}{175} + \frac{(2x_2 - x_1)^2}{17} - 13$ $f_3(\vec{x}) = \frac{((3x_1 - 2)(x_2 + 4))^2}{8} + \frac{(x_1 - x_2 + 1)^2}{27} + 15$	$-4 \leq x_i \leq 4$	3	2	Convex	

Table 38: WFG suite, shape functions of the Pareto front.  
 In all cases,  $x_1, \dots, x_{M-1} \in [0,1]$ .  $A, \alpha$  and  $\beta$  are constants.

Linear	$linear_1(x_1, \dots, x_{M-1}) = \prod_{i=1}^{M-1} x_i$ $linear_{m=2:M-1}(x_1, \dots, x_{M-1}) = \left( \prod_{i=1}^{M-m} x_i \right) (1 - x_{M-m+1})$ $linear_M(x_1, \dots, x_{M-1}) = 1 - x_M$
When $h_{m=1:M} = linear_m$ , the Pareto optimal front is a linear hyperplane, where $\sum_{m=1}^M h_m = 1$	
Convex	$convex_1(x_1, \dots, x_{M-1}) = \prod_{i=1}^{M-1} (1 - \cos(x_i \pi/2))$ $convex_{m=2:M-1}(x_1, \dots, x_{M-1}) = \left( \prod_{i=1}^{M-m} (1 - \cos(x_i \pi/2)) \right) (1 - \sin(x_{M-m+1} \pi/2))$ $convex_M(x_1, \dots, x_{M-1}) = 1 - \sin(x_1 \pi/2)$
When $h_{m=1:M} = convex_m$ , the Pareto optimal front is purely convex.	
Concave	$concave_1(x_1, \dots, x_{M-1}) = \prod_{i=1}^{M-1} \sin(x_i \pi/2)$ $concave_{m=2:M-1}(x_1, \dots, x_{M-1}) = \left( \prod_{i=1}^{M-m} \sin(x_i \pi/2) \right) \cos(x_{M-m+1} \pi/2)$ $concave_M(x_1, \dots, x_{M-1}) = \cos(x_1 \pi/2)$
When $h_{m=1:M} = concave_m$ , the Pareto optimal front is purely concave, and a region of hyper-sphere of radius one centred at the origin, where $\sum_{m=1}^M h_m^2 = 1$	
Mixed convex/concave ( $\alpha > 0, A \in \{1, 2, \dots\}$ )	$mixed_M(x_1, \dots, x_{M-1}) = \left( 1 - x_1 - \frac{\cos(2A\pi x_1 + \pi/2)}{2A\pi} \right)$
Causes the Pareto optimal front to contain both convex and concave segments, the number of which is controlled by A. The overall shape is controlled by $\alpha$ : when $\alpha > 1$ or when $\alpha < 1$ , the overall shape is convex or concave respectively. When $\alpha = 1$ , the overall shape is linear.	
Disconnected ( $\alpha, \beta > 0, A \in \{1, 2, \dots\}$ )	$disc_M(x_1, \dots, x_{M-1}) = (1 - (x_1)^\alpha \cos^2(A(x_1)^\beta \pi))$
Causes the Pareto optimal front to have disconnected regions, the number of which is controlled by A. The overall shape is controlled by $\alpha$ : when $\alpha > 1$ or when $\alpha < 1$ , the overall shape is convex or concave respectively. When $\alpha = 1$ , the overall shape is linear. $\beta$ influences the location of the disconnected regions (Larger values push the location of the disconnected regions towards larger values of $x_1$ , and vice versa).	

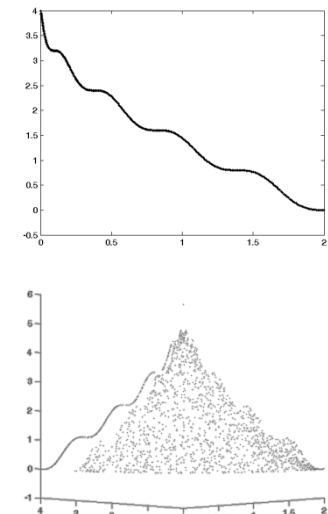
Table 39: WFG Suite, Transformation Functions (bias, shift, reduction)  
 All parameters  $\in [0,1]$ .  $A$ ,  $\alpha$  and  $\beta$  are constants.  $u$  is a reduction function.

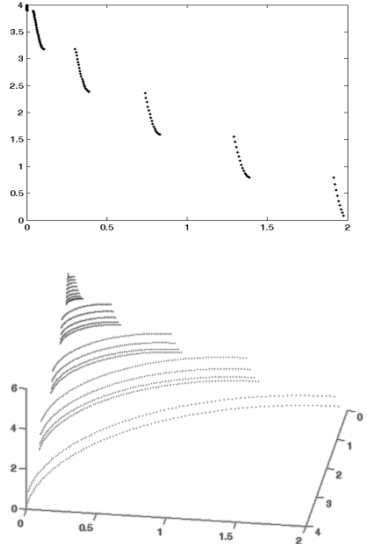
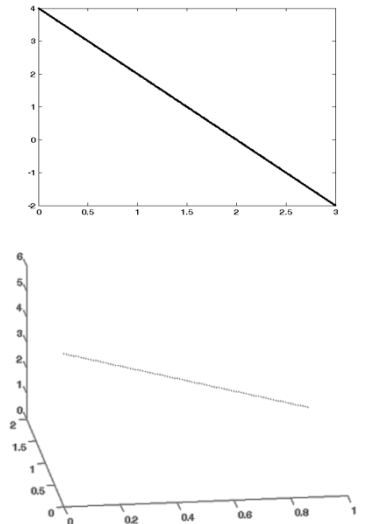
<p>Bias: Polynomial (<math>\alpha &gt; 0, \alpha \neq 1</math>)</p> $b\_poly(y, \alpha) = y^\alpha$ <p>when <math>\alpha &gt; 1</math> or when <math>\alpha &lt; 1</math>, <math>y</math> is biased towards zero or towards one respectively.</p>
<p>Bias: Flat Region (<math>A, B, C \in [0,1], B &lt; C, B=0 \Rightarrow A = 0 \wedge C \neq 0, C = 1 \Rightarrow A = 1 \wedge B</math>)</p> $b\_param(y, y', A, B, C) = A + \min(0, [y - B]) \frac{A(B-y)}{B} - \min(0, [C-y]) \frac{(1-A)(y-C)}{1-C}$ <p>Values of <math>y</math> between <math>B</math> and <math>C</math> (the area of the flat region) are all mapped to the value <math>A</math>.</p>
<p>Bias: Parameter Dependent (<math>A \in (0,1), 0 &lt; B &lt; C</math>)</p> $b\_param(y, y', A, B, C) = y^{B+(C-B)v(u(y'))}$ $v(u(y')) = A - (1-2u(y')) \lfloor -u(y') \rfloor + A \lfloor -u(y') \rfloor$ <p><math>A, B, C</math> and the secondary parameter vector <math>y'</math> together determine the degree to which <math>y</math> is biased by being raised to an associated power: values of <math>u(y') \in [0, 0.05]</math> are mapped linearly onto <math>[B, B+(C-B)A]</math>, and values of <math>u(y') \in [0.5, 1]</math> are mapped linearly onto <math>[B+(C-B)A, C]</math>.</p>
<p>Shift: linear (<math>A \in (0,1)</math>)</p> $s\_linear(y, A) = \frac{ y-A }{ A-y +A}$ <p><math>A</math> is the value for which <math>y</math> is mapped to zero.</p>
<p>Shift: Deceptive (<math>A \in (0,1), 0 &lt; B \ll 1, 0 &lt; C \ll 1, A - B &gt; 0, A + B &lt; 1</math>)</p> $s\_decept(y, A, B, C) = 1 + ( y-A  - B) \times \left( \frac{ y-A+B (1-C+\frac{A-B}{B})}{A-B} + \frac{ A+B-y (1-C+\frac{1-A-B}{B})}{1-A-B} + \frac{1}{B} \right)$ <p><math>A</math> is the value at which <math>y</math> is mapped to zero, and the global minimum of the transformation. <math>B</math> is the “aperture” size of the well/basin leading to the global minimum at <math>A</math>, and <math>C</math> is the value of the deceptive minima (there are always two deceptive minima).</p>
<p>Shift: Multi-Modal (<math>A \in \{1, 2, \dots\}, B \geq 0, (4A + 2)\pi \geq 4B, C \in (0,1)</math>)</p> $s\_multi(y, A, B, C) = \frac{1 + \cos\left[(4A+2)\pi\left(0.5 - \frac{ y-C }{2( C-y +C)}\right)\right] + 4B\left(\frac{ y-C }{2( C-y +C)}\right)^2}{B+2}$ <p><math>A</math> controls the number of minima, <math>B</math> controls the magnitude of the “hill sizes” of the multi-modality, and <math>C</math> is the value for which <math>y</math> is mapped to zero. When <math>B=0</math>, <math>2A+1</math> values of <math>y</math> (one at <math>C</math>) are mapped to zero, and when <math>B \neq 0</math>, there are <math>2A</math> local minima, and one global minimum at <math>C</math>. Larger values of <math>A</math> and smaller values of <math>B</math> generate more challenging problems.</p>
<p>Reduction: Weighted Sum (<math> w  =  y , w_1, \dots, w_{ y } &gt; 0</math>)</p> $r\_sum(y, w) = \left( \sum_{i=1}^{ y } w_i y_i \right) / \sum_{i=1}^{ y } w_i$ <p>By varying the constants of the weight vector <math>w</math>, EAs can be forced to treat parameters differently.</p>
<p>Reduction: Non-separable (<math>A \in \{1, \dots,  y \},  y  \bmod A = 0</math>)</p> $r\_sum(y, A) = \frac{\sum_{i=1}^{ y } (y_i)^A + \sum_{k=0}^{A-2}  y_i^{-y_1+(j+k) \bmod  y } }{\frac{ y }{A} \lfloor \frac{A}{2} \rfloor (1+2A-2\lfloor A/2 \rfloor)}$ <p><math>A</math> controls the degree of non-separability (noting that <math>r\_nonsep(y, 1) = r\_sum(y, \{1, \dots, 1\})</math>).</p>

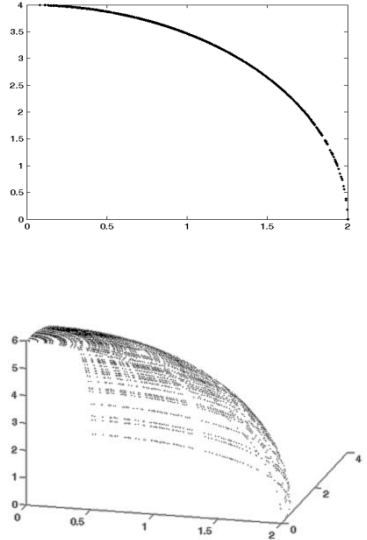
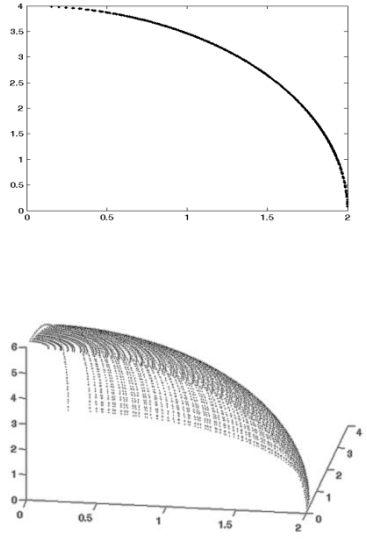
Table 40: WFG test suite

The number of position-related parameters  $k$  must be divisible by the number of underlying position parameters  $M-1$ . For WFG2 and WFG2, 1 must be a multiple of two. For readability, let's define a transition vector  $y = t^{i-1}$ . For  $t^1, y = z_{[0,1]} = \{z_1/2, \dots, z_1/(2n)\}$

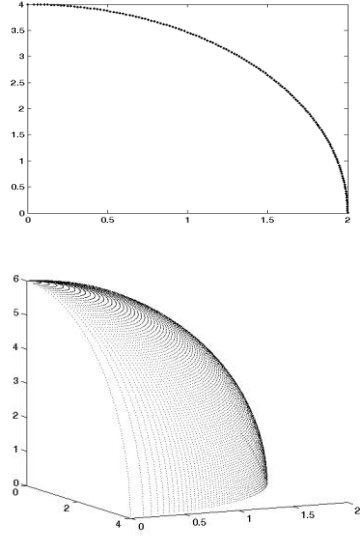
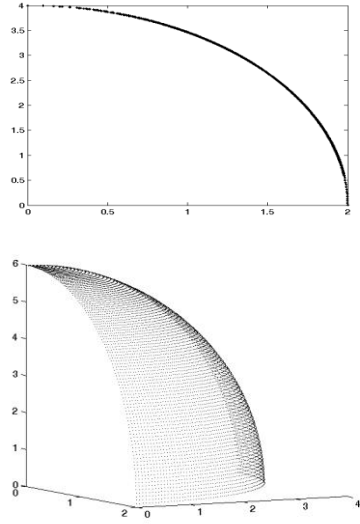
Problem	Type	Settings	Obj	Var.	Geometry
All	Constants	$S_{m=1:M} = 2m$ $D = 1$ $A_1 = 1$ $A_{2:M-1} = \begin{cases} 0, & \text{for WFG3} \\ 1, & \text{otherwise} \end{cases}$ <p>The settings for <math>S_{1:M}</math> ensures the Pareto optimal fronts have dissimilar tradeoff magnitudes, and the settings for <math>A_{1:M-1}</math> ensures the Pareto optimal fronts are not degenerate, except in the case of WFG3 which has a one dimensional Pareto optimal front.</p>			
All	Domains	$z_{i=1:N,max} = 2i$ <p>The working parameters have domains of dissimilar magnitude.</p>			
WFG1	Shape	$h_{m=1:M-1} = \text{convex}_m$ $h_M = \text{mixed}_M \text{ (with } \alpha=1 \text{ and } A=5)$ $t_{i=1:k}^1 = y_i$ $t_{i=k+1:n}^1 = s\_linear(y, 0.35)$ $t_{i=1:k}^2 = y_i$ $t_{i=k+1:n}^2 = b\_flat(y, 0.8, 0.75, 0.85)$ $t_{i=1:n}^3 = b\_poly(y_i, 0.2)$ $t_{i=1:M-2}^4 = r\_sum(\{y_{(i-1)k/(M-1)+1}, \dots, y_{ik/(M-1)}\}, \{2((i-1)k/(M-1)+1), \dots, 2ik/(M-1)\})$ $t_M^4 = r\_sum(\{y_{k+1}, \dots, y_n\}, \{2(k+1), \dots, 2n\})$	2/3	6	Convex concave mixed



WFG2		$h_{m=1:M-1} = \text{convex}_m$ $h_M = \text{disc}_M \text{ (with } \alpha=\beta=1 \text{ and } A=5)$ <p>As <math>t^1</math> from WFG1. (linear shift)</p> $t_{i=k+1:k+l/2}^2 = r_{\text{nonsep}}(\{y_{k+2(i-k)}, y_{k+2(i-k)}\}, 2)$ $t_{i=1:M-1}^3 = r_{\text{sum}}(\{y_{(i-1)k/(M-1)+1}, \dots, y_{ik/(M-1)}\}, \{1, \dots, 1\})$ $t_M^3 = r_{\text{sum}}(\{y_{k+1}, \dots, y_{k+l/2}\}, \{1, \dots, 1\})$	2/3	6	Convex, disconnected	
WFG3		$h_{m=1:M} = \text{linear}_m(\text{degenerate})$ <p>As <math>t^{1:3}</math> from WFG2. (linear shift, non-separable reduction, and weighted sum reduction)</p>	2/3	6	Linear, degenerate	

WFG4		$h_{m=1:M} = \text{concave}_m$ $t_{i=1:n}^1 = s\_multi(y_i, 30, 10, 0.35)$ $t_{i=1:M-1}^2 = r\_sum(\{y_{(i-1)k/(M-1)+1}, \dots, y_{ik/(M-1)}\}, \{1, \dots, 1\})$ $t_M^2 = r\_sum(\{y_{k+1}, \dots, y_n\}, \{1, \dots, 1\})$	2/3	6	Concave	 <p>The top plot is a 2D graph showing a concave curve on a coordinate system where both axes range from 0 to 2. The curve starts at (0, 4) and ends at (2, 0). The bottom plot is a 3D surface plot of a concave surface, with the x and y axes ranging from 0 to 2 and the z-axis ranging from 0 to 6. The surface is highest at the origin and slopes down to zero at the edges of the xy-plane.</p>
WFG5		$h_{m=1:M} = \text{concave}_m$ <p>As <math>t^1</math> from WFG1. (linear shift)</p> $t_{i=1:n}^1 = s\_decept(y_i, 0.35, 0.001, 0.05)$ <p>As <math>t^2</math> from WFG4. (weighted sum reduction)</p>	2/3	6	Concave	 <p>The top plot is a 2D graph showing a concave curve on a coordinate system where both axes range from 0 to 2. The curve starts at (0, 4) and ends at (2, 0). The bottom plot is a 3D surface plot of a concave surface, with the x and y axes ranging from 0 to 2 and the z-axis ranging from 0 to 6. The surface is highest at the origin and slopes down to zero at the edges of the xy-plane.</p>



WFG6		$h_{m=1:M} = \text{concave}_m$ <p>As <math>t^1</math> from WFG1. (linear shift)</p> $t_{i=1:M-1}^2 = r\_nonsep(\{y_{(i-1)k/(M-1)+1}, \dots, y_{ik/(M-1)}\}, k/(M-1))$ $t_M^2 = r\_sum(\{y_{k+1}, \dots, y_n\}, l)$	2/3	6	Concave	
WFG7		$h_{m=1:M} = \text{concave}_m$ $t_{i=1:k}^1 = b\_param\left(y_i, r\_sum(\{y_{(i-1)k/(M-1)+1}, \dots, y_{ik/(M-1)}\}, \{1, \dots, 1\}) \frac{0.98}{49.98}, 0.002, 50\right)$ $t_{i=k+1:n}^1 = y_i$ <p>As <math>t^1</math> from WFG1. (linear shift)</p> <p>As <math>t^2</math> from WFG4. (weighted sum reduction)</p>	2/3	6	Concave	

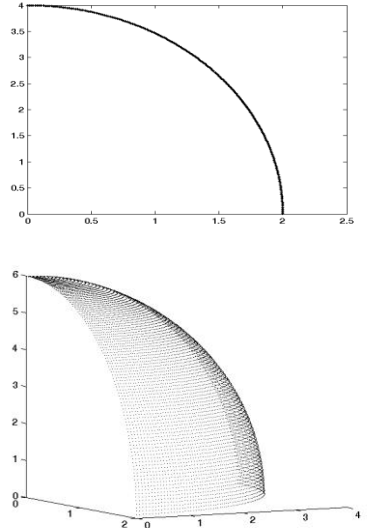
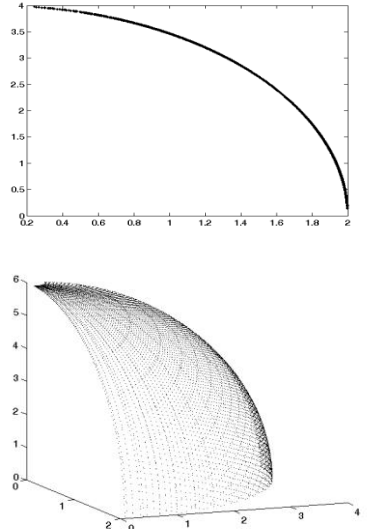
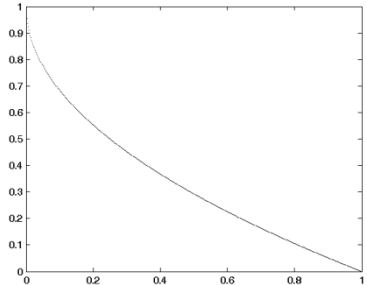
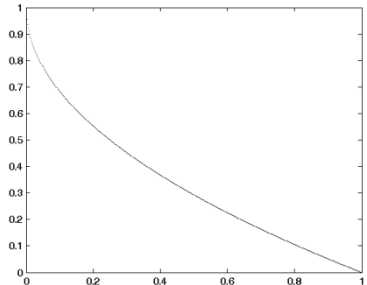
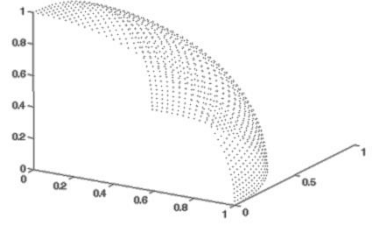
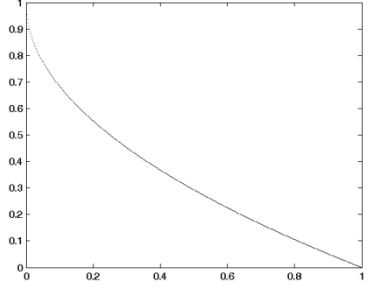
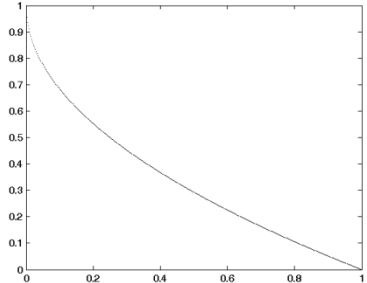
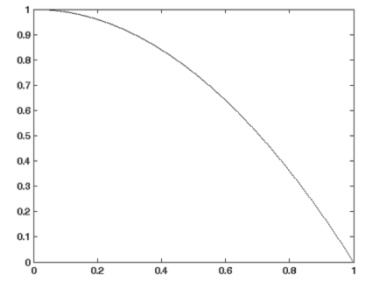
WFG8		$h_{m=1:M} = \text{concave}_m$ $t_{i=1:k}^1 = y_i$ $t_{i=1:k}^1 = b\_param\left(y_i, r\_sum(\{y_{(i-1)k/(M-1)+1}, \dots, y_{ik/(M-1)}\}, \{1, \dots, 1\})^{\frac{0.98}{49.98}}, 0.002, 50\right)$ <p>As <math>t^1</math> from WFG1. (linear shift) As <math>t^2</math> from WFG4. (weighted sum reduction)</p>	2/3	6	Concave	
WFG9		$h_{m=1:M} = \text{concave}_m$ $t_{i=1:n-1}^1 = b\_param\left(y_i, r\_sum(\{y_{(i-1)k/(M-1)+1}, \dots, y_{ik/(M-1)}\}, \{1, \dots, 1\})^{\frac{0.98}{49.98}}, 0.002, 50\right)$ $t_n^1 = y_n$ $t_{i=1:k}^2 = s\_decept(y_i, 0.35, 0.001, 0.05)$ $t_{i=k+1:n}^2 = s\_multi(y_i, 30, 10, 0.35)$ <p>As <math>t^2</math> from WFG6. (Non-separable reduction)</p>	2/3	6	Concave	

Table 41: LZ\_09 test suite

Problems	Type	Settings	No. Objectives	No. Variables	Geometry	
LZ_F1	$f_1(\vec{x}) = x_1 + \frac{2}{ J_1 } \sum_{j \in J_1} (x_j - x_1^{0.5(1.0 + \frac{3(j-2)}{n-2})^2})^2$ $f_2(\vec{x}) = 1 - \sqrt{x_1} + \frac{2}{ J_2 } \sum_{j \in J_2} (x_j - x_1^{0.5(1.0 + \frac{3(j-2)}{n-2})^2})^2$ <p><math>J_1 = \{j   j \text{ is odd and } 2 \leq j \leq n\}</math> and <math>J_2 = \{j   j \text{ is even and } 2 \leq j \leq n\}</math></p>	$0 \leq x_j \leq 1$	2	30	Convex	
LZ_F2	$f_1(\vec{x}) = x_1 + \frac{2}{ J_1 } \sum_{j \in J_1} (x_j - \sin(6\pi x_1 + \frac{j\pi}{n}))^2$ $f_2(\vec{x}) = 1 - \sqrt{x_1} + \frac{2}{ J_2 } \sum_{j \in J_2} (x_j - \sin(6\pi x_1 + \frac{j\pi}{n}))^2$ <p><math>J_1</math> and <math>J_2</math> idem LZ_F12</p>	$0 \leq x_0 \leq 1$ $-1 \leq x_j \leq 1$ $j \neq 0$	2	30	Convex	

LZ_F3	$f_1(\vec{x}) = x_1 + \frac{2}{ J_1 } \sum_{j \in J_1} (x_j - 0.8x_1 \cos(6\pi x_1 + \frac{j\pi}{n}))^2$ $f_2(\vec{x}) = 1 - \sqrt{x_1} + \frac{2}{ J_2 } \sum_{j \in J_2} (x_j - 0.8x_1 \sin(6\pi x_1 + \frac{j\pi}{n}))^2$ <p style="text-align: center;"><math>J_1</math> and <math>J_2</math> idem LZ_F1</p>	$0 \leq x_0 \leq 1$ $-1 \leq x_j \leq 1$ $j \neq 0$	2	30	Convex	
LZ_F4	$f_1(\vec{x}) = x_1 + \frac{2}{ J_1 } \sum_{j \in J_1} (x_j - 0.8x_1 \cos(\frac{6\pi x_1 + j\pi}{3}))^2$ $f_2(\vec{x}) = 1 - \sqrt{x_1} + \frac{2}{ J_2 } \sum_{j \in J_2} (x_j - 0.8x_1 \sin(6\pi x_1 + \frac{j\pi}{n}))^2$ <p style="text-align: center;"><math>J_1</math> and <math>J_2</math> idem LZ_F1</p>	$0 \leq x_0 \leq 1$ $-1 \leq x_j \leq 1$ $j \neq 0$	2	30	Convex	
LZ_F5	$f_1(\vec{x}) = x_1 + \frac{2}{ J_1 } \sum_{j \in J_1} \{x_j - [0.3x_1^2 \cos(24\pi x_1 + \frac{4j\pi}{n}) + 0.6x_1] \cos(6\pi x_1 + \frac{j\pi}{n})\}^2$ $f_2(\vec{x}) = 1 - \sqrt{x_1} + \frac{2}{ J_2 } \sum_{j \in J_2} \{x_j - [0.3x_1^2 \cos(24\pi x_1 + \frac{4j\pi}{n}) + 0.6x_1] \sin(6\pi x_1 + \frac{j\pi}{n})\}^2$ <p style="text-align: center;"><math>J_1</math> and <math>J_2</math> idem LZ_F1</p>	$0 \leq x_0 \leq 1$ $-1 \leq x_j \leq 1$ $j \neq 0$	2	30	Convex	

LZ_F6	$f_1(\vec{x}) = \cos(0.5x_1\pi)\cos(0.5x_2\pi) + \frac{2}{ J_1 } \sum_{j \in J_1} (x_j - 2x_2 \sin(2\pi x_1 + \frac{j\pi}{n}))^2$ $f_2(\vec{x}) = \cos(0.5x_1\pi)\sin(0.5x_2\pi) + \frac{2}{ J_2 } \sum_{j \in J_2} (x_j - 2x_2 \sin(2\pi x_1 + \frac{j\pi}{n}))^2$ $f_3(\vec{x}) = \sin(0.5x_1\pi) + \frac{2}{ J_3 } \sum_{j \in J_3} (x_j - 2x_2 \sin(2\pi x_1 + \frac{j\pi}{n}))^2$ $J_1 = \{j   3 \leq j \leq n, \text{ and } j - 1 \text{ is a multiple of } 3\}$ $J_2 = \{j   3 \leq j \leq n, \text{ and } j - 2 \text{ is a multiple of } 3\}$ $J_3 = \{j   3 \leq j \leq n, \text{ and } j \text{ is a multiple of } 3\}$	$0 \leq x_0 \leq 1$ $0 \leq x_1 \leq 1$ $-1 \leq x_j \leq 1$ $j \neq 0,1$	3	10	Concave	
LZ_F7	$f_1(\vec{x}) = x_1 + \frac{2}{ J_1 } \sum_{j \in J_1} (4y_j^2 - \cos(8y_j\pi + 1.0))$ $f_2(\vec{x}) = 1 - \sqrt{x_1} + \frac{2}{ J_2 } \sum_{j \in J_2} (4y_j^2 - \cos(8y_j\pi + 1.0))$ $J_1 \text{ and } J_2 \text{ idem LZ_F1 and } y_j = x_j - x_1^{0.5(1.0 + \frac{3(j-2)}{n-2})}, J = 2, \dots, n.$	$0 \leq x_j \leq 1$	2	10	Convex	

LZ_F8	$f_1(\vec{x}) = x_1 + \frac{2}{ J_1 } \left( 4 \sum_{j \in J_1} y_j^2 - 2 \prod_{j \in J_1} \cos\left(\frac{20y_j\pi}{\sqrt{j}}\right) + 2 \right)$ $f_2(\vec{x}) = 1 - \sqrt{x_1} + \frac{2}{ J_2 } \left( 4 \sum_{j \in J_2} y_j^2 - 2 \prod_{j \in J_2} \cos\left(\frac{20y_j\pi}{\sqrt{j}}\right) + 2 \right)$ <p><math>J_1</math> and <math>J_2</math> idem LZ_F1 and <math>y_j = x_j - x_1^{0.5(1.0+\frac{3(j-2)}{n-2})}</math>, <math>J = 2, \dots, n</math>.</p>	$0 \leq x_j \leq 1$	2	10	Convex	
LZ_F9	$f_1(\vec{x}) = x_1 + \frac{2}{ J_1 } \sum_{j \in J_1} \left( x_j - \sin\left(6\pi x_1 + \frac{j\pi}{n}\right) \right)^2$ $f_2(\vec{x}) = 1 - x_1^2 + \frac{2}{ J_2 } \sum_{j \in J_2} \left( x_j - \sin\left(6\pi x_1 + \frac{j\pi}{n}\right) \right)^2$ <p><math>J_1</math> and <math>J_2</math> idem LZ_F1 and <math>y_j = x_j - x_1^{0.5(1.0+\frac{3(j-2)}{n-2})}</math>, <math>J = 2, \dots, n</math>.</p>	$0 \leq x_0 \leq 1$ $-1 \leq x_j \leq 1$ $j \neq 0$	2	30	Concave	

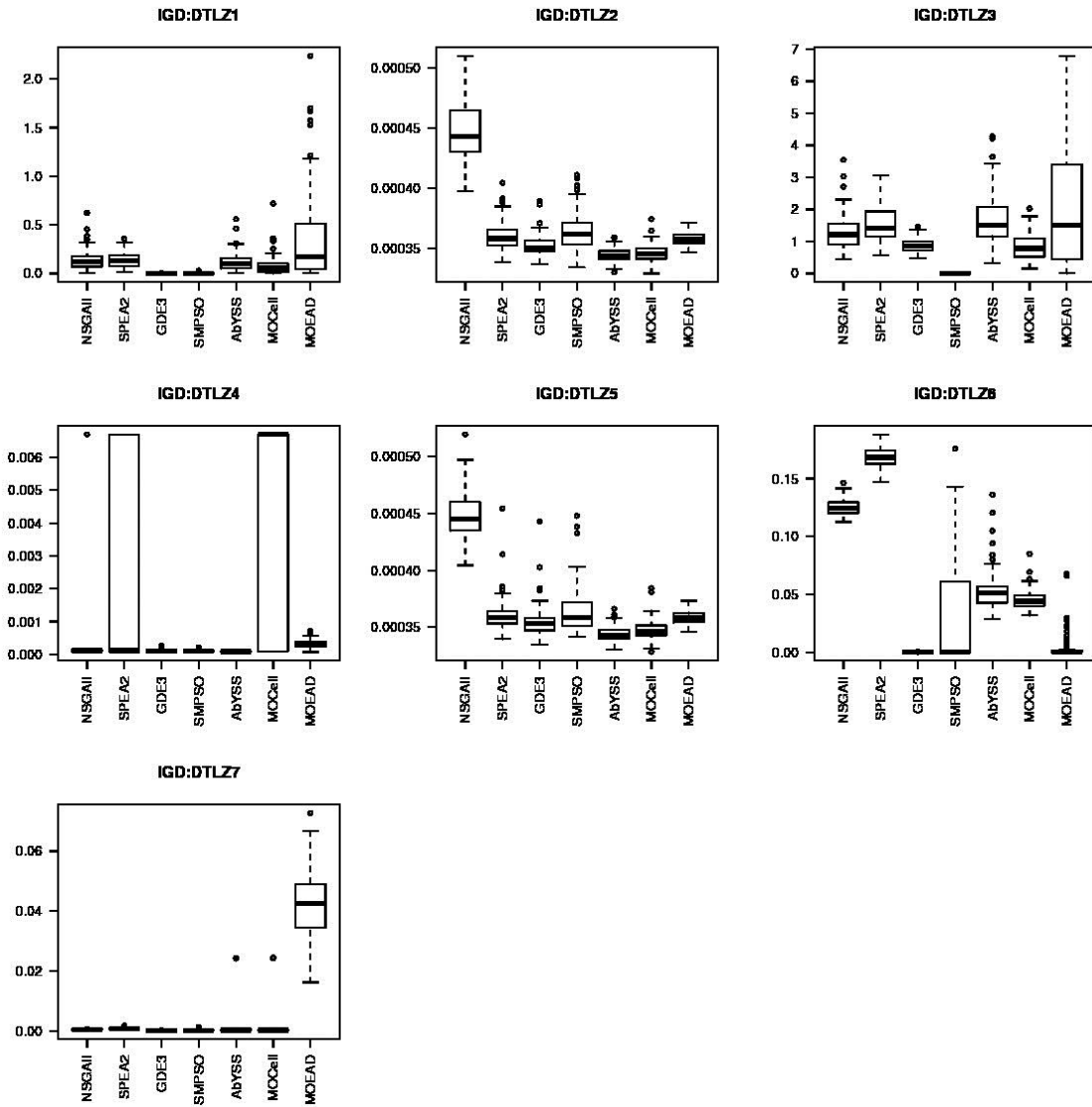


Figure 57: IGD boxplots for DTLZ bi-objective problems

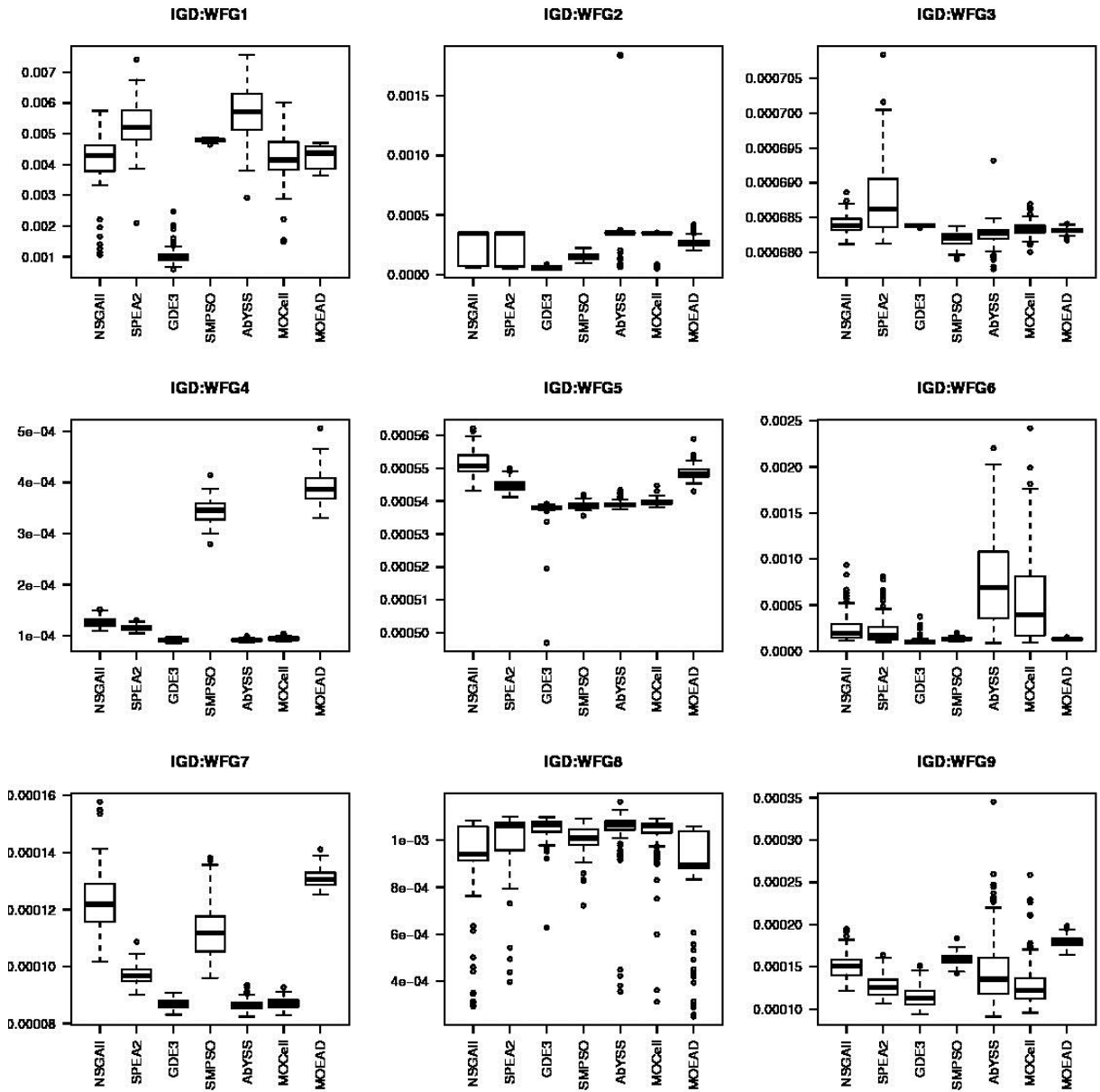


Figure 58: IGD boxplots for WFG bi-objective problems



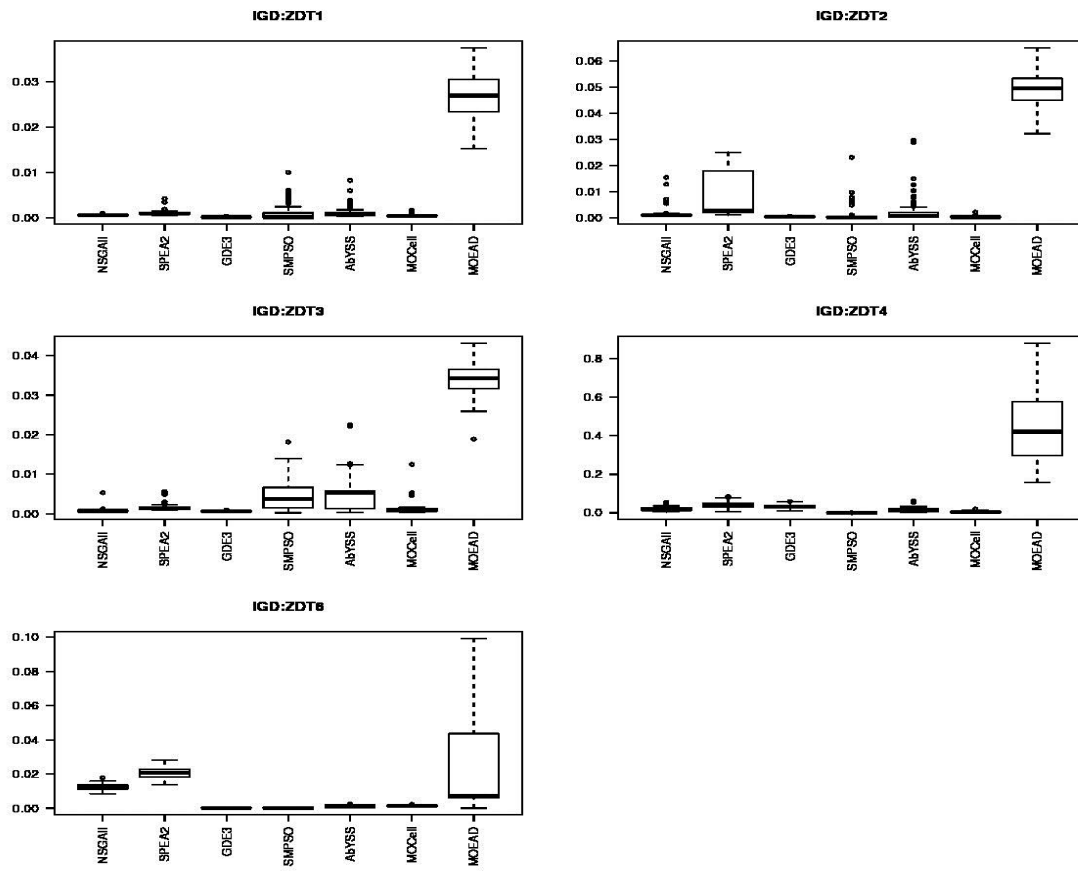


Figure 59: IGD boxplots for ZDT bi-objective problems

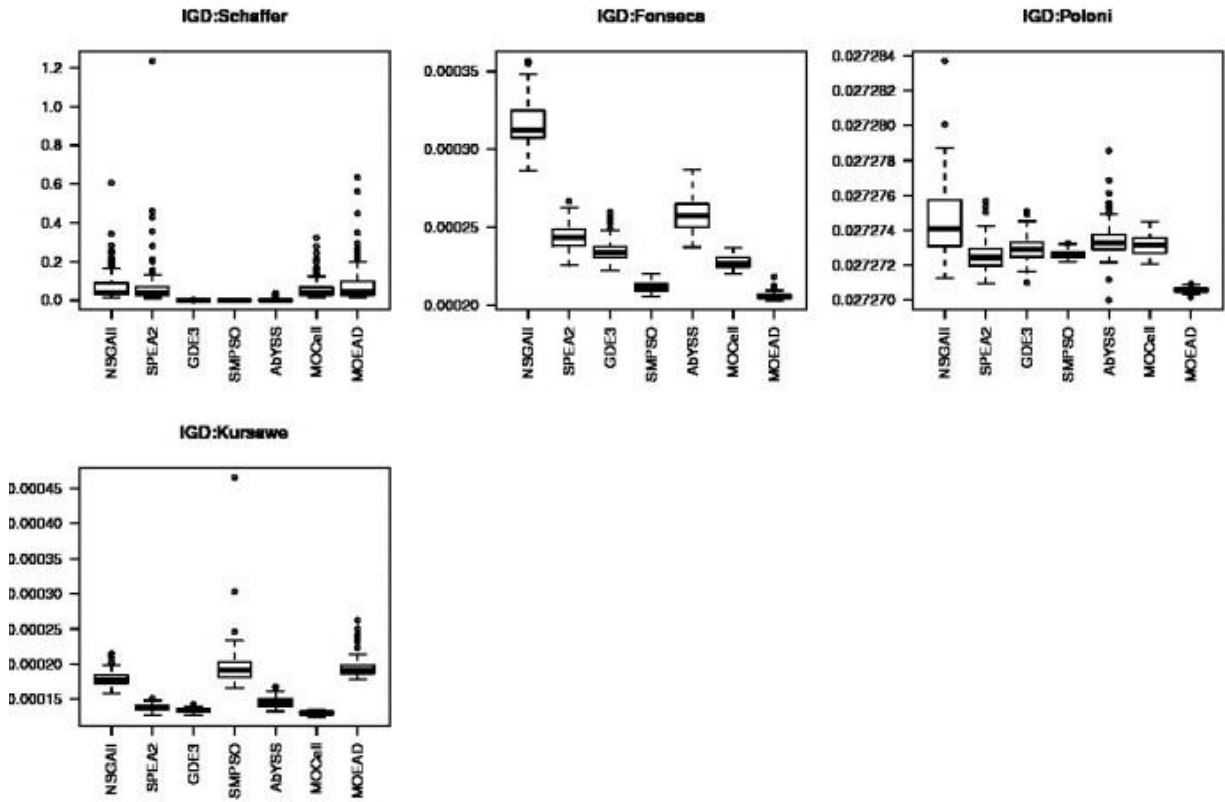


Figure 60: IGD boxplots for Van Veldhuizen's Bi-Objective problems

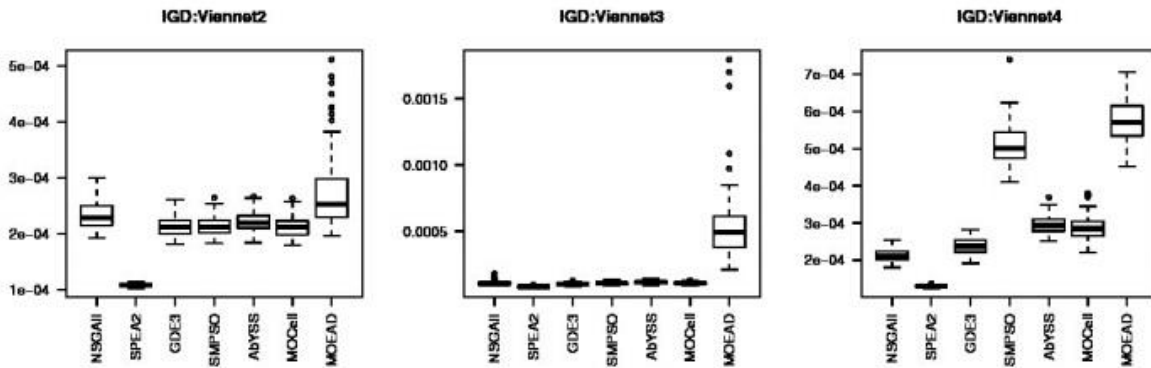


Figure 61: IGD boxplots for the Viennet three-objective problems

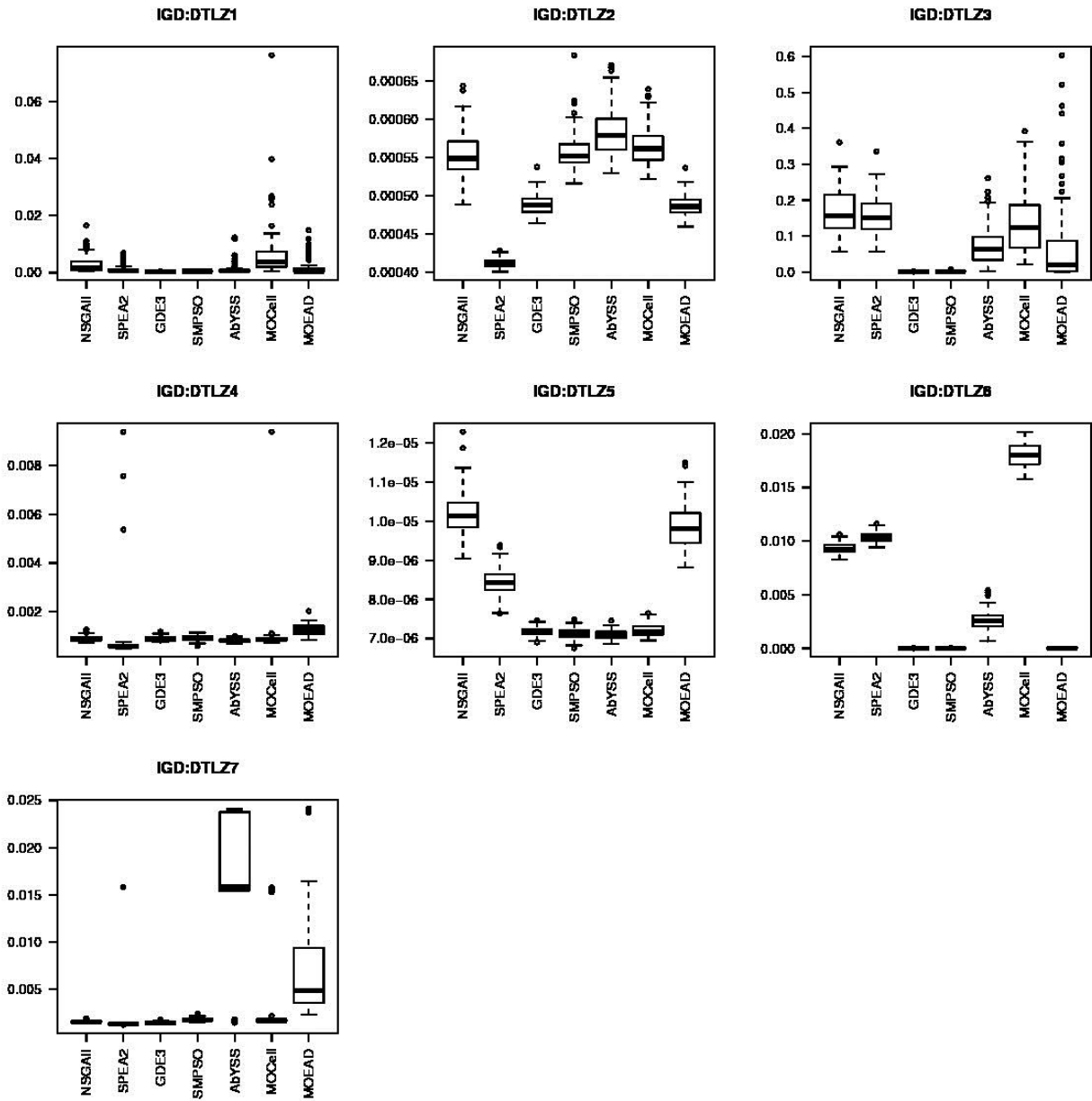


Figure 62: IGD boxplots for DTLZ three-objective problems

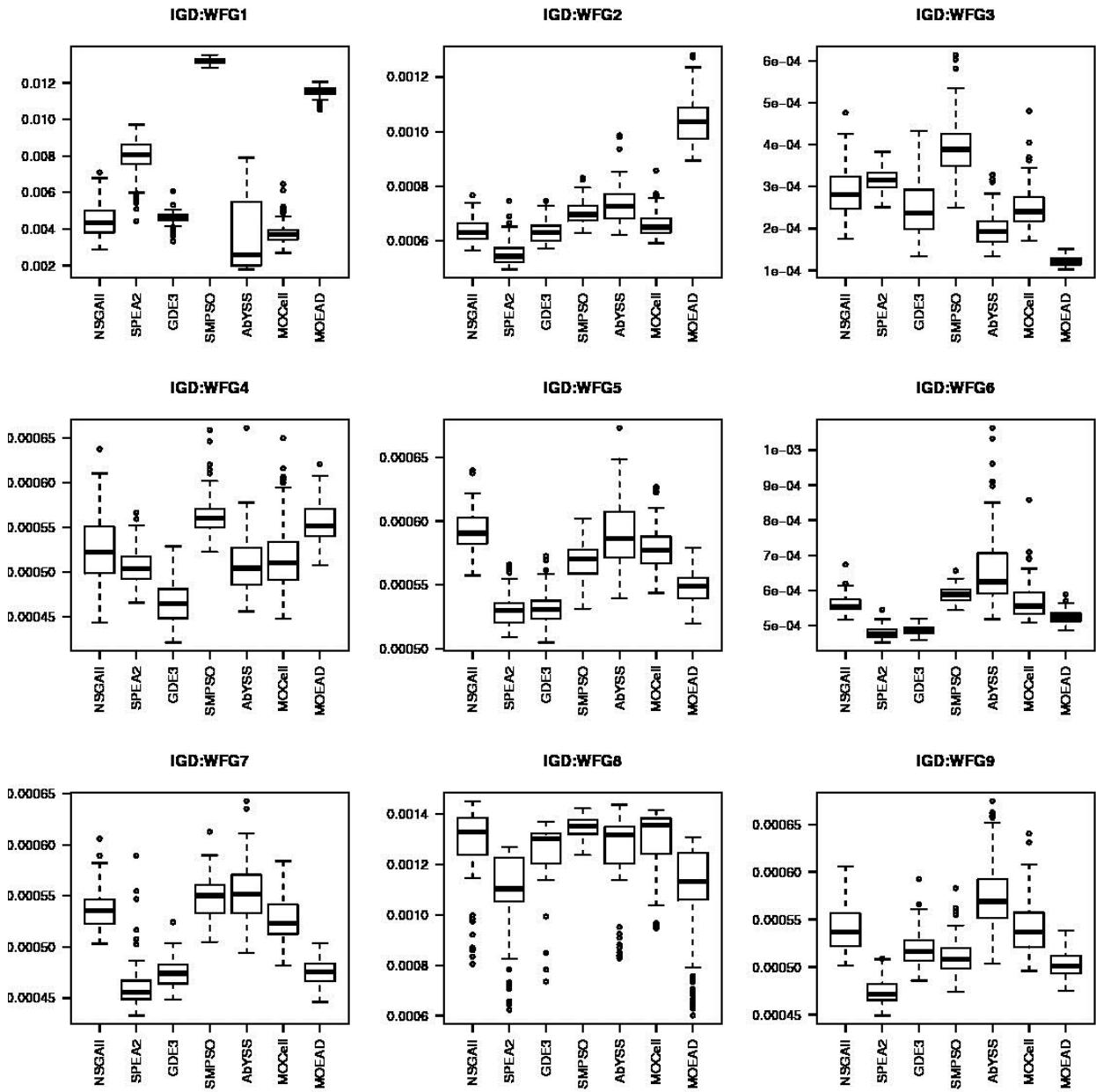


Figure 63: IGD boxplots for WFG three-objective problems

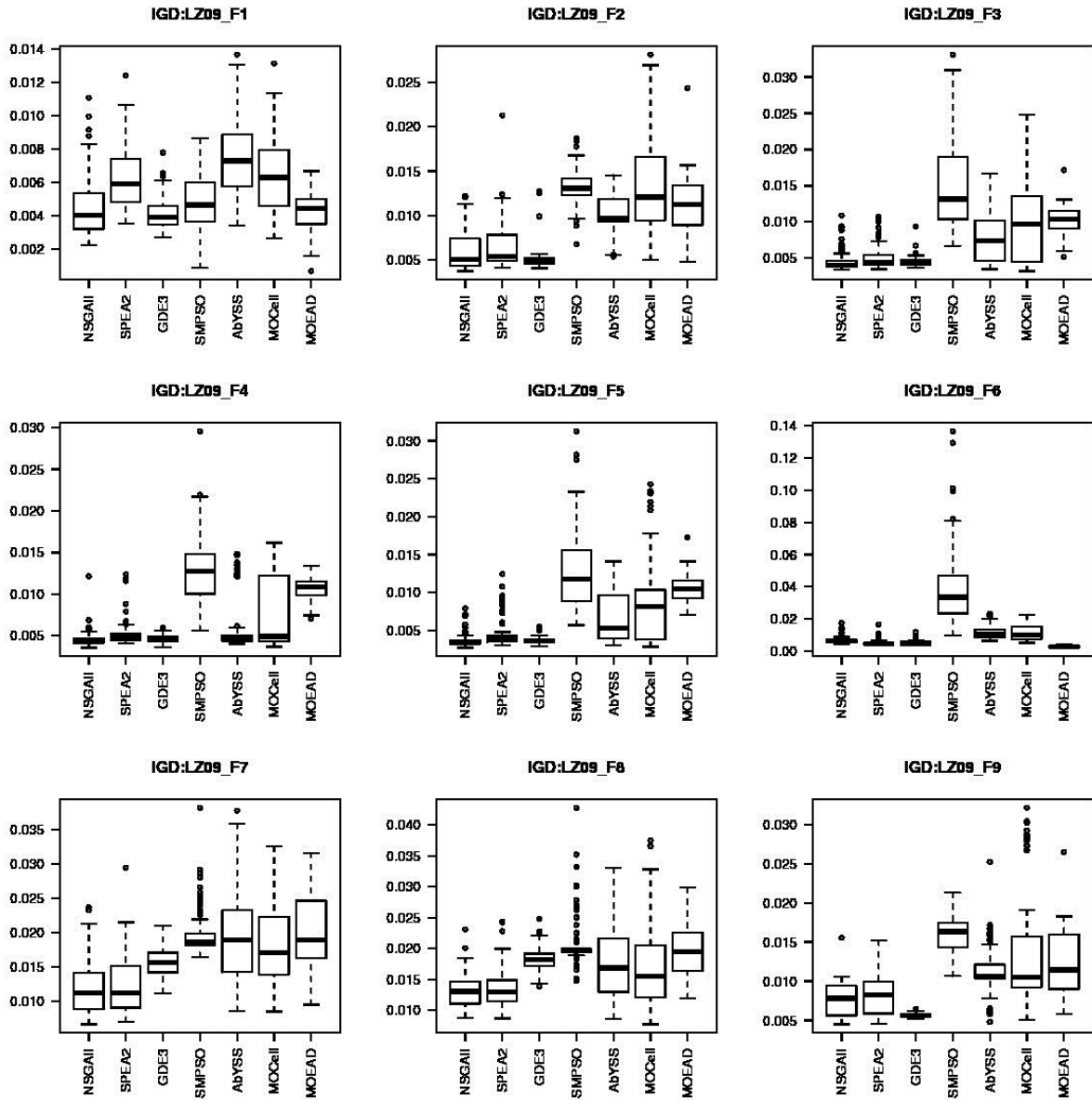


Figure 64: IGD boxplots of LZ\_09 problems

Table 42: HV. Mean and standard deviation for bi-objective problems

	NSGAI1	SPEA2	GDE3	SMPSO	AbySS	MOCcell	MOEAD
Schaffer	$2.90e - 01_{2.5e-01}$	$3.05e - 01_{2.6e-01}$	$8.30e - 01_{3.5e-05}$	$8.30e - 01_{2.9e-05}$	$7.99e - 01_{7.9e-02}$	$3.12e - 01_{2.5e-01}$	$2.83e - 01_{2.6e-01}$
Fonseca	$3.08e - 01_{3.8e-04}$	$3.10e - 01_{2.2e-04}$	$3.11e - 01_{1.9e-04}$	$3.12e - 01_{6.8e-05}$	$3.09e - 01_{4.4e-04}$	$3.11e - 01_{1.8e-04}$	$3.12e - 01_{6.4e-05}$
Poloni	$0.00e + 00_{0.0e+00}$	$0.00e + 00_{0.0e+00}$	$0.00e + 00_{0.0e+00}$	$0.00e + 00_{0.0e+00}$	$0.00e + 00_{0.0e+00}$	$0.00e + 00_{0.0e+00}$	$0.00e + 00_{0.0e+00}$
Kursawe	$3.99e - 01_{3.2e-04}$	$4.00e - 01_{2.8e-04}$	$4.01e - 01_{1.6e-04}$	$3.98e - 01_{8.3e-04}$	$4.00e - 01_{3.3e-04}$	$4.01e - 01_{2.4e-04}$	$3.98e - 01_{6.2e-04}$
ZDT1	$6.36e - 01_{4.5e-03}$	$6.18e - 01_{9.5e-03}$	$6.56e - 01_{2.4e-03}$	$6.14e - 01_{7.9e-02}$	$6.21e - 01_{2.4e-02}$	$6.43e - 01_{7.6e-03}$	$1.14e - 02_{2.4e-02}$
ZDT2	$2.81e - 01_{3.3e-02}$	$1.53e - 01_{1.1e-01}$	$3.20e - 01_{3.7e-03}$	$3.08e - 01_{6.3e-02}$	$2.68e - 01_{7.6e-02}$	$3.20e - 01_{5.7e-03}$	$0.00e + 00_{0.0e+00}$
ZDT3	$4.96e - 01_{4.0e-03}$	$4.78e - 01_{9.7e-03}$	$5.05e - 01_{2.8e-03}$	$4.17e - 01_{7.8e-02}$	$4.69e - 01_{3.5e-02}$	$4.92e - 01_{1.4e-02}$	$2.40e - 02_{2.5e-02}$
ZDT4	$1.41e - 01_{1.4e-01}$	$1.54e - 02_{5.2e-02}$	$1.10e - 02_{3.5e-02}$	$6.60e - 01_{6.4e-04}$	$2.71e - 01_{1.8e-01}$	$5.50e - 01_{1.0e-01}$	$0.00e + 00_{0.0e+00}$
ZDT6	$1.15e - 01_{2.7e-02}$	$2.67e - 02_{2.0e-02}$	$4.01e - 01_{1.1e-04}$	$4.01e - 01_{2.5e-04}$	$3.55e - 01_{1.4e-02}$	$3.50e - 01_{7.9e-03}$	$6.94e - 02_{1.1e-01}$
DTLZ1	$1.96e - 02_{6.3e-02}$	$7.12e - 03_{3.7e-02}$	$4.83e - 01_{9.5e-03}$	$4.64e - 01_{7.4e-02}$	$5.49e - 02_{1.3e-01}$	$1.15e - 01_{1.9e-01}$	$6.74e - 02_{1.3e-01}$
DTLZ2	$2.10e - 01_{2.8e-04}$	$2.11e - 01_{1.9e-04}$	$2.12e - 01_{5.3e-05}$	$2.11e - 01_{2.5e-04}$	$2.12e - 01_{1.5e-04}$	$2.12e - 01_{1.6e-04}$	$2.10e - 01_{2.6e-04}$
DTLZ3	$0.00e + 00_{0.0e+00}$	$0.00e + 00_{0.0e+00}$	$0.00e + 00_{0.0e+00}$	$1.58e - 01_{5.9e-02}$	$0.00e + 00_{0.0e+00}$	$0.00e + 00_{0.0e+00}$	$1.03e - 02_{3.7e-02}$
DTLZ4	$1.65e - 01_{8.5e-02}$	$1.51e - 01_{9.4e-02}$	$2.10e - 01_{1.4e-03}$	$2.10e - 01_{2.9e-04}$	$2.10e - 01_{1.3e-04}$	$9.66e - 02_{1.0e-01}$	$2.06e - 01_{1.5e-03}$
DTLZ5	$2.10e - 01_{2.9e-04}$	$2.11e - 01_{2.0e-04}$	$2.12e - 01_{5.0e-05}$	$2.11e - 01_{2.7e-04}$	$2.12e - 01_{1.6e-04}$	$2.12e - 01_{1.7e-04}$	$2.10e - 01_{2.9e-04}$
DTLZ6	$0.00e + 00_{0.0e+00}$	$0.00e + 00_{0.0e+00}$	$2.12e - 01_{3.4e-05}$	$1.43e - 01_{9.6e-02}$	$0.00e + 00_{0.0e+00}$	$0.00e + 00_{0.0e+00}$	$1.94e - 01_{4.3e-02}$
DTLZ7	$3.21e - 01_{3.0e-03}$	$3.06e - 01_{8.6e-03}$	$3.34e - 01_{3.9e-04}$	$3.33e - 01_{4.9e-03}$	$3.05e - 01_{4.6e-02}$	$3.06e - 01_{4.6e-02}$	$2.24e - 03_{7.9e-03}$
WFG1	$2.98e - 01_{7.4e-02}$	$2.06e - 01_{6.4e-02}$	$4.93e - 01_{5.3e-02}$	$1.06e - 01_{3.4e-03}$	$1.15e - 01_{6.7e-02}$	$2.74e - 01_{8.2e-02}$	$1.36e - 01_{1.7e-02}$
WFG2	$5.61e - 01_{1.4e-03}$	$5.60e - 01_{1.4e-03}$	$5.63e - 01_{4.2e-04}$	$5.54e - 01_{2.6e-03}$	$5.55e - 01_{1.5e-02}$	$5.60e - 01_{1.1e-03}$	$5.58e - 01_{1.1e-03}$
WFG3	$4.40e - 01_{5.0e-04}$	$4.40e - 01_{6.1e-04}$	$4.42e - 01_{1.4e-04}$	$4.39e - 01_{6.1e-04}$	$4.39e - 01_{2.2e-03}$	$4.40e - 01_{5.8e-04}$	$4.40e - 01_{2.7e-04}$
WFG4	$2.16e - 01_{4.3e-04}$	$2.17e - 01_{4.8e-04}$	$2.19e - 01_{2.4e-04}$	$1.95e - 01_{1.8e-03}$	$2.18e - 01_{4.3e-04}$	$2.17e - 01_{5.4e-04}$	$1.94e - 01_{2.3e-03}$
WFG5	$1.95e - 01_{3.2e-04}$	$1.95e - 01_{1.6e-04}$	$1.96e - 01_{2.7e-04}$	$1.96e - 01_{6.9e-05}$	$1.96e - 01_{8.9e-05}$	$1.96e - 01_{7.8e-05}$	$1.94e - 01_{1.6e-04}$
WFG6	$1.96e - 01_{1.1e-02}$	$1.98e - 01_{1.0e-02}$	$2.07e - 01_{3.9e-03}$	$2.05e - 01_{1.1e-03}$	$1.67e - 01_{2.7e-02}$	$1.79e - 01_{2.6e-02}$	$2.06e - 01_{6.7e-04}$
WFG7	$2.08e - 01_{3.9e-04}$	$2.09e - 01_{3.4e-04}$	$2.11e - 01_{6.6e-05}$	$2.06e - 01_{8.1e-04}$	$2.10e - 01_{4.6e-04}$	$2.09e - 01_{3.2e-04}$	$2.07e - 01_{4.3e-04}$
WFG8	$1.46e - 01_{1.1e-02}$	$1.43e - 01_{6.0e-03}$	$1.39e - 01_{1.8e-03}$	$1.42e - 01_{2.2e-03}$	$1.40e - 01_{7.4e-03}$	$1.43e - 01_{6.3e-03}$	$1.51e - 01_{1.1e-02}$
WFG9	$2.36e - 01_{1.6e-03}$	$2.37e - 01_{1.5e-03}$	$2.38e - 01_{1.5e-03}$	$2.33e - 01_{5.4e-04}$	$2.34e - 01_{3.8e-03}$	$2.36e - 01_{2.8e-03}$	$2.32e - 01_{5.0e-04}$

Table 43: HVR. Mean and standard deviation for bi-objective problems

	NSGAI1	SPEA2	GDE3	SMPSO	AbYSS	MOCcell	MOEAD
Schaffer	$3.27e-01_{3.1e-01}$	$3.58e-01_{2.9e-01}$	$9.98e-01_{3.8e-05}$	$9.98e-01_{3.6e-05}$	$9.61e-01_{9.5e-02}$	$4.01e-01_{3.1e-01}$	$2.98e-01_{2.9e-01}$
Fonseca	$9.76e-01_{1.2e-03}$	$9.82e-01_{7.0e-04}$	$9.84e-01_{6.2e-04}$	$9.88e-01_{2.2e-04}$	$9.79e-01_{1.4e-03}$	$9.84e-01_{5.7e-04}$	$9.88e-01_{2.0e-04}$
Poloni	$0.00e+00_{0.0e+00}$	$0.00e+00_{0.0e+00}$	$0.00e+00_{0.0e+00}$	$0.00e+00_{0.0e+00}$	$0.00e+00_{0.0e+00}$	$0.00e+00_{0.0e+00}$	$0.00e+00_{0.0e+00}$
Kursawe	$9.88e-01_{7.9e-04}$	$9.90e-01_{6.9e-04}$	$9.92e-01_{4.0e-04}$	$9.84e-01_{2.0e-03}$	$9.91e-01_{8.1e-04}$	$9.92e-01_{5.9e-04}$	$9.85e-01_{1.5e-03}$
ZDT1	$9.55e-01_{6.7e-03}$	$9.27e-01_{1.4e-02}$	$9.84e-01_{3.6e-03}$	$9.22e-01_{1.2e-01}$	$9.33e-01_{3.6e-02}$	$9.65e-01_{1.1e-02}$	$1.71e-02_{3.6e-02}$
ZDT2	$8.45e-01_{9.9e-02}$	$4.60e-01_{3.5e-01}$	$9.63e-01_{1.1e-02}$	$9.25e-01_{1.9e-01}$	$8.05e-01_{2.3e-01}$	$9.61e-01_{1.7e-02}$	$0.00e+00_{0.0e+00}$
ZDT3	$9.59e-01_{7.7e-03}$	$9.25e-01_{1.9e-02}$	$9.77e-01_{5.5e-03}$	$8.06e-01_{1.5e-01}$	$9.08e-01_{6.8e-02}$	$9.52e-01_{2.6e-02}$	$4.65e-02_{4.8e-02}$
ZDT4	$2.11e-01_{2.1e-01}$	$2.31e-02_{7.8e-02}$	$1.65e-02_{5.3e-02}$	$9.91e-01_{9.6e-04}$	$4.06e-01_{2.6e-01}$	$8.25e-01_{1.6e-01}$	$0.00e+00_{0.0e+00}$
ZDT6	$2.86e-01_{6.8e-02}$	$6.65e-02_{4.9e-02}$	$9.99e-01_{2.7e-04}$	$9.98e-01_{6.3e-04}$	$8.83e-01_{3.4e-02}$	$8.72e-01_{2.0e-02}$	$1.73e-01_{2.7e-01}$
DTLZ1	$3.93e-02_{1.3e-01}$	$1.43e-02_{7.4e-02}$	$9.70e-01_{1.9e-02}$	$9.32e-01_{1.5e-01}$	$1.10e-01_{2.7e-01}$	$2.31e-01_{3.7e-01}$	$1.35e-01_{2.7e-01}$
DTLZ2	$9.81e-01_{1.3e-03}$	$9.85e-01_{9.1e-04}$	$9.90e-01_{2.5e-04}$	$9.86e-01_{1.1e-03}$	$9.89e-01_{7.0e-04}$	$9.87e-01_{7.5e-04}$	$9.80e-01_{1.2e-03}$
DTLZ3	$0.00e+00_{0.0e+00}$	$0.00e+00_{0.0e+00}$	$0.00e+00_{0.0e+00}$	$7.38e-01_{2.8e-01}$	$0.00e+00_{0.0e+00}$	$0.00e+00_{0.0e+00}$	$4.81e-02_{1.7e-01}$
DTLZ4	$7.75e-01_{4.0e-01}$	$7.09e-01_{4.4e-01}$	$9.88e-01_{6.5e-03}$	$9.86e-01_{1.4e-03}$	$9.89e-01_{6.0e-04}$	$4.54e-01_{4.9e-01}$	$9.68e-01_{7.2e-03}$
DTLZ5	$9.81e-01_{1.3e-03}$	$9.85e-01_{9.5e-04}$	$9.90e-01_{2.3e-04}$	$9.86e-01_{1.3e-03}$	$9.89e-01_{7.7e-04}$	$9.87e-01_{8.1e-04}$	$9.80e-01_{1.4e-03}$
DTLZ6	$0.00e+00_{0.0e+00}$	$0.00e+00_{0.0e+00}$	$9.91e-01_{1.6e-04}$	$6.69e-01_{4.5e-01}$	$0.00e+00_{0.0e+00}$	$0.00e+00_{0.0e+00}$	$9.05e-01_{2.0e-01}$
DTLZ7	$9.50e-01_{8.9e-03}$	$9.05e-01_{2.5e-02}$	$9.89e-01_{1.1e-03}$	$9.86e-01_{1.5e-02}$	$9.02e-01_{1.4e-01}$	$9.04e-01_{1.3e-01}$	$6.62e-03_{2.3e-02}$
WFG1	$4.69e-01_{1.2e-01}$	$3.24e-01_{1.0e-01}$	$7.75e-01_{8.4e-02}$	$1.66e-01_{5.3e-03}$	$1.81e-01_{1.1e-01}$	$4.31e-01_{1.3e-01}$	$2.14e-01_{2.7e-02}$
WFG2	$9.94e-01_{2.5e-03}$	$9.93e-01_{2.5e-03}$	$9.97e-01_{7.4e-04}$	$9.81e-01_{4.7e-03}$	$9.83e-01_{2.6e-02}$	$9.93e-01_{2.0e-03}$	$9.89e-01_{2.0e-03}$
WFG3	$8.83e-01_{1.0e-03}$	$8.82e-01_{1.2e-03}$	$8.86e-01_{2.8e-04}$	$8.80e-01_{1.2e-03}$	$8.81e-01_{4.5e-03}$	$8.84e-01_{1.2e-03}$	$8.83e-01_{5.5e-04}$
WFG4	$9.74e-01_{1.9e-03}$	$9.78e-01_{2.1e-03}$	$9.85e-01_{1.1e-03}$	$8.80e-01_{8.3e-03}$	$9.84e-01_{1.9e-03}$	$9.79e-01_{2.4e-03}$	$8.72e-01_{1.0e-02}$
WFG5	$8.32e-01_{1.4e-03}$	$8.35e-01_{6.7e-04}$	$8.38e-01_{1.2e-03}$	$8.38e-01_{3.0e-04}$	$8.38e-01_{3.8e-04}$	$8.38e-01_{3.3e-04}$	$8.31e-01_{6.6e-04}$
WFG6	$9.26e-01_{5.3e-02}$	$9.32e-01_{4.7e-02}$	$9.77e-01_{1.8e-02}$	$9.67e-01_{5.4e-03}$	$7.90e-01_{1.3e-01}$	$8.45e-01_{1.2e-01}$	$9.70e-01_{3.2e-03}$
WFG7	$9.73e-01_{1.8e-03}$	$9.76e-01_{1.6e-03}$	$9.84e-01_{3.1e-04}$	$9.63e-01_{3.8e-03}$	$9.80e-01_{2.2e-03}$	$9.79e-01_{1.5e-03}$	$9.67e-01_{2.0e-03}$
WFG8	$6.88e-01_{5.2e-02}$	$6.75e-01_{2.8e-02}$	$6.55e-01_{8.5e-03}$	$6.70e-01_{1.1e-02}$	$6.57e-01_{3.5e-02}$	$6.71e-01_{3.0e-02}$	$7.10e-01_{5.3e-02}$
WFG9	$9.58e-01_{6.4e-03}$	$9.63e-01_{6.0e-03}$	$9.67e-01_{6.0e-03}$	$9.49e-01_{2.2e-03}$	$9.54e-01_{1.5e-02}$	$9.60e-01_{1.1e-02}$	$9.43e-01_{2.0e-03}$

Table 44: Hypervolume Ratio Mean and Standard Deviation for Three-Objective Problems

	NSGAI1	SPEA2	GDE3	SMPSO	AbYSS	MOCcell	MOEAD
DTLZ1	$5.78e - 01_{3.4e-01}$	$8.42e - 01_{1.7e-01}$	$9.59e - 01_{2.1e-03}$	$9.33e - 01_{3.9e-03}$	$8.05e - 01_{2.8e-01}$	$3.63e - 01_{3.3e-01}$	$7.30e - 01_{3.6e-01}$
DTLZ2	$8.60e - 01_{6.8e-03}$	$9.08e - 01_{2.2e-03}$	$8.87e - 01_{6.2e-03}$	$8.32e - 01_{7.4e-03}$	$8.76e - 01_{6.9e-03}$	$8.56e - 01_{8.2e-03}$	$8.66e - 01_{7.3e-03}$
DTLZ3	$0.00e + 00_{0.0e+00}$	$0.00e + 00_{0.0e+00}$	$8.95e - 01_{5.4e-03}$	$8.19e - 01_{1.0e-01}$	$1.11e - 02_{8.1e-02}$	$0.00e + 00_{0.0e+00}$	$2.48e - 01_{3.6e-01}$
DTLZ4	$9.55e - 01_{6.2e-03}$	$9.41e - 01_{1.7e-01}$	$9.77e - 01_{6.0e-03}$	$9.29e - 01_{2.6e-02}$	$9.78e - 01_{6.3e-03}$	$9.04e - 01_{2.3e-01}$	$8.97e - 01_{6.1e-02}$
DTLZ5	$9.89e - 01_{9.8e-04}$	$9.89e - 01_{9.7e-04}$	$9.97e - 01_{1.0e-04}$	$9.95e - 01_{2.4e-04}$	$9.96e - 01_{1.6e-04}$	$9.94e - 01_{5.0e-04}$	$9.86e - 01_{7.3e-04}$
DTLZ6	$0.00e + 00_{0.0e+00}$	$0.00e + 00_{0.0e+00}$	$1.01e + 00_{9.2e-05}$	$1.01e + 00_{1.4e-04}$	$1.96e - 02_{5.8e-02}$	$0.00e + 00_{0.0e+00}$	$1.01e + 00_{1.6e-04}$
DTLZ7	$8.95e - 01_{8.3e-03}$	$9.03e - 01_{1.4e-02}$	$9.52e - 01_{4.4e-03}$	$9.15e - 01_{8.6e-03}$	$8.02e - 01_{1.0e-01}$	$8.67e - 01_{2.9e-02}$	$5.66e - 01_{1.3e-01}$
WFG1	$7.33e - 01_{6.8e-02}$	$6.31e - 01_{4.3e-02}$	$8.13e - 01_{4.3e-02}$	$1.23e - 01_{1.4e-02}$	$8.78e - 01_{1.1e-01}$	$7.98e - 01_{6.1e-02}$	$2.71e - 01_{1.1e-02}$
WFG2	$9.79e - 01_{1.8e-03}$	$9.86e - 01_{1.0e-03}$	$9.84e - 01_{1.6e-03}$	$9.71e - 01_{2.2e-03}$	$9.78e - 01_{2.5e-03}$	$9.79e - 01_{1.9e-03}$	$9.69e - 01_{3.4e-03}$
WFG3	$9.74e - 01_{4.2e-03}$	$9.16e - 01_{9.4e-03}$	$9.85e - 01_{3.2e-03}$	$9.44e - 01_{6.8e-03}$	$9.83e - 01_{5.3e-03}$	$9.78e - 01_{4.3e-03}$	$9.76e - 01_{2.4e-03}$
WFG4	$8.56e - 01_{8.6e-03}$	$9.01e - 01_{3.9e-03}$	$9.03e - 01_{5.8e-03}$	$7.76e - 01_{7.1e-03}$	$8.98e - 01_{6.4e-03}$	$8.69e - 01_{6.7e-03}$	$8.36e - 01_{7.0e-03}$
WFG5	$7.78e - 01_{7.7e-03}$	$8.18e - 01_{8.4e-03}$	$8.03e - 01_{4.9e-03}$	$7.81e - 01_{7.1e-03}$	$7.98e - 01_{6.7e-03}$	$7.94e - 01_{6.2e-03}$	$8.00e - 01_{4.0e-03}$
WFG6	$8.31e - 01_{1.8e-02}$	$8.71e - 01_{1.7e-02}$	$8.94e - 01_{5.1e-03}$	$8.14e - 01_{8.4e-03}$	$7.67e - 01_{7.1e-02}$	$8.27e - 01_{4.5e-02}$	$8.72e - 01_{4.8e-03}$
WFG7	$8.37e - 01_{8.4e-03}$	$8.80e - 01_{3.9e-03}$	$8.75e - 01_{5.6e-03}$	$8.08e - 01_{1.0e-02}$	$8.70e - 01_{6.6e-03}$	$8.57e - 01_{7.4e-03}$	$8.69e - 01_{5.6e-03}$
WFG8	$5.72e - 01_{4.2e-02}$	$6.44e - 01_{5.0e-02}$	$5.96e - 01_{3.1e-02}$	$5.58e - 01_{9.9e-03}$	$5.96e - 01_{5.1e-02}$	$5.77e - 01_{3.1e-02}$	$6.59e - 01_{8.2e-02}$
WFG9	$8.42e - 01_{7.2e-03}$	$8.76e - 01_{4.9e-03}$	$8.53e - 01_{6.4e-03}$	$8.38e - 01_{7.3e-03}$	$8.39e - 01_{1.4e-02}$	$8.41e - 01_{1.0e-02}$	$8.68e - 01_{5.1e-03}$
Viennet2	$9.93e - 01_{7.3e-04}$	$9.96e - 01_{2.0e-04}$	$9.94e - 01_{3.6e-04}$	$9.94e - 01_{4.3e-04}$	$9.94e - 01_{5.0e-04}$	$9.94e - 01_{4.4e-04}$	$9.96e - 01_{3.8e-04}$
Viennet3	$9.95e - 01_{2.9e-04}$	$9.90e - 01_{5.7e-04}$	$9.97e - 01_{1.9e-04}$	$9.96e - 01_{2.5e-04}$	$9.96e - 01_{3.1e-04}$	$9.97e - 01_{2.3e-04}$	$9.98e - 01_{2.3e-04}$
Viennet4	$9.84e - 01_{1.3e-03}$	$9.90e - 01_{5.4e-04}$	$9.86e - 01_{1.0e-03}$	$1.00e + 00_{4.7e-03}$	$9.83e - 01_{1.5e-03}$	$9.84e - 01_{1.2e-03}$	$9.96e - 01_{4.6e-03}$



Table 45: HV Mean and Standard Deviation for Three-Objective Problems

	NSGAI1	SPEA2	GDE3	SMPSO	AbySS	MOCcell	MOEAD
DTLZ1	$4.77e-01_{2.8e-01}$	$6.95e-01_{1.4e-01}$	$7.92e-01_{1.7e-03}$	$7.70e-01_{3.3e-03}$	$6.64e-01_{2.3e-01}$	$3.00e-01_{2.8e-01}$	$6.03e-01_{2.9e-01}$
DTLZ2	$4.02e-01_{3.2e-03}$	$4.25e-01_{1.0e-03}$	$4.15e-01_{2.9e-03}$	$3.89e-01_{3.5e-03}$	$4.10e-01_{3.2e-03}$	$4.01e-01_{3.8e-03}$	$4.05e-01_{3.4e-03}$
DTLZ3	$0.00e+00_{0.0e+00}$	$0.00e+00_{0.0e+00}$	$4.16e-01_{2.5e-03}$	$3.80e-01_{4.7e-02}$	$5.14e-03_{3.8e-02}$	$0.00e+00_{0.0e+00}$	$1.15e-01_{1.7e-01}$
DTLZ4	$4.02e-01_{2.6e-03}$	$3.96e-01_{7.2e-02}$	$4.12e-01_{2.5e-03}$	$3.91e-01_{1.1e-02}$	$4.12e-01_{2.6e-03}$	$3.81e-01_{9.6e-02}$	$3.78e-01_{2.6e-02}$
DTLZ5	$9.46e-02_{9.4e-05}$	$9.46e-02_{9.3e-05}$	$9.53e-02_{1.0e-05}$	$9.51e-02_{2.3e-05}$	$9.52e-02_{1.5e-05}$	$9.50e-02_{4.8e-05}$	$9.42e-02_{7.0e-05}$
DTLZ6	$0.00e+00_{0.0e+00}$	$0.00e+00_{0.0e+00}$	$9.61e-02_{8.8e-06}$	$9.61e-02_{1.3e-05}$	$1.87e-03_{5.5e-03}$	$0.00e+00_{0.0e+00}$	$9.61e-02_{1.5e-05}$
DTLZ7	$2.92e-01_{2.7e-03}$	$2.94e-01_{4.5e-03}$	$3.10e-01_{1.4e-03}$	$2.98e-01_{2.8e-03}$	$2.62e-01_{3.3e-02}$	$2.83e-01_{9.5e-03}$	$1.85e-01_{4.3e-02}$
WFG1	$6.94e-01_{6.5e-02}$	$5.97e-01_{4.1e-02}$	$7.70e-01_{4.1e-02}$	$1.17e-01_{1.3e-02}$	$8.31e-01_{1.0e-01}$	$7.55e-01_{5.8e-02}$	$2.57e-01_{1.0e-02}$
WFG2	$9.13e-01_{1.7e-03}$	$9.20e-01_{9.7e-04}$	$9.17e-01_{1.5e-03}$	$9.05e-01_{2.1e-03}$	$9.12e-01_{2.4e-03}$	$9.13e-01_{1.8e-03}$	$9.03e-01_{3.2e-03}$
WFG3	$3.20e-01_{1.4e-03}$	$3.01e-01_{3.1e-03}$	$3.23e-01_{1.0e-03}$	$3.10e-01_{2.2e-03}$	$3.23e-01_{1.7e-03}$	$3.21e-01_{1.4e-03}$	$3.20e-01_{7.7e-04}$
WFG4	$3.95e-01_{4.0e-03}$	$4.15e-01_{1.8e-03}$	$4.16e-01_{2.7e-03}$	$3.58e-01_{3.3e-03}$	$4.14e-01_{3.0e-03}$	$4.01e-01_{3.1e-03}$	$3.85e-01_{3.2e-03}$
WFG5	$3.66e-01_{3.6e-03}$	$3.85e-01_{4.0e-03}$	$3.78e-01_{2.3e-03}$	$3.68e-01_{3.3e-03}$	$3.76e-01_{3.2e-03}$	$3.74e-01_{2.9e-03}$	$3.77e-01_{1.9e-03}$
WFG6	$3.92e-01_{8.5e-03}$	$4.11e-01_{7.8e-03}$	$4.22e-01_{2.4e-03}$	$3.84e-01_{4.0e-03}$	$3.62e-01_{3.3e-02}$	$3.90e-01_{2.1e-02}$	$4.12e-01_{2.3e-03}$
WFG7	$3.89e-01_{3.9e-03}$	$4.09e-01_{1.8e-03}$	$4.06e-01_{2.6e-03}$	$3.75e-01_{4.7e-03}$	$4.04e-01_{3.0e-03}$	$3.98e-01_{3.4e-03}$	$4.04e-01_{2.6e-03}$
WFG8	$2.71e-01_{2.0e-02}$	$3.05e-01_{2.3e-02}$	$2.82e-01_{1.5e-02}$	$2.64e-01_{4.7e-03}$	$2.82e-01_{2.4e-02}$	$2.73e-01_{1.5e-02}$	$3.12e-01_{3.9e-02}$
WFG9	$3.86e-01_{3.3e-03}$	$4.02e-01_{2.2e-03}$	$3.91e-01_{2.9e-03}$	$3.84e-01_{3.3e-03}$	$3.85e-01_{6.3e-03}$	$3.86e-01_{4.8e-03}$	$3.98e-01_{2.4e-03}$
Viennet2	$9.25e-01_{6.8e-04}$	$9.28e-01_{1.8e-04}$	$9.26e-01_{3.3e-04}$	$9.26e-01_{4.0e-04}$	$9.26e-01_{4.7e-04}$	$9.26e-01_{4.1e-04}$	$9.28e-01_{3.5e-04}$
Viennet3	$8.37e-01_{2.5e-04}$	$8.33e-01_{4.8e-04}$	$8.38e-01_{1.6e-04}$	$8.38e-01_{2.1e-04}$	$8.38e-01_{2.6e-04}$	$8.38e-01_{2.0e-04}$	$8.39e-01_{2.0e-04}$
Viennet4	$8.63e-01_{1.2e-03}$	$8.69e-01_{4.7e-04}$	$8.65e-01_{8.8e-04}$	$8.81e-01_{4.1e-03}$	$8.62e-01_{1.4e-03}$	$8.63e-01_{1.0e-03}$	$8.74e-01_{4.0e-03}$

Table 46: Hypervolume Ratio Mean and Standard Deviation for LZ\_09 Problems

	NSGAI1	SPEA2	GDE3	SMPSO	AbYSS	MOCcell	MOEAD
LZ09F1	$8.82e-01_{1.4e-02}$	$8.53e-01_{1.8e-02}$	$8.73e-01_{8.3e-03}$	$8.39e-01_{6.0e-02}$	$8.25e-01_{2.3e-02}$	$8.57e-01_{2.1e-02}$	$8.73e-01_{2.8e-02}$
LZ09F2	$7.51e-01_{6.3e-02}$	$7.51e-01_{6.1e-02}$	$7.67e-01_{3.0e-02}$	$4.33e-01_{7.0e-02}$	$6.80e-01_{6.2e-02}$	$5.94e-01_{1.3e-01}$	$5.94e-01_{7.5e-02}$
LZ09F3	$8.18e-01_{3.0e-02}$	$8.04e-01_{3.7e-02}$	$8.01e-01_{1.8e-02}$	$4.18e-01_{2.1e-01}$	$7.75e-01_{5.7e-02}$	$7.39e-01_{1.5e-01}$	$5.53e-01_{7.7e-02}$
LZ09F4	$8.49e-01_{2.9e-02}$	$8.28e-01_{4.6e-02}$	$8.28e-01_{1.6e-02}$	$4.44e-01_{1.4e-01}$	$8.00e-01_{9.2e-02}$	$7.54e-01_{1.4e-01}$	$5.64e-01_{5.3e-02}$
LZ09F5	$8.61e-01_{1.9e-02}$	$8.43e-01_{3.4e-02}$	$8.40e-01_{1.3e-02}$	$4.95e-01_{2.0e-01}$	$8.17e-01_{6.6e-02}$	$7.96e-01_{1.5e-01}$	$5.43e-01_{7.3e-02}$
LZ09F6	$3.89e-01_{9.5e-02}$	$5.37e-01_{7.8e-02}$	$6.22e-01_{5.1e-02}$	$1.54e-02_{4.0e-02}$	$2.61e-01_{1.1e-01}$	$2.57e-01_{1.5e-01}$	$7.43e-01_{3.4e-02}$
LZ09F7	$5.51e-01_{1.0e-01}$	$5.71e-01_{7.6e-02}$	$3.67e-01_{8.8e-02}$	$4.79e-02_{4.6e-02}$	$4.85e-01_{1.2e-01}$	$5.22e-01_{1.0e-01}$	$1.71e-01_{1.5e-01}$
LZ09F8	$4.37e-01_{1.0e-01}$	$4.43e-01_{9.4e-02}$	$2.79e-01_{6.5e-02}$	$2.04e-02_{4.6e-02}$	$4.56e-01_{9.6e-02}$	$4.77e-01_{1.1e-01}$	$1.18e-01_{9.2e-02}$
LZ09F9	$4.93e-01_{1.1e-01}$	$5.00e-01_{1.1e-01}$	$5.88e-01_{2.9e-02}$	$1.81e-01_{7.7e-02}$	$4.67e-01_{9.3e-02}$	$4.39e-01_{1.4e-01}$	$4.32e-01_{9.0e-02}$

Table 47: Hypervolume Mean and Standard Deviation for LZ\_09 Problems

	NSGAI1	SPEA2	GDE3	SMPSO	AbYSS	MOCcell	MOEAD
LZ09F1	$5.87e-01_{9.1e-03}$	$5.68e-01_{1.2e-02}$	$5.81e-01_{5.5e-03}$	$5.58e-01_{4.0e-02}$	$5.49e-01_{1.5e-02}$	$5.70e-01_{1.4e-02}$	$5.81e-01_{1.9e-02}$
LZ09F2	$5.00e-01_{4.2e-02}$	$5.00e-01_{4.1e-02}$	$5.10e-01_{2.0e-02}$	$2.88e-01_{4.7e-02}$	$4.52e-01_{4.1e-02}$	$3.95e-01_{8.9e-02}$	$3.96e-01_{5.0e-02}$
LZ09F3	$5.45e-01_{2.0e-02}$	$5.35e-01_{2.5e-02}$	$5.33e-01_{1.2e-02}$	$2.78e-01_{1.4e-01}$	$5.16e-01_{3.8e-02}$	$4.92e-01_{1.0e-01}$	$3.68e-01_{5.1e-02}$
LZ09F4	$5.65e-01_{1.9e-02}$	$5.51e-01_{3.1e-02}$	$5.51e-01_{1.1e-02}$	$2.96e-01_{9.4e-02}$	$5.33e-01_{6.1e-02}$	$5.02e-01_{9.1e-02}$	$3.75e-01_{3.5e-02}$
LZ09F5	$5.73e-01_{1.2e-02}$	$5.61e-01_{2.3e-02}$	$5.59e-01_{8.6e-03}$	$3.30e-01_{1.3e-01}$	$5.44e-01_{4.4e-02}$	$5.30e-01_{1.0e-01}$	$3.62e-01_{4.9e-02}$
LZ09F6	$1.78e-01_{4.4e-02}$	$2.46e-01_{3.6e-02}$	$2.85e-01_{2.3e-02}$	$7.05e-03_{1.8e-02}$	$1.20e-01_{4.9e-02}$	$1.18e-01_{6.7e-02}$	$3.41e-01_{1.6e-02}$
LZ09F7	$3.67e-01_{6.9e-02}$	$3.80e-01_{5.1e-02}$	$2.44e-01_{5.8e-02}$	$3.19e-02_{3.1e-02}$	$3.23e-01_{7.7e-02}$	$3.48e-01_{6.9e-02}$	$1.14e-01_{1.0e-01}$
LZ09F8	$2.91e-01_{6.8e-02}$	$2.95e-01_{6.2e-02}$	$1.86e-01_{4.3e-02}$	$1.36e-02_{3.1e-02}$	$3.03e-01_{6.4e-02}$	$3.17e-01_{7.4e-02}$	$7.88e-02_{6.1e-02}$
LZ09F9	$1.64e-01_{3.6e-02}$	$1.66e-01_{3.6e-02}$	$1.95e-01_{9.6e-03}$	$6.01e-02_{2.6e-02}$	$1.55e-01_{3.1e-02}$	$1.46e-01_{4.8e-02}$	$1.43e-01_{3.0e-02}$

**Appendix B: Meteorological Data for Toronto Area Used in the  
Photovoltaic Energy System Design Case Study**

Table 48: Monthly average hourly direct normal beam irradiance: Latitude 43.45° / Longitude -79.25° (kWh/m<sup>2</sup>)

Time	Jan	Feb	Mar	Apr	May	Jun	Jul	Aug	Sep	Oct	Nov	Dec
0:00	0.0000	0.0000	0.0000	0.0000	0.0000	0.0000	0.0000	0.0000	0.0000	0.0000	0.0000	0.0000
1:00	0.0000	0.0000	0.0000	0.0000	0.0000	0.0000	0.0000	0.0000	0.0000	0.0000	0.0000	0.0000
2:00	0.0000	0.0000	0.0000	0.0000	0.0000	0.0000	0.0000	0.0000	0.0000	0.0000	0.0000	0.0000
3:00	0.0000	0.0000	0.0000	0.0000	0.0000	0.0000	0.0000	0.0000	0.0000	0.0000	0.0000	0.0000
4:00	0.0000	0.0000	0.0000	0.0000	0.0000	0.0000	0.0000	0.0000	0.0000	0.0000	0.0000	0.0000
5:00	0.0000	0.0000	0.0000	0.0047	0.1467	0.1583	0.1481	0.0153	0.0000	0.0000	0.0000	0.0000
6:00	0.0000	0.0000	0.0157	0.1577	0.3369	0.2626	0.3119	0.2088	0.1339	0.0018	0.0000	0.0000
7:00	0.0000	0.0234	0.2203	0.2634	0.4185	0.3398	0.3781	0.3113	0.3508	0.1634	0.0173	0.0000
8:00	0.0939	0.1708	0.3429	0.3327	0.4887	0.3896	0.4438	0.3813	0.4098	0.2218	0.0572	0.0659
9:00	0.1796	0.2569	0.3795	0.3745	0.4609	0.4468	0.4807	0.4104	0.4506	0.2570	0.1045	0.1436
10:00	0.2627	0.3035	0.3546	0.4053	0.4430	0.4467	0.5061	0.4117	0.4401	0.3320	0.1753	0.2243
11:00	0.3075	0.3277	0.3287	0.4304	0.4369	0.4531	0.5313	0.3910	0.4126	0.3312	0.1804	0.2444
12:00	0.3193	0.3500	0.3615	0.4094	0.4189	0.4398	0.5115	0.4044	0.4388	0.3034	0.2146	0.2718
13:00	0.3112	0.3291	0.3097	0.3829	0.3665	0.4108	0.4417	0.3821	0.4557	0.2903	0.2041	0.2671
14:00	0.2777	0.3139	0.2867	0.3373	0.3548	0.3649	0.3760	0.3616	0.4058	0.3043	0.1816	0.1803
15:00	0.2312	0.3128	0.2617	0.3486	0.3073	0.3333	0.3492	0.3488	0.3314	0.2685	0.0903	0.1191
16:00	0.1149	0.2586	0.2118	0.3050	0.2622	0.3139	0.3437	0.3249	0.2570	0.1759	0.0244	0.0029
17:00	0.0000	0.0565	0.1342	0.2282	0.1894	0.2753	0.2803	0.2428	0.1505	0.0139	0.0000	0.0000
18:00	0.0000	0.0000	0.0000	0.0610	0.0922	0.1934	0.2078	0.1399	0.0143	0.0000	0.0000	0.0000
19:00	0.0000	0.0000	0.0000	0.0000	0.0055	0.0903	0.0740	0.0016	0.0000	0.0000	0.0000	0.0000
20:00	0.0000	0.0000	0.0000	0.0000	0.0000	0.0000	0.0000	0.0000	0.0000	0.0000	0.0000	0.0000
21:00	0.0000	0.0000	0.0000	0.0000	0.0000	0.0000	0.0000	0.0000	0.0000	0.0000	0.0000	0.0000
22:00	0.0000	0.0000	0.0000	0.0000	0.0000	0.0000	0.0000	0.0000	0.0000	0.0000	0.0000	0.0000
23:00	0.0000	0.0000	0.0000	0.0000	0.0000	0.0000	0.0000	0.0000	0.0000	0.0000	0.0000	0.0000

Table 49: Monthly average hourly horizontal diffuse irradiance: Latitude 43.45° / Longitude -79.25° (kWh/m<sup>2</sup>)

Time	Jan	Feb	Mar	Apr	May	Jun	Jul	Aug	Sep	Oct	Nov	Dec
0:00	0.0000	0.0000	0.0000	0.0000	0.0000	0.0000	0.0000	0.0000	0.0000	0.0000	0.0000	0.0000
1:00	0.0000	0.0000	0.0000	0.0000	0.0000	0.0000	0.0000	0.0000	0.0000	0.0000	0.0000	0.0000
2:00	0.0000	0.0000	0.0000	0.0000	0.0000	0.0000	0.0000	0.0000	0.0000	0.0000	0.0000	0.0000
3:00	0.0000	0.0000	0.0000	0.0000	0.0000	0.0000	0.0000	0.0000	0.0000	0.0000	0.0000	0.0000
4:00	0.0000	0.0000	0.0000	0.0001	0.0012	0.0079	0.0048	0.0005	0.0000	0.0000	0.0000	0.0000
5:00	0.0000	0.0000	0.0004	0.0086	0.0281	0.0389	0.0322	0.0190	0.0029	0.0000	0.0000	0.0000
6:00	0.0000	0.0017	0.0156	0.0411	0.0701	0.0816	0.0647	0.0591	0.0368	0.0088	0.0003	0.0000
7:00	0.0049	0.0199	0.0483	0.0957	0.1220	0.1354	0.1033	0.1118	0.0786	0.0444	0.0156	0.0013
8:00	0.0280	0.0556	0.0967	0.1378	0.1657	0.1902	0.1443	0.1609	0.1160	0.0921	0.0526	0.0197
9:00	0.0686	0.0960	0.1439	0.1843	0.2215	0.2298	0.1782	0.2155	0.1595	0.1415	0.0986	0.0610
10:00	0.1056	0.1267	0.1752	0.2339	0.2605	0.2803	0.2083	0.2637	0.1977	0.1802	0.1278	0.0943
11:00	0.1282	0.1522	0.2018	0.2314	0.2779	0.3088	0.2373	0.2937	0.2267	0.1920	0.1351	0.1016
12:00	0.1331	0.1699	0.1868	0.2255	0.2909	0.3202	0.2673	0.2943	0.2199	0.2039	0.1316	0.0993
13:00	0.1223	0.1817	0.1875	0.2105	0.2927	0.3171	0.2858	0.2796	0.2015	0.1868	0.1128	0.0892
14:00	0.0936	0.1507	0.1721	0.1915	0.2654	0.2889	0.2783	0.2463	0.1907	0.1427	0.0813	0.0755
15:00	0.0608	0.1040	0.1390	0.1498	0.2040	0.2339	0.2409	0.1998	0.1535	0.1018	0.0460	0.0415
16:00	0.0320	0.0596	0.0930	0.1078	0.1601	0.1715	0.1764	0.1511	0.1008	0.0532	0.0156	0.0073
17:00	0.0063	0.0293	0.0393	0.0597	0.1022	0.1190	0.1194	0.0992	0.0493	0.0103	0.0012	0.0006
18:00	0.0000	0.0032	0.0068	0.0190	0.0475	0.0660	0.0682	0.0461	0.0098	0.0007	0.0000	0.0000
19:00	0.0000	0.0000	0.0002	0.0029	0.0030	0.0245	0.0279	0.0123	0.0009	0.0000	0.0000	0.0000
20:00	0.0000	0.0000	0.0000	0.0000	0.0001	0.0036	0.0038	0.0003	0.0000	0.0000	0.0000	0.0000
21:00	0.0000	0.0000	0.0000	0.0000	0.0000	0.0000	0.0000	0.0000	0.0000	0.0000	0.0000	0.0000
22:00	0.0000	0.0000	0.0000	0.0000	0.0000	0.0000	0.0000	0.0000	0.0000	0.0000	0.0000	0.0000
23:00	0.0000	0.0000	0.0000	0.0000	0.0000	0.0000	0.0000	0.0000	0.0000	0.0000	0.0000	0.0000

Table 50: Monthly averaged hourly solar azimuth angles due south (degrees 43.45° / Longitude -79.25°)

Time	Jan	Feb	Mar	Apr	May	Jun	Jul	Aug	Sep	Oct	Nov	Dec
0:00	n/a	n/a	n/a	n/a	n/a	n/a	n/a	n/a	n/a	n/a	n/a	n/a
1:00	n/a	n/a	n/a	n/a	n/a	n/a	n/a	n/a	n/a	n/a	n/a	n/a
2:00	n/a	n/a	n/a	n/a	n/a	n/a	n/a	n/a	n/a	n/a	n/a	n/a
3:00	n/a	n/a	n/a	n/a	n/a	n/a	n/a	n/a	n/a	n/a	n/a	n/a
4:00	n/a	n/a	n/a	n/a	n/a	n/a	n/a	n/a	n/a	n/a	n/a	n/a
5:00	n/a	n/a	n/a	n/a	-116.0	-119.5	-119.4	n/a	n/a	n/a	n/a	n/a
6:00	n/a	n/a	n/a	-100.0	-106.1	-109.8	-109.5	-103.8	n/a	n/a	n/a	n/a
7:00	n/a	n/a	-82.8	-89.8	-96.3	-100.4	-99.9	-93.8	-84.1	-75.0	n/a	n/a
8:00	-60.0	-66.0	-72.0	-80.0	-86.1	-90.6	-90.1	-83.3	-74.0	-64.0	-57.0	-55.0
9:00	-49.0	-55.0	-60.0	-67.0	-75.0	-80.0	-79.0	-72.0	-61.0	-51.0	-45.0	-44.0
10:00	-36.0	-42.0	-46.0	-52.0	-60.0	-66.0	-65.0	-57.0	-46.0	-37.0	-32.0	-32.0
11:00	-23.0	-27.0	-29.0	-33.0	-38.0	-44.0	-45.0	-37.0	-27.0	-20.0	-17.0	-18.0
12:00	-7.0	-10.0	-10.0	-8.0	-8.0	-11.0	-15.0	-11.0	-5.0	-1.0	-1.0	-3.0
13:00	8.0	8.0	11.0	18.0	25.0	27.0	21.0	18.0	18.0	17.0	15.0	12.0
14:00	23.0	25.0	31.0	41.0	50.0	54.0	49.0	43.0	38.0	34.0	30.0	26.0
15:00	37.0	40.0	48.0	58.0	68.0	72.0	68.0	61.0	54.0	49.0	43.0	39.0
15:00	49.0	53.0	61.0	72.0	81.0	84.0	81.0	74.0	68.0	61.0	55.0	51.0
17:00	60.0	65.0	73.0	83.0	91.0	95.0	92.0	86.0	79.0	72.0	n/a	n/a
18:00	n/a	n/a	84.0	94.0	101.0	104.0	102.0	96.0	90.0	n/a	n/a	n/a
19:00	n/a	n/a	n/a	n/a	111.0	114.0	111.0	106.0	n/a	n/a	n/a	n/a
20:00	n/a	n/a	n/a	n/a	n/a	n/a	n/a	n/a	n/a	n/a	n/a	n/a
21:00	n/a	n/a	n/a	n/a	n/a	n/a	n/a	n/a	n/a	n/a	n/a	n/a
22:00	n/a	n/a	n/a	n/a	n/a	n/a	n/a	n/a	n/a	n/a	n/a	n/a
23:00	n/a	n/a	n/a	n/a	n/a	n/a	n/a	n/a	n/a	n/a	n/a	n/a

Table 51: Monthly averaged hourly solar Angles relative to the horizon (degrees): 43.45° / Longitude -79.25°

	Jan	Feb	Mar	Apr	May	Jun	Jul	Aug	Sep	Oct	Nov	Dec
0:00	n/a	n/a	n/a	n/a	n/a	n/a	n/a	n/a	n/a	n/a	n/a	n/a
1:00	n/a	n/a	n/a	n/a	n/a	n/a	n/a	n/a	n/a	n/a	n/a	n/a
2:00	n/a	n/a	n/a	n/a	n/a	n/a	n/a	n/a	n/a	n/a	n/a	n/a
3:00	n/a	n/a	n/a	n/a	n/a	n/a	n/a	n/a	n/a	n/a	n/a	n/a
4:00	n/a	n/a	n/a	n/a	n/a	n/a	n/a	n/a	n/a	n/a	n/a	n/a
5:00	n/a	n/a	n/a	n/a	0.3	2.9	0.6	n/a	n/a	n/a	n/a	n/a
6:00	n/a	n/a	n/a	3.5	10.4	12.7	10.4	5.7	n/a	n/a	n/a	n/a
7:00	n/a	n/a	4.9	14.3	21.1	23.2	20.9	16.4	10.8	4.4	n/a	n/a
8:00	1.4	6.9	15.5	25.1	32.0	34.1	31.8	27.2	21.4	14.5	7.3	2.4
9:00	10.1	16.3	25.4	35.6	42.7	44.9	42.6	37.8	31.4	23.6	15.7	10.6
10:00	17.4	24.3	34.1	44.9	52.7	55.3	52.9	47.6	40.1	31.1	22.3	17.2
11:00	22.7	30.3	40.8	52.2	60.9	64.2	61.8	55.6	46.5	36.1	26.7	21.7
12:00	25.4	33.7	44.3	56.0	65.2	69.3	67.2	59.9	49.5	38.0	28.3	23.6
13:00	25.3	33.7	44.1	55.0	63.4	67.7	66.4	59.1	48.2	36.4	26.9	22.6
14:00	22.3	30.6	40.0	49.5	56.7	60.5	60.0	53.5	43.0	31.6	22.6	18.9
15:00	16.8	24.6	33.1	41.2	47.3	50.7	50.6	44.9	35.1	24.3	16.0	12.9
16:00	9.4	16.7	24.2	31.3	36.8	40.1	40.1	34.8	25.5	15.3	7.7	5.2
17:00	0.5	7.3	14.1	20.6	26.0	29.2	29.2	24.0	15.1	5.3	n/a	n/a
18:00	n/a	n/a	3.5	9.8	15.2	18.5	18.4	13.2	4.3	n/a	n/a	n/a
19:00	n/a	n/a	n/a	n/a	4.8	8.3	8.0	2.5	n/a	n/a	n/a	n/a
20:00	n/a	n/a	n/a	n/a	n/a	n/a	n/a	n/a	n/a	n/a	n/a	n/a
21:00	n/a	n/a	n/a	n/a	n/a	n/a	n/a	n/a	n/a	n/a	n/a	n/a
22:00	n/a	n/a	n/a	n/a	n/a	n/a	n/a	n/a	n/a	n/a	n/a	n/a
23:00	n/a	n/a	n/a	n/a	n/a	n/a	n/a	n/a	n/a	n/a	n/a	n/a

Table 52: The solutions having achieved the lowest (best) IGD found by LSMPSO.

$K$	$H$ (m)	$\beta$ ( $^{\circ}$ )	$D$ (m)	$\gamma$ ( $^{\circ}$ )	$E$ (m)	Absorbed light $Q$ (MWh)	Installation cost $C$ (\$)
1	0.20	27.99	0.80	-5.60	1.60	2096.65	924.88
2	0.20	1.00	2.50	-6.15	2.00	3815.93	1849.76
1	0.51	22.58	0.80	-3.49	0.57	5368.79	2378.47
1	0.71	26.85	2.44	-1.26	1.38	7403.44	3273.18
1	0.83	25.07	2.31	-1.44	1.49	8662.61	3832.38
1	0.97	24.63	1.21	-8.39	1.25	10168.81	4497.36
1	1.11	29.51	0.87	-19.49	0.96	11559.18	5143.03
2	0.63	29.20	1.03	-3.52	1.25	13000.40	5787.78
1	1.41	22.36	1.04	6.58	0.77	14478.91	6505.77
2	0.77	29.80	1.76	-4.59	1.19	16059.47	7133.96
1	1.77	22.80	0.87	10.64	0.50	17944.05	8182.17
2	0.97	24.39	1.34	-9.87	0.80	19967.88	8957.01
3	0.70	17.92	0.80	-4.53	0.67	21707.83	9759.59
3	0.76	36.96	1.42	-4.54	1.07	23234.71	10504.09
2	1.22	24.60	1.24	-6.74	1.00	25237.36	11256.60
2	1.31	19.29	1.77	9.60	1.08	26489.56	12079.14
4	0.69	32.52	1.49	-19.89	0.94	28562.13	12840.05
5	0.58	24.66	0.87	-17.96	1.10	30097.73	13475.27
3	1.03	32.47	1.50	-23.35	1.17	31350.21	14276.49
3	1.07	34.00	2.13	-17.02	1.54	32995.91	14795.13
5	0.67	31.89	1.63	-22.76	0.92	34149.94	15486.95
4	0.88	18.04	0.80	-5.38	0.61	36217.93	16315.34
4	0.92	27.72	1.31	-0.04	0.93	37571.92	16983.11
3	1.27	29.20	1.47	-4.26	0.80	39268.07	17596.30
2	2.00	23.71	1.12	-19.58	0.53	40828.55	18497.64
3	1.38	20.22	0.86	-9.34	0.55	42175.48	19179.96
4	1.08	31.12	1.63	-11.39	1.31	44522.33	19985.25
5	0.89	20.71	0.92	-2.84	0.91	46051.59	20687.16
5	0.92	22.51	1.14	-1.72	0.81	47654.75	21356.02
4	1.20	27.09	1.00	-6.73	0.57	49234.81	22173.53
4	1.24	20.80	1.34	-17.61	0.73	51052.72	22972.20
5	1.02	24.31	0.92	-8.65	0.81	52460.23	23591.23
5	1.05	21.05	0.89	-14.85	0.51	53707.01	24185.71
5	1.07	27.01	1.65	-0.58	1.25	55132.25	24780.00
5	1.10	23.82	1.65	-8.95	0.52	56921.83	25434.26
4	1.42	26.02	1.40	-4.64	0.74	58442.40	26215.61
6	0.97	31.07	1.09	-7.65	0.83	59494.66	26880.17
4	1.49	21.28	1.37	-8.89	0.88	61262.14	27528.40
5	1.22	17.51	1.50	-14.57	0.61	62371.42	28130.27
5	1.24	28.28	1.31	-17.95	0.95	63808.04	28724.45
4	1.59	22.12	1.21	-7.22	0.80	65168.39	29360.00
6	1.10	18.03	0.93	-14.73	0.77	67507.80	30521.11
5	1.36	25.49	1.24	2.02	0.60	69505.86	31533.07
5	1.40	22.03	0.93	-8.57	0.54	71722.93	32406.32
5	1.44	25.78	1.36	-4.70	0.93	73892.39	33197.91
5	1.47	25.64	1.21	-3.86	0.62	75392.47	33896.72
5	1.51	26.54	1.23	-2.88	0.89	77391.28	34915.10
6	1.29	25.17	0.88	-11.47	0.62	78733.19	35695.55
5	1.58	21.98	1.30	-6.03	0.87	80828.29	36487.44

6	1.35	25.49	0.90	-12.19	0.61	82541.77	37428.63
5	1.66	25.58	1.14	-11.16	0.59	84629.14	38330.87
5	1.70	23.07	1.20	-11.21	0.63	86696.78	39194.14
5	1.72	20.89	1.23	-6.84	0.62	88363.43	39844.72
8	1.10	30.92	1.16	-9.02	0.61	89270.11	40694.82
5	1.79	23.16	1.17	-9.86	0.56	90940.58	41403.50
6	1.51	20.12	1.35	-8.25	0.92	93125.54	41961.29
5	1.85	28.77	1.65	-6.05	0.58	94581.89	42814.91
5	1.88	23.46	1.32	-11.17	0.68	96303.39	43545.52
6	1.60	22.09	1.21	-3.14	0.82	98326.04	44332.76
6	1.63	20.88	1.00	-6.60	0.67	99924.07	45201.85
6	1.66	23.06	1.18	-15.50	0.69	101930.40	46008.35
6	1.69	23.23	1.00	-11.21	0.57	103305.00	46900.85
7	1.48	22.79	1.14	-13.42	0.59	105843.80	47796.70
6	1.75	23.81	1.76	-3.99	0.60	108220.70	48480.48
7	1.54	20.41	1.39	-8.45	0.96	110941.40	49985.71
6	1.82	21.69	1.12	-5.74	0.64	111576.80	50439.03
7	1.58	20.16	1.40	-8.65	0.94	113826.90	51300.28
6	1.89	23.18	1.33	-8.42	0.54	115856.10	52331.06
6	1.93	19.64	1.20	-10.92	0.50	117915.60	53462.56
6	1.96	21.25	1.23	-11.08	0.50	120230.40	54516.23
6	1.99	20.31	1.49	-8.39	0.50	122571.00	55335.11
7	1.76	24.07	1.12	8.20	0.83	123131.30	56840.10
7	1.76	18.83	0.98	-7.23	0.55	125596.40	57057.91
7	1.78	27.37	0.99	-7.35	0.97	126387.90	57729.43
7	1.80	25.60	0.98	-8.94	0.94	128236.60	58402.99
7	1.82	21.16	1.53	-12.29	0.58	130430.30	58863.70
7	1.85	21.28	1.26	-6.75	0.57	132295.00	59757.17
7	1.90	14.80	1.09	-19.38	0.53	133104.80	61474.28
7	1.91	19.00	1.03	-0.86	0.72	136048.00	61801.25
7	1.93	23.12	1.34	-7.54	0.53	138072.90	62436.63
7	1.98	20.66	1.30	-3.00	0.50	141755.60	64098.10
7	2.00	26.72	1.49	-2.38	0.50	142966.00	64741.76
8	1.80	23.13	1.10	5.67	0.90	145174.00	66656.12
8	1.82	23.08	1.08	6.46	0.90	146283.30	67273.02
8	1.85	17.38	1.16	-22.21	0.52	147766.30	68553.70
8	1.89	16.48	0.80	-7.83	0.50	152689.00	69798.92
8	1.91	15.94	0.80	-8.55	0.50	154142.10	70497.19
8	1.95	16.67	1.13	-23.16	0.50	154830.70	71970.45
8	1.95	17.53	0.86	-12.53	0.57	157725.40	72097.10
8	1.97	21.67	1.23	-6.65	0.50	160795.80	72768.46
9	1.77	19.07	0.89	-3.23	0.54	161563.20	73467.99
8	2.00	21.64	1.31	-0.83	0.50	163402.80	73990.58
9	1.87	10.98	0.80	-2.87	0.50	169285.30	78024.63
9	1.90	10.41	1.28	-11.96	1.10	171353.60	79236.14
9	1.94	14.19	0.80	-8.51	0.50	175850.30	80655.51
9	2.00	34.92	1.14	0.00	0.50	176145.40	83191.66
9	2.00	21.14	1.20	-8.28	0.50	183542.70	83239.40
10	1.91	14.42	1.11	16.13	0.58	184676.00	88116.69

**Appendix C: Electricity Import/Export Capacities in the Province of  
Ontario**



Table 53: Zonal electricity maximum import (MWh)

	2012	2013	2014	2015	2016	2017	2018	2019	2020	2021	2022	2023	2024	2025
Bruce	0	0	0	0	0	0	0	0	0	0	0	0	0	0
West	2000	2000	2000	2000	2000	2000	2000	2000	2000	2000	2000	2000	2000	2000
SW	0	0	0	0	0	0	0	0	0	0	0	0	0	0
Niagara	1300	1300	1300	1300	1300	1300	1300	1300	1300	1300	1300	1300	1300	1300
Toronto	0	0	0	0	0	0	0	0	0	0	0	0	0	0
East	800	800	800	1550	1550	1550	1550	1550	1550	1550	1550	800	800	800
Ottawa	1200	1200	1200	1950	1950	1950	1950	1950	1950	1950	1950	1200	1200	1200
Essa	0	0	0	0	0	0	0	0	0	0	0	0	0	0
NE	70	70	70	570	570	570	570	570	570	570	570	70	70	70
NW	300	300	300	500	500	500	500	500	500	500	500	300	300	300

Table 54: Zonal electricity maximum export (MWh)

	2012	2013	2014	2015	2016	2017	2018	2019	2020	2021	2022	2023	2024	2025
Bruce	0	0	0	0	0	0	0	0	0	0	0	0	0	0
West	9999	9999	9999	9999	9999	9999	9999	9999	9999	9999	9999	9999	9999	9999
SW	0	0	0	0	0	0	0	0	0	0	0	0	0	0
Niagara	9999	9999	9999	9999	9999	9999	9999	9999	9999	9999	9999	9999	9999	9999
Toronto	0	0	0	0	0	0	0	0	0	0	0	0	0	0
East	9999	9999	9999	9999	9999	9999	9999	9999	9999	9999	9999	9999	9999	9999
Ottawa	9999	9999	9999	9999	9999	9999	9999	9999	9999	9999	9999	9999	9999	9999
Essa	0	0	0	0	0	0	0	0	0	0	0	0	0	0
NE	9999	9999	9999	9999	9999	9999	9999	9999	9999	9999	9999	9999	9999	9999
NW	9999	9999	9999	9999	9999	9999	9999	9999	9999	9999	9999	9999	9999	9999

## Bibliography

1. Deb K. *Current trends in evolutionary multi-objective optimization*. Int. J. Simul. Multidisci. Des. Optim., Vol. 1, No. 1, pp. 1–8, 2007.
2. Deb K. *Multi-objective Optimization Using Evolutionary Algorithms*. Wiley: New York, 2001, ISBN: 978-0471873396.
3. Nebro A. J., Durillo J. J., Coello Coello C. A., Luna F., and Alba E. *A Study of Convergence Speed in Multi-Objective Metaheuristics*. Parallel Problem Solving from Nature(PPSN X), Springer, Lecture Notes in Computer Science, Vol. 5199, Dortmund, Germany, pp. 763-772, 2008.
4. Durillo J.J., Nebro A.J., Luna F., Coello Coello C.A., and Alba E. *Convergence Speed in Multi-Objective Metaheuristics: Efficiency Criteria and Empirical Study*. International Journal for Numerical Methods in Engineering, Vol. 83, No. 3, pp. 1344–1375, 2010.
5. Talbi E. *Metaheuristics from Design to Implementation*. John Wiley & Sons Publication Inc., pp. 308-320, 2009.
6. Zhang Q. and Li H. *MOEA/D: A Multiobjective Evolutionary Algorithm Based on Decomposition*. IEEE Transactions on Evolutionary Computation, Vol. 11, No. 6, pp. 712-731, 2007.
7. Li Q. and Zhang H. *Multiobjective Optimization Problems with Complicated Pareto Sets, MOEA/D and NSGA-II*. IEEE Trans on Evolutionary Computation, Vol. 2, No. 12, pp. 284-302, 2009.

8. Nebro A.J., Durillo J.J., Coello Coello C.A. *Analysis of leader selection strategies in a multi-objective Particle Swarm Optimizer*. IEEE Congress on Evolutionary Computation 2013, Cancun, Mexico, pp. 3153-3160, 2013.
9. Durillo J.J., Nebro A.J., Coello Coello C.A., Garcia-Nieto J., Luna F., and Alba E. *A Study of Multiobjective Metaheuristics When Solving Parameter Scalable Problems*. IEEE Transactions On Evolutionary Computation, Vol. 14, No. 4, pp. 618-636, 2010.
10. Coello Coello C. A. *Evolutionary Multi-Objective Optimization: Current and Future Research Trends*. Plenary Talk in the 9th International Conference on Intelligent Systems Design and Applications (ISDA09), Pisa, Italy, 2009.
11. Deb K. *Optimization for Engineering Design: Algorithms and Examples*. Prentice-Hall of India Pvt. Ltd, 2002.
12. Feoktistov, V., *Differential Evolution*. In Search of Solutions. Springer, USA, 2006.
13. Reyes Sierra M., and Coello Coello C. A. *Improving PSO-Based Multi-objective Optimization Using Crowding, Mutation and Dominance*. In Evolutionary Multi-Criterion Optimization (EMO 2005), LNCS 3410, Guanajuato, Mexico, pp 505-519, 2005.
14. Rahnamayan S., Tizhoosh H.R., Salama M.M.A. *Opposition-Based Differential Evolution*. IEEE Transactions on Evolutionary Computation, Vol. 12, No. 1, pp. 64-79, 2008.
15. Bourennani, F., Rahnamayan, S., and Naterer, G. F. *OGDE3: Opposition-Based Third Generalized Differential Evolution*. Journal of Advanced Computational Intelligence and Intelligent Informatics, Vol. 16, No. 3, pp. 469-480, 2012.

16. Rahnamayan S. *Opposition-Based Differential Evolution*. Ph.D. Thesis, Department of Systems Design Engineering, University of Waterloo, Waterloo, Ontario, Canada, May, 2007.
17. Deb K. *Tutorial on Evolutionary Multi-Criterion Optimization* . IEEE Congress on Evolutionary Computation, Cancun, Mexico, pp 1-23, 2013.
18. Lin H., and Xingshi H. *A novel opposition-based particle swarm optimization for noisy problems*. in Proceedings of the Third International Conference on Natural Computation, ICNC, Vol. 3, pp. 624–629, 2007.
19. Wolpert D. H. and Macready W. G. *No free lunch theorem for search*. Santa Fe Institute, Res. Rep. SFI-TR-95-02-010, 1995.
20. Wolpert D.H., and Macready W.G. *Coevolutionary free lunches*. IEEE Transactions on Evolutionary Computation, Vol. 9, No. 6, pp. 721–735, 2005.
21. Schutze O, Lara A, and Coello A. C. C. *On the Influence of the Number of Objectives on the Hardness of a Multiobjective Optimization Problem*. IEEE Transactions on Evolutionary Computation, Vol. 15, No. 4, pp. 444-455, 2011.
22. Adra S. F. and Fleming P.J. *Diversity Management in Evolutionary Many-Objective Optimization*. IEEE Transactions On Evolutionary Computation, Vol. 15, No. 2, pp. 183-195, 2011.

23. Van Veldhuizen D.A. and Lamont G.B. *On Measuring Multiobjective Evolutionary Algorithm Performance*. In proceedings of the 2000 Congress on Evolutionary Computation, Vol. 1, La Jolla, CA , USA , pp. 204–211, 2000.
24. Collette Y. and Siarry P. *Multiobjective Optimization Principles and Case Studies*. Springer-Verlag Berlin Heidelberg, ISBN: 9783540401827, 2003.
25. Zitzler E. and Thiele L. *Multiobjective evolutionary algorithms: A comparative case study and the strength pareto approach*. IEEE Transactions Evolutionary Computation, Vol. 3, No. 4, pp. 257–271, November, 1999.
26. Tukey J.W. *Exploratory Data Analysis*. Addison-Wesley, 1977.
27. Deb K., Pratap A., Agarwal S., and Meyerivan T. *A fast and elitist multiobjective genetic algorithm: NSGA-II*. IEEE Transactions on Evolutionary Computation, Vol. 6, No. 2, pp. 182–197, 2002.
28. Zitzler E., Laumanns M., and Thiele L. *SPEA2: Improving the Strength Pareto Evolutionary Algorithm*. EUROGEN 2001, Vol. 3242, No. 103, pp. 95–100, 2002.
29. Kukkonen S., and Lampinen J. *GDE3: the third evolution step of generalized differential evolution*. IEEE Congress on Evolutionary Computation (CEC'2005), Edinburgh, U.K., pp. 443–450, 2005.
30. Nebro A. J., Luna F., Alba E., Dorronsoro B., Durillo J. J., and Beham A. *AbYSS: Adapting scatter search to multiobjective optimization*. IEEE Transactions on Evolutionary Computation, Vol. 12, No. 4, pp. 439-457, 2008.

31. Nebro A. J., Durillo J. J., Luna F., Dorronsoro B., and Alba E. *A cellular genetic algorithm for multiobjective optimization*. In *Nature Inspired Cooperative Strategies for Optimization (NICSO 2006)*, Grenada, Spain, pp. 25–36, 2006.
32. Nebro A., Durillo J., García-Nieto J., Coello C. C., Luna F., Alba E. *SMPSO: a new PSO-based metaheuristic for multi-objective optimization*. *Proceedings of the IEEE Symposium Series on Computational Intelligence*, Nashville, TN, U.S.A., pp. 66–73, 2009.
33. Zitzler E., Deb K., Thielier L. *Comparison of multiobjective evolutionary algorithms: Empirical results*. *IEEE Trans. on Evol. Computation*, Vol. 8, pp. 173–195, 2000.
34. Deb K., Thiele L., Laumanns M., and Zitzler E. *Scalable Test Problems for Evolutionary Multiobjective Optimization*. In *Evolutionary Multiobjective Optimization. Theoretical Advances and Applications*, Abraham A, Jain L, Goldberg R (eds), Springer USA, pp. 105–145, 2005.
35. Huband S., Hingston P., Barone L., and While L. *A Review of Multiobjective Test Problems and a Scalable Test Problem Toolkit*. *IEEE Transactions on Evolutionary Computation*, Vol. 10, No. 5, pp. 477–506, 2007.
36. Van Veldhuizen OHD. A. *Multiobjective Evolutionary Algorithms: Classifications, Analyzes, and New Innovations*. Ph.D. Dissertation, Air Force Institute of Technology, Wright-Patterson AFB, Jun. 1999.

37. Karthikeyan K. *A Comparative Study of Multiobjective Shortest Path Problems*. International Journal of Engineering Science and Technology (IJEST), Vol. 3, No. 4, pp. 2875-2879, 2011.
38. Duran F.E.C., Cotta C., Fernández-Leiva A.J. *A Comparative Study of Multi-objective Evolutionary Algorithms to Optimize the Selection of Investment Portfolios with Cardinality Constraints*. Applications of Evolutionary Computation Lecture Notes in Computer Science, Vol. 7248, pp 165-173, 2012.
39. Zhang Q., Zhou A., Zhao S., Suganthan P.N., Liu W. and Tiwari S. *Multiobjective optimization Test Instances for the CEC 2009 Special Session and Competition*. Working Report, CES-887, School of Computer Science and Electrical Engineering, University of Essex, 2008.
40. Deb K., Ruiz F., Luque M., Tewari R., Cabello J.M., Cejudo J.M. *On the sizing of a solar thermal electricity plant for multiple objectives using evolutionary optimization*. Applied Soft Computing, Vol. 12, No. 10, pp. 3300-3311, 2012.
41. Poloni C., Mosetti G., and Contessi S. *Multi objective optimization by GAs: Application to system and component design*. in Proc. Comput. Methods in Applied Sciences'96: Invited Lectures and Special Technological Sessions of the 3rd ECCOMAS Comput. Fluid Dynamics Conf. and the 2nd ECCOMAS Conf. Numerical Methods in Engineering, pp. 258–264, 1996.

42. Kursawe K. *A Variant of Evolution Strategies for Vector Optimization*. Parallel Problem Solving for Nature, volume 496 of Lecture Notes in Computer Science, pages 193-197, Berlin, Germany, Springer-Verlag, 1990.
43. Schaffer D. *Multiple Objective Optimization with Vector Evaluated Genetic Algorithms*. Proc. of the First International Conference on Genetic Algorithms (ICGA), Hillsdale, NJ, pp 93-100, 1987.
44. Fonseca C.M. and Fleming P.J. *Multiobjective Optimization and Multiple Constraint Handling with Evolutionary Algorithms - Part II: Application Example*. IEEE Transactions on Systems, Man and Cybernetics, 28, pp.38-47, 1998.
45. Viennet R., Fonteix C., and Marc I. *Multicriteria optimization using a genetic algorithm for determining a Pareto set*. J. Syst. Sci., Vol. 27, No. 2, pp. 255–260, 1996.
46. Deb K. *Multi-objective genetic algorithms: Problem difficulties and construction of test problems*. Evol. Comput., Vol. 7, No. 3, pp. 205–230, 1999.
47. Durillo J.J., Nebro A.J., and Alba E. *The jMetal Framework for Multi-Objective Optimization: Design and Architecture*. IEEE-CEC 2010, pp. 4138-4325, July, 2010.
48. Lampinen J. *DE's selection rule for multiobjective optimization*. Technical report, Lappeenranta University of Technology, Department of Information Technology, 2001.
49. Sheskin D.J. *Handbook of Parametric and Nonparametric Statistical Procedures*. 4th ed. New York: Chapman & Hall/CRC Press, 2007.



50. Billinton B., and Billinton R. *Evaluation of different operating strategies in small standalone power systems*. IEEE Trans Energy Convers, Vol. 20, No. 3, pp. 654–660, 2005.
51. Muselli M, Notton G, Louche A. *Design of hybrid-photovoltaic power generator, with optimization of energy management*. Solar Energy, Vol. 65, No. 3, pp. 143–157, 1999.
52. Ashraf I, Iqbal A., Md. Amanur Rahman, Chandra A. *Multi-objective optimisation of renewable energy systems for pollution mitigation – a case study of Kavaratti Island, India*. International Journal of Sustainable Energy, Vol. 27, No. 4, pp. 165-171, 2008.
53. Koroneos C., Michailidis M., Moussiopoulos N. *Multi-objective optimization in energy systems: the case study of Lesvos Island, Greece*. Renewable and Sustainable Energy Reviews, Vol. 8, pp. 91–100, 2004.
54. Ghoneim, A.A. *Design optimization of photovoltaic powered water pumping systems*. Energy Conversion and Management, Vol. 47, pp. 1449–1463, 2006.
55. Elhadidy MA, Shaahid SM. *Parametric study of hybrid (wind + solar + diesel) power generating systems*. Renew Energy, Vol. 21, No. 2, pp. 129–139, 2000.
56. Kyung S.P., Soung H.K. *Artificial intelligence approaches to determination of CNC machining parameters in manufacturing: a review*. Artificial Intelligence Eng., Vol. 12 , pp. 121–134, 1998.
57. Bernal-Agustin J. L. and Dufo-Lopez R. *Simulation and optimization of stand-alone hybrid renewable energy systems*. Renewable and Sustainable Energy Reviews, Vol. 13, No. 8, pp. 2111–2118, 2009.

58. Bilgena S., Keles S., Kaygusuzb A., Saric A., Kaygusuz K. *Global warming and renewable energy sources for sustainable development: A case study in Turkey*. Renewable and Sustainable Energy Reviews, Vol. 12, No. 2, pp. 372–396, 2008.
59. Overstraeten RJ V., Mertens RP. *Physics, technology and use of photovoltaics*. Bristol and Boston: Adam Hilger, pp. 187–191, 1986.
60. Borowy BS, Salameh ZM. *Methodology for optimally sizing the combination of a battery bank and PV array in a wind/PV hybrid system*. IEEE Trans Energy Conversion, Vol. 11, No. 2, pp.367–373, 1996.
61. Jones AD, Underwood CP. *A modeling method for building-integrated photovoltaic power supply*. Building Services Engineering Research and Technology, Vol. 23, No. 3, pp. 167–177, 2002.
62. Kerr MJ, Cuevas A. *Generalized analysis of the illumination intensity vs. opencircuit voltage of PV modules*. Solar Energy, Vol. 76, No. 1–3, pp.263–267, 2003.
63. Nishioka K., Hatayama T., Uraoka Y., Fuyuki T., Hagihara R., Watanabe M. *Field-test analysis of PV system output characteristics focusing on module temperature*. Solar Energy Materials and Solar Cells, Vol. 75, No. 3, pp. 665–671, 2003.
64. Stamenic L, Smiley E, and Karim K. *Low light conditions modeling for building integrated photovoltaic (BIPV) systems*. Solar Energy, Vol. 77, No. 1, pp. 37-45, 2004.
65. Zhou W, Yang HX, and Fang ZH. *A novel model for photovoltaic array performance prediction*. Applied Energy, Vol. 84, No. 12, pp. 1187–1198, 2007.

66. Mondol J.D., Yohanis Y.G., Smyth M., Norton B. *Long-term validated simulation of a building integrated photovoltaic system*. Solar Energy, Vol. 78, No. 2, pp. 163–176, 2005.
67. Ghali F. M.A, Abd El Aziz M.M., Syam F. A. *Simulation and analysis of hybrid systems using probabilistic techniques*. In proceedings of Power conversion conference-Nagaoka, Vol. 2, pp. 831–835, 1997.
68. Borowy BS, Salameh ZM. *Optimum photovoltaic array size for a hybrid wind/PV system*. IEEE Transactions Energy Conversion, Vol. 9, No.3, pp. 482–488, 1994.
69. Karaki SH, Chedid RB, Ramadan R. *Probabilistic performance assessment of autonomous solar-wind energy conversion systems*. IEEE transactions on energy conversion, Vol. 14, No. 3, pp 766–772, 1999.
70. Nehrir, M.H. *An Approach to Evaluate the General Performance of Stand-Alone Wind/Photovoltaic Generating Systems*. IEEE Transactions on Energy Conversion, Vol. 15, No. 4, pp. 433-439, 2000.
71. Muljadi E., Butterfield C.P. *Pitch-controlled variable-speed wind turbine generation*. IEEE Transactions Industry Applications, Vol. 37, No. 1, pp. 240–246, 2001.
72. Zamani MH, Riahy GH. *Introducing a new method for optimal sizing of a hybrid (wind/PV/battery) system considering instantaneous wind speed variations*. Energy for Sustainable Development, Vol. 12, No.2, pp. 27–33, 2008.

73. Naterer G.F., Fowler M. , Cottonc J., and K. Gabriela. *Synergistic roles of off-peak electrolysis and thermochemical production of hydrogen from nuclear energy in Canada*. International Journal of Hydrogen Energy, Vol. 33, No. 23, pp. 6849-6857, 2008.
74. Vanhanen J.P., Kauranen P.S., Lund P.D., Manninen L.M. *Simulation of Solar Hydrogen Energy Systems*. Solar Energy, Vol. 53, No. 3, pp. 267–278, 1994.
75. Amphlett J.C., Baumert R.M., Mann R.F., Peppley B.A., Roberge P.R., Rodrigues A. *Parametric modeling of the performance of a 5 kW proton-exchange membrane fuel cell stack*. Journal of Power Sources, Vol. 49, No. 1-3, pp. 349–356, 1994.
76. Kim J, Lee SM, Srinivasan S, Chamberlin CE. *Modeling of proton exchange membrane fuel cell performance with an empirical equation*. Journal of Electrochemical Society, Vol. 142, No. 8, pp. 2670–2674, 1995.
77. Lee JH, Lalk TR, Appleby AJ. *Modeling electrochemical performance in large scale proton exchange membrane fuel cell stack*. Journal of Power Sources, Vo. 70, No. 2, pp.258–268, 1998.
78. Mann R.F., Amphlett J.C., Hooper M.A.I., Jensen H.M., Peppley B.A., Roberge P.R. *Development and application of a generalized steady-state electrochemical model for a PEM fuel cell*. Journal of Power Sources, Vol. 86, No. 1-2, pp. 173–180, 2000.
79. Fowler M.W., Mann R.F., Amphlett J.C., Peppley B.A., Roberge P.R. *Incorporation of voltage degradation into a generalized steady state electrochemical model for a PEM fuel cell*. Journal of Power Sources, Vol. 106, No. 1-2, pp. 274–283, 2002.

80. Cheddie D., Munroe N. *Review and comparison of approaches to proton exchange membrane fuel cell modeling*. Journal of Power Sources, Vol. 147, No. 1-2 , pp. 72–84, 2005.
81. Mann R.F., Amphlett J.C., Peppley B.A., Thurgood C.P. *Henry's law and the solubilities of reactant gases of reactant gases in the modeling of PEM fuel cells*. Journal of Power Sources, Vol. 161, No. 2, pp. 768–774, 2006.
82. —. *Anode polarization on Pt(h k l) electrodes in dilute sulphuric acid electrolyte*. Journal of Power Sources, Vol. 163, No. 1, pp. 679–687, 2007.
83. Deshmukh SS, Boehm RF. *Review of modeling details related to renewably powered hydrogen systems*. Renewable and Sustainable Energy Reviews, Vol. 12, No.9, pp. 2301-2330, 2008.
84. Bañosa R., Manzano-Agugliarob F., Montoyab F.G., Gila C., Alcaydeb A., Gómezc J. *Optimization methods applied to renewable and sustainable energy: A review*. Renewable and Sustainable Energy Reviews, Vol. 15, No. 4, pp. 1753-1766, 2011.
85. TS, Wu JC and Liu. *A sliding-mode approach to fuzzy control design*. IEEE Transactions on Control Systems Technology, 1996, 4(2), pp 141–151.
86. HOMER (The Hybrid Optimization Model for Electric Renewables). [Online] [Cited: 04 22, 2010.] <https://analysis.nrel.gov/homer/>.
87. Shaahid SM, Elhadidy MA. *Technical and economic assessment of grid-independent hybrid photovoltaic–diesel–battery power systems for commercial loads in desert environments*. Renewable Sustainable Energy Review, 2007, 11(8), pp. 1794–1810.

88. Shaahid SM, El-Amin I. *Techno-economic evaluation of off-grid hybrid photovoltaic–diesel–battery power systems for rural electrification in Saudi Arabia—a way forward for sustainable development*. Renewable and Sustainable Energy Reviews, 2009, 13(3), pp. 625-633.
89. Li C.H., Zhua X.J., Caoa G.Y., Suia S. and Hua M.R. *Dynamic modeling and sizing optimization of stand-alone photovoltaic power systems using hybrid energy storage technology*. Renewable Energy, 2008, 34(3), pp. 815-826.
90. Wies RW, Johnson RA, Agrawal AN, Chubb TJ. *Simulink model for economic analysis and environmental impacts of a PV with Diesel–Battery system for remote villages*. IEEE Trans Power Systems, 2005, 20(2), pp. 692–700.
91. Himri Y, Boudghene Stambouli A, Draoui B, Himri S. *Techno-economical study of hybrid power system for a remote village in Algeria*. Energy, 2008, 33(7), pp 1128–1136.
92. Lu L., Yang H., Burnett J. *Investigation on wind power potential on Hong Kong islands—an analysis of wind power and wind turbine characteristics*. Renewable Energy, 2002, 27, pp. 1–12.
93. McGowan JG and Manwell JF. *Hybrid wind/PV/diesel system experiences*. Renew Energy, Vol. 16, No. 1–4, pp. 928–933, 1999.
94. Hybrid2. *RERL - Research, Hybrid Power*. [Online] [Cited: 04 20, 2010.] <http://www.ceere.org/rerl/projects/software/hybrid2/>.

95. McGowan JG, Manwell JF, Avelar C, Warner CL. *Hybrid wind/PV/diesel hybrid power systems modelling and South American applications*. *Renew Energy*, 1996, 9(1–4), pp. 836–847.
96. Elhadidy MA. *Performance evaluation of hybrid (wind/solar/diesel) power systems*. *Renew Energy*, Vol. 26, No. 3, pp. 401–413, 2002.
97. Nfah EM, Ngundam JM, Tchinda R. *Modelling of solar/diesel/battery hybrid power systems for far-north Cameroon*. *Renew Energy*, 2007, 32(5), pp. 832–844.
98. Diaf S, Notton G, Belhamel M, Haddadi M, Louche A. *Design and technoeconomical optimization for hybrid PV/wind system under various meteorological conditions*. *Applied Energy*, 2008, 85(10), pp 968–987.
99. Dalton GJ, Lockington DA, Baldock TE. *Feasibility analysis of stand-alone renewable energy supply options for a large hotel*. *Renewable Energy*, 2008, 33 (7), pp. 1475–1490.
100. Mondal M.A.H. and Denich M. *Assessment of renewable energy resources potential for electricity generation in Bangladesh*. *Renewable and Sustainable Energy Reviews*, Vol. 14, No. 8, 2010, pp. 2401-2413.
101. Prodromidis G.N., Coutelieris F.A. *Simulation and optimization of a stand-alone power plant based on renewable energy sources*. *International Journal of Hydrogen Energy*, Vol. 35, No. 19, 2010, pp. 10599-10603.

102. Balamurugana P, Ashok S, Jose TL. *Optimal Operation of Biomass/Wind/PV Hybrid Energy System for Rural Areas*. International Journal of Green Energy, Vol. 6, No. 1, 2009, pp. 104–116.
103. Dufo-López R, Bernal-Agustín JL, Mendoza F. *Design and economical analysis of hybrid PV–wind systems connected to the grid for the intermittent production of hydrogen*. Energy Policy, 2009, 37(8), pp. 3082–3095.
104. Zervas PL, Sarimveis H, Palyvos JA, Markatos NCG. *Model-based optimal control of a hybrid power generation system consisting of photovoltaic arrays and fuel cells*. Journal of Power Sources, Vol. 181, No. 2, pp. 327–338.
105. Koutroulis E., Kolokotsa D., Potirakis A. and Kalaitzakis K. *Methodology for optimal sizing of stand-alone photovoltaic/wind-generator systems using genetic algorithms*. Solar Energy, 2006, 80(9), pp 1072–1088.
106. Weinstock, D. and Appelbaum, J. *Optimal Solar Field Design of Stationary Collectors*. Journal of Solar Energy Engineering, 126(3), 2004, pp.898-906.
107. Ashok, S. *Optimised model for community-based hybrid energy system*. Renewable Energy, 2007, 32(7), pp. 1155–1164.
108. Yang, H., Zhou, W. and Lou, C. *Optimal design and techno-economic analysis of a hybrid solar–wind power generation system*. Applied Energy, 2009, 86(2), pp. 163–169.
109. Tina G, Gagliano S and Raiti S. *Hybrid solar/wind power system probabilistic modeling for long-term performance assessment*. Solar Energy, 2006, 80(5), pp. 578–588.



110. Dufo-López R, Bernal-Agustín JL. *Design and control strategies of PV–diesel systems using genetic algorithms*. Solar Energy, 2005, 79(1), pp.33–46.
111. Esfandyar M., Jiayun Z., Nurcin C., Seungho L., Young-Jun S. and Larry H. *Hybrid simulation and optimization-based design and operation of integrated photovoltaic generation, storage units, and grid*. Simulation Modelling Practice and Theory, 2011, pp. 463–481.
112. Glover F., Kelly J., Laguna M. *The OptQuest Callable Library User's Documentation*. Optimization Technologies Inc., Boulder, Colorado, 1999.
113. Giannakoudis G., Papadopoulos A.I., Seferlis P., Voutetakis S. *Optimum design and operation under uncertainty of power systems using renewable energy sources and hydrogen storage*. International Journal of Hydrogen Energy, Vol. 35, 2010, pp. 872-891.
114. Kaabeche A., Belhamel M., Ibtouen R. *Sizing optimization of grid-independent hybrid photovoltaic/wind power generation system*. Energy, Vol. 36, No.2, 2011, pp. 1214-1222.
115. Zhao M., Chen Z., Blaabjerg F. *Optimization of electrical system for offshore wind farms via genetic algorithm*. IEEE Transactions on Renewable Power Generation, Vol. 3, N. 2, pp. 205–216.
116. Senjyu T, Hayashi D, Yona A, Urasaki N, Funabashi T. *Optimal configuration of power generating systems in isolated island with renewable energy*. Renewable Energy, Vol 32, No. 11, 2007, pp. 1917-1933.

117. Kaviani AK, Riahy GH, Kouhsari SHM. *Optimal design of a reliable hydrogenbased stand-alone wind/PV generating system, considering component outages*. Renewable Energy, Vol. 34, No.11, 2009, pp. 2380–2390.
118. Hakimi SM, Moghaddas-Tafreshi SM. *Optimal sizing of a stand-alone hybrid power system via particle swarm optimization for Kahnouj area in south-east of Iran*. Renewable Energy, Vol. 34, No. 7, 2009, pp. 1855–1862.
119. Dufo-López R., José L., Bernal-Agustín J.L. *Design of isolated hybrid systems minimizing costs and pollutant emissions*. Renewable Energy, 2006, 31 (14), pp. 2227–2244.
120. Dufo-López R., José L., Bernal-Agustín J.L. *Multi-objective design of PV-Wind-Diesel-Hydrogen-Battery systems*. Renewable Energy, Vol. 33, No. 12, pp. 2559-2572, 2008.
121. Bernal-Agustín J., Dufo-López R. *Multi-objective design and control of hybrid systems minimizing costs and unmet load*. Electric Power Systems Research, 2009, Vol. 79, No. 1, pp. 170-180.
122. HOGA (Hybrid Optimization by Genetic Algorithms). [Online] [Cited: 07 01, 2010.] <http://www.unizar.es/rdufo/hoga-eng.htm>.
123. Dipama J., Teyssedou A., Aubé F., and Lizon-A-Lugrin L. *A grid based multi-objective evolutionary algorithm for the optimization of power plants*. Applied Thermal Engineering, 30(8-9) , pp. 807-816, 2010.
124. Meza J. L. C., Yildirim M. B., and Masud A. S. M. *A Multiobjective Evolutionary Programming Algorithm and Its Applications to Power Generation Expansion Planning*.

IEEE Transactions on Systems, Man, and Cybernetics - Part A: Systems and Humans, 39 (5), pp. 1086-1096, 2009.

125. Niknam T., Kavousifard A., Tabatabaei S., Aghaei j. *Optimal operation management of fuel cell/wind/photovoltaic power sources connected to distribution networks*. Journal of Power Sources, Vol. 196, No. 20, pp.8881-8897, 2011.

126. Ould B, Sambou V, Ndiaye PA, Kébé CMF, Ndongo M. *Optimal design of a hybrid solar-wind-battery system using the minimization of the annualized cost system and the minimization of the loss of power supply probability (LPSP)*. Renewable Energy, Vol. 35, No, 10, 2010, pp. 2388–2390.

127. Katsigiannis YA, Georgilakis PS, Karapidakis ES. *Multiobjective genetic algorithm solution to the optimum economic and environmental performance problem of small autonomous hybrid power systems with renewables*. IET Renewable Power Generation, Vol. 4, No. 5, 2010, pp. 404–19.

128. Branke J., Deb K., Miettinen K. *Multiobjective optimization: interactive and evolutionary approaches*. Springer, ISBN: 978-3540889076, 2008.

129. Beyer HG and Sendhoff B. *Robust optimization – A comprehensive survey*. Computer Methods in Applied Mechanics and Engineering, Vol. 196, No. 33-34, pp. 3190-3218, 2007.

130. <http://physicsworld.com>. Birds flock with scale invariance. [Online] [Cited: 12 16, 2013.] <http://physicsworld.com/cws/article/news/2010/jul/06/birds-flock-with-scale-invariance>.

131. School of fish ball protecting from predators. [Online] 12 16, 2013. <http://pandawhale.com/post/4265/school-of-fish-ball-protecting-from-predators-aka-bait-ball>.
132. Kennedy J., and Eberhart R.C. *Particle Swarm Optimization*. In: Proceedings of the 1995 IEEE International Conference on Neural Networks, Piscataway, New Jersey, pp. 1942–1948, 1995.
133. Reyes-sierra M, and Coello CAC. *Multi-objective particle swarm optimizers: A survey of the state-of-the-art*. International Journal of Computational Intelligence Research, Vol. 2, No. 3, pp. 287-308, 2006.
134. J. Moore, R. Chapman, and G. Dozier. *Multiobjective particle swarm optimization*. In Proceedings of the 38th Annual on Southeast Regional Conference, ser. ACM-SE 38. New York, NY, USA: ACM, pp. 56–57, 2000.
135. Jeddy M.J., and Kumar D.N. *An efficient multi-objective optimization algorithm based on swarm intelligence for engineering design*. Engineering Optimization, Vol. 39, No. 1, pp. 49–68, 2007.
136. Santana R. A., Pontes M. R., and Bastos-Filho C. J. A. *A multiple objective particle swarm optimization approach using crowding distance and roulette wheel*. in Proceedings of the 2009 Ninth International Conference on Intelligent Systems Design and Applications, ser. ISDA '09. Washington, DC, USA: IEEE Computer Society, pp. 237–242, 2009.

137. Hernández-Domínguez JS, Pulido GT, Coello CAC. *A Multi-objective Particle Swarm Optimizer Enhanced with a Differential Evolution Scheme*. Artificial Evolution, pp. 169-180, 2011.
138. Bartz-Beielstein T., Limbourg P., Mehnen J., Schmitt K., and Parsopoulos K. *Particle swarm optimizers for pareto optimization with enhanced archiving techniques*. The 2003 Congress in Evolutionary Computation, CEC '03 , Vol. 3, pp. 1780–1787, 2003.
139. Dupont G., Adam S., Lecourtier Y., and Grilhere B. *Multi objective particle swarm optimization using enhanced dominance and guide selection*. International Journal of Computational Intelligence Research, Vol. 4, No. 2, pp. 145–158, 2008.
140. Coello Coello C., and Lechuga M. *Mopso: a proposal for multiple objective particle swarm optimization*. in Proceedings of the 2002 Congress on Evolutionary Computation 2002, CEC '02 , Vol. 2, pp. 1051 –1056, 2002.
141. Mostaghim S., and Teich J. *Strategies for finding good local guides in multi-objective particle swarm optimization (mopso)*. Proceedings of the 2003 IEEE in Swarm Intelligence Symposium, SIS '03, pp. 26 – 33, 2003.
142. Xu H. Wang Y, Xu X. *Dominating Global Best Selection for Multi-objective Particle Swarm Optimization*. Proceedings of the 2nd International Conference on Computer Science and Electronics Engineering (ICCSEE 2013), pp. 1503-1505, 2012.

143. Castro Junior O.R., de Britto A.B., Pozo A. *A Comparison of methods for leader selection in many-objective problems*. IEEE Congress on Evolutionary Computation, Brisbane, Australia, pp. 1-8, 2012.
144. Schlaich J., Bergermann R., Schiel W. & Weinrebe G. *Design of Commercial Solar Updraft Tower Systems—Utilization of Solar Induced Convective Flows for Power Generation*. Journal of Solar Energy Engineering, Vol. 127, pp. 117-125, 2005.
145. Price H., Lüpfer E., Kearney D., Zarza E., Cohen G., Gee R. & Mahoney R. *Advances in parabolic trough Solar power technology*. Journal of Solar Energy Engineering, vol. 124, no2, pp. 109-125, 2002.
146. Sheskin D.J. *Handbook of Parametric and Nonparametric Statistical Procedures*. 4th ed, New York: Chapman & Hall/CRC Press, 2007.
147. Varun S. *Thermal performance optimization of a flat plate solar air heater using genetic algorithm*. Applied Energy, Vol. 87, No. 5, pp. 1793–1799, 2000.
148. Thiaux Y., Seigneurbieux J., Multon B. & Ben Ahmed H. *Load profile impact on the gross energy requirement of stand-alone photovoltaic systems*. Renewable Energy, Volume 35, Issue 3, pp. 602-613, 2010.
149. Yang H., Lu L. and Zhou W. *A novel optimization sizing model for hybrid solar-wind power generation system*. Solar Energy, Vol.81, No.1, pp.76-84, 2007.
150. Chang Y. *Optimal the tilt angles for photovoltaic modules in Taiwan*. International Journal of Electrical Power & Energy Systems, Vol. 32, No. 9, pp. 956-964, 2010.

151. Sadineni S., Boehm R. & Hurt R. *Spacing Analysis of an Inclined Solar Collector Field*. ASME 2nd International Conference on Energy Sustainability, Jacksonville, Florida, 2008.
152. Myers B., Bernardi M. & Grossman J. C. *Three-dimensional photovoltaics*. Applied Physics Letters, Vol. 96, 2010.
153. Y, Ekren O. & Ekren B. *Size optimization of a PV/wind hybrid energy conversion system with battery storage using simulated annealing*. Applied Energy, Volume 87, Issue 2, pp. 592-598.
154. Appelbaum, D. Weinstock & J. *Optimal Solar Field Design of Stationary Collectors*. J. Sol. Energy Eng., 2004, Vol. 126, n. 4, pp. 363-371.
155. Appelbaum, D. Weinstock and J. *Optimization of Solar Photovoltaic Fields*. ASME Journal of Solar Energy Engineering, 2009, Vol. 131, n. 3.
156. Bourennani F., Rizvi R., & Rahnamayan S. *Optimal Photovoltaic Solar Power Farm Design using the Differential Evolution Algorithms*. International Conference on Clean Energy (ICCI'10), Gazimagusa, N. Cyprus, ref. 7-20, pp. 1-8, 2010.
157. Ibrahim, A., Bourennani, F., Rahnamayan, S, and Naterer, G. F. *Optimal Photovoltaic Farm Design Using Multi-objective Optimization*. International Journal of Applied Metaheuristic Computing, (In press), pp. 1-15, 2013 .
158. NCDIA. Monthly Averaged Hourly Solar Angles Relative To The Horizon and Solar Azimuth Angles Due south in degrees. National Climate Data and Information Archive Retrieved August 3 2012. [Online] 2012. [http://climat.meteo.gc.ca/prods\\_servs/index\\_e.html](http://climat.meteo.gc.ca/prods_servs/index_e.html).

159. NASA. Monthly Averaged Hourly Solar Angles Relative To The Horizon(Degrees) and Monthly Averaged Hourly Solar Azimuth Angles(Degrees), 2012. *Atmospheric Science data center. NASA Surface meteorology and Solar Energy Information, August 3, 2012.* [Online] <http://eosweb.larc.nasa.gov>.
160. altestore. Solar Panels at Affordable Prices. *The Alternative Energy Store, Retrieved August 3, 2012, from* . [Online] <http://www.altestore.com/store/Solar-Panels/c541/>.
161. Rahnamayan S., Tizhoosh H. R., and Salama M. M. A. *Opposition versus randomness in soft computing techniques.* Applied Soft Computing Journal, Vol. 8, No. 2, pp. 906–918, 2008.
162. Rahnamayan S., Wang G.G., Ventresca M. *An intuitive distance-based explanation of opposition-based sampling.* Applied Soft Computing, Vol. 12, No. 9, pp. 2828-2839, 2012.
163. Tizhoosh H. R. *Opposition-based learning: A new scheme for machine intelligence.* in Proceedings of the International Conference on Computational Intelligence for Modelling, Control and Automation, CIMCA 2005 and International Conference on Intelligent Agents, Web Technologies and Internet, Vol. 1, pp. 695–701, 2005.
164. Tizhoosh H. R., and Ventresca M. *Oppositional Concepts in Computational Intelligence.* Vol. 155 of Studies in Computational Intelligence, 2008.
165. Rahnamayan S., Tizhoosh H. R., and Salama M. M. A. *Opposition-based differential evolution algorithms.* in IEEE Congress on Evolutionary Computation, pp. 2010–2017, 2006.



166. Rahnamayan S., Tizhoosh H. R., and Salama M. M. A. *A novel population initialization method for accelerating evolutionary algorithms*. Computers and Mathematics with Applications, Vol. 53, No. 10, pp. 1605–1614, 2007.
167. Rahnamayan S. and Wang G. *Solving large scale optimization problems by opposition-based differential evolution (ODE)*. WSEAS Transactions on Computers, Vol. 7, No. 10, pp. 1792–1804, 2008.
168. Rahnamayan S., Tizhoosh H. R., and Salama M. M. A. *Opposition-based differential evolution for optimization of noisy problems*. in IEEE Congress on Evolutionary Computation, CEC, pp. 1865–1872, 2006.
169. Rahnamayan S., Tizhoosh H. R., and Salama M. M. A. *Quasioppositional differential evolution*. in IEEE Congress on Evolutionary Computation, CEC 2007, pp. 2229–2236, 2008.
170. Rahnamayan S., Tizhoosh H. R., and Salama M. M. A. *Opposition-based differential evolution (ODE) with variable jumping rate*. In Proceedings of the 2007 IEEE Symposium on Foundations of Computational Intelligence, FOCI, pp. 81–88, 2007 .
171. Omran M. G. H., and Al-Sharhan S. *Using opposition-based learning to improve the performance of particle swarm optimization*. in IEEE Swarm Intelligence Symposium, SIS, St. Louis, MO, 2008.

172. Al-Qunaieer F.S., Tizhoosh H.R., and Rahnamayan S. *Opposition Based Computing - A Survey*. IEEE International Joint Conference on Neural Networks (IJCNN), Barcelona, Spain, pp. 3183-3189, July 18-23, 2010.
173. Peng L., Wang Y., and Dai A. G. *A Novel Opposition-Based Multi-objective Differential Evolution Algorithm for Multi-objective Optimization*. Advances in Computation and Intelligence, pp. 162-170, 2008.
174. Knowles J. D., and Corne D. W. *The Pareto Archived Evolution Strategy: A New Baseline Algorithm for Multiobjective Optimisation*. In Proceedings of the Congress on Evolutionary Computation, Washington D.C., USA, pp. 98–105, 1999.
175. Ishibuchi H., Tsukamoto N., Nojima Y. *Iterative approach to indicator-based multiobjective optimization*. In proceedings of the IEEE Congress on Evolutionary Computation, CEC 2007, Singapore, pp. 3967 - 3974, 2007 .
176. Wang N., and Dong Y. *Multiobjective Differential Evolution Based on Opposite Operation*. International Conference on Computational Intelligence and Security (CIS '09), Beijing, China, pp. 123 - 127, 2009.
177. Zhang Q., Zhou A., and Jin Y. *RM-MEDA: A regularity model-based multiobjective estimation of distribution algorithm*. IEEE Trans. Evolutionary Computation, Vol. 12, No. 1, pp. 41-63, 2008.

178. Teo T. G., and Tan J. *Evolving Opposition-Based Pareto Solutions: Multiobjective Optimization Using Competitive Coevolution*. In H. R. Tizhoosh and M. Ventresca (Eds), *Oppositional Concepts in Computational Intelligence*, Springer, Vol. 155, pp. 161-206, 2008.
179. Schott J.R. *Fault Tolerant Design Using Single and Multicriteria Genetic Algorithm Optimization*. Masters thesis, Department of Aeronautics and Astronautics, Massachusetts Institute of Technology, Cambridge, Massachusetts, 1995.
180. Eiben G., and Schut M. *New Ways to Calibrate Evolutionary Algorithms*. In P. Siarry and Z. Michalewicz, editors, *Advances in Metaheuristics for Hard Optimization*, Natural Computing, pages 153–177. Springer, Heidelberg, Germany, 2008.
181. Sheskin D. J. *Handbook of Parametric and Nonparametric Statistical Procedures*. 4th ed. New York: Chapman & Hall/CRC Press, 2007.
182. Das S. *Differential Evolution: A Survey of the State-of-the-Art*. *IEEE Transactions on Evolutionary Computation*, Vol. 15, No. 1, pp. 4-31, 2011.
183. Price, R. Storn and K. *Differential evolution - a simple and efficient heuristic for global optimization over continuous spaces*. *Journal of Global Optimization*, Vol. 11, pp. 341–359, 1997.
184. Bourennani F., Rahnamayan S., Naterer G.F. *Leaders and speed constraint multi-objective particle swarm optimization*. *IEEE Congress on Evolutionary Computation 2013*, Cancun, Mexico, pp. 908-915.

185. Canada, Natural Resources. Canada's Energy Outlook: The Reference Case 2006. [Online] 2006. <http://www.nrcan.gc.ca/publications/energy-outlook/788> accessed 11-15-2013.
186. Hajimiragha A, Fowler MW, Canizares CA. *Hydrogen economy impact on optimal planning and operation of integrated energy systems*. In: Proc. international conference & workshop on Micro-Cogeneration Technologies & Applications, Ottawa, Canada, pp. 1-11, 2008.
187. Bourennani, F., Rahnamayan, S., and Naterer, G. F. *Applications of Multi-Objective Optimization to Energy System Design*. International Conference on Clean Energy (ICCI'10), Gazimagusa, N. Cyprus, ref. 6-05, pp. 1-8, 2010.
188. Bourennani, F., Rahnamayan, S., and Naterer, G. F. *Methods of Optimization based Control for Renewable Energy Systems*. International Conference on Clean Energy (ICCI'10), Gazimagusa, N. Cyprus, ref. 7-08, pp. 1-8, 2010.
189. Agency, International Energy. *Key world energy statistics*. [Online] 2006. <http://www.iea.org/>.
190. Canada, Transport. [Online] Transport Canada. <http://www.tc.gc.ca/environment/menu.htm#climatechange>.
191. Socorro M.A.R. *Measuring the oil vulnerability of Canadian cities*. Simon Fraser University, available online: <http://ir.lib.sfu.ca/bitstream/1892/4211/1/etd2765.pdf>, accessed 11-15-2013.

192. Adamson K. *Hydrogen from renewable resourcesd - the hundred year commitment*. Energy Policy, Vol. 32, No. 10, pp. 1231–1242.
193. Rifkin J. *The hydrogen economy: the creation of the worldwide energy web and the redistribution of power on earth*. New York: Penguin Putnam, 2002.
194. McDowall W. and Eames M. *Forecasts, scenarios, visions, backcasts and roadmaps to the hydrogen economy: a review of the hydrogen futures literature*. Energy Policy, Vol. 34, No. 11, pp. 1236–1250, 2006.
195. Felder FA and Hajos A. *Using restructured electricity markets in the hydrogen transition: the PJM case*. In: Proc. IEEE special issue on the hydrogen economy, Vol. 94, No. 10, pp. 1864–1879, 2006.
196. Taljan G, Fowler M, Canizares C, Verbic G. *Hydrogen storage for mixed wind–nuclear power plants in the context of a hydrogen economy*. Int J Hydrogen Energy, Vol. 33, No. 17, pp. 4463–4475, 2008.
197. Hajimiragha A., Fowler M.W., Cañizares C.A. *Hydrogen economy transition in Ontario – Canada considering the electricity grid constraints*. International Journal of Hydrogen Energy, Vol. 34, No. 13, pp. 5275-5293, 2009.
198. Ontario transmission system. *Independent Electricity System Operator (IESO)*.  
[Online] 2012.[accessed: 10 25, 2013.]  
[http://www.theimo.com/imoweb/pubs/marketReports/OntTxSystem\\_2012nov.pdf](http://www.theimo.com/imoweb/pubs/marketReports/OntTxSystem_2012nov.pdf).

199. Ontario Power Authority. ElectrON: planning Ontario's electricity system. *Ontario Power Authority*. [Online] [Cited: 10 2008, 25.] <<http://www.powerauthority.on.ca/electron/>.
200. Authority, Ontario Power. Ontario's integrated power system plan; scope and overview. *Ontario Power Authority*. [Online] 2006.  
[http://www.powerauthority.on.ca/Storage/24/1922\\_OPA\\_-\\_IPSP\\_Scope\\_and\\_Overview.pdf](http://www.powerauthority.on.ca/Storage/24/1922_OPA_-_IPSP_Scope_and_Overview.pdf).
201. Authority, Ontario Power. Nuclear resources for baseload. Submission to the Ontario Energy Board. *EB-2007-0707, Exhibit D, Tab 6, Schedule 1*). Toronto, Ontario, Canada, 2007. [Cited: 10 1, 2013.]  
[http://www.ontarioenergyboard.ca/documents/cases/EB-2007-0707/dec\\_reasons\\_OPA\\_20080326.pdf](http://www.ontarioenergyboard.ca/documents/cases/EB-2007-0707/dec_reasons_OPA_20080326.pdf).
202. Authority, Ontario Power. Determining resource requirements. Submission to the Ontario Energy Board. (*EB-2007-0707, Exhibit D, Tab 3, Schedule 1*). Toronto, Ontario, 2008. [Accessed: 09-15-2013] [http://www.ontarioenergyboard.ca/documents/cases/EB-2007-0707/exhibits\\_issues/exhibit\\_5\\_pollution\\_probe\\_20080115.pdf.pdf](http://www.ontarioenergyboard.ca/documents/cases/EB-2007-0707/exhibits_issues/exhibit_5_pollution_probe_20080115.pdf.pdf).
203. Latella A. *Shortcircuiting system for use in monopolar and bipolar electrolyzers*. US Patent 5431796, 1995.
204. (IESO), Independent Electricity System Operator. Market data. [Online] [Accessed: 10 01, 2013.] <http://www.ieso.ca/imoweb/marketdata/marketData.asp>.
205. Prince-Richard S., Whale M., Djilali N. *A techno-economic analysis of decentralized electrolytic hydrogen production for fuel cell vehicles*. *Int. J. Hydrogen Energy*, Vol. 30, No. 11, pp. 1159–1179, 2005.

206. Parker N. *Optimizing the design of biomass hydrogen supply chains using real-world spatial distributions: A case study using California rice straw*. Institute of Transportation Studies. Paper UCD-ITS-RR-07-13. Available online from:  
[http:// repositories.cdlib.org/itsdavis/UCD-ITS-RR-07-13](http://repositories.cdlib.org/itsdavis/UCD-ITS-RR-07-13)
207. Canada, Natural Resources. *Canadian vehicle survey, summary report 2007*. Available:  
<http://oee.nrcan.gc.ca/publications/statistics/cvs07/index.cfm>, accessed 11-25-2013.
208. Canada, Statistics. Available:  
<<http://www.statcan.ca/Daily/English/080327/d080327d.htm>>, accessed: 11-12-2008.
209. Brey J.J., Brey R., Carazo A.F., Contreras I., Hernandez-Diaz A.G., Castro A. *Planning the transition to a hydrogen economy in Spain*. *Int J Hydrogen Energy*, Vol. 32, No. 10–11, pp. 1339–1346, 2007.
210. Logistic solution builders Inc. Operating costs of trucks in Canada. [Online] 2005.  
[http://publications.gc.ca/collections/collection\\_2011/tc/T46-14-2005-eng.pdf](http://publications.gc.ca/collections/collection_2011/tc/T46-14-2005-eng.pdf).
211. Gomez-Exposito A, Conejo AJ, Canizares CA editors. *Electric energy systems: analysis and operation*. CRC Press, 2008.